SPARK PLASMA SINTERING OF MULTIWALL CARBON NANOTUBES REINFORCED TITANIUM-ALUMINIUM-VANADIUM BASED NANOCOMPOSITES

BY

AVWEROSUOGHENE MOSES OKORO

217092263

ARTICLE BASED THESIS

SUBMITTED IN FULFILLMENT OF THE REQUIREMENTS FOR THE AWARD OF DOCTORAL DEGREE IN METALLURGY

FACULTY OF ENGINEERING AND BUILT ENVIRONMENT, UNIVERSITY OF JOHANNESBURG

SUPERVISOR: PROF. PETER A. OLUBAMBI

CO-SUPERVISOR: DR. RONALD MACHAKA

SEPTEMBER 2019

DECLARATION

I, the author of this work, write to affirm that this dissertation is a combination of papers from my PhD research titled ‘‘Spark plasma sintering of multiwall carbon nanotubes reinforced titanium-aluminium-vanadium-based nanocomposites’’ which I hereby submit for the award of

DOCTORAL DEGREE (Ph.D.) IN METALLURGY

to the University of Johannesburg, Department of Metallurgy, is my personal work beside the acknowledged support of my supervisors and has never been submitted by me or anyone elsewhere to acquire a research degree.

Signature: …… ……..……

AVWEROSUOGHENE MOSES OKORO

Date: ……26…/……09……. /…2019…….....

DEDICATION

This research is dedicated to my beloved parent, Mr. and Mrs. Okoro and my lovely aunt Mrs. Roseline Omotoyinbo and above all, to Almighty God the giver of life.

ACKNOWLEDGMENT

My profound appreciation goes to my mentor and supervisor Prof. Peter Apata Olubambi, the head, Centre for Nanoengineering and Tribocorrosion, Department of Metallurgy, University of Johannesburg, South Africa. I am grateful to him for seeing a prospect in me and giving me the privilege to conduct my doctoral research under his guidance and supervision. He has been a mentor, father, teacher and research coach which has inspired me to succeed in this research journey. From the depth of my heart, I dedicate this section of my thesis to the Godfather and words are not enough to express my sincere gratitude for his system of leadership that motivate all his students to go beyond their limits.

I would like to appreciate my co-supervisor Dr Ronald Machaka for his sincerity about this research and consistent contributions to the success of my PhD studies. He is also a shoulder to stand on to see this far in my research journey. Special thanks to Dr Samuel Ranti Oke and Dr Oluwasegun Falodun for their incessant supports during struggling times in this research. Also, my profound appreciation to my project colleagues Miss Senzeni Sipho Lephuthing, Mrs Mary Ajimegoh Awotunde and Mr Oluwaniyi Ajiteru. It's a great privilege to be associated with you guys during this research journey and I am forever grateful for your contributions towards the success of this work.

My sincere thanks to the Global Excellence and Stature (GES) of the University of Johannesburg and the National Research Foundation of South Africa in association with the World Academy of Science for Funding my doctoral research from 2017 to 2019.

My profound gratitude to my mentors from the Department of Metallurgical and Materials Engineering, the Federal University of Technology Akure, Nigeria Prof J.A. Omotoyinbo, Prof B.O. Borode, Prof. K.K. Alaneme, Dr. I.O. Oladele and Dr. M.O. Bodurin. Your imparts during my undergraduate and master's degree programmes has made me who I am today.

Special thanks to the Institute of Nanoengineering Research (INER) in the Department of Chemical and Metallurgical and Materials Engineering, Tshwane University of Technology for opening their doors to me to carry out the consolidation of the samples using their spark plasma sintering facility. I appreciate Mr Mdu for assisting with the sintering and Mr Brayner for assistance with SEM characterization. Also, Thanks to Miss Rhandzu for assisting me with the TEM characterization of my powder samples.

I would like to recognize my beloved friends and colleagues from my research centre in UJ, Olufunsho Olotu, Adeola Borode, Kesta Segun, Sanumi Femi, Lesufi Miltia, Akinwamide Samuel, Mosima Maja, Olusoji Ayodele for their support

Lastly, I appreciate the incessant motivation and prayers from my aunt Mrs Roseline Omotoyinbo and my uncle, Mr Sunday Onoguere. I am grateful for all your financial support, love and encouragements in my career journey. Thank you.

ABSTRACT

Innovations in materials development has engendered the improvement of the properties of titanium alloys for diverse engineering applications. In this study, titanium alloy (Ti6Al4V) and multiwall carbon nanotubes (MWCNT) were mixed using shift-speed ball milling (SSBM) technique to achieve the uniform dispersion of MWCNT in the Ti6Al4V matrix. The starting and admixed powders were characterized using scanning electron microscopy equipped Energy dispersive X-Ray spectroscopy (SEM-EDS), X-ray diffraction (XRD), Raman spectroscopy and Transmission electron microscopy (TEM). Detailed TEM characterization was carried out to reveal the structural evolutions of the MWCNT during the dispersion process using selected area diffraction and fast Fourier transform pattern. The admixed powders were then consolidated using the spark plasma sintering machine (model HHPD-25, FCT GmbH Germany). Furthermore, various characterization technique such as XRD, SEM-EDS, optical microscopy (OM) was employed to understand the phase evolutions, morphology, microstructural changes and fractography of the fabricated nanocomposites. The mechanical properties of the fabricated materials were further investigated using the Vickers microhardness tester (FALCON 500 series) and the nanoindentation technique (ultra nanoindenter) UNHT. The study resulted in five (5) research articles, each article investigated the following respectively; (1) the previous works that have been conducted in SPS of titanium-based nanocomposites reinforced with MWCNT, (2) the dispersibility, structural evolutions and interfacial bonding of MWCNT in Ti6Al4V powders using the SSBM technique, (3) the evaluation of the influence of varying sintering temperature on the sintering and densification behaviours and microhardness of the fabricated alloy and nanocomposites, (4) the effects of MWCNT addition on the change in microstructures and mechanical properties of the fabricated nanocomposites, and (5) the influence of MWCNT on the nanomechanical properties of the fabricated nanocomposites.

During the dispersion process, the Raman and XRD pattern of the admixed powders showed that mechanical stresses were induced on the walls of the nanotubes which does not result in defects on the MWCNT. Optimal dispersion of MWCNT was achieved on the nanocomposite grades comprising of 0.5 and 1.0 wt.% nanotubes. Additionally, the dispersibility decreased with the increase in concentration of the MWCNT in the Ti6Al4V matrix. Meanwhile, the nanocomposite grades with higher fraction of MWCNT experienced higher deformation of the nanotubes during the dispersion process. The optimal dispersion of MWCNT in Ti6Al4V matrix with minimal

structural deformation was achieved when the powders were mixed with the following milling parameters; 8 h, 150 rpm, 10:1 of BPR and 10 min of relaxation time and 1 h, 100 rpm, 10:1 and 10 min of relaxation time during low-speed ball milling and high-speed ball milling respectively. Furthermore, during the consolidation of the Ti6Al4V alloy and the nanocomposites at varying sintering temperature, it was observed that the densification of the materials improved with the increase in sintering temperature. Conversely, the relative density of the nanocomposites decreased with the addition of MWCNT into the Ti6Al4V matrix. The optimal densification of both the sintered Ti6Al4V and the nanocomposites was achieved using the following sintering parameters; sintering temperature of 1100 ^{o}C, holding time of 10 min, heating rate of 100 ^{o}C/min, and compressive pressure of 50 MPa. It was also realized that after the sintering of the materials various phases such as the alpha-titanium, beta-titanium and the titanium carbide phases were observed which helped in improving the mechanical properties of the fabricated materials.

Additionally, improvement in Vickers microhardness value was recorded in the composite grades fabricated with the aforementioned sintering parameters. Also, the sintering process was retarded by the addition and increase in the concentration of MWCNT. However, all the nanocomposite grades exhibited similar sintering and densification behaviour. The microhardness of the fabricated materials improved with the increase in sintering temperature. Also, the microhardness and nanomechanical properties of the fabricated nanocomposites improved with the increase in concentration of the MWCNT in the Ti6Al4V matrix. Furthermore, a linear correlation ($H_V = 0.0316H_N + 294.72$) relating the Vickers microhardness and nanohardness was established for the fabricated materials at an indentation load of 100 mN. It was observed that the nanomechanical properties of the fabricated materials decreased with the increase in nanoindentation loads. The elastic recovery index $\left({}^{W_e}/_{W_t}\right)$, nanohardness ($H_N$), reduced elastic modulus (E_r), resistance to elastic deformation $\left({}^{H}/_{E_r}\right)$ and anti-wear behaviour $\left({}^{H^3}/_{E_r^2}\right)$ of the fabricated materials at the maximum load improved with the addition of MWCNT. Conversely, the fabricated Ti6Al4V alloy exhibited the highest plastic deformation, thus, having the highest plasticity index $\left({}^{W_p}/_{W_t}\right)$at all the indentation loads. Irrespective of the agglomeration observed in the nanocomposite grade comprising of 1.5 wt.%, this nanocomposite grade fabricated at the optimal sintering parameters exhibited the highest mechanical properties tested in this study.

Table of Contents

Cover page i
Declaration ii
Dedication iii
Acknowledgment iv
Abstract vi
Table of Contents viii
List of Figures xiii
List of Tables xviii
List of Acronyms xviv

CHAPTER ONE 1
INTRODUCTION 1
1.1 Background of Research 1
1.2 Problem statements 4
1.3 Aim and Objectives 6
1.4 Research Questions 7
1.5 Justification of the Research 7
1.6 Scope of the Study 9
1.7 Structure of the Thesis 10
Reference 13
CHAPTER TWO 18
Paper 1: A Review of Spark Plasma Sintering of Carbon Nanotubes Reinforced Titanium-based Nanocomposites: Fabrication, Densification and Mechanical Properties. 20
Abstract 20
1. Introduction 20
2. Properties of CNTs for TMNC Applications 23
3. Fabrication of CNT-TMNC by SPS 25
3.1 Overview on SPS for Fabrication of TMNC 25
4. Densification of CNT-TMNC Fabricated by SPS 27
4.1 Effect of sintering parameters and CNT addition to the densification behavior of SPS-based TMNC 30
5. Mechanical properties of CNT-TMNC 37

5.1 Effect of sintering parameters and CNT addition on the mechanical properties of CNT-TMNC 38
6. Potential Applications of SPSed CNT-TMNC 51
7. Conclusions and Future Prospect 51
Acknowledgements 52
Conflict of interest 52
Reference 53
CHAPTER THREE 59
PUBLISHED INVESTIGATIONS FROM THIS STUDY 59
3.1 Synopsis 59
3.2 Summary of written/published articles from the study 59
3.3 The Enclosed Articles 59
Paper 2: Dispersion characteristics, interfacial bonding and nanostructural evolution of 61
MWCNT in Ti6Al4V powders prepared by shift speed ball milling technique 61
Abstract 61
1. Introduction 62
2. Materials and Method 65
2.1 Starting materials 65
2.2 Dispersion of MWCNT in Ti6Al4V powders by shift speed ball milling (SSBM) 66
2.3 Characterization of the starting and admixed powders after SSBM 67
3. Results and Discussion 67
3.1 Microstructural evolution of MWCNT after dispersion in Ti6Al4V powders 67
3.1.1 Mechanism of ball milling of MWCNT in Ti6Al4V using low-speed and high-speed ball mill 74
3.2 Structural evolution and interfacial bonding of MWCNT in Ti6Al4V Powders 74
3.2.1 TEM analysis of the dispersion characteristics, interfacial bonding and structural 76
evolution of MWCNT in Ti6Al4V powders 77
3.2.2 Raman spectroscopic analysis of MWCNT in Ti6Al4V powders. 79
3.3 XRD analysis of the MWCNT-Ti6Al4V powders 82
4. Conclusion 83
Acknowledgement 84
Reference 85

Paper 3: Evaluation of the sinterability, densification behaviour and microhardness of spark plasma sintered multiwall carbon nanotubes reinforced Ti6Al4V nanocomposites 92
Abstract 92
1. Introduction 92
2. Materials and Method 95
2.1. Starting materials 95
2.2. Milling of starting powders using shift speed ball milling technique 96
2.3. Fabrication of the Ti6Al4V and nanocomposites using SPS technique 96
2.4. Characterization of as-received, admixed powders and sintered MWCNT-Ti6Al4V nanocomposites 97
2.5. Density measurement and microhardness test of the sintered Ti6Al4V and MWCNT-Ti6Al4V nanocomposites 98
3. Results and Discussion 99
3.1. Microstructural evolution of as-received, admixed powders, sintered Ti6Al4V and the MWCNT-Ti6Al4V nanocomposites 99
3.2. XRD analysis of the starting, admixed powders, sintered Ti6Al4V and MWCNT-Ti6Al4V nanocomposites 106
3.3 Raman spectroscopic analysis of starting, admixed powders and sintered MWCNT-Ti6Al4V nanocomposites 110
3.4 Sintering behaviours of the sintered Ti6Al4V and MWCNT-Ti6Al4V nanocomposites..114
3.5 Densification behaviour of the sintered Ti6Al4V and MWCNT-Ti6Al4V nanocomposites 117
3.6 Relative density of the sintered Ti6Al4V and MWCNT-Ti6Al4V nanocomposites 119
3.7 Microhardness of the sintered Ti6Al4V and MWCNT-Ti6Al4V nanocomposites 120
4. Conclusion 122
Acknowledgement 123
Reference 124
Paper 4: Influence of multiwall carbon nanotubes addition on the microstructural evolution and mechanical properties of spark plasma sintered Ti6Al4V nanocomposites 131
Abstract 131
1. Introduction 132
2. Materials and Method 135
2.1. As-received materials 135
2.2 Dispersion of MWCNT in Ti6Al4V matrix using shift speed ball milling technique 135

2.3. Sintering of the Ti6Al4V and Ti6Al4V nanocomposites using SPS technique.....136
2.4. Characterization of starting, admixed powders and fabricated MWCNT-Ti6Al4V nanocomposites.....137
2.5. Densification and mechanical test of the fabricated Ti6Al4V and MWCNT-Ti6Al4V nanocomposites.....138
3. Results and discussion.....139
3.1 Microstructural analysis of starting and mixed MWCT-Ti6Al4V powders.....139
3.2 Influence of SSBM on the dispersion features of MWCNT in Ti6Al4V powders.....140
3.3. Microstructural evolution of fabricated Ti6Al4V and MWCNT-Ti6Al4V nanocomposites after SPS.....144
3.4 Fracture morphology of the fabricated Ti6Al4V and MWCNT-Ti6Al4V nanocomposites 146
3.5 X-Ray diffraction pattern of the starting powders, mixed powders, fabricated Ti6Al4V, and MWCNT-Ti6Al4V nanocomposites.....147
3.6 Raman spectra of the starting, mixed powders, fabricated Ti6Al4V and Ti6Al4V nanocomposites.....149
3.7 Densification of the fabricated Ti6Al4V and Ti6Al4V based nanocomposites.....153
3.8 Mechanical properties of the fabricated Ti6Al4V and Ti6Al4V based nanocomposites ..154
3.8.1 Micro and Nanohardness values of the fabricated Ti6Al4V and Ti6Al4V based nanocomposites.....154
3.8.2 Load-displacement the fabricated Ti6Al4V and Ti6Al4V nanocomposites.....156
3.8.3 Elastic modulus of the fabricated Ti6Al4V and Ti6Al4V nanocomposites.....157
4. Conclusion.....158
Acknowledgement.....159
Reference.....160
Paper 5: Nanoindentation studies of the mechanical behaviours of spark plasma sintered multiwall carbon nanotubes reinforced Ti6Al4V nanocomposites.....168
Abstract.....168
1. Introduction.....168
2. Materials and Methods.....171
2.1 Mixing and fabrication of Ti6Al4V and MWCNT-Ti6Al4V nanocomposites by SPS.....172
2.2 Microstructural evolution of sintered Ti6Al4V and MWCNT-Ti6Al4V nanocomposites172
2.3 Nanoindentation and Nanomechanics of the mechanical properties of the sintered Ti6Al4V and MWCNT-Ti6Al4V nanocomposites.....173
3. Results and Discussion.....176

3.1 Microstructures of the sintered Ti6Al4V and Ti6Al4V nanocomposites 177
3.2 Nanoindentation studies of the mechanical properties of the sintered Ti6Al4V and Ti6Al4V nanocomposites.....178
3.2.1 Load-displacement and depth-time curves of the sintered Ti6Al4V and Ti6Al4V nanocomposites 178
3.2.2 Nanohardness and reduced elastic modulus of the sintered ti6al4v and ti6al4v nanocomposites 180
3.2.3 Mechanical and anti-wear behaviours of the sintered Ti6Al4V and Ti6Al4V nanocomposites 182
4. Conclusion 184
Acknowledgement 184
Reference 185
CHAPTER FOUR.....191
DISCUSSIONS ON SUBJECTS CONSIDERED BY THE ARTICLES 191
4.1 The Ideas of the Dissertation 191
4.2 Subjects on the novelty and contributions of the study to knowledge.....191
4.2.1 Subjects considered from the reviewed articles on SPS of titanium-based nanocomposites 192
4.2.2 Achieving the dispersion of MWCNT in Ti6Al4V matrix 193
4.2.3 Effects of sintering temperature during spark plasma sintering.....194
4.2.4 Effect of MWCNT addition on the microstructural evolution of the nanocomposites...196
4.2.5 Ascertaining the mechanical integrity of the nanocomposite system by nanoindentation 198
4.3 Conclusions.....200
4.4 Recommendations.....201

LIST OF FIGURES

Paper One

Figure 1. Illustrates the structures of CNTs; SWCNT (a), DWCNT (b) and MWCNT(c) [39] Reprinted with permission from Ref. 39.....25
Figure 2. Illustrates the schematic of SPS apparatus [42]. Reprinted with permission from Ref. 42 26
Figure 3. Illustrates the sintering changes due to the densification of and grain growth in the powder compact.....28
Figure 4. Illustrates the SEM images of the polished cross section of (a, b, c) Ti-0CNT, (d, e, f) Ti-5CNT, and (g, h, i) Ti-10CNT sintered at 800 °C, 1000 °C and 1200 °C, respectively [48]. Reprinted with permission from Ref.48.....31
Figure 5. Illustrates the influence of sintering parameters (time and temperature) and CNT addition in the densification of CNT-Ti composites [48]. Reprinted with permission from Ref. 48.....32
Figure 6. Illustrates the influence of the sintering temperature and CNT addition in the densification behavior of SPSed CNT-Ti6Al4V composites [49]. Reprinted with permission from Ref. 49.....33
Figure 7(a & b). Illustrates the SEM images of Ti-0.5 CNT sintered at 800 °C and 900 °C, respectively [52]. Reprinted with permission from Ref. 52.....34
Figure 8. Illustrates the stress-strain curve of the sintered CNT-Ti composites [60]. Reprinted with permission from Ref. 60 39
Figure 9. Illustrates the stress–strain curves of extruded CNT-Ti [61]. Reprinted with permission from Ref. 61.....40
Figure 10. Illustrates the effects of the temperature on the mechanical properties of SPS Ti/TMC-CNT [62]. Reprinted with permission from Ref. 62.....41
Figure 11(a-c). Illustrates the effects of CNT addition on the mechanical properties of TMC [50]. Reprinted with permission from Ref.50.....43
Figure 12 (a &b). Illustrates the TEM and HRTEM of 1.0 wt.% CNT-TMNC with CNT located at the grain boundary of the titanium matrix [50]. Reprinted with permission from Ref. 50.....43
Figure 13. Illustrates a (elastic modulus and nanohardness) and b (fracture toughness) of the SPSed Ti-B-CNT nanocomposites [15]. Reprinted with permission from Ref. 15 45

Figure 14.Illustrates the microhardness of CNT-Ti6Al4V with varied CNT contents [49]. Reprinted with permission from Ref. 49.....47
Figure 15Illustrates the nanohardness/elastic modulus of sintered Ti-CNT at 800 and 900°C, respectively [52]. Reprinted with permission from Ref. 52.....47

Paper Two

Fig.1. Illustrates schematics of the SSBM of MWCNT in Ti6Al4V using batch 1 & 2 processing routes.....67
Fig.2. Illustrates high-resolution TEM & SEM images of the starting powders Ti6Al4V (a) and MWCNT (b-d).....70
Fig.3. Illustrates the high-resolution SEM image (a) and EDX (b) of MWCNT dispersed in Ti6Al4V powders by low-speed ball milling for 6 h.....71
Fig. 4. Illustrates the high-resolution SEM image (a) and EDX (b) of MWCNT dispersed in Ti6Al4V powders by low-speed ball milling for 8 h.....72
Fig.5. Illustrates the high-resolution SEM images (a) and EDX (b) of MWCNT dispersed in Ti6Al4V powders by SSBM using Batch 1.....73
Fig.6. Illustrates the high-resolution SEM images (a) and EDX (b) of MWCNT dispersed in Ti6Al4V powders by SSBM using Batch 2.....74
Fig.7. Illustrates the dispersion mechanism of MWCNT in Ti6Al4V using low-speed and high-speed ball milling techniques.....77
Fig.8. Illustrates the high-resolution TEM images (a & c), SAED (b) and FFT (d) of MWCNT dispersed in Ti6Al4V powders by SSBM using Batch 1.....77
Fig.9. Illustrates high-resolution TEM images (a & c), SAED (b) and FFT (d) of MWCNT dispersed in Ti6Al4V powders by SSBM using Batch B.....79
Fig.10. Raman spectra of starting powders and admixed MWCNT-Ti6Al4V composite powders (a) Pristine Ti6Al4V (b) Pristine MWCNT (c) 1.0 wt. % MWCNT-Ti6Al4V produced in batch 1 (d) and 1.0 wt. % MWCNT-Ti6Al4V produced in batch 2.....81
Fig. 11. XRD patterns of starting powders and admixed MWCNT-Ti6Al4V composite powders (a) Pristine MWCNT, (b) as-received Ti64, (c) 1.0 wt. % MWCNT-Ti6Al4V produced by batch 1 (d) and 1.0 wt. % MWCNT-Ti6Al4V produced by batch 2.....83

Paper Three

Figure 1. Schematic diagram of the preparation of the composite powders using shift speed ball milling technique (SSBM) [20] 96
Figure 2. Schematic diagram of the SPS technique 97
Figure 3. SEM and TEM images of the as-received Ti6Al4V (a) and MWCNT (b-d) powders 101
Figure 4. SEM images of the Admixed composite powders (MWCNT-Ti6Al4V) containing 0.5 wt.% (a), 1.0 wt.% (b) and 1.5 wt.% (c) and their corresponding EDX (d-f).....102
Figure 5. TEM images of the admixed composite powders (MWCNT-Ti6Al4V) comprise 0.5 wt.% (a), 1.0 wt.% (b) and 1.5 wt.% (c) of MWCNT 104
Figure 6. SEM images of the Ti6Al4V sintered at 900 ^{o}C (a), 1000 ^{o}C (b), 1100 ^{o}C (c), 0.5 wt.% MWCNT- Ti6Al4V sintered at 900 ^{o}C (d), 1000 ^{o}C (e), 1100 ^{o}C (f), 1.0 wt.% MWCNT-Ti6Al4V sintered at 900 ^{o}C (g) 1000 ^{o}C (h), 1100 ^{o}C (i) and 1.5 wt.% MWCNT- Ti6Al4V sintered at 900 ^{o}C (g) 1000 ^{o}C (h), 1100 ^{o}C (i) 106
Figure 7: XRD patterns of starting and admixed MWCNT-Ti6Al4V composite powders (a) pristine MWCNT, (b) pristine Ti6Al4V, (c) 0.5 wt.% MWCNT-Ti6Al4V, (d)1.0 wt.% MWCNT-Ti6Al4V and (e) 1.5 wt.% MWCNT-Ti6Al4V nanocomposite powders.....107
Figure 8: XRD patterns of the sintered Ti6Al4V and sintered nanocomposites MWCNT-Ti6Al4V comprising 0.5, 1.0, 1.5 wt.% of MWCNT sintered at (a) 900 ^{o}C, (b) 1000 ^{o}C and (c) 1100 ^{o}C respectively 109
Figure 9: Raman spectra of the starting powders and admixed nanocomposite powders; (a) Pristine Ti6Al4V powders, (b) Pristine MWCNT, (c) 0.5 wt.% MWCNT-Ti6Al4V, (d) 1.0 wt.% MWCNT-Ti6Al4V and (e) 1.5 wt.% MWCNT-Ti6Al4V 112
Figure 10. Raman spectra of pristine MWCNT and sintered MWCNT-Ti6Al4V nanocomposites at 1000 ^{o}C (a) sintered Ti6Al4V powders, (b) Pristine MWCNTs, (c) 0.5 wt.% MWCNT-Ti6Al4V, (d) 1.0 wt.% MWCNT-Ti6Al4V, and (e) 1.5 wt.% MWCNT-Ti6Al4V.....113
Figure 11. Sintering behaviour of the Ti6Al4V and the fabricated nanocomposites (a-c) and the displacement curves of the punches (d-f) during sintering at 900 ^{o}C, 1000 ^{o}C, and 1100 ^{o}C respectively. 115
Figure 12. Shrinkage rate against sintering time of the Ti6Al4V and the fabricated nanocomposites (a-c) during sintering at 900 ^{o}C, 1000 ^{o}C and 1100 ^{o}C respectively.....118

Figure 13. The relative density of the fabricated Ti6Al4V and nanocomposites sintered at 900 ^{o}C, 1000 ^{o}C and 1100 ^{o}C respectively. 119
Figure 14. Microhardness of the fabricated Ti6Al4V and nanocomposites sintered at 900 ^{o}C, 1000 ^{o}C, and 1100 ^{o}C respectively 121

Paper Four

Figure 1: Schematic diagram of the processing of nanocomposite powders [8] 136
Figure 2. SEM of the starting Ti6Al4V (a), MWCNT (b), and TEM images of MWCNT (c-d) powders 140
Figure 3: SEM results of the mixed composite powders (MWCNT-Ti6Al4V) comprising of 0.5 wt.% (a), 1.0 wt.% (b) and 1.5 wt.% MWCNT (c) and their conforming EDX (d-f).....142
Figure 4: HRTEM images of MWCNT-Ti6Al4V comprises of 0.5 wt.% (a & b), 1.0 wt.% (c &d), and 1.5 wt.% MWCNT (e & f) after SSBM process. 144
Figure 5: SEM images of the fabricated Ti6Al4V (a) and MWCN-Ti6Al4V nanocomposites comprising of 0.5 wt.% (b), 1.0 wt.% (c), and 1.5 wt.% (d) MWCNT 145
Figure 6: Optical micrographs of the fabricated Ti6Al4V (a) and MWCN-Ti6Al4V nanocomposites comprising of 0.5 wt.% (b), 1.0 wt.% (c), and 1.5 wt.% (d) MWCNT.....146
Figure 7: Fractured morphology of the fabricated Ti6Al4V (a) and MWCN-Ti6Al4V nanocomposites comprising of 0.5 wt.% (b), 1.0 wt.% (c), and 1.5 wt.% (d) MWCNT.....147
Figure 8: X-Ray diffraction patterns of starting powders (a) MWCNT, (b) starting Ti6Al4V, and mixed nanocomposite powders comprising of (c) 0.5 wt.% MWCNT (d)1.0 wt.% MWCNT, and (e) 1.5 wt.% MWCNT 148
Figure 9: X-Ray diffraction patterns of the fabricated Ti6Al4V and Ti6Al4V nanocomposites comprising of MWCNT (0.5-1.5 wt.%).....149
Figure 10: Raman spectra of starting powders (a) Ti6Al4V, (b) starting MWCNT, and mixed nanocomposite powders comprising of (c) 0.5 wt.% MWCNT (d)1.0 wt.% MWCNT, and (e) 1.5 wt.% MWCNT.....151
Figure 11: Raman spectra of starting MWCNT (a) fabricated Ti6Al4V (b) and consolidated nanocomposites comprising of (c) 0.5 wt.% MWCNT (d)1.0 wt.% MWCNT, and (e) 1.5 wt.% MWCNT 153
Figure 12: Densification of the consolidated Ti6Al4V and Ti6Al4V based nanocomposites 154

Figure 13. Micro and nanohardness of the fabricated Ti6Al4V and nanocomposites.....156
Figure 14. Load-displacement curves of the fabricated Ti6Al4V (a), and Ti6Al4V nanocomposites comprising of 0.5 wt.% MWCNT(b), 1.0 wt.% MWCNT, and 1.5 wt.% MWCNT.....157
Figure 15. Elastic Modulus of the fabricated Ti6Al4V and nanocomposites.....158

Paper Five

Figure 1: Mathematical derivation of the contact area of a Berkovich indenter (A).....175
Figure 2: Nanoindentation parameters for the evaluation of mechanical properties.....176
Figure 3: SEM images of the Ti6Al4V (a), 0.5 wt.% MWCNT- Ti6Al4V (b), and 1.0 wt.% MWCNT- Ti6Al4V (c).....177
Figure 4. Load-displacement curves of the sintered Ti6Al4V and Ti6Al4V nanocomposites under indentation loads of 50 mN (a), 75 mN (b), and 100 mN (c) respectively. 179
Figure 5. Displacement-time curves of the sintered Ti6Al4V and Ti6Al4V nanocomposites under indentation loads of 50 mN (a), 75 mN (b), and 100 mN (c) respectively. 180
Figure 6. Nanohardness (a) and reduced elastic modulus (b) of the sintered Ti6Al4V and Ti6Al4V nanocomposites under indentation loads of 50 mN, 75 mN, and 100 mN respectively.....182
Figure 7. Elastic recovery and plasticity index (a), and elastic strain resistance to failure and yield pressure (b) of the sintered Ti6Al4V and Ti6Al4V nanocomposites under indentation load of 100 mN.....183

LIST OF TABLES

Paper One

Table 1: Illustrates the effect of the sintering temperature and CNT content on the densification of the SPSed CNT-TMNC. 37
Table 2: Illustrates a summary list of CNT-TMNC fabricated by SPS 48

Paper Three

Table 1: Shows the sintering parameters, density and the microhardness values of the Ti6Al4V and nanocomposites 122

LIST OF ACRONYMS

A / Ac	Area / Contact Area
AFM	Atomic Force Microscopy
Al	Aluminium
AM	Additive Manufacturing
ASTM	American Standard Testing Method
BH	Brinell Hardness
CNTs	Carbon nanotubes
CoF	Coefficient of Friction
D	Diameter
DWCNT	Double Wall Carbon Nanotubes
DSS	Duplex Stainless Steel
E / Er	Elastic Modulus / Reduced Elastic Modulus
EDS	Energy Dispersive Spectroscopy
FAST	Field Assisted Sintering
Fe	Iron
FESEM	Field Emission Scanning Electron microscope
FFT	Fast Fourier Transform
FGM	Functional Graded Materials
GNDs	Geometrically Necessary Dislocations
H / HIT	Hardness
HEBM	High Energy Ball Mill
HRTEM	High Resolution Transmission Electron Microscope
HSBM	High Speed Ball Milling
HIP	Hot Isostatic Pressing
HSPS	Hybrid Spark Plasma Sintering
IAF	Indenter Area Function
ISE	Indentation Size Effects
ISO	International Organization for Standardization
KHN	Knoop Hardness Number
L / P	Load

LSPM	Low Speed Ball Milling
MMC	Metal Matrix Composite
MMNC	Metal Matrix Nanocomposite
MWCNT	Multiwall Carbon Nanotubes
Ni	Nickel
OM	Optical Microscope
PAM	Powder Additive Manufacturing
PECS	Pulsed Electric Current Sintering
PIM	Powder Injection Moulding
PMAX	Maximum Load
PREN	Pitting Resistance Equivalent
SAED	Selected Area Diffraction Pattern
SEM	Scanning Electron Microscope
SLS/SLM	Selective Lase Sintering/Melting
SPS	Spark Plasma Sintering
SSBM	Shift Speed Ball Milling
SWCNT	Single Wall Carbon Nanotubes
UNHT	Ultra Nanoindenter High Temperature
TAF	Tip Area Function
TEM	Transmission Electron Microscope
Ti	Titanium
Ti6Al4V	Titanium-Aluminium-Vanadium Alloy
TiC	Titanium Carbide
TMNC	Titanium Matrix Nanocomposite
3D Printing	Three-Dimensional Printing
TiN	Titanium Nitride
VHN	Vickers Hardness Number
XRD	X-ray Diffraction
EBSD	Electron Backscattered Diffraction

CHAPTER ONE

INTRODUCTION

1.1 Background of Research

Structural and industrial demands for novel engineering materials with improved properties have paved way for the reinforcement of metals with ceramics or other metals to form metal matrix composites. Metal matrix composites (MMC) are recognized for their ability to withstand high temperatures and structural loading conditions. MMC exhibit better performance at elevated temperatures because of their higher tensile strength, hardness, Young's modulus, and better wear resistance, compared to unreinforced metals and alloys (Bakshi *et al.*, 2010). Owing to these superior mechanical, thermal, and physical properties, MMC are considered as innovative engineering materials for aerospace, automobile, electronic, thermal, and wear applications (Koli, Agnihotri and Purohit, 2015).

Over the years, extensive research has been carried to improve the properties of MMC as these materials have the potential to replace the existing conventional materials in many engineering applications. Past studies have emphasized that the mechanical and wear behavior of MMC for high temperature applications is exceptionally better than unreinforced alloys because of their unique properties. Alloys alone are not capable of providing strength and stiffness to structures simultaneously so it is expected that MMC has reinforcements to deliver strength and stiffness with the metal matrix delivering ductility and strength to the composite structure (Bakshi, Lahiri and Agarwal, 2010a; Tjong, 2013).

Basically, the improved properties of MMC are linked to the appropriate selection of reinforcement and metal matrix systems. Meanwhile, the volume fraction, shape, size, and orientation of reinforcements in metal matrix play an important role in determining the properties of MMC. Many combinations for metal matrix composites are available in literatures for a wide range of applications. A wide range of metal systems and reinforcements are available for MMC, such as, Al, Mg, Ni, Ti, Cu, Fe, etc., and reinforcement systems in the form of whiskers, fibers, and particulates (e.g., boron, carbon fiber, carbon nanotubes, graphene, Kevlar, SiC) (Munir, Kingshott and Wen, 2015).

Owing to industrial and structural demands for lightweight materials with high corrosion resistance and specific strength, titanium and its alloys has spurred considerable interest in recent times. They have gained significant attentions because of their uses in aerospace, petrochemical and many other industries due to their attractive properties such as relatively low densities, high-specific strength, excellent oxidation, biocompatibility, nonmagnetic properties, high melting point, corrosion resistance and adequate creep resistance at temperatures up to 400 ^{0}C (Yamaguchi, Inui and Ito, 2000; Lephuthing *et al.*, 2018; Falodun *et al.*, 2019).

Amongst the various grades of titanium alloys, Ti6Al4V has attracted the attentions of materials scientist and researchers in recent decades. Ti6Al4V is a grade 5 titanium alloy and it is the most commonly used titanium alloy owing to its strength and heat-treatability. It comprises of chemical composition of 6% Al, 4% V, 0.25% (maximum) Fe, and 0.2% (maximum) O. In addition, It is significantly stronger than commercially pure titanium while having the same stiffness and thermal properties (excluding thermal conductivity, which is about 60% lower in Grade 5 than in CP Ti) (Donachie, 2000).

In addition, it is heat treatable and can be welded by conventional welding techniques such as gas-tungsten arc welding , plasma arc welding, laser-beam welding, gas-metal arc welding (MIG) among others (Ahmed, Sahari and Ishak, 2012). Which implies that it has an excellent combination of strength, corrosion resistance, weldability and fabricability. It is made up of alpha-beta phase which makes it the workhorse alloy of the titanium industry. It uses span across many aerospace airframe, engine components and major non-aerospace applications such as marine, offshore and power generation industries. Other key applications include: Blades, discs, rings, fasteners, components, vessels, cases, hubs, forgings and biomedical implants. Generally, Ti6Al4V is used in applications up to 400 ^{o}C. Its density is roughly 4420 kg/m^{3}, Young's modulus of up to 120 GPa, and tensile strength of about 1000 MPa (Boyer, 1996)**.**

Despite the attributes of Ti6Al4V, however, it was reported that it possess some inferior properties such as ease of oxidation, high coefficient of friction and it undergoes ductile-brittle failure (Leyens and Peters, 2003). Additionally, it has restricted use up to 400 ^{o}C, limited creep resistance up to 300 ^{o}C, low wear resistance, low Young’s modulus, hardness, and lower heat resistance when compared

with carbon nanomaterials. Meanwhile, it suffers considerable loss in mechanical strength at high temperatures (Leyens and Peters, 2003; A.M. Okoro *et al.*, 2018). These inferior properties have limited their widespread use in intrinsic components in automobile and aerospace industries.

In a bid to minimize the fuel consumptions for global sustainability, it has become compelling to develop lightweight, high strength and cost-effective structural materials which is achievable by nanotechnology. The advancement of nanotechnology has fostered the utilization of carbon nanomaterials in synthesizing advanced materials (Titanium matrix composites TMC) with enhanced mechanical and wear properties than titanium and its alloys. Typical examples of such carbon nanomaterials are carbon nanotubes (CNT) and graphene.

Over the years, CNT has emerged as remarkable reinforcing materials for composites production owing to its excellent mechanical and thermal properties (Bakshi *et al.*, 2010b; Munir *et al.*, 2015). it can be classified based on it structural morphology as single walls (SWCNT), double walls (DWCNT), and multiwall carbon nanotubes (MWCNT) (Tjong, 2013). Since the discovery of CNT in 1991 by Iijima, (1991), it has spurred unprecedented attention across materials research community. It is recognized for its lightweight (~1.7 –2.0 g/cm3), tubular morphology and ultra-high aspect ratios (~100 –100,000).

Additionally, its Young's modulus is in the range of Tera Pascal (TPa), strength up to 100 GPa which is highly required to fabricate high strength composites for aerospace and automotive industries (Chen *et al.*, 2017). The distinctive properties of CNT is attributed to its continuous cylindrical morphology and presence of strong sp^2 carbon-carbon (C–C) bonds in its outer layer (Munir *et al.*, 2015). The sp^2 C–C bonds forms a closed honeycomb lattice and such sp2 hybridization provides CNT a high value of bond energy (614 kJ/mol) (Munir *et al.*, 2016; Zhai *et al.*, 2017). Therefore, CNT reinforced titanium metal matrix composites (TMC) have the potentials to replace unreinforced titanium alloys and the conventional engineering materials used for aerospace applications.

The quest to fabricate titanium-based nanocomposites with improved properties has engendered the application of innovative sintering technique with outstanding features called spark plasma sintering (SPS). SPS technique has been effectively employed to fabricate various advanced materials ranging from functionally graded materials (FGM), fine ceramics, advanced composites, biomaterials,

thermo-electric conductors and highly densified nanostructured materials (Tokita, 2013). It is a powder metallurgy (PM) sintering technique that offers numerous advantages over conventional sintering processes such as hot pressing, hot isostatic pressing, pressureless sintering and the others (Munir *et al.*, 2006). It has an improved heating mechanism which includes lower sintering temperature and cooling time, fast sintering process resulting from its exceedingly great heating rate tendencies up to 1000 ^{o}C/min and excellent heat distribution on compacted materials at both macroscopic and microscopic level (Ujah *et al.*, 2019; Falodun *et al.*, 2018). The major advantages of this technique over other conventional sintering technique is that high densification can be achieved within a limited sintering time (Munir, Anselmi-Tamburini and Ohyanagi, 2006; Falodun *et al.*, 2019).

Extensive studies have been done to explore the potentials of MWCNT for the fabrication of metal matrix composites using the SPS technique (Goh *et al.*, 2006; Kondoh *et al.*, 2009; Kwon *et al.*, 2009; Chen *et al.*, 2015; Munir *et al.*, 2017). Which have resulted in the fabrication of composite materials with outstanding mechanical and thermal properties, however, limited studies have been carried out to improve the mechanical properties of Ti6Al4V by exploiting the potentials of MWCNT.

Therefore, this study provides information on the synthesis and characterization of Ti6Al4V based nanocomposites fabricated by SPS technique. The dispersion characteristics and the nanostructural evolution of the MWCNT in the titanium alloy was evaluated. Furthermore, the effect of MWCNT on the densification behaviour, phase and microstructural evolution and mechanical behaviour of the fabricated nanocomposites was also assessed.

1.2 Problem statements

Extensive studies from the fabrication of advanced materials using conventional manufacturing techniques have revealed the difficulties of producing near-net shapes with homogeneous microstructures, fully dense structure and improved properties (Suarez *et al.*, 2013). Conventional fabrication techniques such as hot pressing, hot isostatic pressing, and casting have been utilized over the years to fabricated alloys and composites with improve the mechanical, thermal and electrical

properties of the materials. However, using these manufacturing techniques to fabricate near-net shapes with outstanding density and mechanical properties has been a day-dreaming adventure.

SPS is a non-equilibrium fabrication technique that has spurred research interests in recent years in comparison with conventional sintering methods, such as HP, HIP and HP-HT. It employs high pressure and relatively low sintering temperature to consolidate powder compacts within a limited time. Meanwhile, appropriate selection of sintering parameters during SPS is essential to achieve fully dense composite with improved properties.

Meanwhile, Ti6Al4V which are majorly employed for aerospace components possesses some inferior properties such as ease of oxidation, high coefficient of friction and undergo ductile-brittle failure during service conditions. It has restricted use at elevated temperatures above 400 ^{o}C and is invariably prone to creep failure above 300 ^{o}C. They also have low mechanical properties (hardness and elastic modulus) when compared to nickel-based alloys and super-duplex steels used in the fabrication of turbine blades for aerospace application (Leyens and Peters, 2003). These inferior properties have limited the application of the alloy in various components in aircraft engine (Donachie, 2000).

Furthermore, in order to improve the properties of the titanium alloy using carbon nanomaterials such as graphene or MWCNT, past research outputs have emphasized that these nanomaterials have the tendencies of agglomerating into clusters during composite production (Esawi *et al.*, 2010). This dispersion characteristics of the nanomaterials are detrimental to the transfer of their unique and excellent properties into the titanium alloys (Munir *et al.*, 2015). During the synthesis of MWCNT reinforced titanium matrix composites, achieving a uniform dispersion of MWCNT in the Ti metal matrix while retaining their sp^2 carbon-carbon network is a significant challenge. The dispersion behaviour of MWCNT is traceable to their nanoscale dimensions, high aspect ratio and the strong Van der Waals forces among the individual nanotubes (Thostenson, 2001).

Over the years, various powder metallurgy techniques such as ultrasonication (Munkhbayar *et al.*, 2013; Munir *et al.*, 2015), low-speed ball milling (Okoro *et al.*, 2018), freeze drying (Khaleghi *et al.*, 2012), and high energy ball milling (HEBM) (Kim *et al.*, 2006) have been explored to achieve uniform dispersion of MWCNT in metal matrices. However, HEBM has proven to be the most

effective method of dispersing MWCNT in metal matrices. Meanwhile, this technique has the tendency of destroying the tubular structure of MWCNT during the dispersion process by creating wall defects such as vacancies and open edges which are potential sites for interfacial reactions (Paramsothy *et al.*, 2010; Gill and Munroe, 2012). The application of HEBM usually creates defects on the nanotubes especially when harsh milling operations is carried out during the milling of the powders. This adverse milling condition promotes the uniform dispersion of MWCNT in the metal matrix but at the expense of the structural integrity of the nanotubes. Furthermore, the harsh milling condition results in the deterioration of the strong sp^2 carbon-carbon network and properties of the nanotubes by forming a highly reactive sp^3 carbon-carbon network (amorphous carbon) which in turn triggers interfacial reactions between the metal matrix and the carbon nanomaterials.

Consequently, after the fabrication of the nanostructured titanium-based nanocomposites, assessing the materials integrity by mechanical testing is very paramount. Over the years, conventional mechanical tests have been used on bulky samples which can only assess the general properties of materials (Gao and Liu, 2017). These features makes the application of conventional mechanical testing technique less fit for ascertaining the mechanical properties of the fabricated titanium-based nanocomposites at a micro and nanoscale (Attar *et al.*, 2017).

Meanwhile, nanoindentation study allows the probing of small samples and carrying out an in-situ evaluation of the mechanical properties of materials without impelling the microstructural features of the materials at micrometer and nanoscale (Attar *et al.*, 2017).

1.3 Aim and Objectives

This project synthesize and evaluate the dispersion characteristics and nanostructural evolution of MWCNT in Ti6Al4V matrix during shift speed ball milling (SSBM) and studied the densification and mechanical behaviours of MWCNT reinforced Ti6Al4V nanocomposites after SPS. This is directed toward enhancing the properties of Ti6Al4V.

The aim of the research was achieved through the following objectives:

1. Shift speed ball milling and characterization of as-received & admixed powders (MWCNT & Ti64);

2. Evaluation of the influence of milling parameters on the dispersion characteristics and nanostructural evolution of MWCNT and their interactions with the Ti6Al4V matrix of the admixed powders in 1);
3. Sintering of the admixed powders in 1) to form MWCNT-Ti6Al4V nanocomposites via SPS;
4. Investigate the influence of sintering temperature on the densification behaviours, microhardness, microstructural and phase evolution of the fabricated nanocomposites;
5. Assess the influence of MWCNT additions on the microstructural evolution, mechanical and fracture behaviour of the sintered nanocomposites; and
6. Nanoindentation studies of the mechanical and anti-wear behaviour of the MWCNT reinforced Ti6Al4V nanocomposites.

1.4 Research Questions

The following research questions were addressed during the study:

a) What is the role of SSBM on the dispersion characteristics, structural integrity and nanocrostructural evolution of MWCNT in Ti6Al4V?
b) What are the influences of increase in MWCNT concentration on their dispersion characteristics in Ti6Al4V matrix?
c) What is the role of sintering temperatures during SPS on the phase evolution, densification behaviour and microstructural evolution of the fabricated Ti6Al4V based nanocomposites?
d) What are the influences of increase in MWCNT concentration on the densification and microhardness of the fabricated nanocomposites?
e) Why does the addition and increase of MWCNT in Ti6Al4V matrix affects the phase and microstructural evolution, and the mechanical properties of the sintered nanocomposites?
f) What are the influences of varying indentation loads on the nanomechanical and anti-wear properties of the fabricated alloy and Ti6Al4V based nanocomposites?

1.5 Justification of the Research

Rapid technological advancement around the world has attracted the interest of materials scientist towards utilizing the benefits of nanotechnology to herald new industrial revolution. Nanostructured materials which are subset of nanotechnology are expected to have major impact across all industries

and improve our everyday lives. This ideas has helped to fabricate metallic-based nanocomposites reinforced MWCNT with superior physical, mechanical and thermal properties (Dresselhaus and Avouris, 2001). Meanwhile, these nanocomposites finds a wide range of engineering applications in automotive, aerospace and industrial sectors (Miracle, 2005).

Extensive research has been carried out to synthesis MWCNT reinforced with commercially pure titanium using the PM technique, however, there exist few literatures on the incorporation of MWCNT to reinforced Ti6Al4V matrix. Specifically, when the MWCNT is effectively dispersed within the alloy without compromising its structural integrity during dispersion. Although, the available literature on the SPS of MWCNT reinforced Ti6Al4V matrix, reported the destruction of the structural integrity of the MWCNT using HEBM in a bid to achieve uniform dispersion of the nanotubes (Adegbenjo *et al.*, 2017). To the best of our knowledge, SSBM has not been employed to disperse MWCNT in Ti6Al4V matrix before the SPS. Thus, achieving a uniform dispersion of MWCNT in the metal matrix and good interfacial bonding without compromising the structural integrity of the nanotubes. Which will promote effective load transfer from the matrix to the reinforcement under load bearing conditions. Meanwhile, SSBM has been effectively employed to uniformly disperse MWCNT in aluminium matrix, which in turn improves the load bearing capabilities of the fabricated nanocomposites (Chen *et al.*, 2018).

Furthermore, past studies (Kaya *et al.*, 2008; Adegbenjo *et al.*, 2017) have been conducted to assess the reinforcing capabilities of MWCNT both as coatings and reinforcement in Ti6Al4V matrix via electrophoretic deposition and SPS. However, there are inadequate information that addressed the densification mechanisms of the Ti6Al4V when MWCNT is incorporated into its matrix. Hence, the grasp of the influence of sintering temperature on the densification mechanism is still not yet reported especially, during sintering of the nanocomposites. Additionally, there exist a gap in understanding the sintering behaviour of MWCNT reinforced Ti6Al4V nanocomposites and how the addition and increase in the concentration of the nanotubes affects the sinterability of the nanocomposites. Despite past study by Adegebenjo *et al.*,(2017) reported the usual reduction in density and increase in hardness of the sintered nanocomposites, there are still gaps on densification mechanism and nanomechanical properties of the sintered nanocomposites.

Moreover, information on the elastic-plastic deformation of the nanocomposites during indentation and unloading of the nanocomposites is very essential to assess the nanomechanical behaviour of the composite. This will enhance the application of the fabricated nanocomposites in various engineering applications. The fabrication of MWCNT reinforced Ti6Al4V nanocomposites has great economic viability. The specific strength of the nanocomposite will help to reduce the weight of the Ti6Al4V and cut-down the cost of fuel when its employed in the production of automobile and aircraft components. Meanwhile, by saving energy, it can be employed in the fabrication of brake rotors, connecting rods, valve lifters, exhaust nozzles, links, blades, cases, shafts, and fuselage structures.

1.6 Scope of the Study

The scope of this study involved the utilization of SSBM technique to disperse quantified amount of MWCNT (diameter, 9.5 nm and length, 1.5 mm) in Ti6Al4V powders (~25 mm) to achieve homogeneous dispersion, interfacial bonding without compromising the structural integrity of the nanotubes. Varying proportion (0.5, 1.0, 1.5 wt.%) of the MWCNT were dispersed in the Ti6Al4V using low-speed ball mill for preliminary milling operation. The preliminary milling was conducted using milling speed of 150 rpm, for 8 h and employing balls to powder ratio (BPR) of 10:1 to promote the dispersion of the MWCNT in the Ti6Al4V matrix. Furthermore, a supplementary milling operation was conducted on the pre-milled powders using high-speed ball mill with a speed of 100 rpm, for 1 h and using BPR of 10 :1. The supplementary milling of the powders was conducted to exert sufficient impact energy to overcome the strong van der Waal forces present in the nanotubes. The starting and admixed powders were characterized using scanning electron microscope (SEM), transmission electron microscope (TEM), X-Ray diffraction technique (XRD) and Raman spectroscopy to understand the dispersion characteristics, nanostructural evolution of the MWCNT and interfacial bonding between the nanotubes and the Ti6Al4V particles. Afterwards, SPS of the admixed powders were conducted by to consolidate the powders. The nanocomposites were sintered at varying sintering temperature to evaluate the influence of sintering temperature on the density, hardness, microstructural and phase evolutions of the composites. Detail characterization of the sintered nanocomposites were conducted using SEM, XRD and Raman to assess the microstructure and fractured surface, phase evolution and structural integrity respectively. Furthermore,

nanoindentation was carried out to understand the elastic-plastic behaviour and the nanomechanical properties of the sintered nanocomposites.

1.7 Structure of the Thesis

The **Chapter one** of this thesis provides information on the general overview of titanium alloys specifically, Ti6Al4V and the problems associated with the widespread application of the alloy. The motivation for improving the properties of Ti6Al4V using MWCNT as reinforcement, aim and objectives of the research, justification and scope of the research are presented in this chapter. Furthermore, a compilation of five (5) articles from the investigations of this research published and/or submitted to peer-review ISI journals are enclosed in the second and third chapters. In **Paper 1,** which is in **Chapter Two,** gives a comprehensive review of past and current works on the spark plasma sintering of carbon nanotubes reinforced titanium-based nanocomposites with emphasis on the sintering, densification, microstructural changes and mechanical properties of the nanocomposite. Subsequently, **Chapter Three** comprises of the summary of all the written articles from this study and their connectivity with each other. Meanwhile, all the articles are arranged consecutively to achieve the stated objectives of the work.

Papers 2 and 3 comprises of the publications on the dispersion characteristics of MWCNT in Ti6Al4V matrix and the sintering behaviour of the sintered nanocomposites. **Paper 2** reported the application of SSBM for effective dispersion of MWCNT in Ti6Al4V matrix. The dispersion characteristics, interfacial bonding between the composite components, nanostructural evolutions of the MWCNT after dispersion and the structural morphology of the nanotubes after dispersion was assessed. **Paper 3** elucidated the influence of varying sintering temperature during SPS on the densification behaviour and sinterability of the nanocomposites. Investigation was conducted to assess the density and the microhardness of the sintered nanocomposites in this article. In addition, the influence of MWCNT concentration on the densification and sintering behaviour of the nanocomposites was explained. The densification, phase and microstructural evolutions, fracture surface, mechanical behaviours and the influence of MWCNT additions on the properties of the nanocomposites were investigated in **Paper 4** and **Paper 5**. The influence of MWCNT addition on the microstructural and phase evolution, mechanical and fracture behaviour of the nanocomposites was reported in **Paper 4.** While in **Paper 5,** nanoindentation studies of the mechanical behaviour

and anti-wear properties were reported. The influence of MWCNT and the variation of indentation loads on the nanohardness and reduced elastic modulus was explained in this article.

The papers that originated from this research are listed below:

Paper 1: **Okoro, A. M.**, Lephuthing, S. S., Oke, S. R., Falodun, O. E., Awotunde, M. A., & Olubambi, P. A. (2019). A review of spark plasma sintering of carbon nanotubes reinforced titanium-based nanocomposites: Fabrication, densification, and mechanical properties. The Journal of The Minerals, Metals & Materials Society (TMS), 71(2), 567-584.

Paper 2: **Okoro, A. M.,** Machaka, R., Lephuthing, S. S., Awotunde, M. A., Oke, S. R., Falodun, O. E., & Olubambi, P. A. (2019). Dispersion characteristics, interfacial bonding and nanostructural evolution of MWCNT in Ti6Al4V powders prepared by shift speed ball milling technique. Journal of Alloys and Compounds, 785, 356-366.

Paper 3: **Okoro, A. M.,** Machaka, R., Lephuthing, S. S., Oke, S. R., Awotunde, M. A., P. A. Olubambi (2019). Evaluation of the sinterability, densification behaviour and microhardness of spark plasma sintered multiwall carbon nanotubes reinforced Ti6Al4V nanocomposites. Ceramics International 45(16), pp.19864-19878

Paper 4: **Okoro, A. M.**, Machaka, R., Lephuthing, S. S., Oke, S. R., Awotunde, M. A., P. A. Olubambi (2019). Influence of multiwall carbon nanotubes addition on the microstructural evolution and mechanical properties of spark plasma sintered Ti6Al4V nanocomposites. Composite Part B (submitted to Journal)

Paper 5: **Okoro, A. M.**, Machaka, R., Lephuthing, S. S., Oke, S. R., Awotunde, M. A., P. A. Olubambi (2019). Nanoindentation studies of the mechanical behaviours of spark plasma sintered multiwall carbon nanotubes reinforced Ti6Al4V nanocomposites. Journal of Materials Science and Engineering: A, p.138320.

The **Chapter Four** of the thesis recapitulate all the enlisted articles, their correlations and present logical explanation of the novelty and contribution of this study to existing knowledge and spark plasma sintering of MWCNT reinforced Ti6Al4V nanocomposite. Conclusions were drawn from the investigations and recommendations were made.

Reference

Adegbenjo, A.O., Olubambi, P.A., Potgieter, J.H., Shongwe, M.B. and Ramakokovhu, M., 2017. Spark plasma sintering of graphitized multi-walled carbon nanotube reinforced Ti6Al4V. Materials & Design, 128, pp.119-129.

Attar, H., Ehtemam-Haghighi, S., Kent, D., Okulov, I.V., Wendrock, H., Bönisch, M., Volegov, A.S., Calin, M., Eckert, J. and Dargusch, M.S., 2017. Nanoindentation and wear properties of Ti and Ti-TiB composite materials produced by selective laser melting. Materials Science and Engineering: A, 688, pp.20-26.

Bakshi, S.R., Lahiri, D. and Agarwal, A., 2010a. Carbon nanotube reinforced metal matrix composites-a review. International materials reviews, 55(1), pp.41-64.

Bakshi, S.R., Lahiri, D. and Agarwal, A., 2010b. Carbon nanotube reinforced metal matrix composites-a review. International materials reviews, 55(1), pp.41-64.

Boyer, R.R., 1996. An overview on the use of titanium in the aerospace industry. Materials Science and Engineering: A, 213(1-2), pp.103-114.

Chen, B., Li, S., Imai, H., Jia, L., Umeda, J., Takahashi, M. and Kondoh, K., 2015. Load transfer strengthening in carbon nanotubes reinforced metal matrix composites via in-situ tensile tests. Composites Science and Technology, 113, pp.1-8.

Chen, B., Shen, J., Ye, X., Jia, L., Li, S., Umeda, J., Takahashi, M. and Kondoh, K., 2017. Length effect of carbon nanotubes on the strengthening mechanisms in metal matrix composites. Acta Materialia, 140, pp.317-325.

Chen, M., Fan, G., Tan, Z., Xiong, D., Guo, Q., Su, Y., Zhang, J., Li, Z., Naito, M. and Zhang, D., 2018. Design of an efficient flake powder metallurgy route to fabricate CNT/6061Al composites. Materials & Design, 142, pp.288-296.

Donachie, M.J., 2000. Titanium. A Technical Guide, ASM International, Materials Park, OH.

Dresselhaus, M.S. and Avouris, P., 2001. Introduction to carbon materials research. In Carbon nanotubes (pp. 1-9). Springer, Berlin, Heidelberg.

Esawi, A.M.K., Morsi, K., Sayed, A., Taher, M. and Lanka, S., 2010. Effect of carbon nanotube (CNT) content on the mechanical properties of CNT-reinforced aluminium composites. Composites Science and Technology, 70(16), pp.2237-2241.

Falodun, O.E., Obadele, B.A., Oke, S.R., Ige, O.O. and Olubambi, P.A., 2018. Effect of TiN and TiCN additions on spark plasma sintered Ti–6Al–4V. Particulate Science and Technology, pp.1-10.

Falodun, O.E., Obadele, B.A., Oke, S.R., Okoro, A.M. and Olubambi, P.A., 2019. Titanium-based matrix composites reinforced with particulate, microstructure, and mechanical properties using spark plasma sintering technique: a review. The International Journal of Advanced Manufacturing Technology, pp.1-13.

Gao, C. and Liu, M., 2017. Instrumented indentation of fused silica by Berkovich indenter. Journal of Non-Crystalline Solids, 475, pp.151-160.

Gill, P. and Munroe, N., 2012. Study of carbon nanotubes in Cu-Cr metal matrix composites. Journal of materials engineering and performance, 21(11), pp.2467-2471.

Goh, C.S., Wei, J., Lee, L.C. and Gupta, M., 2006. Simultaneous enhancement in strength and ductility by reinforcing magnesium with carbon nanotubes. Materials Science and Engineering: A, 423(1-2), pp.153-156.

Iijima, S., 1991. Helical microtubules of graphitic carbon. nature, 354(6348), p.56.

Kaya, C., Singh, I. and Boccaccini, A.R., 2008. Multi-walled carbon nanotube-reinforced hydroxyapatite layers on Ti6Al4V medical implants by Electrophoretic Deposition (EPD). Advanced Engineering Materials, 10(1-2), pp.131-138.

Khaleghi, E., Torikachvili, M., Meyers, M.A. and Olevsky, E.A., 2012. Magnetic enhancement of thermal conductivity in copper–carbon nanotube composites produced by electroless plating, freeze drying, and spark plasma sintering. Materials Letters, 79, pp.256-258.

Kim, K.T., Cha, S.I., Hong, S.H. and Hong, S.H., 2006. Microstructures and tensile behavior of carbon nanotube reinforced Cu matrix nanocomposites. Materials Science and Engineering: A, 430(1-2), pp.27-33.

Kondoh, K., Threrujirapapong, T., Imai, H., Umeda, J. and Fugetsu, B., 2009. Characteristics of powder metallurgy pure titanium matrix composite reinforced with multi-wall carbon nanotubes. Composites Science and Technology, 69(7-8), pp.1077-1081.

Kwon, H., Estili, M., Takagi, K., Miyazaki, T. and Kawasaki, A., 2009. Combination of hot extrusion and spark plasma sintering for producing carbon nanotube reinforced aluminum matrix composites. Carbon, 47(3), pp.570-577.

Lephuthing, S.S., Okoro, A.M., Lesufi, M., Ige, O.O. and Olubambi, P.A., 2018, September. Effect of milling parameters on the dispersion characteristics of multi-walled carbon nanotubes in transition metal oxides. In IOP Conference Series: Materials Science and Engineering (Vol. 430, No. 1, p. 012002). IOP Publishing.

Leyens, C. and Peters, M., 2003. Titanium and Titanium Alloys: Fundamentals and Applications; Willey.

Miracle, D.B., 2005. Metal matrix composites–from science to technological significance. Composites science and technology, 65(15-16), pp.2526-2540.

Munir, K.S., Li, Y., Liang, D., Qian, M., Xu, W. and Wen, C., 2015. Effect of dispersion method on the deterioration, interfacial interactions and re-agglomeration of carbon nanotubes in titanium metal matrix composites. Materials & Design, 88, pp.138-148.

Munir, K.S., Qian, M., Li, Y., Oldfield, D.T., Kingshott, P., Zhu, D.M. and Wen, C., 2015. Quantitative Analyses of MWCNT-Ti Powder Mixtures using Raman Spectroscopy: The Influence of Milling Parameters on Nanostructural Evolution. Advanced Engineering Materials, 17(11), pp.1660-1669.

Munir, K.S., Li, Y., Qian, M. and Wen, C., 2016. Identifying and understanding the effect of milling energy on the synthesis of carbon nanotubes reinforced titanium metal matrix composites. Carbon, 99, pp.384-397.

Munir, K.S., Zheng, Y., Zhang, D., Lin, J., Li, Y. and Wen, C., 2017. Microstructure and mechanical properties of carbon nanotubes reinforced titanium matrix composites fabricated via spark plasma

sintering. Materials Science and Engineering: A, 688, pp.505-523.

Munir, K.S., Kingshott, P. and Wen, C., 2015. Carbon nanotube reinforced titanium metal matrix composites prepared by powder metallurgy—a review. Critical Reviews in Solid State and Materials Sciences, 40(1), pp.38-55.

Munir, Z.A., Anselmi-Tamburini, U. and Ohyanagi, M., 2006. The effect of electric field and pressure on the synthesis and consolidation of materials: A review of the spark plasma sintering method. Journal of Materials Science, 41(3), pp.763-777.

Munkhbayar, B., Nine, M.J., Jeoun, J., Bat-Erdene, M., Chung, H. and Jeong, H., 2013. Influence of dry and wet ball milling on dispersion characteristics of the multi-walled carbon nanotubes in aqueous solution with and without surfactant. Powder technology, 234, pp.132-140.

Okoro, A.M., Awotunde, M., Ajiteru, O.A., Lephuthing, S.S., Olubambi, P.A. and Machaka, R., 2018, February. Effects of carbon nanotubes on the mechanical properties of spark plasma sintered titanium matrix composites—A review. In 2018 IEEE 9th International Conference on Mechanical and Intelligent Manufacturing Technologies (ICMIMT) (pp. 54-59). IEEE.

Okoro, A.M., Machaka, R., Lephuthing, S.S., Awotunde, M. and Olubambi, P.A., 2018, September. Structural integrity and dispersion characteristics of carbon nanotubes in titanium-based alloy. In IOP Conference Series: Materials Science and Engineering (Vol. 430, No. 1, p. 012004). IOP Publishing.

Okoro, A.M., Machaka, R., Lephuthing, S.S., Awotunde, M.A., Oke, S.R., Falodun, O.E. and Olubambi, P.A., 2019. Dispersion characteristics, interfacial bonding and nanostructural evolution of MWCNT in Ti6Al4V powders prepared by shift speed ball milling technique. Journal of Alloys and Compounds, 785, pp.356-366.

Paramsothy, M., Hassan, S.F., Srikanth, N. and Gupta, M., 2010. Simultaneous enhancement of tensile/compressive strength and ductility of magnesium alloy AZ31 using carbon nanotubes. Journal of nanoscience and nanotechnology, 10(2), pp.956-964.

Suárez, M., Fernández, A., Menéndez, J.L., Torrecillas, R., Kessel, H.U., Hennicke, J., Kirchner, R.

and Kessel, T., 2013. Challenges and opportunities for spark plasma sintering: a key technology for a new generation of materials. In Sintering Applications. IntechOpen.

Thostenson, E.T., Ren, Z. and Chou, T.W., 2001. Advances in the science and technology of carbon nanotubes and their composites: a review. Composites science and technology, 61(13), pp.1899-1912.

Tjong, S.C., 2013. Recent progress in the development and properties of novel metal matrix nanocomposites reinforced with carbon nanotubes and graphene nanosheets. Materials Science and Engineering: R: Reports, 74(10), pp.281-350.

Tokita, M., 2013. Spark plasma sintering (SPS) method, systems and applications. Handbook of advanced ceramics, pp.1149-1177.

Ujah, C.O., Popoola, O.M. and Aigbodion, V.S., 2019. Optimisation of spark plasma sintering parameters of Al-CNTs-Nb nano-composite using Taguchi Design of Experiment. The International Journal of Advanced Manufacturing Technology, 100(5-8), pp.1563-1573.

Yamaguchi, M., Inui, H. and Ito, K., 2000. High-temperature structural intermetallics. Acta materialia, 48(1), pp.307-322.

Zhai, W., Srikanth, N., Kong, L.B. and Zhou, K., 2017. Carbon nanomaterials in tribology. Carbon, 119, pp.150-171.

CHAPTER TWO

This chapter presents a review of the past research on the improvement of the properties of spark plasma sintered titanium-based nanocomposites using carbon nanotubes as reinforcement phase.

Over the years, various research has been conducted where SPS technique was used to fabricated titanium-based nanocomposites reinforced with MWCNT for diverse engineering applications. In this article, efforts were made to review past works on the SPS of CNT reinforced titanium-based matrices to acquire thorough understanding of previous findings and identify a research gap and niche for this study. In the review article, attempt was made to understand the reinforcing capabilities of CNT, the effects of CNT on the microstructural and phase evolution of the composites, the role of SPS on the densification behaviours and various mechanical properties of the fabricated nanocomposites was explored. Extensive information on the roles of sintering parameters on the densification behaviour, phase evolution and mechanical properties of SPSed titanium-based nanocomposites were provided. Additionally, emphasis was made on the current and potential applications of the fabricated nanocomposites.

It was realized from the study that CNT has extraordinary reinforcing capabilities to augment the mechanical, thermal and electrical properties of titanium and its alloys. The transfer of the outstanding properties of the CNT into the titanium-based matrices is a function of their homogeneous dispersion in the matrix materials. Furthermore, the integration of CNT into the titanium-based matrices results in microstructural and phase evolution which translates to improvement in mechanical properties. Although the increase in CNT content decrease the densification of the fabricated nanocomposites.

Additionally, it was deduced that the application of an effective dispersion method to promote the homogeneous dispersion of CNT in Ti6Al4V without damaging the nanostructure of the nanotubes has not been significantly investigated. Information on the application of nanoindentation technique to ascertain the mechanical properties of Ti6Al4V based nanocomposites after effective dispersion of MWCNT is yet to be reported in literatures.

JOM, Vol. 71, No. 3, 2019
https://doi.org/10.1007/s11837-018-3277-2

A Review of Spark Plasma Sintering of Carbon Nanotubes Reinforced Titanium-Based Nanocomposites: Fabrication, Densification, and Mechanical Properties

AVWEROSUOGHENE MOSES OKORO,[1,2] SENZENI SIPHO LEPHUTHING,[1] SAMUEL RANTI OKE,[1] OLUWASEGUN ESO FALODUN,[1] MARY AJIMEGOH AWOTUNDE,[1] and PETER APATA OLUBAMBI[1]

1.—Centre for Nanoengineering and Tribocorrosion, Department of Metallurgy, School of Mining, Metallurgy and Chemical Engineering, University of Johannesburg, Johannesburg, Republic of South Africa. 2.—e-mail: okoromoses@gmail.com

The quest to consistently develop improved materials for direct application in automotive, aerospace, and other industries has led to the synthesis of titanium-based composites—with current research efforts being directed toward the utilization of carbon nanotubes (CNTs) as reinforcement. CNTs constitute an outstanding reinforcement for titanium-based matrixes, owing to their extraordinary physical, electrical, mechanical, and thermal properties. Powder metallurgy (PM) routes have been adjudged the most promising technique for synthesizing CNT-reinforced titanium. However, past reviews have highlighted various PM techniques, reinforcement efficiency, and effective methods for dispersing CNTs in metal matrixes. Among the various PM techniques, spark plasma sintering (SPS) has gained popularity in the synthesizing of titanium-based nanocomposites (TMNCs). Hence, this review focused on past works on the SPS of TMNCs reinforced with CNTs. The properties of CNTs, their fabrication method, their densification mechanism, and the mechanical properties of sintered TMNCs were discussed in detail.

INTRODUCTION

Titanium metals and their alloys have spurred considerable interest in various advanced applications in recent years. This is due to their unique properties that include good mechanical properties, light weight, and excellent corrosion resistance.[1] However, for them to compete with the Ni-based alloys and high-strength steels used in critical applications, it is imperative to improve their properties (strength, toughness, and stiffness) by developing titanium-based composites. Titanium matrix composites (TMCs) are potential alternatives in the endeavor to increase the stiffness and specific strength of titanium and its alloys.[1] Among the TMC family, short fibers or particulate-reinforced TMCs are fascinating. This is because of their isotropic behavior that encourages their usage in widespread applications.[2]

The incessant need to enhance the properties of titanium and its alloys has paved way for the utilization of carbon nanotubes (CNTs) with unique and outstanding properties as reinforcing materials, to develop titanium-based composites. Over the years, CNTs have emerged as essential and novel reinforcing materials for functional devices and structural engineering applications. This is due to their unique mechanical properties, low thermal expansion coefficient, excellent thermal and electrical conductivity, and low friction coefficient.[3–5] They have been extensively used in enhancing the properties of various metals and their alloys, such as aluminum,[6–8] copper,[9–11] magnesium,[12–14] and titanium.[15,16] Due to their nanostructural morphologies and high aspect ratio, past works have established their advantages over micro and sub-micron reinforcements, which have negative impacts on the ductility and tensile properties of developed metal

(Published online December 17, 2018)

Paper 1: A Review of Spark Plasma Sintering of Carbon Nanotubes Reinforced Titanium-based Nanocomposites: Fabrication, Densification and Mechanical Properties.

Status: Published with The Journal of The Minerals, Metals & Materials Society (TMS), 71(2), 567-584

https://link.springer.com/article/10.1007/s11837-018-3277-2

Abstract

The quest to consistently develop improved materials for direct application in the automotive, aerospace and other industries have led to the synthesis of titanium-based composites with current research efforts deviating towards the utilization of carbon nanotube (CNTs) as reinforcement. CNTs are outstanding reinforcement for titanium-based matrix owing to their extraordinary physical, electrical, mechanical and thermal properties. In recent times, the powder metallurgy (PM) routes have been adjudged the most promising technique for synthesizing titanium-based composites reinforced with CNTs. However, past reviews have highlighted various PM techniques, reinforcement efficiency and effective dispersion methods of carbon nanotubes in metal matrix. Amongst the PM techniques, spark plasma sintering (SPS) has gained much attention for synthesizing titanium-based nanocomposites. Hence, this review focused on past works on SPS of titanium-based nanocomposites reinforced with CNTs. The properties of CNTs, fabrication method, densification mechanism and mechanical properties of sintered titanium-based nanocomposites were discussed in detail.

1. Introduction

Titanium metals and its alloys have spurred considerable interest in various advanced applications in recent years due to their unique properties which include; good mechanical properties, light weight and excellent corrosion resistance [1]. However, to be competitive with Ni-based alloys and high strength steels in critical applications, it is worthwhile to improve its properties (strength, toughness and stiffness) by developing titanium-based composites. Titanium matrix composites (TMCs) are potential alternatives to increase the stiffness and specific strength of titanium and its alloys [1].

Amongst the TMCs family, short fibres or particulate reinforced TMCs are very fascinating because of their isotropic behaviour that encourages their usage in widespread applications [2].

The incessant needs to enhance the properties of titanium and its alloys have paved way for the utilization of carbon nanotubes (CNTs) with unique and outstanding properties as reinforcing materials to develop titanium-based composites.

Over the years, CNTs have emerged as essential and novel reinforcing materials for functional devices and structural engineering applications because of their unique mechanical properties, low coefficient of thermal expansion, excellent thermal and electrical conductivity and low coefficient of friction [3–5]. They have been extensively and effectively utilized in enhancing the properties of various metals and their alloys such as Aluminium [6–8], Copper [9–11], Magnesium [12–14] and Titanium [15,16]. Due to their nanostructural morphologies and high aspect ratio, past works have established their advantages over micro and sub-micron reinforcements; which have negative impacts on the ductility and tensile properties of developed metal matrix composites since these composites are susceptible to the presence of defects (cracks) during mechanical testing [5]. This has encouraged the reinforcement of titanium-based materials using carbon nanotubes to form nanocomposites with improved mechanical properties. The mechanisms responsible for the significant improvements in mechanical properties is the collective influence of Orowan strengthening and Hall Petch strengthening mechanisms. These strengthening mechanisms have been extensively discussed in past literature [5,17–19].

Due to the significant enhancements in properties that can be achieved by the incorporation of nanomaterials into titanium-based materials, titanium nanocomposites have spurred unprecedented attention in the past two decades. Titanium matrix nanocomposites TMNC) have emerged as high-performance materials with exclusive design potentials to overcome the limitations of titanium-based composites reinforced with micro and sub-microns particles. They have demonstrated unusual potentials for widespread applications ranging from automotive to aerospace industries because of their combination of outstanding properties. These unique properties are linked to the incorporation of nanomaterials which are below materials critical size levels that enhance interfacial reaction and improve the properties of the nanocomposites [20–22]. However, various challenges related to

regulating the elemental compositions and stoichiometry of the nanostructured phases are stumbling block during the fabrication of these nanocomposites.

Recently, powder metallurgy processes have proved effective for the fabrication of TMNC since it allows the synthesis of powders of various sizes, textures, chemical compositions and morphologies to achieve controlled microstructural features and improved properties [23,24]. This manufacturing process involves the synthesis and shaping of powders, consolidation, sintering and post sintering processes to fabricate near-net components [25]. Past works have proved that this route is best fit for the fabrication of nanocomposites because of its flexibility and ability to attain the uniform dispersion of CNTs within the titanium-based matrix since it involves lower processing temperature and regulates interfacial reaction between the composite's components [26]. Additionally, it promotes the achievement of outstanding properties by the application of various steps of densification of the admixed powders and subsequent cold compaction and sintering operations [27,28].

Over the years, technological advancement in powder metallurgy has unveiled the exploration of various methods of compaction and sintering of titanium-based powders for diverse engineering applications. These methods involve the application of both pressureless and pressure assisted techniques which have been extensively and successfully utilized in compacting titanium metals/alloys and its composites. These consolidation techniques include; hot isostatic pressing, hot pressing, laser sintering, vacuum hot sintering, microwave sintering and SPS [29].

Amongst the aforementioned consolidation techniques, SPS proffers numerous benefits over other conventional techniques, due to its flexibility and effective control of sintering energy as well as high sintering speed, high reproducibility, safety and reliability [26]. Additionally, this method allows a heating rate of up to 1000 ^{0}C which is a function of the size, electrical and thermal properties of the sample and the electric power supply of the sintering system.

Structural demands for the synthesis of fully dense nanocomposites have encouraged substantial advancements in SPS technique. This sintering method has unveiled new potentials of CNTs reinforced titanium-based materials which is recognised for their outstanding mechanical and physical properties. Basically, it is an exceptional powder metallurgy technique for producing nanocomposites which restrict grain enlargements and supports hot compaction up to full densification within a limited time [30].

Additionally, it is a fast sintering method that activates necking process between nanoparticles and rapid densification of powder materials. Past investigations by Tiwari and Tokita [29,30] revealed the mechanism responsible for the fast sintering operation of powders during SPS, they stated that the captured gases between powder particles can be ionized and converted to plasma. The produced plasma and spark discharge promote diffusion bonding between the powder particles and enhance densification of the consolidated powders. While there are controversial deliberations about the mechanisms responsible for sintering during SPS, the various prediction has stated that the major mechanisms are [30,31]:

- Activation by the pulse current
- Heating through the electrical current passage
- Applied external pressure

To date, much efforts have been made to fabricate densified TMNC reinforced with CNTs using the SPS process. Despite numerous reviews on the development of CNT-reinforced metal matrix composites [4,26,32,33], to the best of our knowledge, there is no articulated review on SPS of CNTs reinforced titanium-based composites, especially on the mechanical behaviours and nanostructural evolution of these nanocomposites. Therefore, this article focuses on a review of the effect of CNTs on the densification behaviour and mechanical properties of TMNC developed by SPS, since this is a potential material system that meets the requirements of diverse engineering applications.

2. Properties of CNTs for TMNC Applications

Carbon nanotubes (CNTs) have unique tubular structures with diameters in nanometres and length in micrometre. Their unique structural morphologies have impacted them with outstanding properties for composites applications. These properties include [33,34];

- ✓ exceedingly high elastic modulus (~1 TPa) which makes them 10 times stronger than steels and as hard as diamonds.
- ✓ high strength (up to 40 GPa).
- ✓ great aspect ratio (that lies between ~100-1000).
- ✓ exceedingly light weight (1.5-2 g/cm^3) which makes them six times lighter than steels,

- ✓ exceptional thermal and chemical stabilities (up to 750 and 2800^{0}C in air and vacuum, respectively).
- ✓ high electrical and thermal conductivities (which is greater than diamond and copper wires).

In a nutshell, the combination of outstanding properties makes CNTs potential candidates for reinforcements during the synthesis of advanced composites materials. The use of CNTs as a reinforcement phase in composites has made positive impacts to the properties of materials when compared to other reinforcing materials. Past research had shown that they have great hardening effect even when used at low volume fractions and this is linked to their high aspect ratio.

CNTs can be classified based on their tubular structures into; single wall carbon nanotubes (SWCNTs), double walled carbon nanotubes (DWCNTs) and multiwalled carbon nanotubes (MWCNTs) which is schematically shown in figure 1 below. Amongst these types of CNTs, SWCNTs are considered to have the best mechanical properties (stiffness and strength) because of their high crystalline structures and purity [35–37]. Despite their outstanding mechanical properties, SWCNTs are rarely utilized as reinforcements for composites production due to their high cost of production and purification. However, MWCNTs are cheaper to produce and they are made up of unique layered structures. Meanwhile, during the processing of MWCNTs, there is a tendency of the inner layer to pull out of the outer layer when they are subjected to elongation. This is sometimes considered as telescopic extension of MWCNTs [17]. Characterization using in-situ TEM evaluation on nanotubes revealed that telescopic effects takes place at extremely low friction state that indicates no wear or fatigue at the atomic scale.

Various mechanical testing and characterization techniques have shown that SWCNTs possessed better mechanical properties (Young modulus and tensile strength) than MWCNTs [35–38]. However, MWCNTs are highly desirable for composites applications because of their low cost of production, purification and multiple layered nanostructure. Therefore, during the synthesis of TMNC, MWCNTs are the most reported nanotubes as reinforcements because of its considerable unique properties, excellent reinforcement capabilities and outstanding multi-layered nanostructures.

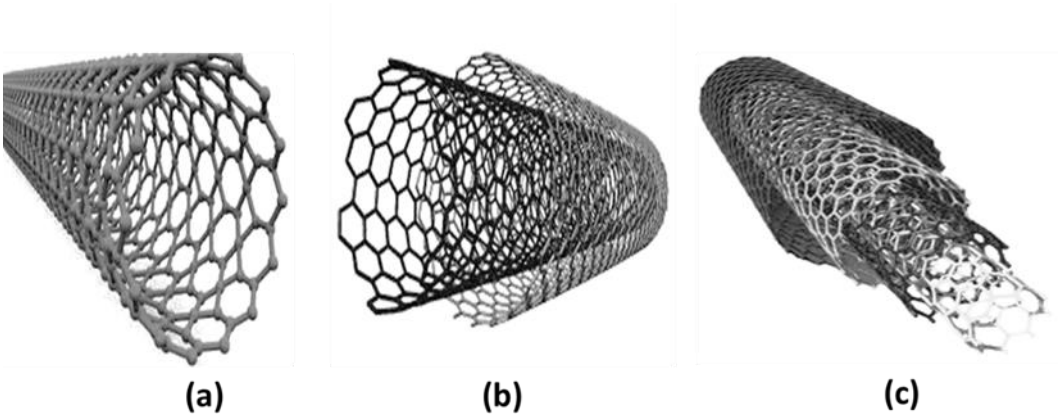

Figure 1. Illustrates the structures of CNTs; SWCNT (a), DWCNT (b) and MWCNT(c) [39]
Reprinted with permission from Ref. 39

3. Fabrication of CNT-TMNC by SPS

Titanium-based nanocomposites reinforced with CNTs can be fabricated by various powder metallurgy techniques; hot pressing, hot isostatic pressing, reactive sintering, self-propagating high-temperature synthesis and SPS. Amongst these fabrication techniques, SPS are highly considered because of it flexibility, simplicity and ability to produce densified TMNC at a fast rate. Additionally, it can be utilized to fabricate porous materials for biomedical applications by selecting the powder particles (size and shape) and optimizing the parameters (pressure, holding and cooling time, heating rate and temperature) during sintering [40].

3.1 Overview on SPS for Fabrication of TMNC.

Technological and industrial demands for fully densified nanostructured composites have paved way for advanced sintering techniques such as S. This sintering method has unveiled innovations on CNT-MMCs with exclusive mechanical properties. It is also called pulse electric current sintering (PECS) since it utilizes uniaxial force and pulsed (on-off) direct electrical current (DC) under reduced atmospheric pressure to carry out fast sintering operations on powder materials [41].

The unique feature of this techniques is that it uses Joule heating effects in sintering the powder materials by the flow of electric current through the powders that promotes the rapid sintering operations. The rapid sintering helps to inhibit grain growth process and regulates the final

microstructures and properties of the sintered material during densification. The schematic diagram of SPS process is shown in figure 2 below:

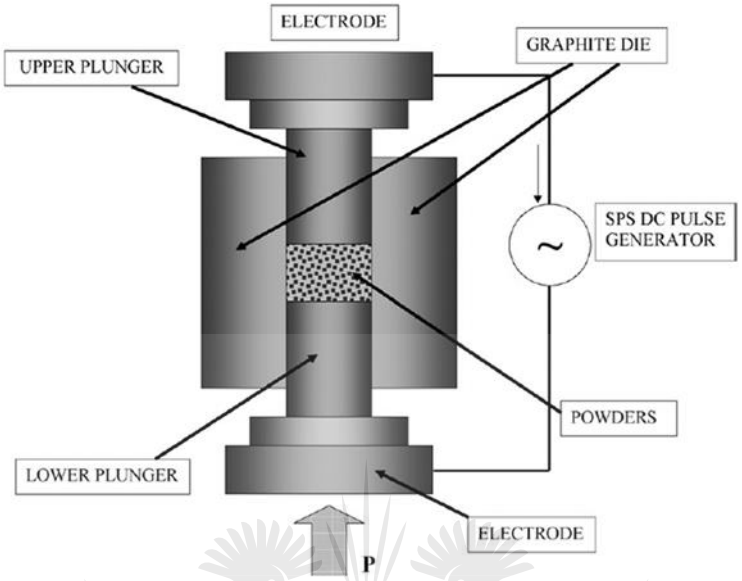

Figure 2. Illustrates the schematic of SPS apparatus [42]. Reprinted with permission from Ref. 42

SPS is considered as a rapid sintering technique, because the heating power is transferred uniformly across the volume of the powder compact where energy is needed for the sintering process at the macrostructure and the microstructure scale, which ensures a favorable sintering process with less grain growth and powder disintegration. This technique offers more benefits than conventional sintering techniques. Such benefits include user-friendliness, precise regulation of sintering energy, as well as high sintering speed, safety and reliability [43]. Specifically, sintering operations using SPS require few minutes to complete, unlike conventional sintering techniques that need hours or days. Moreover, the sintering rate of samples during SPS is amazingly high because of the existence of an internal sample-heating mechanism, contrary to the external heating mechanisms of conventional sintering techniques. This short-time sintering attribute of SPS is also linked to its slight holding time of 5 to 10 minutes, compared to the hours required by conventional sintering. Specifically, SPS can reach a higher heating rate of up to 1000°C /min, which promotes sintering at elevated temperatures in limited time. However, the heating rates of conventional sintering furnaces

range from 5 to 10°C/min; hence, they require a couple of hours to attain temperatures between 1000 and 2000°C [41].

The combined effect of temperature and pressure during SPS – alongside material variables such as chemical composition, size distribution, sizes, shapes and degree of powder agglomeration – determines the full densification and sinterability of powders at lower temperature – especially at short duration – unlike in conventional sintering techniques. This helps to restrict coarsening and grain growth and makes it possible to sinter nano powders. The same cannot be achieved using conventional sintering techniques.

Technological and scientific research in composites engineering has advanced in recent years, as nanostructured composites with full densification and less microstructural defects are in high demand – for various applications. This has given rise to the application of innovative sintering techniques such as SPS. The latter has recently been used to sinter TMNC with excellent mechanical and physical properties. The SPS of TMNC involves feeding the component powders into a graphite die that is then enclosed with the required punches. The graphite die is subsequently transferred into the SPS chamber that is enclosed in vacuum or argon gas. Thereafter, the program is set and the sintering operation is undertaken. Since it is fast, the unwanted reaction that commonly occurs in conventional sintering operations is eradicated. To sinter nanocomposites using SPS – to achieve full densification, outstanding properties and minimal structural defects – certain sintering process parameters need to be optimized, to achieve the full benefits of this technique. Parameters such as the sintering temperature, time and pressure play major roles in the microstructural evolution and densification behavior of the sintered material. In subsequent sections, the densification of CNT-TMNC and the effects of the sintering parameters on the densification behavior of SPS-based CNT-TMNC will be discussed.

4. Densification of CNT-TMNC Fabricated by SPS

The sintering phenomenon plays important roles during the fabrication of CNT-TMNC, as it changes the microstructure of the sintered material and results in the improvement of the properties of the nanocomposites. The principal phenomena that transpire during the sintering of TMNC are grain growth and the densification of the compacted powders, which usually occur in the forms of neck-

size enlargement, decrease in the number of grains, increase in grain size, change in grains' orientation, decrease in surface area and number of pores present in the material. These sintering phenomena are usually facilitated by the decrease of the total interfacial energy of the powder compacts. The total interfacial energy of the powder compact is assigned as γE, where γ is the specific surface energy at the powder interface and E is the total surface area of the powder compact [44]. Therefore, the decrease in the total energy can be expressed as:

$$\Delta(\gamma E) = \Delta\gamma E + \gamma\Delta E \qquad (1)$$

From the above equation, the change in interfacial energy ($\Delta\gamma$) usually occurs due to densification, while grain growth is responsible for the change in the interfacial area (ΔE) of the compacted powders. This decrease in total interfacial energy during sintering significantly improves the densification behaviors and mechanical properties of the sintered material [45]. This is usually achieved at all three stages of the sintering (initial, intermediate and final). During the first sintering stage, necking among the compacted powder particles occurs, which influences the shrinkage of the powder compacts up to 2-3% [44]. This is reinforced at the intermediate sintering stage where up to 93% of the densification occurs, before the segregation of the pores present in the powder compact. During the final stage of sintering, full densification is achieved with the elimination of pores. The schematic representation of the sintering changes due to densification and grain growth is provided in Figure 3 below.

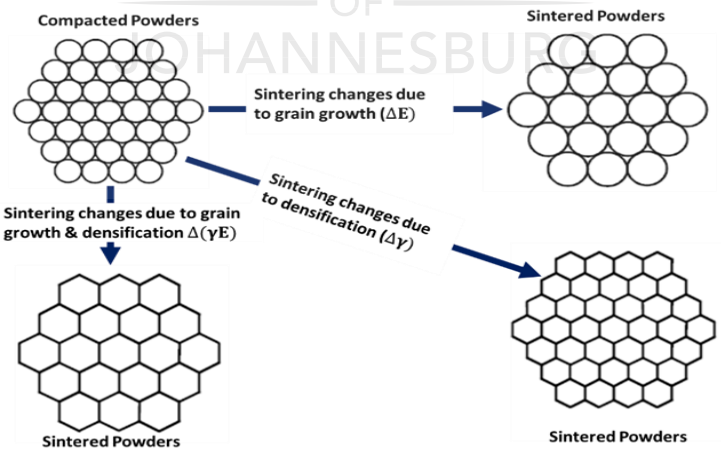

Figure 3. Illustrates the sintering changes due to the densification of and grain growth in the powder compact

To achieve improved properties of powder compacts during sintering operations, full densification and supplementary grain growth are highly desirable. Densification can be expressed as change in porosity after sintering divided by the initial porosity of the compacts. It also indicates the relative variation in density that is determined by the density changes needed for powders to reach their full densification. During a sintering operation, a sintered material can attain full densification (100%) only when all its porosities are eliminated. Porosities are detrimental to the properties of sintered materials.

During densification, the diameters of a material's pores shrink due to grains' coarsening that suppresses the pores in the powder compacts. Densification occurs through bulk transport, since the mass that grows the sinter neck comes from within the grain. The bulk transport mechanisms result in various sintering phenomena such as volume diffusion, grain boundary diffusion, plastic flow, dislocation climb and viscous flow. Plastic flow is particularly significant during heating, before the dislocation density is removed from the material. It is prominent in powder compacts containing dislocation density because of the work-hardening process [45]. The densification is denoted by ψ and can be expressed as:

$$\psi = \frac{f - f0}{1 - f0} \qquad (2)$$

where f represents the fractional sintered density and f_0 is the initial density. During the densification, diffusion along the grain boundaries occurs and may lead to the shrinkage and collapse of the pores that enhance the density and mechanical properties of the sintered material [45].

During the densification of composite materials, the densification rate of the composites can be explained by rules of mixture and Scherer's theory – when the volume fraction of the reinforcement phase is less than 0.12% [50]. However, when the volume fraction of the reinforcement phase is greater than 0.12%, the densification of the composites tends to decrease; in this case, the measured density tends to be lower than the theoretical density of the composite [46].

4.1 Effect of sintering parameters and CNT addition to the densification behavior of SPS-based TMNC

As stated earlier, SPS is a fast-sintering technique that promotes full densification and inhibits the coarsening of grains. During the SPS of TMNC reinforced with CNT, various sintering parameters play significant roles in the densification and overall mechanical properties of the composites. Sintering parameters such as compressive pressure, temperature and holding time are factors that can be optimized to obtain full densification. Furthermore, to obtain full densification during sintering, the powders should be homogeneous. This can be effectively achieved by ball milling that provides adequate energy that fosters the dispersion of the CNT in the titanium-based material and promotes good interfacial powder bonding before compaction.

Apart from the sintering parameters, powder morphologies and sizes have a significant influence on the densification rate of nanocomposites. The densification rate increases with the reduction of powder particles' sizes and increase in sintering temperature, pressure and time, which favors the fabrication of CNT-TMNC [47]. Therefore, the incorporation of nanomaterials (CNT) into titanium-based matrices, alongside the good dispersion of CNT, will promote the densification rate of the nanocomposite.

Considerable research has been conducted to foster the effects of CNT contents and sintering parameters on the densification behavior of spark plasma sintered (SPSed) TMNC. Vasanthakumar et al. [48] adopted SPS in the fabrication of Ti/CNT. They reported an increase in the density of the sintered composite, up to 99%, when sintered at a temperature of 1200°C. They also confirmed that the amount of porosity in the sintered sample increased with the CNT content. This is directly related to the adopted sintering temperature of the composite. At a higher sintering temperature (1200°C), no porosity was revealed. This is because of grain growth, despite the increase in the content of the CNT. However, samples sintered at lower temperatures (800°C and 1000°C) revealed porosity in the sintered composites. The scanning electron microscopy (SEM) images of the sintered samples at various temperatures are shown in Figure 4. They revealed the microstructures of the sintered composites in accordance with the density measurement.

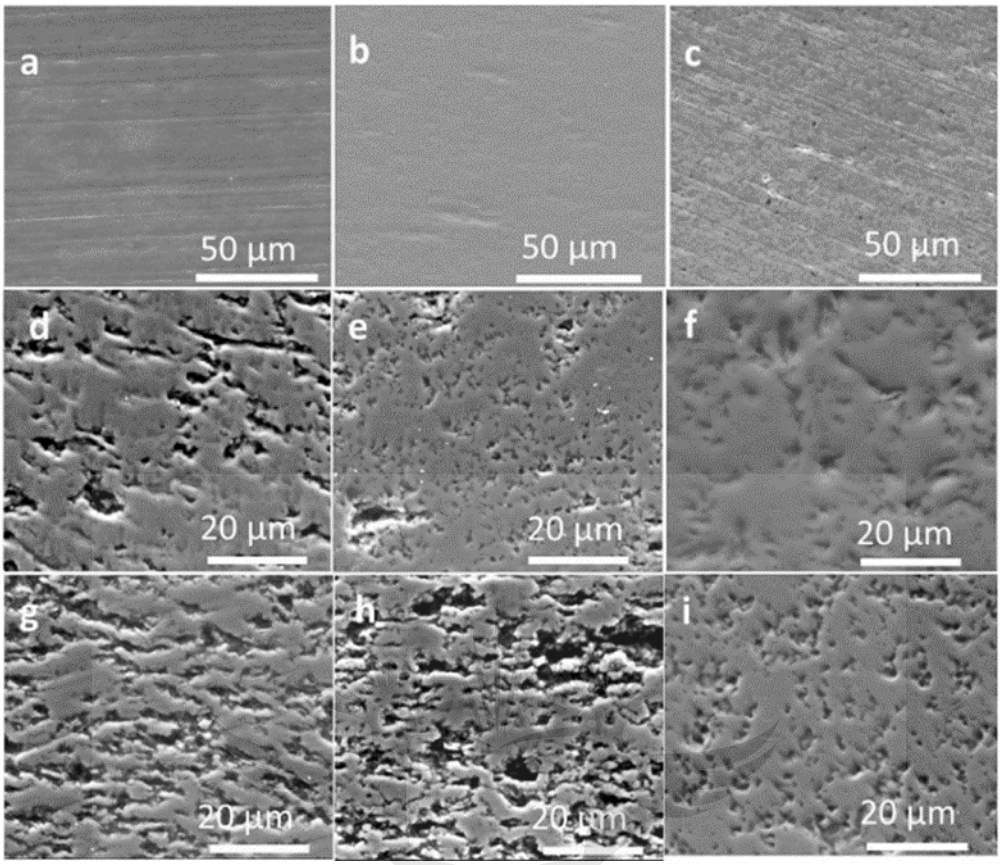

Figure 4. Illustrates the SEM images of the polished cross section of (a, b, c) Ti-0CNT, (d, e, f) Ti-5CNT, and (g, h, i) Ti-10CNT sintered at 800°C, 1000°C and 1200°C, respectively [48]. Reprinted with permission from Ref.48.

From the above SEM images, it is evident that the degree of porosity decreases according to the sintering temperature, despite the increase in the CNT content in the matrix material. This also supports the fact that during sintering, the densification of a material increases with the increase in the sintering temperature. However, the densification rate – which was higher for the sintered pure titanium powders – decreased as the CNT content increased, for samples sintered at 800°C and 1000°C. Hence, the densification increases with CNT contents, for samples sintered at 1200°C. This confirms the closure of pores during sintering at a higher temperature, which reduces the porosity of the sintered sample and eventually enhances the density of the sintered composite. Moreover, Vasanthakumar et al. [48] also reported an increased in densification resulting from the increase in the sintering time, which are shown in Figure 5 (a-c) below. This behavior was ascribed to the

increased in difficulty during the sintering process due to the increase of carbon/titanium ratio in the composite mixture [48].

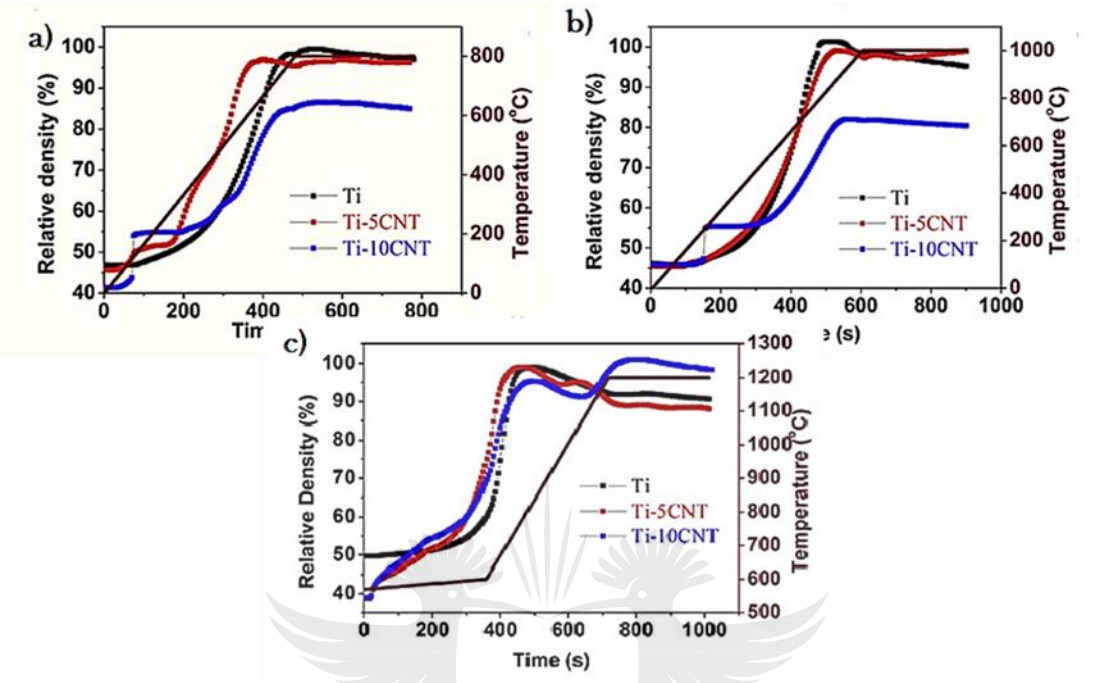

Figure 5. Illustrates the influence of sintering parameters (time and temperature) and CNT addition in the densification of CNT-Ti composites [48]. Reprinted with permission from Ref. 48

Similarly, Adegbenjo et al. [49] reported an increase in density following the increase in the sintering temperature. They further stated an increase in the density of the sintered CNT-Ti6Al4V composites from 98.8% to 99.6% between 850^0C and 1000^0C, respectively – which amounts to a 0.8% increase in density. The improvement in density according to the sintering temperature was attributed to the enhanced diffusion bonding and the mobility of atoms during sintering at higher temperature, which led to the reduction in porosity (closure of pores) within the sintered composites. They further reported similar trend on the densification of the sintered composites, when the CNT content was increased. This implied that the densification of the sintered composites decreased with the increase in CNT content in the composite materials. This confirmed the possible porosity of the composite mixtures containing a higher content of CNT. The densification behavior of the sintered nanocomposites – at varying sintering temperatures – and CNT addition are illustrated in Figure 6 below.

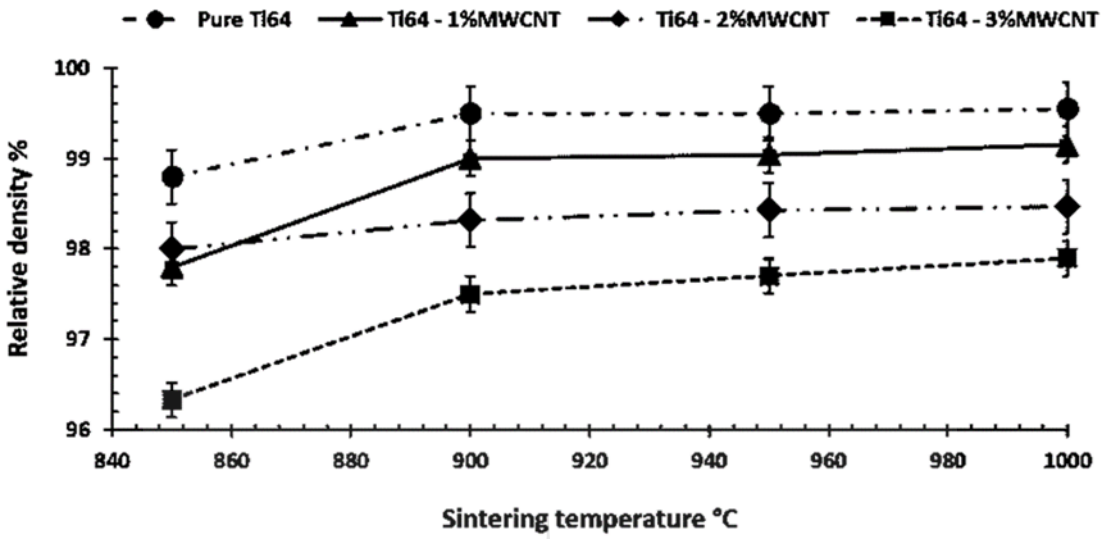

Figure 6. Illustrates the influence of the sintering temperature and CNT addition in the densification behavior of SPSed CNT-Ti6Al4V composites [49]. Reprinted with permission from Ref. 49

Various optimizations of sintering parameters can be adopted, based on the desired properties of the sintered composites. Wang et al. [50] adopted a low-temperature-and-rapid SPS of CNT/Ti composites, where they optimized some sintering parameters to achieve a better densification. They applied preliminary holding pressures of 1 and 300 MPa, respectively, to inhibit grain growth in the titanium matrix and to prevent the formation of titanium carbide during the sintering process. The specific low-sintering temperature and fast-heating rate adopted are 550 °C and 100 °C/min, respectively. These parameters were adopted to minimize the energy required by the atoms of both the CNT and the titanium matrix – to overcome the energy barriers – for reaction to occur. Additionally, the abovementioned parameters were adopted to maintain the structural integrity of the CNT and to reduce the tendency for the formation of titanium carbide phases in the sintered composites. The results of the sintered composites revealed that their densification behavior was not fully influenced by the content of the CNT present in the composites. Nonetheless, slight drop in the density of the sintered samples was observed, as the CNT content increased. The best density of 99.69 %) was achieved for 0.2 wt.%. This behavior is ascribed to the low content of the CNT (0-1.0

wt.%) used to reinforce the titanium matrix, as they have a minimal influence on the densification of the SPSed composites.

Full densification can be achieved at short holding time and high temperatures, especially in a bid to prevent grain growth in material during the SPS process. This was confirmed by Jiang and Gao [51][52] who fabricated CNT-reinforced TiN nanocomposites using the SPS technique. They adopted a sintering temperature of 1250°C at a holding time of 2 minutes and achieved a full densification of 100% for one of the sintered CNT-TiN nanocomposite. However, they observed that the densification of the sintered composites declined with the increase in the content of the CNT. This confirmed the views of past works that indicate that the increase in CNT content in the composites imposes the presence of pores in the sintered material, which will eventually affect the densification and overall properties of the sintered composites.

Contrary to previous reports on the effect of sintering temperatures on the densification behavior of SPS nanocomposites reinforced with CNT, Munir et al. [52] reported a decrease in the relative density of sintered titanium/CNT in line with the increase in the sintering temperature. They fabricated Ti-0.5 wt.% CNT composites using SPS at the sintering temperatures of 800°C and 900°C, respectively. Their findings indicated an average relative density of 99.89% for the fabricated nanocomposites sintered at 800°C. The corresponding SEM micrograph, Figure 7(a), reveals the presence of TiC dispersoids embedded in the Ti matrix. Furthermore, a thorough microstructural examination showed the absence of micropores in the sintered composites. Nevertheless, fine TiC particles were homogeneously dispersed in the Ti matrix. Conversely, samples sintered at 900°C indicated the presence of coarse TiC dispersoids embedded in the Ti matrix, within some parts of the composites. This is shown in the SEM micrograph constituting Figure 7(b). The SEM image also shows the re-agglomeration features of unreacted CNT at higher temperatures. Hence, the average relative density of the sintered composites declined to 98.12%. The authors attributed the low densification behavior to the high heating rates and high sintering temperatures during sintering, which resulted in poor uniformity in the sintered composites as the liquid flow was abated by the applied pressure and short sintering cycles. This might result in the formation of defect zones taking the form of pores and cracks in the composite [52].

Recently, Sribalaja et al. [43] fabricated a ternary composite comprising titanium carbide (TiC), TiC-3.5 wt.% WC (TW) and TiC-3.5 wt% WC-2 wt.% CNT (TWC) pellets using SPS at 1600°C, with a compressive pressure of 50 MPa. It was observed that some of the CNT in the TWC pellets became unzipped and formed in-situ wide graphene nanoribbons (GNR) during the SPS.

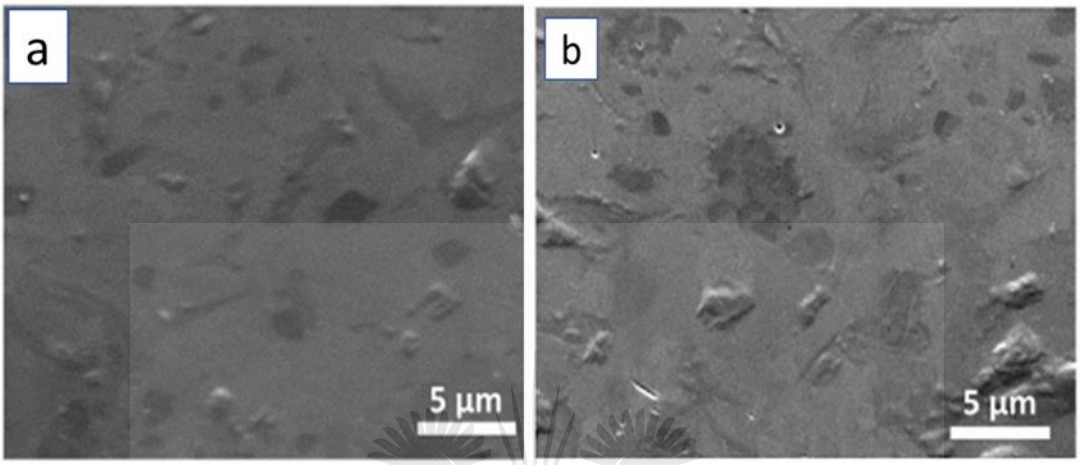

Figure 7(a & b). Illustrates the SEM images of Ti-0.5 CNT sintered at 800°C and 900°C, respectively [52]. Reprinted with permission from Ref. 52

Furthermore, they reported that the addition of CNT and the formation of in-situ GNR enhanced the density (approximately 99.4%) and inhibited the size of the TWC grains up to 54 %. This increase in density was ascribed to the homogeneous dispersion of CNT and the formation of in-situ wide GNRs which possessed a higher thermal conductivity (CNT: 3000 W/m K [9] and GNR: 5200 W/m K [53]), compared to that of TiC (~25 W/m K [53]). Apparently, the homogeneous dispersion of CNT and the in-situ-formed wide GNR led to the homogeneous dissipation of heat in the matrix that induced the partial melting of TiC grains.

Similarly, Karthiselva and Bakshi [15] fabricated a ternary composite containing CNT as reinforcement, using the SPS technique. The fabricated TiB_2-TiC-CNT composites were sintered at a temperature of 1400°C, with a holding time of 10 min under a uniaxial pressure of 50 MPa, at the peak temperature. Furthermore, the sintering temperature, punch displacement and vacuum pressure were plotted against the sintering time to understand the densification behavior of the materials. The results indicated that the relative density of the sintered composites declined as the CNT content increased. However, the authors achieved the best density of 99.3% for the fabricated composites,

which was in line with previous works that confirmed the decrease of the density following the increase in the content of CNT present in the SPSed nanocomposites.

From all indications, the densification behavior of CNT-TMNC fabricated using the SPS technique has a direct relationship with the sintering parameters and the CNT content in the sintered nanocomposites. It was revealed that a higher sintering temperature promotes the closure of pores and enhances the densification of the sintered CNT-TMNC. Furthermore, the incorporation of CNT into a titanium-based matrix does not have adverse effects on the densification of the nanocomposites, especially when the CNT content is below 0.12 wt.%. However, a higher fraction of CNT in the nanocomposites tends to destabilize the structure due to the introduction of pores that eventually decrease the densification of the nanocomposites. Additionally, the homogeneous dispersion of CNT in the matrix material, and a high sintering rate at lower sintering temperature enhance the densification and improve the properties of the resulting nanocomposites. Table I provide the lists of reported works on the effect of the sintering temperature and CNT content on the density of CNT-TMNC.

Table 1: Illustrates the effect of the sintering temperature and CNT content on the densification of the SPSed CNT-TMNC.

Reference	Composite composition	CNT (wt. %)	Sintering Temperature (ºC)	Relative Density (%)
[49]	Ti6Al4V-CNT	1	850, 950,1000	96.3, 98.7, 98.8
		2	850,950,1000	97.9, 98.1, 98.2
		3	850,950,1000	97.3, 97.4, 97.6
[48]	Ti-CNT	5	800,1000,1200	97, 99, 102
		10	800 ,1000,1200	87, 88, 102
[50]	Ti-CNT	0.2		99.69
		0.4		99.44
		0.6	550	99.31
		0.8		99.13
		1.0		99.01
[51]	TiN-CNT	0.1	1250	100
		1		98.6
		5		97.8
[52]	Ti-CNT	0.5	800	99.8 ± 0.07
[54]	TiO_2-CNT	0.5	900	97.68 ± 0.13
		2	1000	98

5. Mechanical properties of CNT-TMNC

In recent years, numerous CNT-TMNC have been fabricated using the SPS technique, with the goal of achieving better mechanical and other properties [55]. As stated earlier, CNT are recognized for their outstanding and exclusive properties that qualify them as reinforcements for various metals and alloys. Due to incessant needs for materials with improved mechanical properties for widespread

applications, researchers have shown interest in fabricating CNT-TMNC using SPS technique. Unlike other composites fabrication techniques, the SPS is a simple and efficient method for the fabrication of CNT-TMNC with excellent mechanical properties, since it has the potential of preventing damages to the CNT, given its short sintering time and high temperatures [26,56]. Nonetheless, the following are the various bottlenecks associated with the fabrication of CNT-TMNC with improved mechanical properties:

- Poor homogeneous dispersion of the CNT within the matrix of the titanium-based material. This is because individual CNT have the tendency to agglomerate, due to the strong Van der Waal forces, high aspect ratio, nanoscale dimension and high surface energy between them.
- Weak interfacial bonding between the CNT and the titanium-based matrix. This minimizes the stress transfer between the matrix and the CNT, thereby affecting the resulting mechanical properties of the fabricated nanocomposites.
- Formation of titanium carbide phases within the interface of the fabricated nanocomposite. This can either strengthen some properties such as hardness and elastic modulus or degrade some properties such as the toughness and ductility of the fabricated nanocomposites.

Basically, to achieve the desired mechanical properties of the fabricated nanocomposites, the bottlenecks need to be addressed using effective dispersion techniques [57]. Additionally, the sintered nanocomposites can be fabricated using optimized sintering parameters, to achieve densified composites with minimal micropores that may eventually inhibit the mechanical properties of the composites [58,59].

5.1 Effect of sintering parameters and CNT addition on the mechanical properties of CNT-TMNC

Various researchers have made efforts to fabricate TMNC reinforced with CNT of outstanding mechanical properties – using SPS technique. Li et al. [60] adopted planetary milling to disperse 0.4–1.0 wt.% CNT in pure titanium powders. They reported the homogeneous dispersion of CNT in the flaked titanium particles, after ball milling for 24 hours. The admixed powders compacts were sintered using SPS at a temperature of 800^{o}C for 1.8 ks and at a pressure of 30 MPa, under a vacuum of 5 Pa, to achieve 42.0 mm diameter and 32.0 mm height samples. After sintering, the composites

were preheated to 1273 K for 3 mins under an argon atmosphere and then extruded using a hydraulic press. A tensile test was carried out at room temperature, to access the mechanical properties of the extruded composites. The results indicated that the tensile properties increased when the CNT content increased from 0.4 to 1.0 wt.%. It was observed that the ultimate tensile strength (UTS) and the yield strength (YS) gradually increased when the CNT content increased from 0.4 to 1.0 wt.%. The results also indicated that the maximum UTS of 1182 MPa was achieved for composites with a composition of 1.0 wt.% CNT, which amounted to an 80.7 % improvement over the pure Ti.

Furthermore, the yield strength of 1.0 wt.% of CNT composition showed tremendous improvement, with a value of 1179 MPa over the pure Ti which has a yield strength value of 484 MPa, that corresponds to a 143.6 % improvement. However, there was a decline in the elongation value, from 29% to 15%, which indicated that the strength was increased at the expense of the ductility. This enhancement of the strength was ascribed to the formation of in-situ TiC particles in the sintered composites, the solution strengthening of the titanium by the carbon element, the grain refinement of the Ti matrix, and the load-bearing transfer from the Ti matrix to the CNT. This occurs through crack bridging, when their end is anchored within the Ti matrix grain [60]. The stress strain curve of the composite's behavior is shown in Figure 8. The stress-strain curve is an indication that CNT addition resulted in the improvement of the strength of the composites.

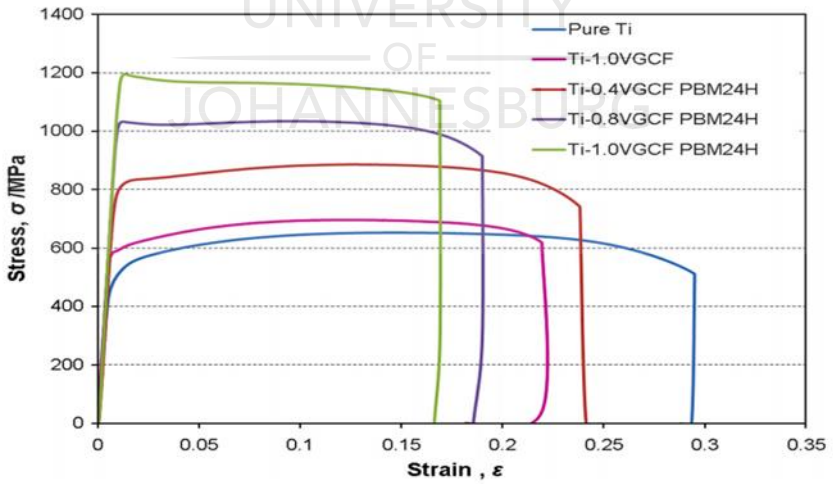

Figure 8. Illustrates the stress-strain curve of the sintered CNT-Ti composites [60]. Reprinted with permission from Ref. 60

Kondoh et al. [61] obtained similar results when they dispersed CNT (0.18- 0.35 wt. %) in pure titanium – using a wet process. The admixed powders were consolidated in a carbon die using a SPS with varying heating steps: 873 K for 3.6 ks – for their removal; and 1073 K for 1.8 ks – for the vacuum sintering. The compressive loads applied during sintering are 20 kN and 41.6 kN, respectively. They indicated that the sintered TMNC had a 43 mm diameter and a height of 15 mm. These were then heated in an argon atmosphere at 1273 K for 3 min, before hot extrusion. The stress-strain curve of the behavior of pure extruded titanium and 0.35 wt. % CNT-reinforced titanium is shown in Figure 9 below. However, the results of the UTS, yield strength and micro Vickerss hardness (Hv) indicated better improvement in properties over the pure titanium, when the CNT content was increased from 0.18 to 0.35 wt. %. Conversely, a decline in the elongation percentage was observed with the increase in CNT content from 0.18 to 0.35 wt. %; although composites with 0.24 wt. % CNT achieved a better elongation percentage. The improvement in UTS, YS and Hv is due to a better dispersion of the unbundled CNT and the in-situ formation of TiC in the sintered composites.

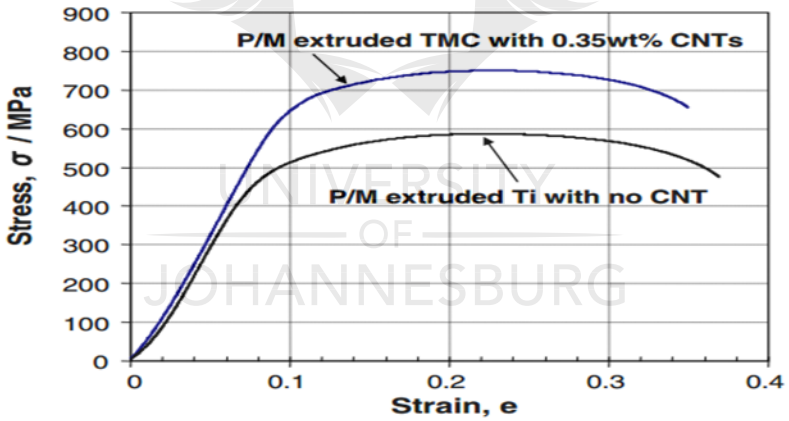

Figure 9. Illustrates the stress–strain curves of extruded CNT-Ti [61]. Reprinted with permission from Ref. 61

Recently, Kondoh et al. [62] adopted another approach to the fabrication of titanium-based composites reinforced with CNT – using SPS – and undertook extrusion on the sintered samples. The CNT (1.0, 2.0 and 3.0 wt.%) were dispersed into the Ti matrix using a wet process. The result of the sintered sample indicated the formation and dispersion of in-situ titanium carbide on the composites. The As-extruded Ti/TiC composite samples were annealed at 473 K for 3.6 ks, to

minimize the presence of residual stresses. After annealing, a tensile test was performed at room and elevated temperatures of 473, 573 and 673 K, respectively. Furthermore, a hardness test was conducted at a temperature of up to 573 K, with a step of 50 K. The results of the mechanical properties of the extruded Ti/CNT composites at an elevated temperature were significantly enhanced by the addition of CNT, compared to those of the extruded Ti matrix. The authors ascribed this improvement to the uniform dispersion of the TiC, which was initiated by the presence of CNT that excellently stabilized the microstructure of the extruded titanium composites by pinning effects. The distributed TiC dispersoids inhibit the deformation of the Ti grains, which eventually sustain their stability during the tensile test at an elevated temperature. Therefore, they reported no coarsening and growth of titanium grains, despite the annealing at 573 K for 36 ks and 673 K for 360 ks, respectively. Moreover, they reported some declination in the yield and the tensile strength of the tested samples, when subjected to high temperatures. This was related to the diffusion creep phenomenon [63–65]. The mechanical behaviors of the sintered samples, when examined at varying temperatures, are illustrated in Figure 10 (a-d) below.

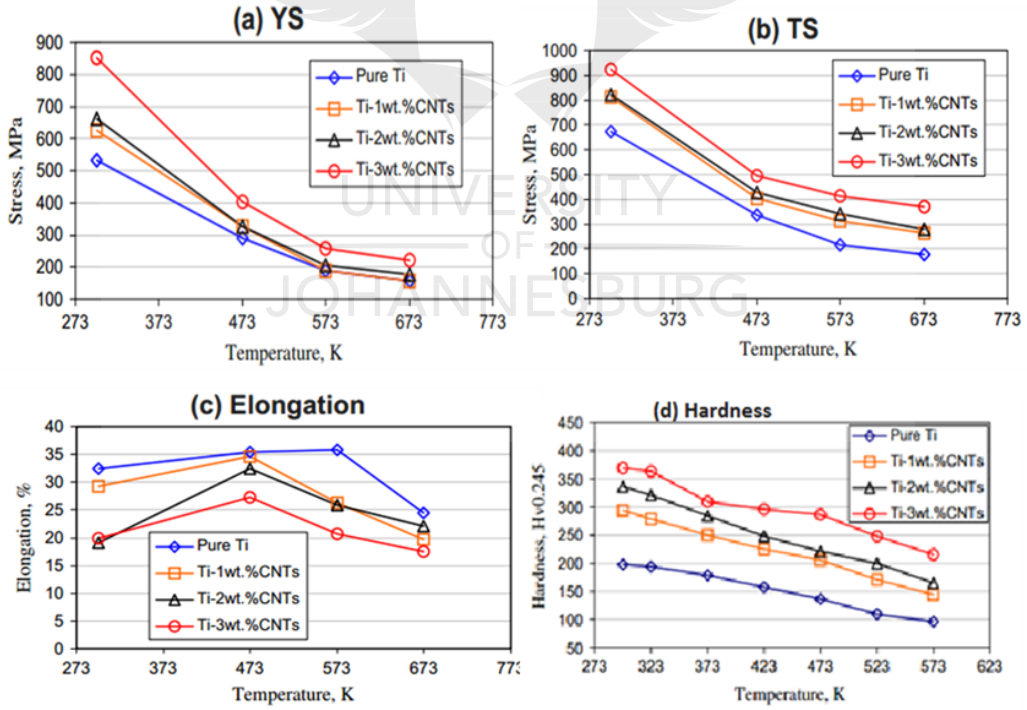

Figure 10. Illustrates the effects of the temperature on the mechanical properties of SPS Ti/TMC-CNT [62]. Reprinted with permission from Ref. 62

Based on Figure 10, it is obvious that the mechanical properties (YS,TS and Hv) of the sintered TMC reinforced with CNT were effectively enhanced by the addition of CNT, when tested at room temperature. Nonetheless, a decline was observed in the percentage elongation of the sintered composites with the increase in CNT content. This is an indication that the sintered composites possessed low ductility in comparison to the sintered pure titanium. This may be the result of the presence of in-situ formed titanium carbide that contributed to the improvement of the strength and hardness of the composites at the expense of the ductility.

Recently, Wang et al. [50] studied the mechanical properties of SPS titanium matrix composites reinforced with CNT (0.1-1.0 wt.%). They fabricated the composites at the low sintering temperatures of 550°C and the high sintering rate of 100°C/min, respectively. The influence of the weight fraction of the CNT on the microstructures and mechanical properties of the composites were examined. They reported (Figure 11 a) an improvement in the microhardness of the sintered CNT-TMNC over the pure titanium metal, with the increase in CNT content in the composites. They attributed this improvement to the addition of CNT that reinforced the properties of the titanium through grain refinement and the texture strengthening resulting from the pinning effect of the CNT. The latter impede the grain growth of the Ti by means of solution strengthening from the carbon atoms, load transfer from the matrix to the strong reinforcement and the dislocation motion impediment emanating from the strain hardening generated by the thermal mismatch between the titanium and the CNT. The variation of the Vickers microhardness – from the nanohardness – was related to the influence of the indentation size [66,67]. Similar trends (Figure 11 b & c) were also reported for the yield strength and the stress-strain behaviors of the sintered composites, although a drop in the tensile properties of the composites containing CNT (0.6-1.0 wt. %) was observed. The decline in the tensile properties of the composite samples containing CNT (0.4-1.0 wt.%) was attributed to the agglomeration of CNT at a higher weight percentage [50]. This confirms that the increase in CNT content leads to a higher tendency of agglomeration, because of the strong Van der Waal forces that exist between individual CNT. Figures 11 (a-c) and 12 (a &b) illustrate the effects of the addition of CNT on the mechanical properties of TMC and the Zener pinning effects of CNT during SPS.

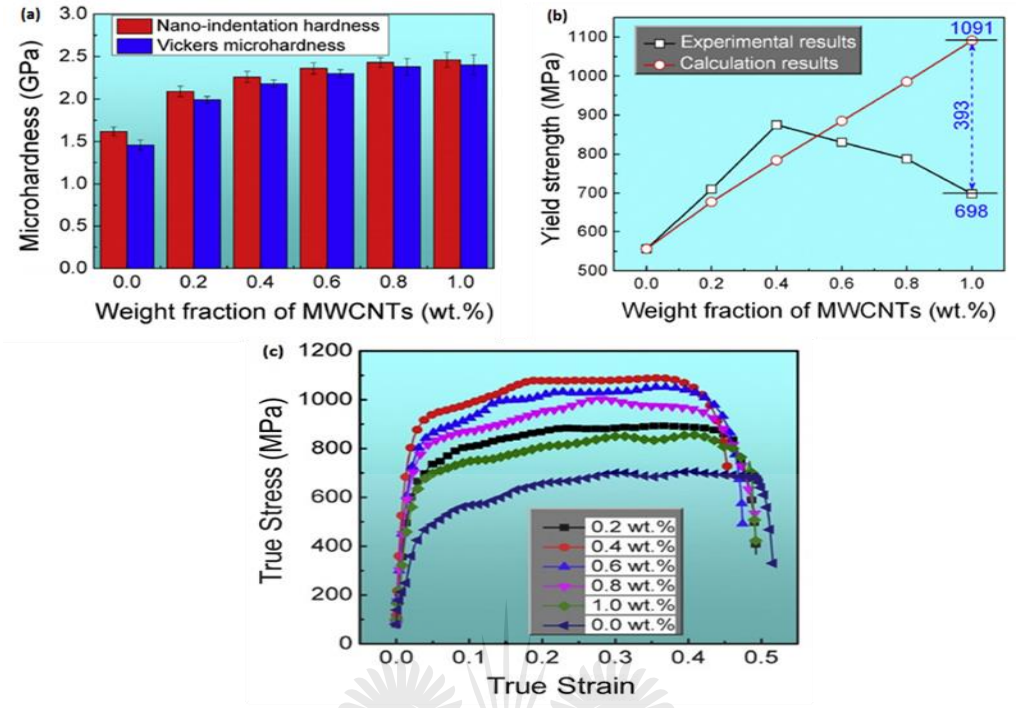

Figure 11(a-c). Illustrates the effects of CNT addition on the mechanical properties of TMC [50]. Reprinted with permission from Ref.50

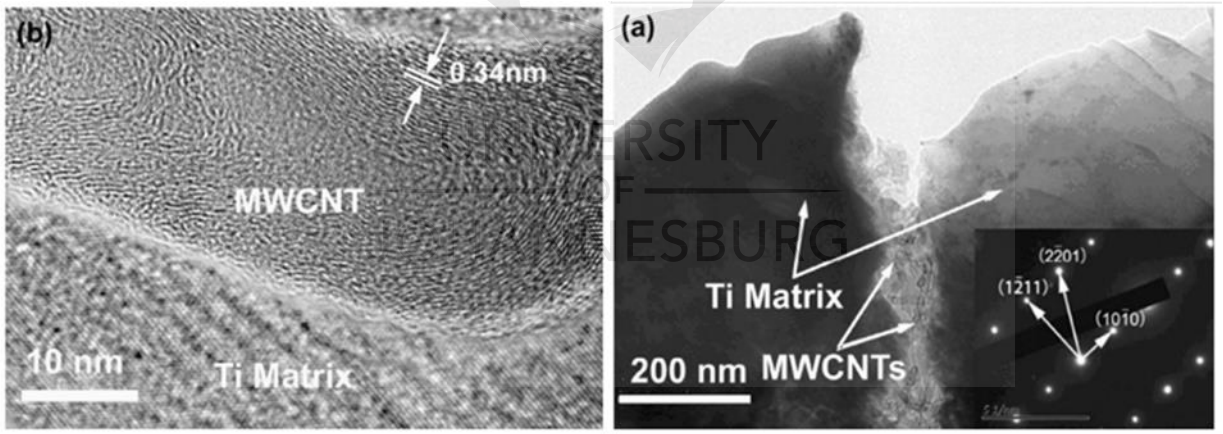

Figure 12 (a &b). Illustrates the TEM and HRTEM of 1.0 wt.% CNT-TMNC with CNT located at the grain boundary of the titanium matrix [50]. Reprinted with permission from Ref. 50

More recently, Debalina et al. [54] reinforced an alloy of titanium using various nanocarbonaceous materials (graphene nanoplatelets, single walled nanorods and CNT). They fabricated titania reinforced with 2 wt % of CNT – using SPS. The CNT were dispersed in the titania using a ball milling process. They reported a slight enhancement in the microhardness and elastic modulus of the

sintered composites, when compared to other nanocarbon reinforcements (graphene nanoplatelete). However, they attributed the slight improvements in the mechanical properties of the sintered composites to the low density of the composites. This is an indication that the composites were not fully densified, unlike the ones reinforced with graphene nanoplateletes which showed better improvements in both their densification and mechanical properties.

Similarly, Kartheselva et al. [15] fabricated titanium-and-boron-based composites reinforced with varying volume percentages of CNT (1,2,4,6) using reactive SPS, to form TiB_2-TiC-CNT hybrid composites. They reported that the reinforcement of titanium and boron retards the formation of TiB_2 which affected the microstructure and mechanical properties of the sintered composites. The mechanical properties were characterized using a nanoindenter to ascertain the elastic modulus and nanohardness. The indentation fracture toughness was evaluated using Vickerss hardness tester, where the crack length was confirmed from SEM images and the fracture toughness was determined using Anstis' equation [68].

$$KIC = 0.016\left(\frac{E}{H}\right)^{1/2}\left(\frac{P}{C^{3/2}}\right) \qquad (5)$$

The denotations KIC, E, H, C and P represent the fracture toughness in $Pa.m^{1/2}$, the elastic modulus in GPa, the hardness in GPa, the crack length in m and the load in N, respectively. It was observed from the results in Figure 13 (a) that the elastic modulus and the nanohardness of the sintered composites reinforced with CNT decreased in comparison to those of the sintered TiB_2. This behavior was ascribed to the high deformability of CNT during the synthesis of the nanocomposites [69], the lubrication ability of CNT between the TiB_2 grains and the change of CNT to graphene-like structures which eventually enhanced slippage. However, all the fabricated composites depict nanohardness and elastic modulus values greater than 425 GPa and 500 GPa, respectively. In addition, samples Ti-B-8h1400C, Ti-B-1CNT and Ti-B-2CNT showed higher elastic modulus values, which was linked to the indentation size effects and the nature of the localized measurement provided by the indentation techniques [70]. Furthermore, they reported that the addition of CNT enhanced the fracture toughness. This was evidenced by the result of the TiB-4CNT which depict the highest fracture toughness value that is 55 % greater than the fracture toughness of Ti-B-8h1400C. Hence the conclusion that CNT addition inhibits grain growth and reduces the grain size,

although it enhances the fracture toughness of the composites. The authors further explained that the influence of grain size on the fracture toughness is linked to the crystal symmetry of the composites. This is a confirmation of past work by Rice [71] which indicated that grain size does not have an adverse influence on polycrystals in cubic symmetry. However, non-cubic symmetry polycrystals revealed an adverse enhancement of the fracture toughness – with the increase in grain size. This improvement in toughness is credited to the thermal expansion mismatch stresses generated in the non-cubic symmetry crystals [72,73]. Figure 13 shows the mechanical properties of the SPS composites.

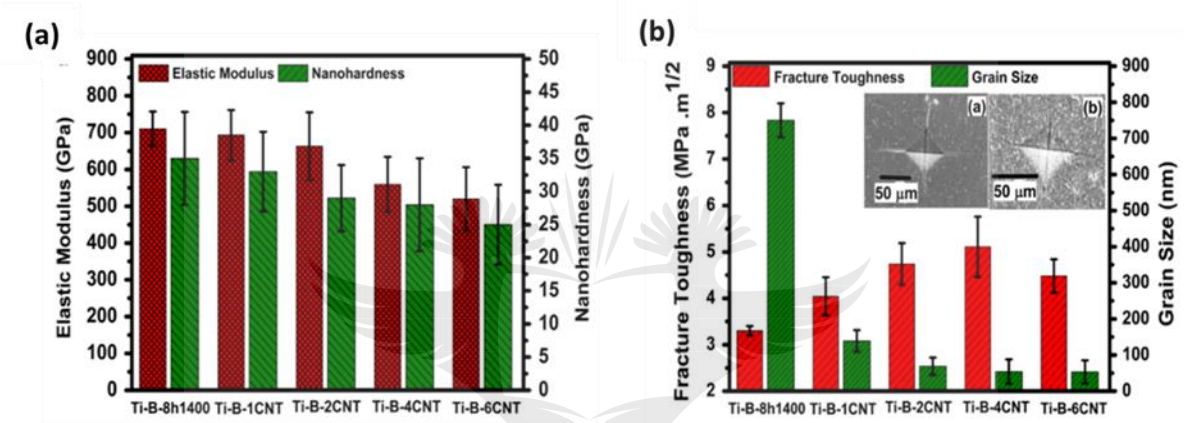

Figure 13. Illustrates a (elastic modulus and nanohardness) and b (fracture toughness) of the SPSed Ti-B-CNT nanocomposites [15]. Reprinted with permission from Ref. 15

Other SPS syntheses have been undertaken to enhance the mechanical properties of titanium and its alloys reinforced with CNT. As reported by Adegbenjo et al. [49], the microhardness of Ti6Al4V was enhanced, when the content of graphitized CNT reinforcement was increased in the fabricated composites. These authors fabricated CNT-Ti6Al4V with varying weight fractions of CNT (1,2 & 3 wt.%) – using SPS. The change in microhardness behavior in relation to the sintering temperature of the fabricated composites is shown in Figure 14 below. It was observed that the microhardness value of the fabricated composites increased with the graphitized CNT content in the composites, at different sintering temperature. They ascribed the improvement of the hardness to the presence of graphitized CNT in the composites and the formation of a titanium carbide phase which resulted from the interfacial reaction between the CNT and the metal matrix during the synthesis. This result

is in line with the findings of other past works on CNT reinforced titanium-based composites [16,62,71–73].

Similar improvements in mechanical properties were reported by Munir et al. [52] when they fabricated a CNT-Ti nanocomposite with (0.5 wt. %) CNT through the use of SPS and the adoption of various dispersion methods, in preparing their composites. Furthermore, they evaluated the mechanical properties and microstructural features of the fabricated composites. During the fabrication of the composites, the impact energy on the CNT was effectively controlled to prevent damages to the CNT and to minimize the formation of TiC during the dispersion and sintering of the composite mixtures. This contibuted to the improvement in the mechanical and tribological properties of the fabricated composites. The authors further reported improvements in the compressive strength, nanohardness, elastic modulus and wear resistance of all the fabricated composites, in contrast to those of pure titanium. Their work also explained the effect of sintering temperatures on the mechanical and tribological properties of the developed composites, as shown in Figure 15 below. This improvement in properties is attributed to various strengthening mechanisms which include grain refinement as a result of CNT pinning effects [59], dispersion strengtheing due to CNT dispersion in the TMNC [74], solution strengthening caused by the incorporation of interstitial atoms in the lattice of metal atoms [75], inhibition of dislocation as a result of the CNT/Ti interface that leads to strain hardening in the composites and thermal mismatch between the CNT and the titanium matrix [66], the formation of TiC dispersoid which enhanced the strength of the composites through orowan looping [60,61,66,76] as well as load transfer mechanism – from the titanium to CNT – enabled by an interfacial shear stress which uses the stiffness of CNT [77].

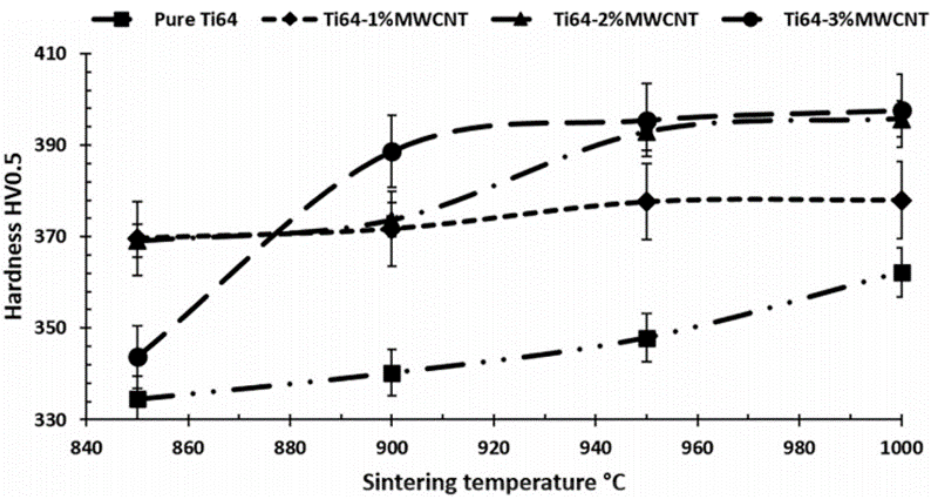

Figure 14. Illustrates the microhardness of CNT-Ti6Al4V with varied CNT contents [49]. Reprinted with permission from Ref. 49

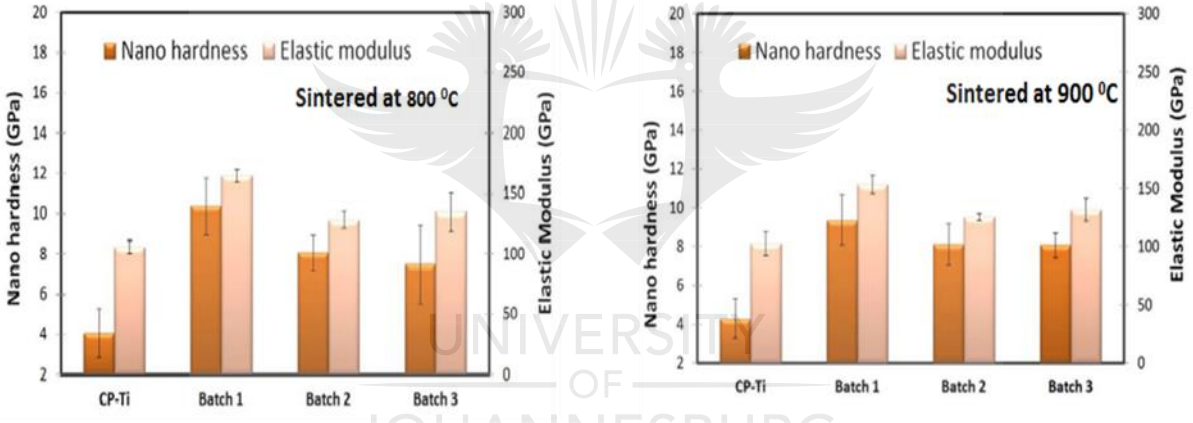

Figure 15. Illustrates the nanohardness/elastic modulus of sintered Ti-CNT at 800 and 900°C, respectively [52]. Reprinted with permission from Ref. 52

From the reviewed literatures of past research, it is glaring that the mechanical behavior of sintered TMNC reinforced with CNT depends on the dispersion methods, sintering parameters and the contents of the CNT in the composites mixture [78]. Additionally, post-sintering operations such as extrusion, rolling, annealing, among others, can play vital roles in improving the microstructural homogeneity and the mechanical properties of sintered TMNC. The summary of the mechanical properties of the SPSed titanium and its alloys reinforced with CNT is provided in Table II.

Table 2: Illustrates a summary list of CNT-TMNC fabricated by SPS

	Composites Composition	Dispersion Methods & Post Sintering Technique	CNTs Content (wt.%)	Sintering Temp (^{0}C)	Mechanical Properties				
					H_V (GPa)	H_N (GPa)	UTS (MPa)	E (GPa)	YS (MPa)
[15]	Ti-B-CNT	HEBM	0	1400	---	35	---	713	---
			1			33		694	
			2			29		663	
			4			27		559	
			6			25		519	
[43]	TiC-WC-CNT	SPRAY DRYING	0	1600	---	28.1	---	329.4	---
			2			33.7		428.5	
[48]	Ti-CNT	HEBM	0	800,1000,1200	---	8,10.5,7.9	---	126,180,167	---
			5			9.5,13.2,18.8		174,212,213	
			10			9.6,10.1,20.1		216,188,286	

[49]	Ti6Al4V-CNT	HEBM	0	850,950,1000	335,347,361				
			1		370,377,378	---	---	---	---
			2		369,393,396				
			3		344,395,398				
[50]	Ti-CNT	SBM	0.0	550	1.43	1.62	715		550
			0.2		1.97	2.09	902	---	707.4
			0.4		2.17	2.26	1098		864.8
			0.6		2.27	2.37	1057		822.5
			0.8		2.35	2.45	1012		784.9
			1.0		2.38	2.47	866		698
[51]	Ti-CNT		0	800, 900	---	4, 4.2	---	106.9,103.7	---
		HEBM	0.5			10.3,9.4		166.1,154.8	
		SBM	0.5			7.4,8.1		135.2,132.7	
[54]	TiO_2 -CNT	SBM	0	1000	---	8.8±1.9	---	237±34	---
			2			11±1.13		250±15	

[60]	Ti-CNT		0	800	---	---	654±6.6	---	654±6.6
		HEBM/EXT	0.4				887±5.2		795±8.5
			0.8				1026±11.5		1017±16.7
			1.0				1182±15.9		1179±15.7
		TM/HEXT	1.0				697±11.6		585±10.5
[61]	Ti-CNT	WET PROCESS	0	800	261	---	591	---	472
			0.18		275		682		590
			0.24		278		704		633
			0.35		285		754		697
[79]	Ti-CNT	ROCKING	0	800	---	---	627	---	387
		MILL	0.1				666		510
			0.2				682		521
			0.3				689		535
			0.4				699		542

EXT-Hot Extrusion, HEBM-High energy ball milling, TM-Table milling, SBM-Solution ball milling

6. Potential Applications of SPSed CNT-TMNC

The constant need for densified nanostructured materials with superlative properties has prompted researchers to fabricate CNT-TMNC using SPS, for various advanced engineering applications. The incorporation of CNT into the structure of titanium metal and its alloys as well as the fabrication of nanocomposites using SPS have resulted in improved mechanical properties of the ensuing composites. Such enhanced attributes include the hardness, the tensile and yield strength [52,80], the toughness and elongation [62], as well as the tribological and thermal properties of titanium metals and their alloys [4,81]. Additionally, this helps to reduce the weight of the nanocomposites since CNT are lighter than titanium-based matrixes.

Apparently, due to the improved mechanical and tribological properties of these nanocomposites, they have potential applications in various part of automobile such as intake valves, engine valves, exhaust valves, exhaust pipes and mufflers [82]. Furthermore, they can be used in various rotating and non-rotating parts of aircraft components. In the rotating parts, these nanocomposites can be utilized for the following parts: disks, blinks, impellers, shafts, fans, compressor blades and spacers. As a result of the light weight and stiffness of the fabricated nanocomposites, they can be applied in non-rotating parts of aircrafts such as ducts and cases, stator vanes, struts, fan and turbine frames, link and actuators, as well as exhaust and sidewalls [83]. Additionally, CNT are biocompatible, and their nanocomposites are not cytotoxic; hence, they can find application as biomedical implants [84,85].

7. Conclusions and Future Prospect

This article has reviewed most of the research findings on the SPS of CNT-reinforced titanium and its alloys nanocomposites as well as their reported experimental outputs. The following summary was produced from the various studies:

- CNT have extraordinary properties such as high stiffness, strength, aspect ratio as well as exceptional thermal and electrical properties that have encouraged their utilization as potential reinforcements for advanced composites production.

- The outstanding features of CNT could be effectively incorporated into titanium metal and its alloys, to enhance their properties. This can only be achieved if there is a homogeneous dispersion of CNT within the titanium-based matrix.
- The addition of CNT to the titanium-based matrix helps to inhibit grain growth during SPS and enhances the densification of the composites. Hence, the increase in CNT content – above 0.12 wt. % – in the composites reduces their density, because of the increase of micropores in the sintered composites.
- The SPS of TMNC reinforced with CNT requires an effective optimization of the sintering parameters, to achieve improved densification and mechanical properties of the sintered nanocomposites.

To sum up, further research should be carried on comparative studies of graphene, graphene nanoplates, graphene nanorods and CNT – with focus on their dispersion characteristics and their enhancement of the properties of titanium and its alloys. This would help to ascertain the best carbon nanomaterials to use as reinforcement for the effective enhancement of the properties of titanium and its alloys. Furthermore, future work should focus on the effect of post-sintering operations on the microstructural evolution and mechanical properties of the SPS TMC reinforced with CNT.

Acknowledgements

The authors would like to extend their appreciation to the National Research Foundation (NRF) of South Africa as well as the Global Excellence and Stature (GES) of the University of Johannesburg, South Africa, for their financial support.

Conflict of interest

The authors declared that they have no conflict of interest.

Reference

1. S. Ranganath, J. Mater. Sci. **32**, 1 (1997).

2. M. A. Lagos, I. Agote, G. Atxaga, O. Adarraga, and L. Pambaguian, Mater. Sci. Eng. A **655**, 44 (2016).

3. E. Neubauer, M. Kitzmantel, M. Hulman, and P. Angerer, Compos. Sci. Technol. **70**, 2228 (2010).

4. S. C. Tjong, Mater. Sci. Eng. R Reports **74**, 281 (2013).

5. A. Dorri Moghadam, E. Omrani, P. L. Menezes, and P. K. Rohatgi, Compos. Part B Eng. **77**, 402 (2015).

6. A. M. K. Esawi, K. Morsi, A. Sayed, M. Taher, and S. Lanka, Compos. Part A Appl. Sci. Manuf. **42**, 234 (2011).

7. A. M. K. Esawi, K. Morsi, A. Sayed, M. Taher, and S. Lanka, Compos. Sci. Technol. **70**, 2237 (2010).

8. T. Kuzumaki, K. Miyazawa, H. Ichinose, and K. Ito, J. Mater. Res. **13**, 2445 (1998).

9. K. T. Kim, S. Il Cha, S. H. Hong, and S. H. Hong, Mater. Sci. Eng. A **430**, 27 (2006).

10. A. Bhat, V. K. Balla, S. Bysakh, D. Basu, S. Bose, and A. Bandyopadhyay, Mater. Sci. Eng. A **528**, 6727 (2011).

11. S. Cho, K. Kikuchi, A. Kawasaki, H. Kwon, and Y. Kim, Nanotechnology **23**, (2012).

12. C. S. Goh, J. Wei, L. C. Lee, and M. Gupta, Mater. Sci. Eng. A **423**, 153 (2006).

13. S. Y. Liu, F. P. Gao, Q. Y. Zhang, X. Zhu, and W. Z. Li, Trans. Nonferrous Met. Soc. China (English Ed. **20**, 1222 (2010).

14. M. Paramsothy, S. F. Hassan, N. Srikanth, and M. Gupta, Compos. Part A Appl. Sci. Manuf. **40**, 1490 (2009).

15. N. S. Karthiselva and S. R. Bakshi, Mater. Sci. Eng. A **663**, 38 (2016).

16. K. S. Munir, Y. Li, D. Liang, M. Qian, W. Xu, and C. Wen, Mater. Des. **88**, 138 (2015).

17. A. D. Moghadam, B. F. Schultz, J. B. Ferguson, E. Omrani, P. K. Rohatgi, and N. Gupta, Jom **66**, 872 (2014).

18. M. Jurczyk and J. Jakubowicz, *Bionanomateriały* (Wydawnictwo Politechniki Poznańskiej, 2008).

19. J. B. Ferguson, F. Sheykh-Jaberi, C. S. Kim, P. K. Rohatgi, and K. Cho, Mater. Sci. Eng. A **558**, 193 (2012).

20. M. Jurczyk, K. Niespodziana, and K. Jurczyk, Obróbka Plast. Met. **19**, 37 (2008).

21. G. K. Stylios, P. V Giannoudis, and T. Wan, Injury **36 Suppl 4**, S6 (2005).

22. H. Agheli, J. Malmström, P. Hanarp, and D. S. Sutherland, Mater. Sci. Eng. C **26**, 911 (2006).

23. K. Niespodziana, K. Jurczyk, and M. Jurczyk, Nanopages **1**, 219 (2006).

24. M. U. Jurczyk, K. Jurczyk, K. Niespodziana, A. Miklaszewski, and M. Jurczyk, Mater. Charact. **77**, 99 (2013).

25. Z. Z. Fang, J. D. Paramore, P. Sun, K. S. R. Chandran, Y. Zhang, Y. Xia, F. Cao, M. Koopman, and M. Free, Int. Mater. Rev. **63**, 407 (2018).

26. A. Azarniya, A. Azarniya, S. Sovizi, H. R. M. Hosseini, T. Varol, A. Kawasaki, and S. Ramakrishna, Prog. Mater. Sci. **90**, 276 (2017).

27. G. S. Upadhyaya, *Powder Metallurgy Technology* (Cambridge Int Science Publishing, 1997).

28. J. Beddoes and M. Bibby, *Principles of Metal Manufacturing Processes* (Butterworth-Heinemann, 1999).

29. D. Tiwari, B. Basu, and K. Biswas, Ceram. Int. **35**, 699 (2009).

30. M. Tokita, in *Mater. Sci. Forum* (Trans Tech Publ, 1999), pp. 83–88.

31. F. V Lenel, JOM **7**, 158 (1955).

32. S. R. Bakshi, D. Lahiri, and A. Agarwal, Int. Mater. Rev. **55**, 41 (2010).

33. E. Thostenson, Compos. Sci. Technol. **61**, 1899 (2001).

34. V. Viswanathan, T. Laha, K. Balani, A. Agarwal, and S. Seal, Mater. Sci. Eng. R Reports **54**, 121 (2006).

35. B. G. Demczyk, Y. M. Wang, J. Cumings, M. Hetman, W. Han, A. Zettl, and R. O. Ritchie, Mater. Sci. Eng. A **334**, 173 (2002).

36. M. F. Yu, O. Lourie, M. J. Dyer, K. Moloni, T. F. Kelly, and R. S. Ruoff, Science **287**, 637 (2000).

37. M.-F. Yu, B. I. Yakobson, and R. S. Ruoff, J. Phys. Chem. B **104**, 8764 (2000).

38. J. Liao and M.-J. Tan, Powder Technol. **208**, 42 (2011).

39. A.M. Okoro, M. Awotunde, O.A. Ajiteru, S.S. Lephuthing, P.A. Olubambi, R. Machaka, in *Mech. Intell. Manuf. Technol. (ICMIMT), 2018 IEEE 9th Int. Conf.* (IEEE, 2018), pp. 54–59.

40. W. M. R. M. Daoush, H. S. Park, F. Inam, B. K. Lim, and S. H. Hong, Metall. Mater. Trans. A **46**, 1385 (2015).

41. M. Suarez, A. Fernandez, J. L. Menendez, R. Torrecillas, H. U., J. Hennicke, R. Kirchner, and T. Kessel, Sinter. Appl. (2013).

42. R. Licheri, S. Fadda, R. Orrù, G. Cao, and V. Buscaglia, J. Eur. Ceram. Soc. **27**, 2245 (2007).

43. M. Sribalaji, B. Mukherjee, A. Islam, and A. Kumar Keshri, Mater. Sci. Eng. A **702**, 10 (2017).

44. S.-J. L. Kang, *Sintering: Densification, Grain Growth and Microstructure* (Elsevier, 2004).

45. R. M. German, in *Proc. 3rd Int. Conf. Sci. Technol. Appl. Sinter.* (2003), pp. 15–17.

46. C. A. Handwerker, J. E. Blendell, and R. L. Coble, in *Sci. Sinter.* (Springer, 1989), pp. 3–37.

47. R. German, *Sintering: From Empirical Observations to Scientific Principles* (Butterworth-Heinemann, 2014).

48. K. Vasanthakumar, N. S. Karthiselva, N. M. Chawake, and S. R. Bakshi, J. Alloys Compd. **709**, 829 (2017).

49. A. O. Adegbenjo, P. A. Olubambi, J. H. Potgieter, M. B. Shongwe, and M. Ramakokovhu,

Mater. Des. **128**, 119 (2017).

50. F. C. Wang, Z. H. Zhang, Y. J. Sun, Y. Liu, Z. Y. Hu, H. Wang, A. V. Korznikov, E. Korznikova, Z. F. Liu, and S. Osamu, Carbon N. Y. **95**, 396 (2015).

51. L. Jiang and L. Gao, Ceram. Int. **34**, 231 (2008).

52. K. S. Munir, Y. Zheng, D. Zhang, J. Lin, Y. Li, and C. Wen, Mater. Sci. Eng. A **688**, 505 (2017).

53. A. I. Khan, I. A. Navid, M. Noshin, H. M. Uddin, F. F. Hossain, and S. Subrina, Electronics **4**, 1109 (2015).

54. B. Debalina, N. Vaishakh, M. Jagannatham, K. Vasanthakumar, N. S. Karthiselva, R. Vinu, P. Haridoss, and S. R. Bakshi, Ceram. Int. **42**, 14266 (2016).

55. W. A. Curtin and B. W. Sheldon, Mater. Today **7**, 44 (2004).

56. A. H. Javadi, S. Mirdamadi, M. A. Faghihisani, S. Shakhesi, and R. Soltani, Xinxing Tan Cailiao/New Carbon Mater. **27**, 161 (2012).

57. A. M. Okoro, R. Machaka, S. S. Lephuthing, M. Awotunde, and P. A. Olubambi, in *IOP Conf. Ser. Mater. Sci. Eng.* (2018), p. 12004.

58. H. Wang, X. Li, J. Ma, G. Li, and T. Hu, Compos. Part A Appl. Sci. Manuf. **43**, 317 (2012).

59. K. G. Dassios, G. Bonnefont, G. Fantozzi, and T. E. Matikas, J. Eur. Ceram. Soc. **35**, 2599 (2015).

60. S. Li, B. Sun, H. Imai, and K. Kondoh, Carbon N. Y. **61**, 216 (2013).

61. K. Kondoh, T. Threrujirapapong, H. Imai, J. Umeda, and B. Fugetsu, Compos. Sci. Technol. **69**, 1077 (2009).

62. K. Kondoh, T. Threrujirapapong, J. Umeda, and B. Fugetsu, Compos. Sci. Technol. **72**, 1291 (2012).

63. F. H. William and H. Hosford, USA Univ. Michigan.Google Sch. (2005).

64. Y. Estrin, G. Gottstein, and L. S. Shvindlerman, Scr. Mater. **50**, 993 (2004).

65. M. J. R. Barboza, E. A. C. Perez, M. M. Medeiros, D. A. P. Reis, M. C. A. Nono, F. P. Neto, and C. R. M. Silva, Mater. Sci. Eng. A **428**, 319 (2006).

66. S. J. Yoo, S. H. Han, and W. J. Kim, Scr. Mater. **68**, 711 (2013).

67. B. Chen, S. Li, H. Imai, L. Jia, J. Umeda, M. Takahashi, and K. Kondoh, Mater. Des. **72**, 1 (2015).

68. G. R. Anstis, P. Chantikul, B. R. Lawn, and D. B. Marshall, J. Am. Ceram. Soc. **64**, 533 (1981).

69. J. Gonzalez-Julian, A. Datye, K.-H. Wu, J. Schneider, and M. Belmonte, Carbon N. Y. **72**, 338 (2014).

70. G. M. Pharr, E. G. Herbert, and Y. Gao, Annu. Rev. Mater. Res. **40**, 271 (2010).

71. R. W. Rice, *Mechanical Properties of Ceramics and Composites: Grain and Particle Effects* (CRC Press, 2000).

72. J. B. Wachtman, W. R. Cannon, and M. J. Matthewson, *Mechanical Properties of Ceramics* (John Wiley & Sons, 2009).

73. F. Xue, S. Jiehe, F. Yan, and C. Wei, Mater. Sci. Eng. A **527**, 1586 (2010).

74. D. H. Nam, S. I. Cha, B. K. Lim, H. M. Park, D. S. Han, and S. H. Hong, Carbon N. Y. **50**, 2417 (2012).

75. J. G. Park, D. H. Keum, and Y. H. Lee, Carbon N. Y. **95**, 690 (2015).

76. S.-H. Jung, M.-R. Kim, S.-H. Jeong, S.-U. Kim, O.-J. Lee, K.-H. Lee, J.-H. Suh, and C.-K. Park, Appl. Phys. A **76**, 285 (2003).

77. J. L. Li, Y. C. Xiong, X. D. Wang, S. J. Yan, C. Yang, W. W. He, J. Z. Chen, S. Q. Wang, X. Y. Zhang, and S. L. Dai, Mater. Sci. Eng. A **626**, 400 (2015).

78. E. O. Hall, Proc. Phys. Soc. B **64**, 747 (1951).

79. S. Li, B. Sun, H. Imai, T. Mimoto, and K. Kondoh, Compos. Part A Appl. Sci. Manuf. **48**, 57 (2013).

80. K. S. Munir, Y. Li, J. Lin, and C. Wen, Materialia (2018).

81. A. Adegbenjo, P. Olubambi, and J. Potgieter, in *Int. Conf. Theor. Appl. Exp. Mech.* (2018), pp. 55–61.

82. H. Fujii, K. Takahashi, and Y. Yamashita, Shinnittetsu Giho 62 (2003).

83. S. Singerman, J. Jackson, and M. Lynn, in *Superalloys 1996, Proc. Eighth Int. Symp. Superalloys* (1996).

84. F. M. Makau, K. Morsi, N. Gude, R. Alvarez, M. Sussman, and K. May-Newman, ISRN Biomater. **2013**, (2013).

85. S. K. Smart, A. I. Cassady, G. Q. Lu, and D. J. Martin, Carbon N. Y. **44**, 1034 (2006).

86. I.M. Robertson, G.B. Schaffer. Powder metallurgy, **53 (**2010) 146-62.

CHAPTER THREE

PUBLISHED INVESTIGATIONS FROM THIS STUDY

3.1 Synopsis

In this study, the influence of MWCNT addition on the dispersion characteristics, microstructural evolution and micro and nanomechanical properties of spark plasma sintered Ti6Al4V nanocomposites was investigated. Prior to the consolidation of the nanocomposites, the MWCNT were dispersed in the Ti6Al4V matrix via the shift-speed ball milling technique. Subsequently, the admixed powders were consolidated using the SPS technique and the sintering data were acquired and evaluated to understand the sinterability and densification behaviour of the alloy and nanocomposites. Various characterizations were conducted on the admixed powders and fabricated materials using SEM, TEM, XRD, EDS, OM, SAED and FFT to understand the dispersion characteristics of the MWCNT, microstructural evolution and phase changes after dispersion and consolidation. Lastly, investigations were carried out to ascertain the effects of MWCNT addition on the on the relative density, microhardness and nanomechanical properties (nanohardness, reduced elastic modulus, elastic recovery index, plasticity index, elastic strain resistance and anti-wear behaviours) of the fabricated Ti6Al4V and its nanocomposites.

3.2 Summary of written/published articles from the study

This study generated a sum of five (5) articles from the investigations with some of the articles already published in reputable DHET accredited peer-reviewed journals. The articles are serially arranged in accordance with the objectives and research questions of the study. Furthermore, each article is comprising of research background, materials used for the research, thorough explanation of the experimentation technique, results achieved and detailed analysis and results discussion. This was accompanied by respective conclusions and acknowledgements of the organizations that funded the research. Meanwhile, cited literatures were appropriately listed at the end of each article. Besides, the opening section of this chapter presents the summary of each articles generated from the research.

3.3 The Enclosed Articles

The current versions of the published articles as appeared in the journal publications and the submitted manuscripts under consideration are shown in the following section.

Journal of Alloys and Compounds 785 (2019) 356–366

Contents lists available at ScienceDirect

Journal of Alloys and Compounds

journal homepage: http://www.elsevier.com/locate/jalcom

Dispersion characteristics, interfacial bonding and nanostructural evolution of MWCNT in Ti6Al4V powders prepared by shift speed ball milling technique

Avwerosuoghene Moses Okoro [a, *], Ronald Machaka [b], Senzeni Sipho Lephuthing [a], Mary Ajimegoh Awotunde [a], Samuel Ranti Oke [a], Oluwasegun Eso Falodun [a], Peter Apata Olubambi [a]

[a] Centre for Nanoengineering and Tribocorrosion, Department of Metallurgy, School of Mining, Metallurgy and Chemical Engineering, University of Johannesburg, South Africa
[b] Council for Scientific and Industrial Research, Pretoria, South Africa

ARTICLE INFO

Article history:
Received 20 November 2018
Received in revised form
12 January 2019
Accepted 14 January 2019
Available online 17 January 2019

Keywords:
Multiwalled carbon nanotubes
Titanium alloys
Dispersion characteristics
Nanostructural evolution
Shift speed ball milling

ABSTRACT

The quest to achieve uniform dispersion of multiwalled carbon nanotubes (MWCNT) in metal matrices without compromising the structural integrity of the nanotubes during the production of metal matrix composites have been a lingering challenge across materials science community. The problem has compelled researchers to explore various techniques of dispersing MWCNT in metal matrices. In this study, 1.0 wt% MWCNT was dispersed in Ti6Al4V powders using shift speed ball milling technique to achieve uniform dispersion, good interfacial bonding and minimal structural strain to the MWCNT after dispersion. Two batches of dispersion techniques were adopted to disperse the nanotubes in the Ti6Al4V matrix. Batch 1 (6 h of low-speed ball milling + 1 h high-speed ball milling) and Batch 2 (8 h of low-speed ball milling + 1 h high-speed ball milling). After dispersion, various advanced characterisation techniques such as high-resolution transmission electron microscopy (HRTEM), scanning electron microscopy (SEM), Raman spectroscopy and X-Ray diffraction (XRD) were utilised to evaluate the dispersion characteristics, interfacial bonding and micro and nanostructural evolution of the MWCNT in Ti6Al4V powders. The results indicated that batch 2 sample showed the best dispersion characteristics of MWCNT, good interfacial bonding with minimal strain to the walls of the MWCNT in the Ti6Al4V powders and this is ascribed to the adequate impact energy exerted on the powders during prolong milling time of low-speed ball milling and the supplementary 1 h of high-speed ball milling.

1. Introduction

Industrial and structural demands for engineering materials with exclusive properties in advanced engineering applications have grown in recent times. This has engendered the utilisation of powder metallurgy and nanotechnology techniques to incorporate nanomaterials into various engineering materials for automobile, biomedical and aerospace applications.

Over the years, nanomaterials such as carbon nanotubes (CNT) have been successfully utilised as reinforcement to enhance the properties of various materials for structural, industrial and biomedical applications because of their superlative properties. Since 1991 when CNT came into limelight, they have emerged as potential materials for diverse engineering applications including advanced composites, biomaterials [1] and various electrical devices [2] because of their exceptional thermal, electrical and mechanical properties which supersede conventional reinforcing materials [3–5]. Carbon nanotubes can exist in two basic defect-free forms namely; single-walled nanotubes and multiwalled nanotubes (MWCNT) which are known for their extraordinary lightweight (~1.7–2.0 g/cm^3), ultra-high aspect ratios (~100–100,000) and unique tubular morphology. In addition, they possessed tensile strength up to 150 GPa and modulus of elasticity in the range of 1 TPa [6,7]. These incomparable (physical and mechanical) properties have credited MWCNT the unfathomable attention in scientific and materials engineering research

* Corresponding author.
E-mail address: okoromo@gmail.com (A.M. Okoro).

https://doi.org/10.1016/j.jallcom.2019.01.174
0925-8388/

Paper 2: Dispersion characteristics, interfacial bonding and nanostructural evolution of MWCNT in Ti6Al4V powders prepared by shift speed ball milling technique

Status: Published in Journal of Alloys and Compounds 785, 356-366

https://doi.org/10.1016/j.jallcom.2019.01.174

Abstract

The quest to achieve uniform dispersion of multiwalled carbon nanotubes (MWCNT) in metal matrices without compromising the structural integrity of the nanotubes during the production of metal matrix composites have been a lingering challenge across materials science community. The problem has compelled researchers to explore various techniques of dispersing MWCNT in metal matrices. In this study, 1.0 wt.% MWCNT was dispersed in Ti6Al4V powders using shift speed ball milling technique to achieve uniform dispersion, good interfacial bonding and minimal structural strain to the MWCNT after dispersion. Two batches of dispersion techniques were adopted to disperse the nanotubes in the Ti6Al4V matrix. Batch 1 (6 h of low-speed ball milling + 1 h high-speed ball milling) and Batch 2 (8 h of low-speed ball milling + 1 h high-speed ball milling). After dispersion, various advanced characterization techniques such as high-resolution transmission electron microscopy (HRTEM), scanning electron microscopy (SEM), Raman spectroscopy and X-Ray diffraction (XRD) were utilized to evaluate the dispersion characteristics, interfacial bonding and micro and nanostructural evolution of the MWCNT in Ti6Al4V powders. The results indicated that batch 2 sample showed the best dispersion characteristics of MWCNT, good interfacial bonding with minimal strain to the walls of the MWCNT in the Ti6Al4V powders and this is ascribed to the adequate impact energy exerted on the powders during prolong milling time of low-speed ball milling and the supplementary 1 h of high-speed ball milling.

Keywords: Multiwalled carbon nanotubes; Titanium alloys; Dispersion characteristics; nanostructural evolution; shift speed ball milling.

1. Introduction

Industrial and structural demands for engineering materials with exclusive properties in advanced engineering applications have grown in recent times. This has engendered the utilisation of powder metallurgy and nanotechnology techniques to incorporate nanomaterials into various engineering materials for automobile, biomedical and aerospace applications.

Over the years, nanomaterials such as carbon nanotubes (CNT) have been successfully utilised as reinforcement to enhance the properties of various materials for structural, industrial and biomedical applications because of their superlative properties. Since 1991 when CNT came into limelight, they have emerged as potential materials for diverse engineering applications including advanced composites, biomaterials [1] and various electrical devices [2] because of their exceptional thermal, electrical and mechanical properties which supersede conventional reinforcing materials [3–5]. Carbon nanotubes can exist in two basic defect-free forms namely; single-walled nanotubes and multiwalled nanotubes (MWCNT) which are known for their extraordinary lightweight (~1.7–2.0 g/cm^3), ultra-high aspect ratios (~100 –100,000) and unique tubular morphology. In addition, they possessed tensile strength up to 150 GPa and modulus of elasticity in the range of 1TPa [6,7]. These incomparable (physical and mechanical) properties have credited MWCNT the unfathomable attention in scientific and materials engineering research communities. The outstanding features of MWCNT are primarily attributed to their quasi-one-dimensional (1D) structures, the graphite-like arrangement of the carbon atoms in their shells, seamless cylindrical morphology and existence of strong sp^2 carbon–carbon (C–C) bonds in their outer shells [8,9].

In recent times, research advances have encouraged the integration of MWCNT into metal matrices to improve their properties. MWCNT have been extensively and successfully used to improve the mechanical, thermal and electrical properties of various metals and their alloys; aluminium [10–12], copper [13,14], magnesium [15,16] and titanium [9,17,18] by adopting several powder metallurgy processing techniques. Among these metals and alloys, titanium and its alloys have spurred considerable interest for automobile, aerospace, biomedical and industrial applications due to their lightweight, corrosion resistance, high melting point, biocompatibility, and unique mechanical properties even at cryogenic temperatures [19–21]. However, past research outputs have indicated that they tend to oxidise easily especially at an elevated temperature which leads to the loss of good

mechanical features. Additionally, they have a low elastic modulus, thermal conductivity, wear resistance and hardness which have limited their demands for some intrinsic parts in industrial applications [18]. Furthermore, these limitations of titanium and its alloys have given significant justification for the incorporation of MWCNT to improve their properties.

The quest to develop engineering materials with outstanding properties to meet the mechanical and thermal properties demands of modern automobile and aerospace industries, have prompted researchers to explore the production of nanostructured materials by integrating MWCNT into titanium-based matrices. MWCNT has layers of tubular structures and is highly desirable for composite production because if one of its layers experience telescopic effects [22] during their incorporation into the titanium-based matrix, the other layers can act as good reinforcements to enhance the properties of the resulting composites. During the integration of MWCNT into the titanium-based matrix, they have the tendency to agglomerate into clusters which inhibits their homogeneous dispersion. However, when harsh dispersion techniques are adopted, it may lead to uniform distribution but at the expense of the structural integrity of the MWCNT [7]. This dispersion characteristics of MWCNT is attributed to the strong Van der Waals forces that exist between them, their high aspect ratio and nanoscale dimensions. In order to achieve the ultimate aim of transfer of the excellent properties of the MWCNT into the titanium-based matrix, homogeneous dispersion, good interfacial bonding and the retainment of the unique tubular morphology of the MWCNT after dispersion in the titanium-based matrix is very paramount [3].

Recently, various efforts have been made to uniformly disperse MWCNT in metal matrices without compromising the structural integrity of the MWCNT after dispersion. In a quest to achieve this, different powder metallurgy dispersion techniques have been adopted which reported high energy ball milling (HEBM) as the most effective powder metallurgy technique to disperse MWCNT in metal matrices [23]. However, this method alone leads to the destruction of the tubular morphology of the nanotubes during dispersion, thereby compromising the excellent properties of MWCNT [23,24]. This was confirmed by Adegbenjo et al. [18] that adopted HEBM in dispersing MWCNT in Ti6Al4V, they achieved uniform dispersion but with severe destruction of the walls of the nanotubes after milling for 6 h and at a speed of 50 rpm. Similarly, Munir et al. [8] reported the formation of non-sp^2 defects in the form of vacancies and open edges in the C-C network of the MWCNT after dispersion in titanium metals using HEBM for 1 h and at a speed of 150 rpm. These are indications

that prolong milling time alongside with low milling speed and short milling time alongside with high milling speed using high energy ball mill have an adverse effect on the structural integrity of MWCNT since it creates structural defects on the walls of the nanotubes. This was buttressed by Morsi and Esawi [25] work where the emphasis was made that extended high energy ball milling time enhanced the deagglomeration and dispersion of MWCNT but results in damages to the nanotubes.

Additionally, Liu et al. [26] reported uniform dispersion of MWCNT in the metal matrix at the expense of the structural integrity of the nanotubes when high energy ball mill was used during the dispersion process for 4 to 12 h. However, the uniform dispersion was achieved after 6 h of milling alongside with the shortening of MWCNT that increased with the milling time which is signs of defects to the nanotubes. These formed defects are eligible sites for the formation of carbide (brittle phase) during milling which may be detrimental in producing composites with high toughness. Nevertheless, the carbide phases which are formed as a result of interfacial reactions between the MWCNT and the metal matrix can augment the strength, hardness and wear resistance of the resulting metal matrix composites [26,27]. The destruction to the walls of the MWCNT during high energy ball milling has prompted researchers to explore other routes of powder metallurgy processing techniques to effectively disperse MWCNT in metal matrixes.

Considering the fact that prolong milling time promotes uniform dispersion of MWCNT, Ostovan et al. [28] adopted low-speed ball mill (Retch PM100) for 0.5h to 12h in dispersing MWCNT in a metal matrix. It was observed that the MWCNT remained entangled until 5 h of milling where considerable dispersion occurred. However, the dispersion of MWCNT increased with extended milling time since the best dispersion was achieved from 5 to 12 h of milling. Specifically, the extended milling time introduced severe strain on the powders which eventually resulted in interfacial reactions between the powders to form carbide phase. To achieve uniform dispersion of MWCNT without compromising the structure of the nanotubes, optimum milling time is very expedient.

More recently, Okoro et al. [29] adopted low-speed ball milling technique to disperse MWCNT in titanium alloy; they reported relative dispersion with some amounts of agglomeration of the nanotubes and this dispersion characteristics were ascribed to insufficient impact energy exerted on the powder mixture during milling.

Furthermore, other powder metallurgy techniques have been used, but they have their peculiar limitations. Techniques such as sonication [8] and low-speed ball milling [29] when used with optimum dispersion parameters, exert inadequate impact energy on the powders during dispersion which is unable to overcome the strong Van der Waals forces that exist among the individual MWCNT and foster the uniform dispersion of the nanotubes. Sonication assisted high-speed ball milling [8] has been reported as a good dispersion method, but there are tendencies of re-agglomeration of the MWCNT especially during the drying of the powder mixture after wet milling. Therefore, it is paramount to adopt a dispersion technique that will exert optimum impact energy to overcome the strong Van der Waals forces of the MWCNT, induce uniform dispersion and good interfacial bonding between the powders without compromising the structural integrity of the nanotubes.

The quest to overcome these challenges of inadequate impact energy on the powders during dispersion and re-agglomeration of the MWCNT during drying process after wet milling have prompted researchers to adopt shift speed ball milling technique in dispersing MWCNT.

Xu et al. [30] adopted this method to achieve a homogeneous dispersion of MWCNT in aluminium matrix where they subjected the powder mixture to 9 h of low-speed ball milling and subsequent 1 h of high-speed ball milling. They reported uniform dispersion of MWCNT alongside with less structural strain after the dispersion process. In this study, efforts have been made to achieve uniform dispersion of MWCNT in Ti6Al4V powders without compromising the structural integrity of the nanotubes using the shift speed ball milling technique. To the best of our knowledge, this method has not been used to disperse MWCNT into Ti6Al4V powders in past studies.

2. Materials and Method

2.1 Starting materials

The MWCNT powders used for this study was supplied by Nanocycl Belgium with percentage purity of (~99.7), it has an average diameter and length of 9.5 nm and 1.5 μm respectively. Argon atomised, prealloyed Ti6Al4V powders with particle size ~25 μm supplied by TLS Technik GmbH & Co. Germany was utilised as the matrix material, and the stearic acid ($C_{18}H_{36}O_2$) with purity of 99.99 % was employed as the process control agent (supplied by Glass blown & Volumetric Glassware & Chemicals in Johannesburg, South Africa).

2.2 Dispersion of MWCNT in Ti6Al4V powders by shift speed ball milling (SSBM)

The MWCNT (1.0 wt.%), stearic acid (1.0 wt.%) and Ti6Al4V powders were weighed and charged into a 250 ml steel vial with inner diameter (ID) = 100 mm and placed into a low-speed ball milling machine (Retsch 100 PM, Germany) for preliminary milling process to disperse the MWCNT in the Ti6Al4V powders. The preliminary dispersion was carried out by adopting the following milling parameters; ball to powder ratio (BPR) 10:1, milling speed of 150 revolutions per minute (rpm) for 6 and 8 h respectively. The milling operation was done using dissimilar steel balls with sizes of 10 mm and 5 mm to enhance collisions of the balls to the powders and prevent subsequent cold welding of the powders. This milling operation was done at an interval of 10 min for every 10 min of milling to prevent the powders from heating up and avoid unwanted reactions between the powders during the milling operation. The admixed powders were further charged into another steel vial and transferred into a high energy ball mill (Retch 400 PM, Germany) for supplementary milling operation. The supplementary milling was carried out to exert sufficient impact energy needed to overcome the strong Van der Waals forces that exist between the MWCNT, deagglomerate and disperse the MWCNT homogeneously in the Ti6Al4V powders.

Additionally, the supplementary milling operation is needed to improve the dispersion of MWCNT and interfacial bonding between the MWCNT and the Ti6Al4V powders, and this was carried out by adopting a high-speed ball milling technique with a speed of 100 rpm while maintaining the other milling parameters used during the preliminary milling operation. In a nutshell, the milling process was done in two batches; batch 1 was done in a low-speed ball mill for 6 h and additional milling for 1 h in a high energy ball mill while batch 2 was carried out in a low-speed ball mill for 8 h and an additional 1 h of high-speed ball milling in a HEBM. The mixed powders from both batches were collected in a glove box to avoid contamination. Figure 1 shows the schematics of the dispersion process using the SSBM technique.

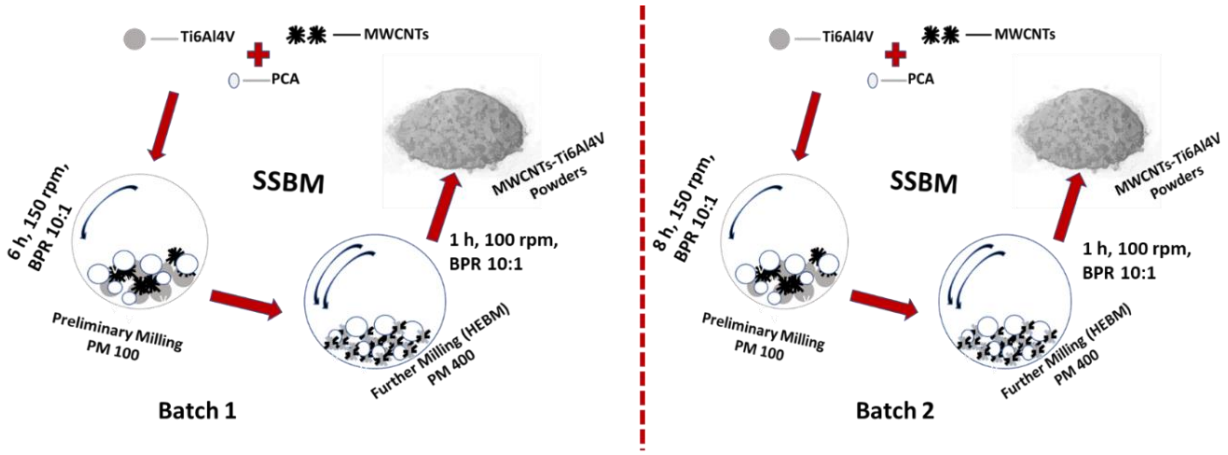

Fig.1. Illustrates schematics of the SSBM of MWCNT in Ti6Al4V using batch 1 & 2 processing routes.

2.3 Characterization of the starting and admixed powders after SSBM

The morphology of both the starting and the admixed powders after SSBM were observed by utilising scanning electron microscopy (SEM), Carl Zeiss Sigma FESEM furnished with energy dispersive X-ray spectrometry (EDX) and transmission electron microscopy (TEM), JEOL-Jem 2100. The TEM was also used to ascertain the structural integrity (walls) of the MWCNT before and after SSBM in the Ti6Al4V. The phase identification and crystalline phases of starting and mixed powders were characterised by X-ray diffractometer (XRD, Rigaku D/max-rB). This was carried out by a scan using Cu-Kα (λ= 0.154 nm) radiation at a scanning rate of 1°/min over the angular range of 10–90°. Furthermore, the structural integrity of the MWCNT was analysed by Raman spectroscopy, In-Via Raman microscope, Renishaw Plc. The Raman scattering was acquired in the spectral range of 200–1800 cm^{-1} on the pristine MWCNT and admixed powder on ten various positions with an acquisition of 50 s using a 514 nm laser (laser beam power = 5.63 mW). The intensity of Raman peaks and their conforming positions were acquired by deconvoluting the Raman spectra into two Gaussian peaks using WITec 2.5 software.

3. Results and Discussion

3.1 Microstructural evolution of MWCNT after dispersion in Ti6Al4V powders

The morphology and the structure of the starting powders; Ti6Al4V and MWCNT are as shown in Figure 2 (a-d). From the SEM image in Figure 2 (a), it was observed that the morphology of the Ti6Al4V depicted a spherical structure with an average particle size of (~25 μm). The SEM image in Figure 2 (b) shows the morphology of the pristine MWCNT, and it was observed that

there are bundling and tangling of the individual nanotubes which may act as obstacles during dispersion into Ti6Al4V powders. This characteristic feature of the MWCNT is ascribed to it exceedingly large aspect ratios which are in the range of (100-100,000), large specific surface area (~250 m^2/g) and the existence of strong Van der Waals forces (~-100 eV/mm) among the individual MWCNT [31].

Similarly, the HRTEM image in Figure 2 (c) shows the morphology of the MWCNT which conforms with the SEM image in Figure 2 (b) that depicts the clustering of the MWCNT. The inset on Figure 2 (c) is the selected area electron diffraction (SAED) pattern acquired for the MWCNT which is used to ascertain the crystalline phase and the amorphous phase formed in the MWCNT after dispersion. From the SAED pattern of the MWCNT, sharp rings patterns of the prominent graphite (002) and (100) planes were observed which is an indication of the high crystalline nature of the MWCNT without distortion on it planes [32,33]. Furthermore, a highly crystalline MWCNT usually have the features of identical chiralities of zigzag type and sharp coaxial rings with less halo ring pattern [34]. The HRTEM image in Figure 2 (d) shows the tubular morphology and undamaged walls of the MWCNT with an interlayer spacing of 0.3461 nm and the inset on the image depicts the fast Fourier transform (FFT) of the MWCNT which is utilized to confirm the crystalline nature or the level of ordered carbon in the MWCNT. Since FFT peaks were protruded with narrower tips, this confirmed the high crystalline nature of the MWCNT [35].

Extensive studies from previous works have emphasised that the effective transfer of the good properties of MWCNT into matrix materials during composites production is a function of the homogeneous dispersion of the MWCNT in the matrix phase and good interfacial bonding without compromising the tubular morphology and large surface area of the MWCNT [36,37]. In addition, adequate impact energy is required to overcome the strong Van der Waals forces between the MWCNT to achieve good dispersion in Ti6Al4V powders. The impact energy needed to de-agglomerate the clustered MWCNT without compromising their tubular morphology during milling operation is a function of the milling method and regulated milling parameters; milling speed, milling time, relaxation time, ball to powder ratio and the presence of process control agent.

Another intriguing factor that exists while incorporating MWCNT into Ti6Al4V powders is the

poor compatibility between the hydrophobic MWCNT and the hydrophilic Ti6Al4V powders which inhibit the homogeneous dispersion of MWCNT into the metallic based powder. This factor can lead to segregation of the MWCNT from the Ti6Al4V particles, poor interfacial bonding, and re-agglomeration of the MWCNT at the interstices of the Ti6Al4V particles. In order to prevent this bottleneck, high-speed ball milling was adopted with regulated milling parameters to further disperse the MWCNT after preliminary milling operation using low-speed ball milling.

Although, it has been established from past studies that HEBM is an effective technique to disperse CNT into various metal matrices [17,29]. However, HEBM alone without regulating the milling parameters can result in the deterioration of the tubular structure of the MWCNT during dispersion and lead to the formation of non-sp^2 defects on the walls of the MWCNT that may exist as open edges, vacancies and deformed side walls [38]. The existence of these defects can act as potential sites for unwanted interfacial reactions between the Ti6Al4V and the MWCNT powders.

In this research 1.0 wt.% of MWCNT was dispersed in batches by the application of low-speed ball milling and further high-speed ball milling. During the dispersion using a low-speed ball mill, stearic acid was adopted as the process control agent to minimise the surface free energy of the Ti6Al4V particles. Since the adopted PCA is known to have a hydrophilic head and hydrophobic end, the hydrophilic head get attached to the surface of the Ti6Al4V particles to reduce the surface free energy and further prevent cold welding of the particles by surrounding them with the hydrophobic tails [39].

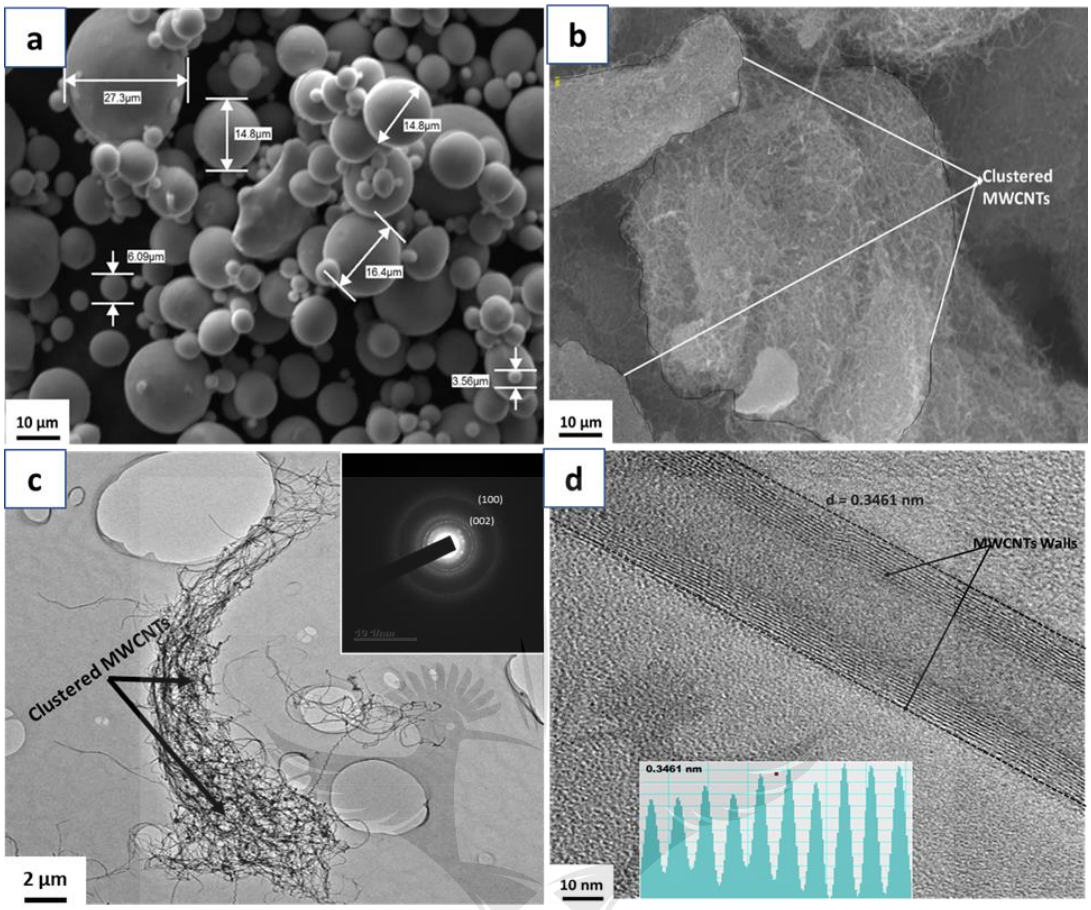

Fig.2. Illustrates high-resolution TEM & SEM images of the starting powders Ti6Al4V (a) and MWCNT (b-d)

Furthermore, the SEM images in Figure 3 and 4 shows the dispersion characteristics of the MWCNT in Ti6Al4V powders after milling for 6 and 8 h respectively using low-speed ball mill. From the SEM images in Figure 3, it was observed that there was some level of dispersion of the MWCNT within the Ti6Al4V particles, but it was seen that the dispersed MWCNT were segregated out as agglomerates in the interstices of the Ti6Al4V particles. This dispersion characteristic is ascribed to the inadequate energy exerted on the powders during dispersion which was unable to overcome the strong Van der Waals forces and unbundle the MWCNT. Besides, good interfacial bonding between the MWCNT and the Ti6Al4V was not observed after dispersion.

Similarly, the SEM images in Figure 4 shows the dispersion characteristics of the MWCNT in Ti6Al4V powders after dispersion in a low-speed ball mill for 8 h. It was observed that there was better dispersion of the MWCNT within the Ti6Al4V powders when compared with the

dispersion for 6 h. This better dispersion characteristic is a function of the prolong milling time where considerable impact energy was exerted on the powders to foster better dispersion of the MWCNT within the Ti6Al4V powders. However, some agglomerations of MWCNT at the interstices of the Ti6Al4V particles and poor interfacial bonding between the MWCNT and the Ti6Al4V powders were observed. This dispersion characteristic is ascribed to the insufficient impact energy exerted on the powders during dispersion even after prolong milling time. Thus, it is expedient to exert adequate impact energy to the powders to promote the dispersion of MWCNT which is adjudged to have a strong Van der Waals forces of (~ -100 eV) among it tubes [31]. All indications from the SEM images in Figure 3 and 4 revealed that the impact energy exerted on the powders was inadequate to uniformly disperse the MWCNT and promote good interfacial bonding between them.

The improvement in the dispersion of MWCNT in Ti6Al4V powders observed after 8 h of low-speed ball milling was achieved because of the continuous increase in the number of collisions and the total number of impact energy exerted on the powders by the cascading motion of the balls [40,41]. This consistent collision of the balls to the powders induced better mechanochemical activation reaction that promotes improved dispersion of the MWCNT than the 6-h of the low-speed ball milling process. However, there is the possibility of decomposition of the powders with prolonging milling time is adopted [41].

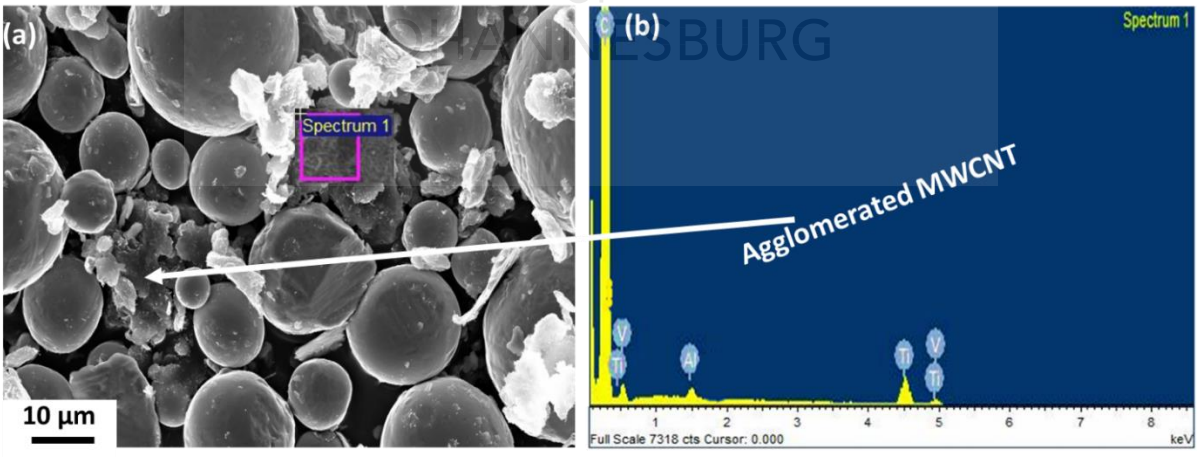

Fig.3. Illustrates the high-resolution SEM image (a) and EDX (b) of MWCNT dispersed in Ti6Al4V powders by low-speed ball milling for 6 h

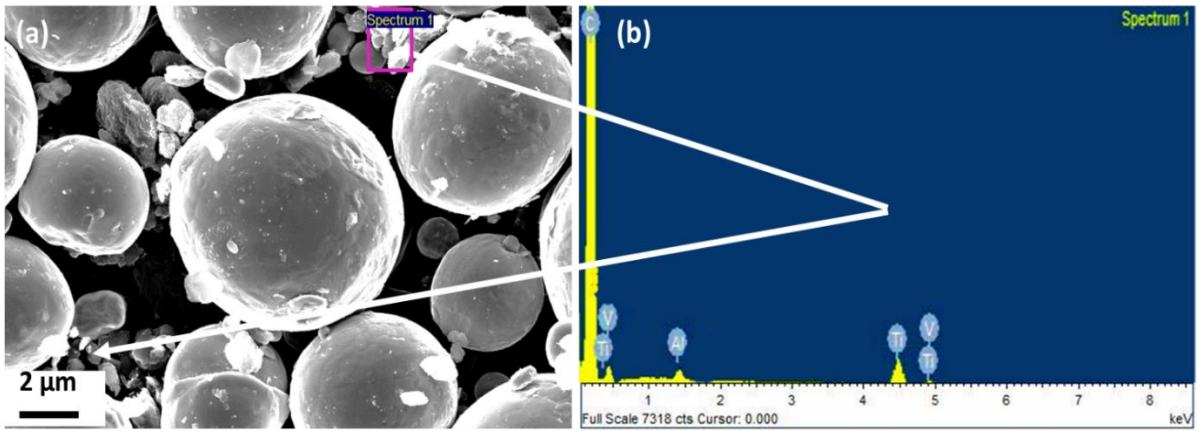

Fig. 4. Illustrates the high-resolution SEM image (a) and EDX (b) of MWCNT dispersed in Ti6Al4V powders by low-speed ball milling for 8 h

Furthermore, efforts were made to mill the admixed powders using HEBM to exert substantial impact energy on the powders to promote homogeneous dispersion, good interfacial bonding between the MWCNT and the TiAl4V powders and retainment of the tubular morphology of the MWCNT after dispersion. This further milling was carried out for 1 h in a high energy ball mill. Figure 5 shows the SEM images obtained for batch 1 processing with the microstructural evolution and dispersion features of the MWCNT in Ti6Al4V powders.

From the SEM images, it was observed that there was no significant difference in term of dispersion of the MWCNT in the Ti6Al4V particles when compared with the dispersion of MWCNT using only low-speed ball mill for 8 h. The MWCNT were segregated into the interstices of the Ti6Al4V because of poor dispersion and inadequate impact energy exerted on the powders to overcome the strong Van der Waals forces present in the MWCNT. However, some reasonable level of interfacial bonding was recorded which may not be satisfactory to improve the load carrying ability of the composite when consolidated. Since the primary aim of incorporating the MWCNT into the Ti6Al4V powders is to enhance the properties of the matrix material. The inset on Figure 5 (a) indicates clustered MWCNT and poor interfacial bonding between the MWCNT and the Ti6Al4V particles when observed in detail.

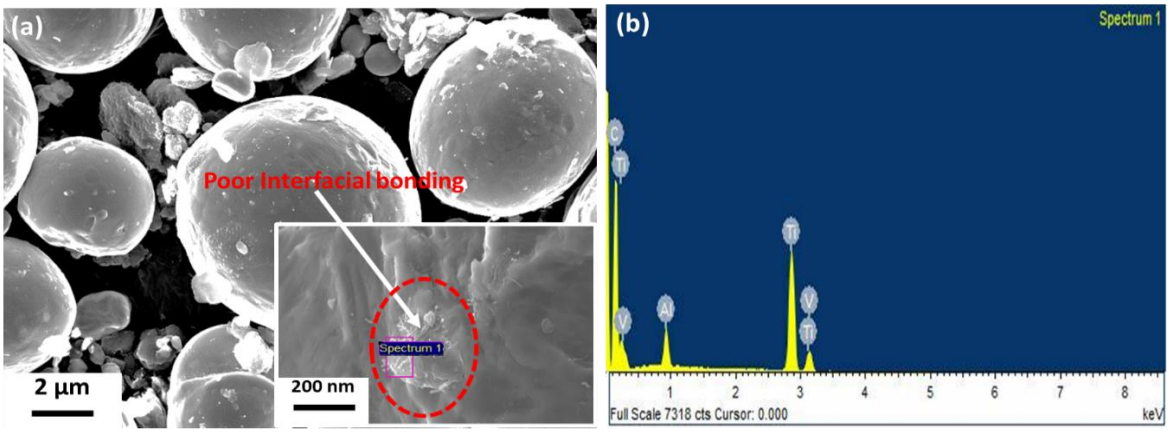

Fig.5. Illustrates the high-resolution SEM images (a) and EDX (b) of MWCNT dispersed in Ti6Al4V powders by SSBM using Batch 1

Similarly, batch 2 processing was carried out by preliminary dispersing 1.0 wt.% MWCNT in Ti6Al4V powders using low-speed ball mill for 8 h, and further milling was done using HEBM for 1 h. As shown in the SEM images, the inset in Figure 6 (a) shows the microstructural evolution, dispersion characteristics and interfacial bonding of the MWCNT in the Ti6Al4V powders after batch 2 processing. From the SEM images, a reasonable level of uniform dispersion of MWCNT in Ti6Al4V powders was recorded with accompanying good interfacial bonding between the powder mixture.

From all indications, there was a significant bonding and embedment of the MWCNT within the Ti6Al4V particles which shows good interfacial bonding between the powders. This dispersion characteristic is a function of the adequate impact energy exerted by the combined effect of low-speed ball milling for 8 h and additional high-speed ball milling for 1 h . It is assumed that the combined milling processes exerted significant impact energy on the powder mixtures that resulted in reasonable dispersion, and embedment of the MWCNT within the Ti6Al4V particles. Furthermore, the significant impact energy is appreciable enough to overcome the strong Van der Waals forces among the MWCNT, disentangle the agglomerated MWCNT seated in the interstices of the Ti6Al4V particles and adhere the nanotubes to the matrix particles. However, if the time of milling using the HEBM is extended, there are high possibilities of compromising the unique structure of the nanotubes.

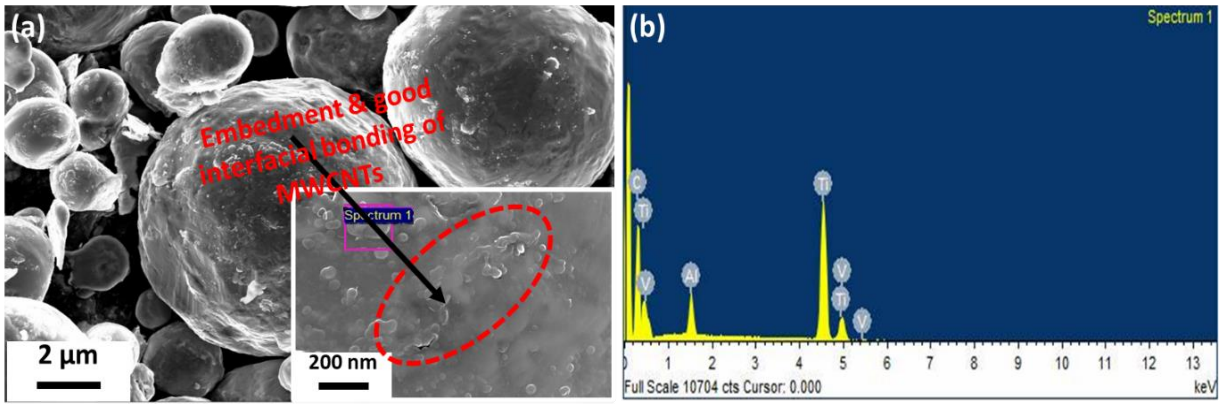

Fig.6. Illustrates the high-resolution SEM images (a) and EDX (b) of MWCNT dispersed in Ti6Al4V powders by SSBM using Batch 2

3.1.1 Mechanism of ball milling of MWCNT in Ti6Al4V using low-speed and high-speed ball mill

The adoption of ball milling technique in dispersing MWCNT into Ti6Al4V powders exerts several (compressive and shear) forces on the powders during the dispersion process. The intensity of the forces exerted on the charged materials is a function of the design of the mill and the adopted milling parameters. High-speed ball mill is designed to exert higher compressive and shearing forces on charged materials than low-speed ball mill which is illustrated in Figure 7 below.

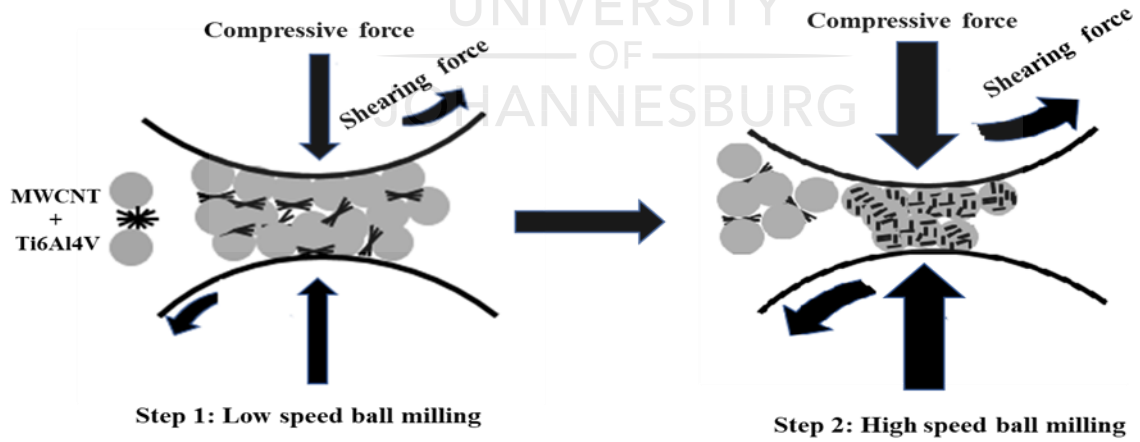

Fig.7. Illustrates the dispersion mechanism of MWCNT in Ti6Al4V using low-speed and high-speed ball milling techniques

This enormous force exerted by high-speed ball mill has the tendency to impose higher impact energy on materials that result in good dispersion of MWCNT but at the expense of the structural integrity

of the nanotubes. The total amount of impact energy exerted by the balls on charged materials is a function of the number of collision of a ball on the walls of the vial and/or on other balls [42]. The effectiveness of the collision is also dependent on the mass of the charged materials (M_s), the milling speed and the milling time. The total impact energy (E_i) during ball milling can be calculated using equation (1), where M_b denotes the mass of the balls, n represents the number of collision between milling balls or against the vial walls per seconds while M_s is the mass of the charged samples and v_j is the relative impact velocity of the balls [42]. Nevertheless, the impact velocity and the number of collisions during milling depends on the design of the milling machine.

$$E_i = \sum_{j=1}^{n} \frac{1}{2M_s} M_b {v_j}^2 \qquad (1)$$

Low-speed ball mill is designed to exert cascading motion of the balls on the powders while high-speed ball milling technique employs the cataracting motion of the balls on the powders [43]. Based on the design of the high-speed ball mill, it has the ability to exert centrifugal forces up to 20 times the gravitational acceleration on charged materials (powders and balls) [44]. These enormous centrifugal forces are usually triggered by the turning of the disc and the independent rotation of the vial on the charges. Since the vial and supporting disc usually moves in opposite directions, the induced centrifugal forces are usually reversed and synchronised [44]. Hence, the balls and the powders alternatively roll on the inner wall of the vial and undergo cataracting motion across the vial at a higher speed which exerts enormous impact energy on the charged materials.

Therefore, the charged materials during the shift speed ball milling of MWCNT in Ti6Al4V powders were subjected to considerable cascading for 8h and subsequent cataracting motion (which exert higher compressive and shear forces) on the powders that promoted the uniform dispersion of the MWCNT and excellent interfacial bonding between the powders.

3.2 Structural evolution and interfacial bonding of MWCNT in Ti6Al4V Powders

In a quest to confirm the interfacial bonding and structural features of the MWCNT after dispersion using the discussed processing batches, high-resolution transmission electron microscope and Raman spectroscopy were used to characterise the admixed powders.

3.2.1 TEM analysis of the dispersion characteristics, interfacial bonding and structural evolution of MWCNT in Ti6Al4V powders

The HRTEM Images in Figure 8 shows the morphology of MWCNT and the structural features after dispersion using batch 1 processing route. From HRTEM image on Figure 8 (a), it was observed that the MWCNT were not properly dispersed that segregated from the Ti6Al4V particles which are clear confirmation of the SEM result discussed in the previous section. This dispersion characteristic is because of insignificant impact energy exerted on the powders during dispersion which is unable to overcome the strong Van der Waals forces present among the MWCNT.

Figure 8 (b) is the selected area diffraction pattern of the MWCNT after dispersion, from the SAED pattern, it was observed that the coaxial and the halo rings were intact as the SAED pattern of the pristine MWCNT discussed in the previous section. Despite the impact energy exerted on the MWCNT during the dispersion process, the prominent graphite planes (002) and (100) were still observed. Also, the rings were entirely circular at these planes which depict lack of crystal defects and deformation (dislocation) to the walls of the MWCNT during dispersion. However, it is believed that the MWCNT were subjected to some level of insignificant strain during dispersion which may stretch their interplanar layers but could not reflect on the SAED patterns of the MWCNT after dispersion. In order to confirm if the interplanar layer of the MWCNT were strained after dispersion, the walls of the MWCNT were critically viewed under high-resolution TEM.

The HRTEM image for the walls of the MWCNT as shown in Figure 8 (c), indicates a slight stretch of the interlayer spacing of the MWCNT from 0.3461 in the pristine MWCNT to 0.3510 nm after dispersion. This is a clear indication that the adopted dispersion route subjected the walls of the MWCNT to some level of strain. However, this does not result in the formation of crystal defects which may have appeared as streaks and extra spots on the SAED pattern discussed earlier. The existence of streaks on the spot in the SAED pattern can arise as a result of precipitates formed (TiC), dislocations and twins on the MWCNT structure during processing [34]. Similarly, the fast Fourier transform image on Figure 8 (d) confirmed the new interlayer spacing of the MWCNT after dispersion via the batch 1 processing route. However, the FFT peaks have narrower tips which are an indication of the presence of crystalline carbon present in the MWCNT in spite of the dispersion route adopted. Therefore, no amorphous phases were formed in the MWCNT during dispersion in

Ti6Al4V powders via the batch 1 route.

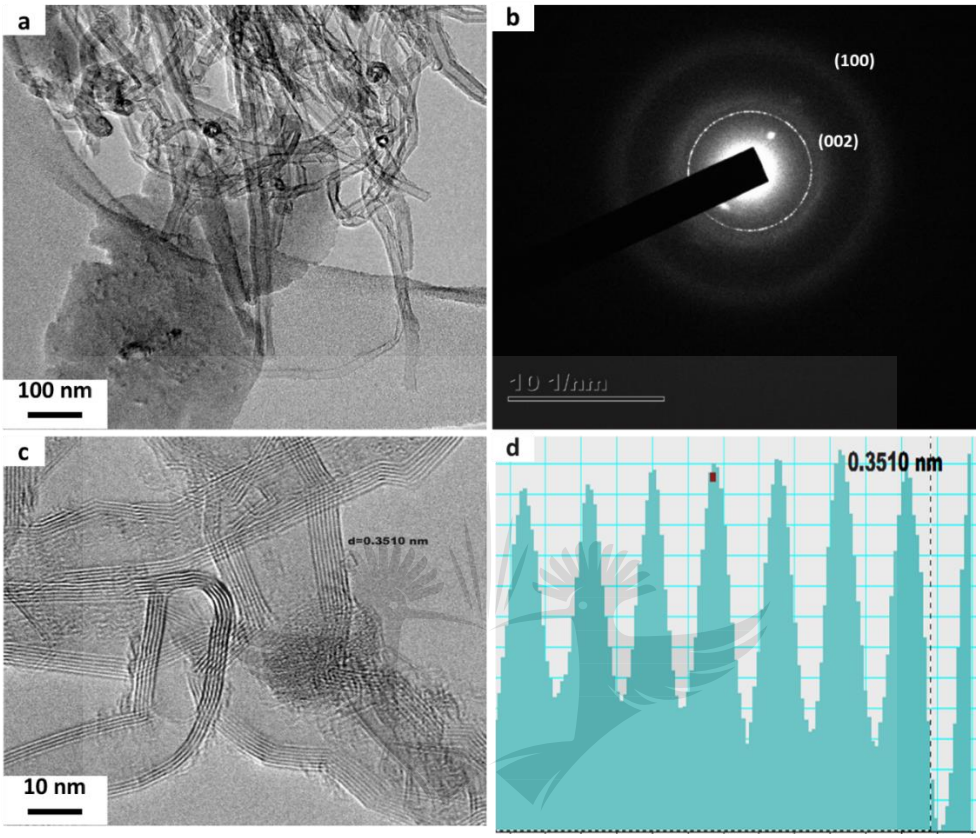

Fig.8. Illustrates the high-resolution TEM images (a & c), SAED (b) and FFT (d) of MWCNT dispersed in Ti6Al4V powders by SSBM using Batch 1

The HRTEM images of the admixed powders processed via batch 2 route are as shown in Figure 9 below. Figure 9 (a) shows the morphology of the dispersion of MWCNT in the Ti6Al4V particles and good interfacial bonding between the powders. This is as a result of the significant impact energy exerted on the powders during dispersion that overcame the strong Van der Waals forces of the MWCNT and embeds them to the Ti6Al4V particles. Additionally, this dispersion characteristic conforms with the SEM images discussed in the earlier section. Figure 9 (b) shows the SAED pattern of the MWCNT after dispersion via batch 2 route. From the SAED pattern, it was observed that the coaxial and halo rings were gradually fading out which is a clear indication of adequate strain on the graphite planes (002) and (100) during dispersion.

Furthermore, the rings were not fully concentric, and there was the formation of extra spots on the rings which may be as a result of crystal defects and dislocations on the MWCNT structure

during dispersion that leads to the presence of amorphous carbon that scatters electrons during diffraction. However, there was no indication of streaks on the spots formed within the coaxial and halo rings which usually exist when there is a severe accumulation of dislocations that deforms the crystal orientations of the MWCNT [34].

In a nutshell, the adequate impact energy on MWCNT during this processing route imposed a considerable strain on the walls of the nanotubes, but this is not capable of forming crystal defects in the MWCNT. The existence of streaks and extra spots in rings pattern is a clear indication of crystal defects that includes staking faults, different type of precipitates such as carbide phases (TiC) and dislocation in the material [34]. Streaks on spot or pseudo-satellites patterns are usually formed by stacking faults of quasi-sphere and rod-like particles of carbides (TiC in the case of CNT-Titanium and its alloys) in the materials. Furthermore, when a SAED pattern of MWCNT reinforced titanium-based pattern shows the formation of streaks on spots, it implies that titanium carbide phases have been formed in the composite material. This is, thus, an indication of the creation of crystal defect sites in the form of open edges and vacancies which consist of non-sp^2 defects in the C-C system of the MWCNT [29,38].

Similarly, from Figure 9 (c), the HRTEM image of the walls of the MWCNT after dispersion via the batch 2 processing route indicates further stretching of the interlayers of the MWCNT that increased the interlayer spacing from 0.3461 in the pristine MWCNT to 0.3521 nm after dispersion. The increase in interlayer spacing of the MWCNT is a result of the strain on the nanotubes due to prolong ball milling condition. However, this strain does not result in the formation of defect sites which usually exist as non-sp^2 defects on the nanotubes during severe milling conditions. Subsequently, the FFT peaks of the MWCNT was captured to confirm the crystalline nature of the MWCNT after dispersion. From Figure 9 (d) which show the FFT peaks, the new interlayer spacing of the MWCNT was confirmed. Nevertheless, there were narrower peaks which established the high degree of crystallinity of the carbon present in the MWCNT.

From all indications, the batch 2 route of dispersing MWCNT in Ti6Al4V powders is the most effective route where adequate impact energy was exerted on the powders that resulted in uniform dispersion and good interfacial bonding between the powder mixtures without compromising the structural integrity of the MWCNT.

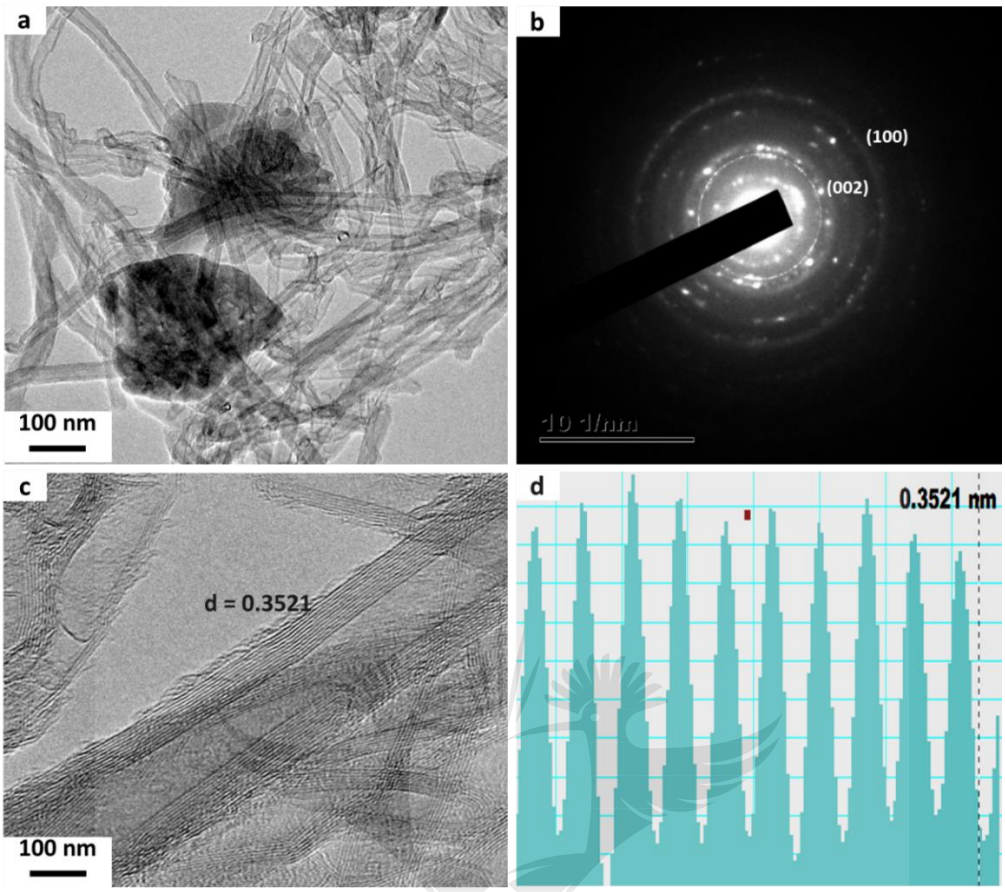

Fig.9. Illustrates high-resolution TEM images (a & c), SAED (b) and FFT (d) of MWCNT dispersed in Ti6Al4V powders by SSBM using Batch B

3.2.2 Raman spectroscopic analysis of MWCNT in Ti6Al4V powders.

The structural evolution of the MWCNT after dispersion in Ti6Al4V powders was investigated to ascertain the extent of the imposed strain on the structural integrity of the nanotubes during the different dispersion routes. Raman spectroscopy was used to characterise the pristine Ti6Al4V, MWCNT and the admixed powders from the two different dispersion routes. Figure 10 (a-d) shows the Raman spectra of the pristine and the admixed powders. It was observed that the spectra of the pristine Ti6Al4V do not depict any major Raman vibration peaks. This is because the Raman technique is usually adopted to ascertain the structural integrity of CNT when used as reinforcements to enhance materials properties during composites production [45].

Recent studies on Raman spectroscopy of MWCNT have highlighted that the D and G band are used to analyse the amount of deformation or structural strain to the nanotubes during dispersion in metal matrices. The D band is associated with sp3 defects in the C-C bonds of the MWCNT,

while the G band is related to the in-plane stretching mode of the C-C bonds in the nanotubes which determines the degree of graphitization, the orderliness of the carbon, metallicity and crystalline nature of the MWCNT [46][48].

Furthermore, the features of the intensity ratio (I_D/I_G) have been used as a suitable approach in previous studies to ascertain the level of crystallinity and damage to MWCNT during their incorporation into metal matrices for composite production. However, the reduction and broadening of the crystalline peak (G band) can be explained as stacking of disorder in the sp^2 C-C system of the MWCNT which may occur as open edges, vacancies and damaged walls [29,48]. The Raman spectra of the pristine MWCNT in Figure 10 (b) indicated the two major graphitic peaks which are narrower and sharper in the spectral range of 200-1800/cm at 1340 and 1580 /cm which corresponds to the characteristic D and G band respectively. From the Raman spectra in Figure 10 (b), the corresponding I_D/I_G ratio of the pristine MWCNT was calculated to be 0.800.

However, when 1.0 wt.% of the MWCNT was dispersed in Ti6Al4V powders using the batch 1 processing route, from Figure 10 (c), the characteristic Raman peaks of the MWCNT in the powder mixture became broadened and the G Band peak shifted to a higher wavenumber from 1580 cm^{-1} in the pristine MWCNT to 1586 cm^{-1} in the admixed powders. This Raman shift of the G band can be ascribed to the exerted stress on the walls of the MWCNT during the milling of the powders that resulted in some strain on the walls of the nanotubes. However, the level of structural strain formed on the MWCNT was not severe, and it is not capable of forming titanium carbide phases on the nanotubes which would have reflected as prominent peaks between 200 and 800 cm^{-1} on the Raman spectra of the powder mixture [49,50].

Furthermore, it was observed that the I_D/I_G ratio of the Raman spectra experienced a slight increased from 0.800 in the pristine MWCNT to 0.830 after dispersion using the batch 1 processing route which amounts to 3.85 %, this confirmed the extent of strain to the walls of the nanotubes after dispersion.

Similarly, the Raman spectra of the admixed powders processed via batch 2 route are shown in Figure 10 (d). From the Raman spectra, it was observed that the characteristic Raman peaks were more broadened and collapsed when compared with the Raman peak of the pristine MWCNT. Additionally, the G band experienced an enormous Raman shift to a higher wave number from 1580 cm^{-1} in the pristine MWCNT to 1588.4 cm^{-1} after dispersion. This incredible Raman shift is

ascribed to the high stress imposed on the MWCNT during dispersion in Ti6Al4V powders. As earlier discussed in the previous section, the dispersion of MWCNT using the batch 2 processing route, subjected considerable impact energy on the powders as a result of prolonging milling time which is capable of imposing structural strain to the MWCNT. Although the level of structural strain does not result in the formation of titanium carbide phase in the admixed powders, it increased the I_D/I_G ratio from 0.800 in the pristine MWCNT to 0.955 which amount to 19.38 % strain.

From all indications, the adopted dispersion method of MWCNT in Ti6Al4V powders resulted in the deformation (strain) of the walls of the nanotubes that increased the interlayer spacing of the MWCNT. However, the severity of the strain does not result in vacancies, open edge and broken walls of the nanotube which would have been potential sites for the formation of titanium carbide phases in the admixed powders.

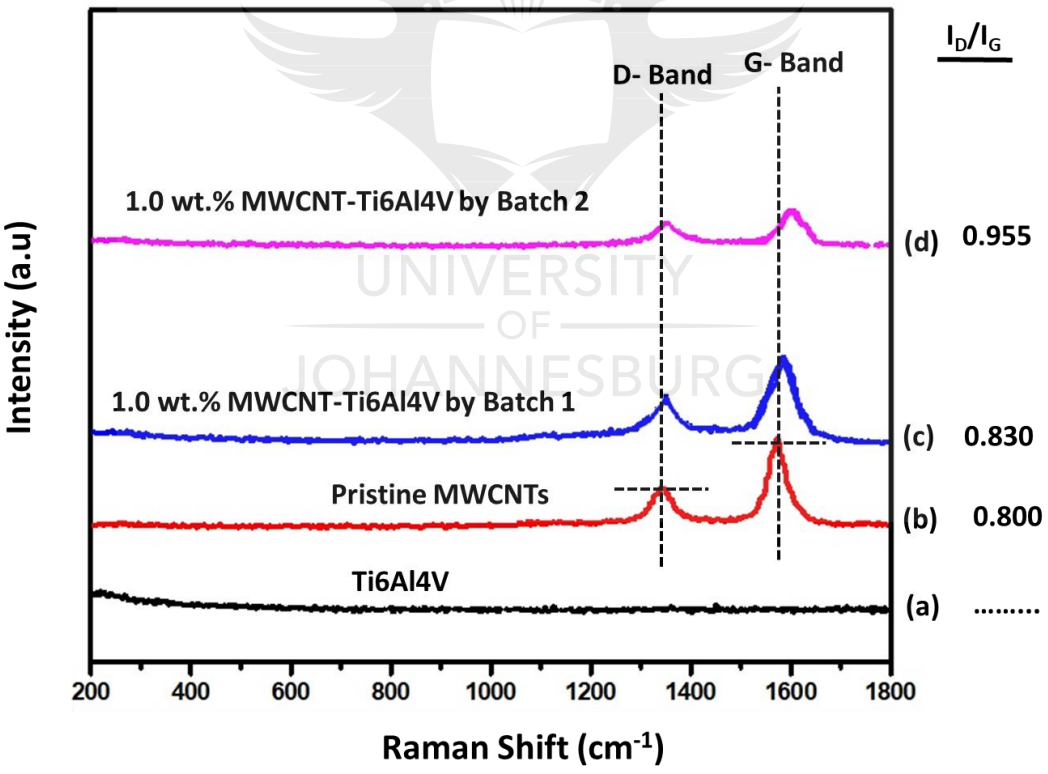

Fig.10. Raman spectra of starting powders and admixed MWCNT-Ti6Al4V composite powders (a) Pristine Ti6Al4V (b) Pristine MWCNT (c) 1.0 wt. % MWCNT-Ti6Al4V produced in batch 1 (d) and 1.0 wt. % MWCNT-Ti6Al4V produced in batch 2.

3.3 XRD analysis of the MWCNT-Ti6Al4V powders

X-ray diffraction technique was utilised to ascertain the phases present in the pristine powders and the evolution of the crystalline phases after dispersion. Figure 11 (a-d) indicates the XRD pattern of the pristine and admixed powders. From Figure 11 (a) which shows the XRD pattern of the pristine MWCNT, the two prominent graphitic peaks were observed at $2\theta = 25.64^{o}$ and 43.34^{o} which correspond to the plane of (002) and (100) respectively. Similarly, Figure 11 (b) shows the XRD pattern of the pristine Ti6Al4V powder, and it was observed that the various α titanium peaks were prominent at $2\theta = 35.48^{o}$,38.68^{o} ,40.52^{o}, 53.43^{o} , 63.85^{o} , 81.10^{o}, 86.92^{o} , 82.84^{o} and 88.42^{o} which corresponds to the planes (100), (002) , (101) , (102), (110), (103), (112), (004) and (202) respectively. It was observed that the β titanium peak was not visible in the XRD pattern. Figure 11 (c) shows the XRD pattern of the admixed powders processed via batch 1 route. From the XRD pattern, there were no prominent structural changes to the Ti6Al4V structure. However, the α titanium peaks were more pronounced, and this may be attributed to the strain on the Ti6Al4V powders during powder processing. Additionally, the incorporation of MWCNT into Ti6Al4V powders via the SSBM technique does not result in the formation of new phases in the admixed powders.

The XRD pattern in Figure 11 (c) of the admixed powders processed via the batch 2 route depicts a similar trend as the admixed powders in Figure 11 (b). However, the α titanium peaks were increased and more prominent. Furthermore, there was no trace of the MWCNT peaks in the XRD pattern of the admixed powders in both processing batches and this is attributed to low weight fraction (1.0 wt.%) of the MWCNT in the admixed powder and the substantial difference of the mass absorption coefficient (for Cu Kα radiations) of Ti and carbon (C) which are 208 and 4.6 m^2/g respectively [51]. From all indications on the XRD pattern of the admixed powders, it was observed that carbide phases were not formed which is in conformity with the SAED patterns and the Raman spectra of the admixed powders. Therefore, the adopted powder processing method in this study does not result in structural changes in the crystalline phases of the titanium alloy.

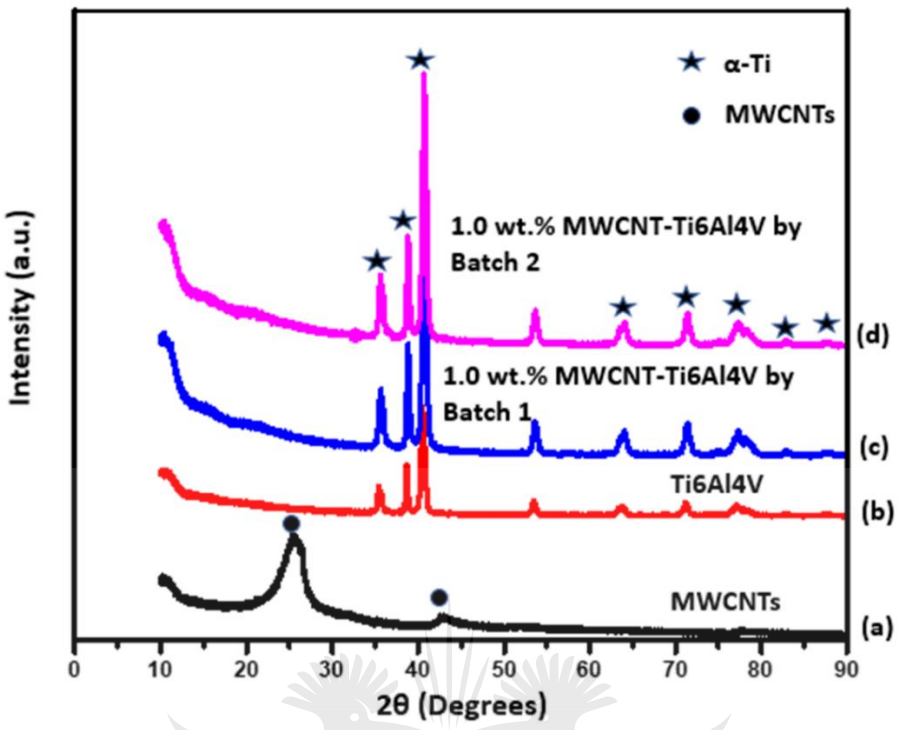

Fig. 11. XRD patterns of starting powders and admixed MWCNT-Ti6Al4V composite powders (a) Pristine MWCNT, (b) as-received Ti64, (c) 1.0 wt. % MWCNT-Ti6Al4V produced by batch 1 (d) and 1.0 wt. % MWCNT-Ti6Al4V produced by batch 2.

4. Conclusion

Shift speed ball milling of MWCNT and Ti6Al4V powders resulted in uniform dispersion of MWCNT alongside with good interfacial bonding of the nanotubes in the Ti6Al4V powders. This signifies that the dispersion technique is very effective during the dispersion of MWCNT in Ti6Al4V powders. Furthermore, the following conclusions were drawn from this study:

1. The SEM images confirmed that subsequent ball milling using HEBM after preliminary low-Speed ball milling resulted in homogeneous dispersion and good interfacial bonding of the MWCNT in the Ti6Al4V powders.
2. The HRTEM images, SAED patterns, and Raman spectra confirmed that shift speedball milling technique deformed the walls of the MWCNT during dispersion in Ti6Al4V powders.
3. The severity of the deformation that the powders underwent does not result in open edges, vacancies and broken walls of the MWCNT because there was no trace of TiC on the SAED patterns, Raman spectra and XRD pattern of the MWCNT.

4. The regulation of milling parameters minimizes the impact stresses on the MWCNT during dispersion in Ti6Al4V powders. However, adequate impact energy is expedient for homogeneous dispersion and excellent interfacial bonding of MWCNT in Ti6Al4V powders.

Acknowledgement

The authors would like to appreciate the National Research Foundation of South Africa in association with the World Academic of Science (NRF-TWAS) and Global Excellence and Stature for funding this research.

Reference

[1] B.S. Harrison, A. Atala, Carbon nanotube applications for tissue engineering, Biomaterials. 28 (2008) 344–353.

[2] A.K. Feldman, M.L. Steigerwald, X. Guo, C. Nuckolls, Molecular electronic devices based on single-walled carbon nanotube electrodes, Acc. Chem. Res. 41 (2008) 1831–1841.

[3] S.R. Bakshi, D. Lahiri, A. Agarwal, Carbon nanotube reinforced metal matrix composites - a review, Int. Mater. Rev. 55 (2010) 41–64. doi:10.1189/095066009X12582530180543.

[4] O.A. Ajiteru, T.S. Tshephe, A.M. Okoro, P.A. Olubambi, S. Lephuthing, M. Lesufi, Evaluation of the methods of dispersion of carbon nanotubes (CNTs) in titanium and its alloys: Literature review, in: Mech. Intell. Manuf. Technol. (ICMIMT), 2018 IEEE 9th Int. Conf., IEEE, 2018: pp. 50–53.

[5] A. Esawi, K. Morsi, Dispersion of carbon nanotubes (CNTs) in aluminum powder, 38 (2008) 646–650. doi:10.1016/j.compositesa.2006.04.006.

[6] B.G. Demczyk, Y.M. Wang, J. Cumings, M. Hetman, W. Han, A. Zettl, R.O. Ritchie, Direct mechanical measurement of the tensile strength and elastic modulus of multiwalled carbon nanotubes, Mater. Sci. Eng. A. 334 (2002) 183–188.

[8] R.S. Ruoff, D. Qian, W.K. Liu, Mechanical properties of carbon nanotubes: theoretical predictions and experimental measurements, Comptes Rendus Phys. 4 (2003) 993–1008.

[8] K.S. Munir, Y. Li, D. Liang, M. Qian, W. Xu, C. Wen, Effect of dispersion method on the deterioration, interfacial interactions and re-agglomeration of carbon nanotubes in titanium metal matrix composites, Mater. Des. 88 (2015) 138–148. doi:10.1016/j.matdes.2015.08.112.

[9] K. Kondoh, T. Threrujirapapong, H. Imai, J. Umeda, B. Fugetsu, Characteristics of powder metallurgy pure titanium matrix composite reinforced with multi-wall carbon nanotubes, Compos. Sci. Technol. 69 (2009) 1088–1081. doi:10.1016/j.compscitech.2009.01.026.

[10] W. Zhou, S. Bang, H. Kurita, T. Miyazaki, Y. Fan, A. Kawasaki, Interface and interfacial reactions in multi-walled carbon nanotube-reinforced aluminum matrix composites, Carbon

N. Y. 96 (2016) 919–928. doi:10.1016/j.carbon.2015.10.016.

[11] J. Liao, M.-J. Tan, I. Sridhar, Spark plasma sintered multi-wall carbon nanotube reinforced aluminum matrix composites, Mater. Des. 31 (2010) S96--S100.

[12] F. Ostovan, K.A. Matori, M. Toozandehjani, A. Oskoueian, H.M. Yusoff, R. Yunus, A.H. Mohamed Ariff, H.J. Quah, W.F. Lim, Effects of CNTs content and milling time on mechanical behavior of MWCNT-reinforced aluminum nanocomposites, Mater. Chem. Phys. 166 (2015) 160–166. doi:10.1016/j.matchemphys.2015.09.041.

[13] K.S. Prakash, T. Thankachan, R. Radhakrishnan, Parametric optimization of dry sliding wear loss of copper--MWCNT composites, Trans. Nonferrous Met. Soc. China. 28 (2018) 628–638.

[14] N. Selvakumar, K. Gangatharan, Electrical resistivity, tribological behaviour of multiwalled carbon nanotubes and nanoboron carbide particles reinforced copper hybrid composites for pantograph application, Adv. Mater. Sci. Eng. 2016 (2016).

[15] Y. Chen, Y. Mao, J. Xie, Z. Zhan, L. Yu, Microstructure and microwave absorption properties of MWCNTs reinforced magnesium matrix composites fabriccated by FSP, Optoelectron. Lett. 13 (2018) 1–4.

[16] S.V. Bhaskar, T. Rajmohan, K. Palanikumar, B.B.G. Kumar, Synthesis and Characterization of Multi Wall Carbon Nanotubes (MWCNT) Reinforced Sintered Magnesium Matrix Composites, J. Inst. Eng. Ser. D. 98 (2016) 59–68.

[18] K.S. Munir, Y. Li, M. Qian, C. Wen, Identifying and understanding the effect of milling energy on the synthesis of carbon nanotubes reinforced titanium metal matrix composites, Carbon N. Y. 99 (2016) 384–398. doi:10.1016/j.carbon.2015.12.041.

[18] A.O. Adegbenjo, P.A. Olubambi, J.H. Potgieter, M.B. Shongwe, M. Ramakokovhu, Spark plasma sintering of graphitized multi-walled carbon nanotube reinforced Ti6Al4V, Mater. Des. 128 (2018) 119–129. doi:10.1016/j.matdes.2018.05.003.

[19] C. Leyens, M. Peters, Titanium and titanium alloys: fundamentals and applications, John Wiley & Sons, 2003.

[20] R. Machaka, Effects of Carbon Nanotubes on the Mechanical Properties of Spark Plasma Sintered Titanium Matrix Composites-A Review, (n.d.).

[21] V.A.R. Henriques, P.P. de Campos, C.A.A. Cairo, J.C. Bressiani, Production of titanium alloys for advanced aerospace systems by powder metallurgy, Mater. Res. 8 (2005) 443–446.

[22] A. Dorri Moghadam, E. Omrani, P.L. Menezes, P.K. Rohatgi, Mechanical and tribological properties of self-lubricating metal matrix nanocomposites reinforced by carbon nanotubes (CNTs) and graphene - A review, Compos. Part B Eng. 88 (2015) 402–420. doi:10.1016/j.compositesb.2015.03.014.

[23] A.M.K. Esawi, K. Morsi, A. Sayed, M. Taher, S. Lanka, Effect of carbon nanotube (CNT) content on the mechanical properties of CNT-reinforced aluminium composites, Compos. Sci. Technol. 80 (2010) 2238–2241. doi:10.1016/j.compscitech.2010.05.004.

[24] S.S. Lephuthing, A.M. Okoro, M. Lesufi, O.O. Ige, P.A. Olubambi, Effect of milling parameters on the dispersion characteristics of multi-walled carbon nanotubes in transition metal oxides, in: IOP Conf. Ser. Mater. Sci. Eng., 2018: p. 12002.

[25] K. Morsi, A. Esawi, Effect of mechanical alloying time and carbon nanotube (CNT) content on the evolution of aluminum (Al)--CNT composite powders, J. Mater. Sci. 42 (2008) 4954–4959.

[26] Z.Y. Liu, S.J. Xu, B.L. Xiao, P. Xue, W.G. Wang, Z.Y. Ma, Effect of ball-milling time on mechanical properties of carbon nanotubes reinforced aluminum matrix composites, Compos. Part A Appl. Sci. Manuf. 43 (2012) 2161–2168.

[28] A.M. Okoro, S.S. Lephuthing, S.R. Oke, O.E. Falodun, M.A. Awotunde, P.A. Olubambi, A Review of Spark Plasma Sintering of Carbon Nanotubes Reinforced Titanium-Based Nanocomposites: Fabrication, Densification, and Mechanical Properties, JOM. (n.d.) 1–18.

[28] F. Ostovan, K.A. Matori, M. Toozandehjani, A. Oskoueian, H.M. Yusoff, R. Yunus, A.H. Mohamed Ariff, Nanomechanical behavior of multi-walled carbon nanotubes particulate reinforced aluminum nanocomposites prepared by ball milling, Materials (Basel). 9 (2016)

140.

[29] A.M. Okoro, R. Machaka, S.S. Lephuthing, M. Awotunde, P.A. Olubambi, Structural integrity and dispersion characteristics of carbon nanotubes in titanium-based alloy, in: IOP Conf. Ser. Mater. Sci. Eng., 2018: p. 12004.

[30] R. Xu, Z. Tan, D. Xiong, G. Fan, Q. Guo, J. Zhang, Y. Su, Z. Li, D. Zhang, Balanced strength and ductility in CNT/Al composites achieved by flake powder metallurgy via shift-speed ball milling, Compos. Part A Appl. Sci. Manuf. 96 (2018) 58–66.

[31] E.W. Wong, P.E. Sheehan, C.M. Lieber, Nanobeam mechanics: elasticity, strength, and toughness of nanorods and nanotubes, Science (80-.). 288 (1998) 1981–1985.

[32] P.S.R. Sreekanth, K. Acharyya, I. Talukdar, S. Kanagaraj, Studies on structural defects on 60Co irradiated multi walled carbon nanotubes., Procedia Mater. Sci. 6 (2014) 1968–1985.

[33] T. Characterization, CHAPTER Acylation of Carbon Nanotubes by Chemical Route and Their Characterization, (n.d.) 105–125.

[34] M.A. Asadabad, M.J. Eskandari, Electron diffraction, in: Mod. Electron Microsc. Phys. Life Sci., InTech, 2016.

[35] J.H. Lehman, M. Terrones, E. Mansfield, K.E. Hurst, V. Meunier, Evaluating the characteristics of multiwall carbon nanotubes, Carbon N. Y. 49 (2011) 2581–2602. doi:10.1016/j.carbon.2011.03.028.

[36] K.S. Munir, Y. Zheng, D. Zhang, J. Lin, Y. Li, C. Wen, Microstructure and mechanical properties of carbon nanotubes reinforced titanium matrix composites fabricated via spark plasma sintering, Mater. Sci. Eng. A. 688 (2018) 505–523. doi:10.1016/j.msea.2018.02.019.

[38] K.S. Munir, Y. Zheng, D. Zhang, J. Lin, Y. Li, C. Wen, Improving the strengthening efficiency of carbon nanotubes in titanium metal matrix composites, Mater. Sci. Eng. A. 696 (2018) 10–25. doi:10.1016/j.msea.2018.04.026.

[38] K.S. Munir, Y. Li, J. Lin, C. Wen, Interdependencies between graphitization of carbon nanotubes and strengthening mechanisms in titanium matrix composites, Materialia. (2018).

[39] A. Nouri, C. Wen, Surfactants in mechanical alloying/milling: a catch-22 situation, Crit. Rev. Solid State Mater. Sci. 39 (2014) 81–108.

[40] B. Rodriguez, A. Bruckmann, C. Bolm, A highly efficient asymmetric organocatalytic aldol reaction in a ball mill, Chem. Eur. J. 13 (2008) 4810–4822.

[41] F. Schneider, A. Stolle, B. Ondruschka, H. Hopf, The Suzuki- Miyaura reaction under mechanochemical conditions, Org. Process Res. Dev. 13 (2008) 44–48.

[42] H. Mio, J. Kano, F. Saito, K. Kaneko, Optimum revolution and rotational directions and their speeds in planetary ball milling, Int. J. Miner. Process. 84 (2004) S85--S92.

[43] C.F. Burmeister, A. Kwade, Process engineering with planetary ball mills, Chem. Soc. Rev. 42 (2013) 8660–8668.

[44] M.S. El-Eskandarany, The history and necessity of mechanical alloying. Mechanical Alloying, (2015).

[45] B.H. Lohse, A. Calka, D. Wexler, Raman spectroscopy as a tool to study TiC formation during controlled ball milling, J. Appl. Phys. 98 (2005) 114912.

[46] A.C. Ferrari, Raman spectroscopy of graphene and graphite: disorder, electron--phonon coupling, doping and nonadiabatic effects, Solid State Commun. 143 (2008) 48–58.

[48] P. Delhaes, M. Couzi, M. Trinquecoste, J. Dentzer, H. Hamidou, C. Vix-Guterl, A comparison between Raman spectroscopy and surface characterizations of multiwall carbon nanotubes, Carbon N. Y. 44 (2006) 3005–3013.

[48] K.S. Munir, D.T. Oldfield, C. Wen, Role of Process Control Agent in the Synthesis of Multi-Walled Carbon Nanotubes Reinforced Titanium Metal Matrix Powder Mixtures, Adv. Eng. Mater. 18 (2016) 294–303. doi:10.1002/adem.201500346.

[49] B.H. Lohse, A. Calka, D. Wexler, Raman spectroscopy sheds new light on TiC formation during the controlled milling of titanium and carbon, J. Alloys Compd. 434 (2008) 405–409.

[50] M. V Klein, J.A. Holy, W.S. Williams, Raman scattering induced by carbon vacancies in Ti C x, Phys. Rev. B. 18 (1988) 1546.

[51] L.L. Ye, M.X. Quan, Synthesis of nanocrystalline TiC powders by mechanical alloying, Nanostructured Mater. 5 (1995) 25–31.

Ceramics International 45 (2019) 19864–19878

Contents lists available at ScienceDirect

Ceramics International

journal homepage: www.elsevier.com/locate/ceramint

Evaluation of the sinterability, densification behaviour and microhardness of spark plasma sintered multiwall carbon nanotubes reinforced Ti6Al4V nanocomposites

Avwerosuoghene Moses Okoro[a,*], Ronald Machaka[b], Senzeni Sipho Lephuthing[a], Samuel Ranti Oke[a], Mary Ajimegoh Awotunde[a], Peter Apata Olubambi[a]

[a] Centre for Nanoengineering and Tribocorrosion, Department of Metallurgy, School of Mining, Metallurgy and Chemical Engineering, University of Johannesburg, South Africa
[b] Council for Scientific and Industrial Research, Pretoria, South Africa

ARTICLE INFO

Keywords:
Multiwall carbon nanotubes
Titanium alloys
Densification behaviours
Sinterability
Microhardness

ABSTRACT

Structural and industrial demands for lightweight engineering materials with exclusive properties have been rising in recent decades for automobile and aerospace applications. This has encouraged various innovations in materials engineering communities to synthesis advanced engineering materials using improved fabrication technique such as spark plasma sintering (SPS). In this study, titanium-based nanocomposites were synthesized by reinforcing Ti6Al4V reinforced with (0.5, 1.0 and 1.5 wt%) multiwall carbon nanotubes (MWCNT) powders. The starting powders were blended by shift-speed ball milling. Thereafter, SPS technique was used to consolidate the admixed powders by employing the following sintering parameters; sintering rate, 100 °C/min, compressive pressure, 50 MPa, holding time, 10 min and sintering temperatures of 900–1100 °C. The influence of MWCNT additions on the sinterability, densification behaviours and microhardness of the sintered nanocomposites were investigated. The results revealed that the densification of the sintered nanocomposites was in the range of 97.51–99.61% which decreased with an increase in concentration of the MWCNT. Meanwhile, the densification and microhardness improved tremendously with an increase in sintering temperatures.

Paper 3: Evaluation of the sinterability, densification behaviour and microhardness of spark plasma sintered multiwall carbon nanotubes reinforced Ti6Al4V nanocomposites

Status: Published in Ceramics International 45(16), pp.19864-19878

https://doi.org/10.1016/j.ceramint.2019.06.242

Abstract

Structural and industrial demands for lightweight engineering materials with exclusive properties have been rising in recent decades for automobile and aerospace applications. This has encouraged various innovations in materials engineering communities to synthesis advanced engineering materials using improved fabrication technique such as spark plasma sintering (SPS). In this study, titanium-based nanocomposites were synthesized by reinforcing Ti6Al4V reinforced with (0.5, 1.0 and 1.5 wt.%) multiwall carbon nanotubes (MWCNT) powders. The starting powders were blended by shift-speed ball milling. Thereafter, SPS technique was used to consolidate the admixed powders by employing the following sintering parameters; sintering rate, 100 ^{o}C/min, compressive pressure, 50 MPa, holding time, 10 min and sintering temperatures of 900-1100 ^{o}C. The influence of MWCNT additions on the sinterability, densification behaviours and microhardness of the sintered nanocomposites were investigated. The results revealed that the densification of the sintered nanocomposites was in the range of 97.51-99.61% which decreased with an increase in concentration of the MWCNT. Meanwhile, the densification and microhardness improved tremendously with an increase in sintering temperatures.

Keywords: Multiwall carbon nanotubes; Titanium alloys; Densification behaviours; Sinterability; Microhardness.

1. Introduction

The emergence of new technologies in fabricating advanced materials with high performance-ability and safety for diverse engineering applications have revolutionized research across materials science and engineering fields. This has encouraged the utilization of novel technologies such as spark plasma sintering (SPS) in fabricating advanced materials.

Since the invention of SPS by Sumitomo Coal Mining Co. Ltd in Japan in 1989 [1], it has spurred great attention in the fabrication of various advanced materials ranging from functionally graded

materials (FGM), fine ceramics, advanced composites, biomaterials, thermo-electric conductors and highly densified nanostructured materials [1]. Additionally, it is an advanced powder sintering technique with numerous advantages over conventional sintering processes such as hot pressing, hot isostatic pressing, pressureless sintering and the others [2]. It has an improved heating mechanism which includes lower sintering temperature and cooling time, fast sintering process as a result of its exceedingly great heating rate tendencies up to 1000 oC/min and excellent heat distribution on compacted materials at both macroscopic and microscopic level [3–5]. The major advantage of this technique over other conventional sintering technique is that high densification can be achieved within a limited sintering time [2,6].

During the SPS process, the uniaxial compression forces from the graphite punches aid the removal of pores from the compacted material, promotes the diffusion of atoms and the necking of particles. The graphite die triggers the transfer of heat from the graphite mould to the compacted materials, thereby activating the rapid heating of samples and the fast sintering process. Additionally, the spark discharge and the produced plasma during the initial stage of SPS promotes the elimination of trapped gases present in the compacted material [7].

The continuous demand for advanced materials with exclusive properties for various engineering applications has engendered the utilization of SPS in the fabrication of advanced alloys and composites. In recent years, this sintering technique has been effectively utilized in the fabrication of various materials with enhanced mechanical, thermal and electrical properties. These materials range from metallic-based composites [8,9], alloys [10,11], polymers [12,13], and ceramics [14,15]. Among these materials, the demands for metallic-based composites with exceptional properties for aerospace, biomedical and automobile applications have grown in recent times. This has redirected research attention into the fabrication of aluminium, titanium and other lightweight metallic based composites using SPS.

Over the years, the use of titanium and its alloys in aerospace, biomedical, marine and automobile industries have attracted much research attention due to their exclusive mechanical properties, high corrosion resistance, high melting point, lightweight and biocompatibility [16–18]. Although they possessed low elastic modulus, low wear resistance and relatively low hardness when compared with super-duplex stainless steel and nickel-based alloys [16,19]. Furthermore, the weak stiffness and

wear resistance of titanium and its alloys have limited their application in high-temperature environments owing to their ease of oxidation at elevated temperature [20].

In a bid to augment the properties of titanium and its alloys, various research efforts have been made where particulates and fibres of different ceramic-based materials were used as a reinforcing phase to synthesize titanium-based composites. However, both the choice of reinforcing phases and fabrication technique have tremendous effects on the properties of the resulting titanium-based composites. This was confirmed by Falodun et al. [5] that achieved over 55% improvement in microhardness of Ti6Al4V by the addition of TiCN and TiN as reinforcements. Similarly, Kondoh et al. [21] fabricated titanium nanocomposites using SPS technique at 800 ^{o}C. They achieved about 19.1%, 34.1%, 5.2% and 6% improvement in tensile strength, yield strength, percentage elongation and microhardness respectively after reinforcing pure titanium metal with 0.24 wt.% multiwall carbon nanotubes (MWCNT).

Recent advancement in materials science and engineering have fostered the fabrication of nanostructured materials for various engineering applications. Nanomaterial such as MWCNT are at the highpoint of materials used as the reinforcing phase for augmenting the properties of titanium and its alloys. Moreover, they are known for their exceedingly great strength of up to 150 GPa, high young modulus in the range of 1 TPa, lightweight (1.7-2.0 g/cm^3) and ultra-high aspect ratios between 100-100000 [22,23]. The exclusive properties of MWCNT are ascribed to their graphitic network of the carbon atoms in their outer shells, quasi-one-dimensional structure, their tubular morphology and the rigid C-C bonds in their shells [24,25].

The quest to improve the properties of titanium and its alloys for various advanced engineering applications have prompted the integration of MWCNT into titanium-based matrices. However, to transfer the unique properties of the MWCNT into the titanium-based matrices requires the effective dispersion of the nanotubes into the matrix material since MWCNT has the tendencies to agglomerate into clusters during the synthesis of the composites [20]. Also, the dispersion features of MWCNT are linked to the great Van der Waals forces between its tubes, nanoscale dimensions and the ultra-high aspect ratio which affects the ease of dispersion of these nanotubes in various matrices [20]. Nevertheless, there is a tendency of compromising the exclusive properties of the nanotubes by the destruction of their structures when adverse dispersion techniques are used [26]. Therefore, it is

paramount to utilize an effective dispersion method to overcome the strong Van der Waals forces without compromising the structural integrity during composites production.

Apart from using the SPS technique in fabricating nanostructured materials, it is expedient to employ optimized sintering parameters to achieve full densification and improved mechanical properties after sintering. In recent years, various research attempts have been made to understand the effects of different sintering parameters during the fabrication of titanium-based nanocomposites. It was reported by Debalina et al. [27] that the densification of titanium-based nanocomposites improved with the increase in sintering temperature. The improvement of density was ascribed to the considerable grain growth that occurred during sintering at higher temperature which filled up micropores present in the compacted material. Similarly, Munir et al. [28] confirmed that the densification and hardness of sintered titanium-based nanocomposites increased with sintering temperature.

Past studies have highlighted the influence of sintering parameters on the densification of sintered titanium-based nanocomposites reinforced with MWCNT. To the best of our knowledge, no research output has explained the mechanisms that take place during the sintering of Ti6Al4V nanocomposites reinforced with MWCNT and how the mechanisms affect the densification and mechanical properties of the nanocomposites. Therefore, this work focuses on the densification, sintering behaviour and microhardness of titanium-based nanocomposites and how the additions of MWCNT affect the densification of the sintered nanocomposites during SPS.

2. Materials and Method

2.1. Starting materials

MWCNT powders utilized for this research were outsourced from Nanocyl Belgium, and it has a high percentage purity of ~99.7 and a length of 1.5 mm and 9.5 nm diameter. Also, argon atomized prealloyed titanium (Ti6Al4V) powders were acquired from TLS Technik GmbH & Co. Germany. This titanium alloy was used as the matrix material and stearic acid acquired from Glassblown & Volumetric Glassware & Chemicals in Johannesburg, South Africa was utilized as process control agent during the milling of the powders.

2.2. Milling of starting powders using shift speed ball milling technique

The MWCNT of various weight fractions (0.5, 1.0 and 1.5 wt.%) were measured alongside the Ti6Al4V powders and 1.0 wt.% stearic acid. The measured powders were charged alongside with steel ball of 10 and 5 mm into a steel vial of 250 mm outer diameter and 100 mm inner diameter. The steel vial was transferred into a low-speed ball mill (Retch 100 PM, Germany) where preliminary milling operations were carried out to foster the dispersion of the MWCNT into the Ti6Al4V powders. The milling parameters used for this preliminary milling operation were; the speed of 150 revolutions per minute (rpm), time of 8 hours (h) and ball to powder ratio (BPR) of 10:1. Various sizes of steel balls were used for the milling of the powders to prevent cold welding and promote effective collision of the balls on the powders. Furthermore, the milling was carried out with a relaxation time of 10 min for every 10 min of milling to prevent the powders from overheating which will eventually promote the interfacial reaction between the powders during the milling operation. Subsequently, the pre-milled powders were charged into another steel vial alongside with steel balls (5 and 10 mm) with a BPR of 10:1. Thereafter, the vial was transferred into a high energy ball mill (Retsch 400 PM, Germany) for further milling operation which was performed at a speed of 100 rpm for 1 h. The further milling operation was carried out to foster the effective dispersion of MWCNT in the titanium alloy and achieve good interfacial bonding between the matrix and the reinforcement. The schematic diagram of the dispersion process is shown below in Figure 1.

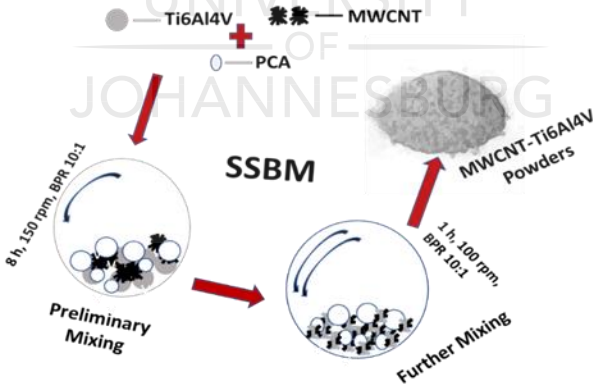

Figure 1. Schematic diagram of the preparation of the composite powders using shift speed ball milling technique (SSBM) [20]

2.3. Fabrication of the Ti6Al4V and nanocomposites using SPS technique

The milled powders were measured and charged into a graphite die of 20 mm diameter and cold compacted with a force of 10 KN to impact the powders with green strength and aid good

conductivity between the powders and the graphite die. The compacted composite powders were then placed into the sintering chamber of the SPS (model HHPD-25, FCT Germany) for sintering operation. A schematic diagram of the SPS equipment is illustrated in Figure 2 below. Furthermore, the sintering was carried out by utilizing the following parameters; compressive pressure of 50 MPa, at a heating rate of 100 ^{o}C/min with a holding time of 10 min and sintering temperature of 900-1100 ^{o}C. Post sintering, the sample was left to cool in the sintering chamber and then sandblasted to remove the graphite foils from the sample surface. The sintering data generated were later acquired and evaluated to understand the sintering behaviour during SPS.

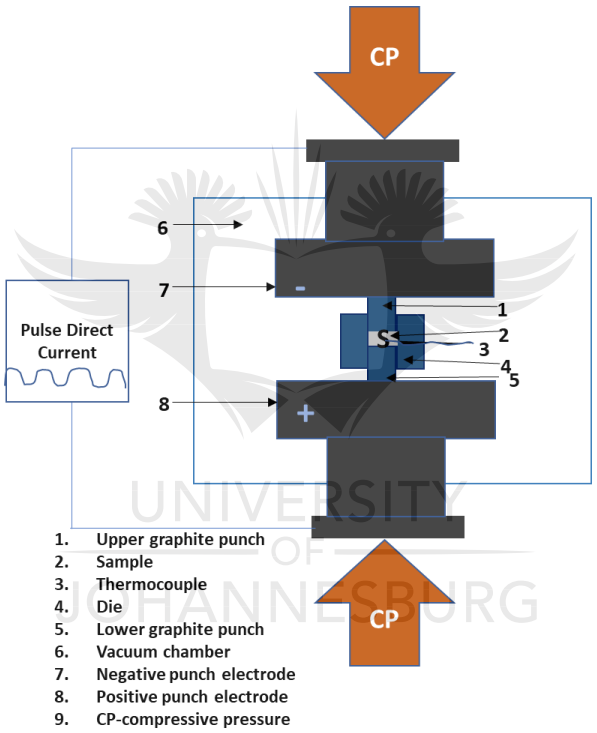

Figure 2. Schematic diagram of the SPS technique

2.4. Characterization of as-received, admixed powders and sintered MWCNT-Ti6Al4V nanocomposites

In a bid to understand the morphology of the starting powders (Ti6Al4V & MWCNT) and the admixed powders after the milling operations, scanning electron microscope (Carl Zeiss Sigma FESEM) equipped with energy dispersive X-ray spectrometry (EDX) and the JOEL-Jem 2100 transmission electron microscope (TEM) were used. TEM was also used to evaluate the walls of the

as-received MWCNT to understand the structural integrity of the nanotubes before the dispersion in the Ti6Al4V matrix. Additionally, TEM was used to capture the fast Fourier transform (FFT) of the as-received MWCNT to confirm the interlayer spacing and the crystalline nature of the nanotubes.

The structural integrity of the as-received MWCNT and the admixed powders were also investigated using Raman spectroscopy (WITEC 2.0). The Raman spectra obtained were in the spectral range of 200-1800 cm^{-1} of the as-received MWCNT and admixed powder on ten different spots on the material with an acquisition of 50 s using a 514 nm laser beam. Subsequently, the intensity of Raman peaks and their corresponding positions were acquired by deconvoluting the Raman spectra into two Gaussian peaks using WITec 2.10 software. The Raman shifts of the D and G band were calibrated in accordance with ASTM E1840-96 [29].

Additionally, X-Ray diffractometer (XRD, Rigaku D/max-rB) was utilized to identify the phase evolution of the starting, admixed powders, and the sintered nanocomposites to understand the phases formed during the processing and sintering of the nanocomposites. This was carried out by scanning the materials with Cu-Kα (λ= 0.154 nm) radiation at a rate of 1 o/min over the angular range of 10-90^{o}. Meanwhile, the ICDD card was used as the reference data for phase identification and analysis.

Subsequently, metallographic preparation was carried out on the sintered nanocomposites where SiC papers of different grit grade (P320-1200) were used for grinding the samples. This was accompanied by polishing with a 6 µm and 2 µm suspension and lastly, fused silica suspension was used to obtain a mirror-like surface of the samples. Thereafter, SEM analysis was performed to investigate the morphology of the sintered samples.

2.5. Density measurement and microhardness test of the sintered Ti6Al4V and MWCNT-Ti6Al4V nanocomposites

The densification of the nanocomposites was ascertained from the theoretical density of the composite mixtures and the quantity of powders used for the milling and sintering operation. The theoretical densities of the starting powders is Ti6Al4V (4.43 g/cm^3) and MWCNT (2.11 g/cm^3), through substituting these values into equation (1) and (2), the theoretical density of the nanocomposites were easily calculated.

$$Q = D_t \pi h r^2 \quad (1)$$

$$\frac{1}{D_c} = \frac{W_m}{D_m} + \frac{W_r}{D_r} \quad (2)$$

From equation (1), Q signifies the quantity of powders in gram charged into the die, and this was computed from the following parameters; D_t, the theoretical density (4.43 g/cm^3) of the powder, h, the estimated height of the sintered sample and r which is the radius of the sintered sample. Additionally, the theoretical density of each of the composite samples were computed from the application of equation (2). From equation (2), D_c represents the calculated theoretical density of the composite, D_m is the theoretical density of the Ti6Al4V matrix, D_r is the theoretical density of the MWCNT reinforcement. While W_m and W_r are the weight fraction of the matrix (Ti6Al4V) and reinforcement (MWCNT) respectively, the density of the sintered samples was evaluated in accordance to ASTM B962 using the Archimedes' principle. While the experimental density was measured by taking the arithmetic mean of five different readings for each sample, the densification of the samples was further calculated by using equation (3).

$$Densification\ (\%) = \frac{Average\ Experimental\ density}{Theoretical\ density} \times 100 \quad (3)$$

Similarly, the microhardness of the sintered nanocomposites was measured by carrying out a Vickers test using a FALCON 500 series microhardness tester. This was achieved by indenting the polished surface of the nanocomposite samples with a diamond indenter load of 100 gf (0.98 N) at dwelling time of 10 s. Different phases of the polished samples were indented and the average value was recorded for the Vickers hardness of the sintered nanocomposites.

3. Results and Discussion

3.1. Microstructural evolution of as-received, admixed powders, sintered Ti6Al4V and the MWCNT-Ti6Al4V nanocomposites

The microstructural features which revealed the morphology of the starting and mixed powders are as shown in the SEM and TEM images in Figure 3 (a-d). It was revealed from the SEM image in Figure 3 (a) that the Ti6Al4V powder particles depicted a spherical morphology. Figure 3 (b) depicts the SEM image of the MWCNT which shows the morphology of the nanotubes where the

agglomeration of the tubes was glaringly observed. Meanwhile, 0.5, 1.0 and 1.5 wt.% concentration of MWCNT were chosen for this study since higher concentration of MWCNT have the tendency of agglomerating into clusters during composite production which is detrimental to the mechanical properties of the resulting composite. The agglomeration of the nanotubes may tend to inhibit their easy dispersion in the metal matrix and this dispersion characteristics of the nanotubes is ascribed to the presence of strong Van der Waals forces (~100 eV/mm) between its individual tubes, great aspect ratios (100-100,000) and huge specific surface area (~250 m^2/g) [30]. In addition, a composite system comprising of reinforcement phase above 0.12 wt.% is usually associated with lower density than the unreinforced matrix which in turn can affect the mechanical properties of the composite [31]. Furthermore, 1.0 wt.% of stearic acid was used as a process control agent to modify the surface of the Ti6Al4V particles, aid better bonding between the MWCNT and Ti6Al4V particles and further prevent cold welding during milling. Moreover, Figure 3 (c) shows the TEM image of the tubular structure of the as-received MWCNT and the inset is the fast FFT which was used to confirm the crystalline nature of the MWCNT [32]. From the high-resolution TEM image in Figure 3 (c), it was observed that the walls of the nanotubes were intact without any prior deformation. Likewise, the inset in Figure 3 (c) shows sharp narrow peaks which confirm the high crystalline nature of the as-received MWCNT. The TEM image in Figure 3 (d) conforms with the SEM image in Figure 3 (b) which shows the entangled nanotubes.

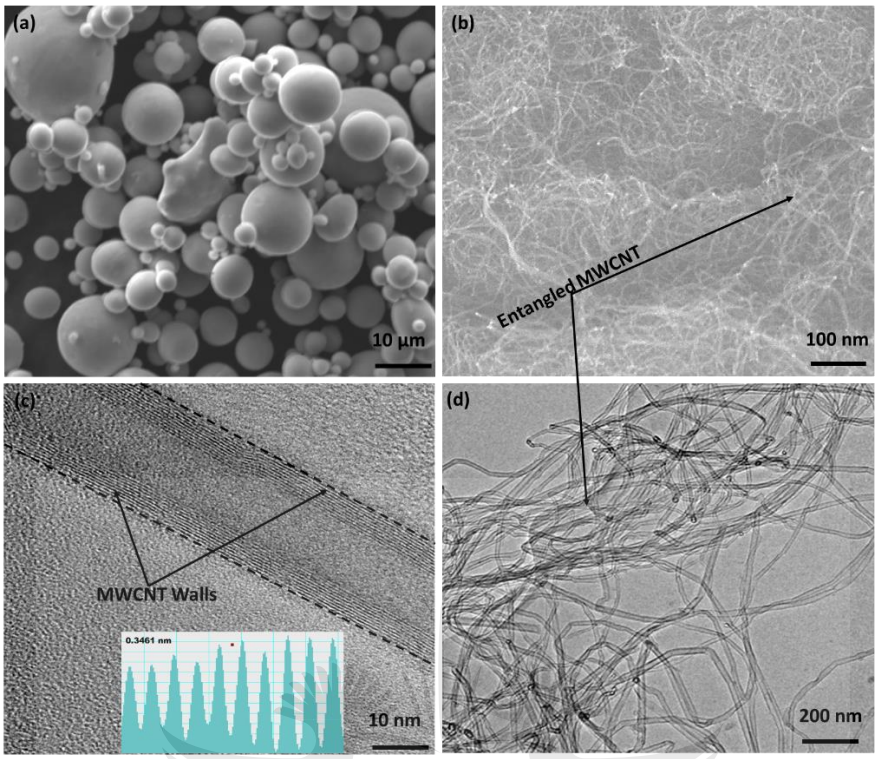

Figure 3. SEM and TEM images of the as-received Ti6Al4V (a) and MWCNT (b-d) powders

In recent years, efforts have been made from past studies which highlighted the importance of transfer of the excellent properties of MWCNT into metal matrices during the synthesis of composites materials. The transfer of these unique properties is dependent on the uniform dispersion of the nanotubes within the matrix material and good interfacial bonding between the MWCNT and the metal matrix. This is achievable using an effective dispersion technique to homogeneously disperse the MWCNT into the metal matrices without severe structural damages to the walls of the nanotubes [20,33,34]. To achieve homogeneous dispersion of the MWCNT in Ti6Al4V, shift speed ball milling technique was employed in this study. The SEM images in Figure 4 (a-c) and the corresponding EDX in Figure 4 (d-f) indicates the dispersion characteristics of the MWCNT in Ti6Al4V powders after mixing using the SSBM technique.

As shown in Figure 4 (a), the SEM image of the admixed 0.5 wt.% MWCNT-Ti6Al4V nanocomposite powder that indicates the microstructural evolution of the SSBM powder, it was observed from the SEM image that the MWCNT were homogeneously dispersed on the surface of the Ti6Al4V particles without any trace of segregated nanotubes around the interstices of the

titanium-based matrix. Furthermore, good interfacial bonding between the MWCNT and Ti6Al4V powder particles were fully observed. The dispersion characteristic of the MWCNT is ascribed to the adequate impact energy exerted on the powder mixture during the SSBM process which was able to overcome the strong Van der Waals forces present between the individual tubes of the MWCNT. This considerable impact energy resulted in uniform dispersion and embedment of the MWCNT into the Ti6Al4V particles.

Similarly, from Figure 4 (b) which shows the SEM image of the 1.0 wt.% MWCNT-Ti6Al4V nanocomposite powders, uniform dispersion of the MWCNT within the Ti6Al4V powders was recorded. Additionally, good interfacial bonding of the MWCNT on the titanium-based matrix was observed, and dispersion characteristics may be ascribed to the considerable impact energy exerted on the powders during the SSBM process that promoted the good dispersion of the MWCNT. Moreover, more nanotubes adhered on the particle of the Ti6Al4V and this dispersion feature is as a result of the increase in the weight fraction of the MWCNT in the composites mixture.

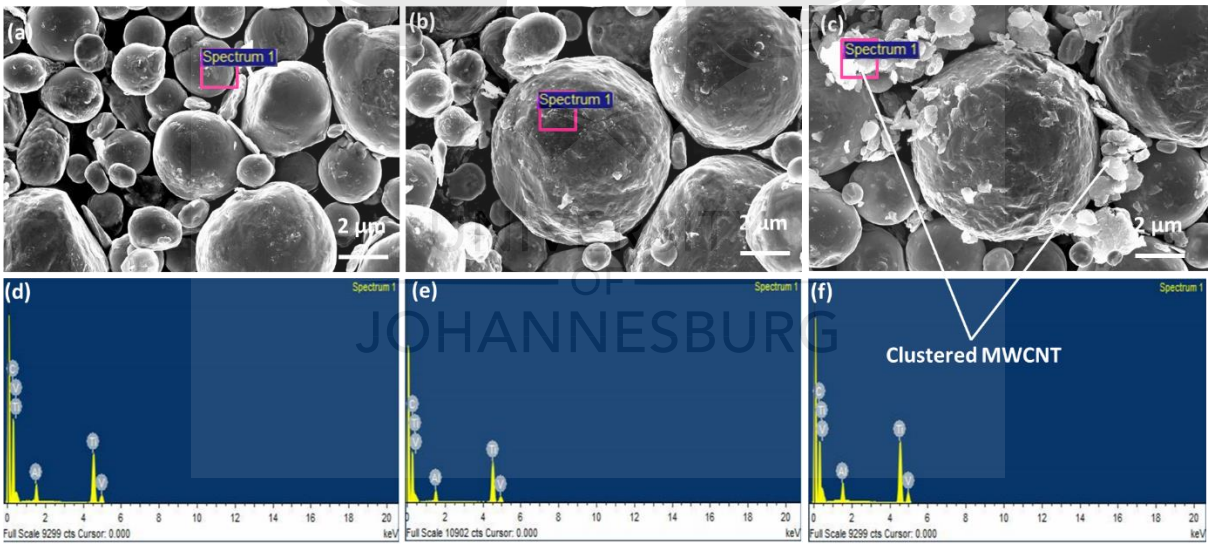

Figure 4. SEM images of the Admixed composite powders (MWCNT-Ti6Al4V) containing 0.5 wt.% (a), 1.0 wt.% (b) and 1.5 wt.% (c) and their corresponding EDX (d-f).

Subsequently, when the MWCNT was increased to 1.5 wt.%, it was observed from the SEM image in Figure 4 (c) that the nanotubes were clustered at the various interstitial position of the Ti6Al4V powder particles. However, some level of good interfacial bonding was observed from the SEM

images. These dispersion characteristics of the MWCNT in the Ti6Al4V powders are linked to the stronger Van der Waals forces present in the MWCNT since it has a higher concentration of MWCNT (1.5 wt.%) in the composite sample. Therefore, it is expedient to increase the milling parameters during SSBM process when the weight fraction of the nanotubes is greater than 1.0 wt.%. This will aid the exertion of adequate impact energy and overcome the stronger Van der Waals forces present in the MWCNT. From all indications, it was observed that the effectiveness of the SSBM technique decreased with increase in the nanotubes above 1.0 wt.%.

Additionally, the homogeneous dispersion and good interfacial bonding of MWCNT in Ti6Al4V has a threshold of less than 1.5 wt.% of MWCNT when the milling parameters employed in this study are used. However, when the weight fraction of the MWCNT was increased to 1.5 wt.%, there is a tendency of forming clusters of MWCNT within the Ti6Al4V powders. These agglomerates can only be overcome by increasing the milling parameters to achieve uniform dispersion of MWCNT in the titanium-based alloy.

To confirm the morphology of the dispersed nanotubes in the admixed powders, the powders were characterized using high-resolution transmission electron microscope. Figure 5 (a-c) shows the TEM images of the admixed powders comprising 0.5-1.5 wt.% of the MWCNT. From Figure 5 (a) which shows the TEM images of the admixed powder comprising 0.5 wt.% of MWCNT, it was observed that the nanotubes were detangled, dispersed and embedded within the Ti6Al4V particles. These dispersion characteristics are ascribed to the adequate impact energy exerted on the powders during the SSBM process, and this result conforms with the SEM results discussed earlier.

Similarly, Figure 5 (b) shows the morphology of the 1.0 wt.% MWCNT in Ti6Al4V powders. From the TEM results, it was observed that the nanotubes were also dispersed and embedded within the Ti6Al4V particles. These dispersion characteristics are in conformation with the SEM image in Figure 4 (b) however, the TEM image in Figure 5 (c) shows the agglomeration of the MWCNT within the Ti6Al4V particles, an indication of the insufficient energy exerted on the powders to overcome the stronger Van der Waals forces when the concentration of the MWCNT was increased to 1.5 wt.%.

These agglomerated nanotubes observed conform with the SEM results where clusters of MWCNT were seen at various interstices of the Ti6Al4V particles.

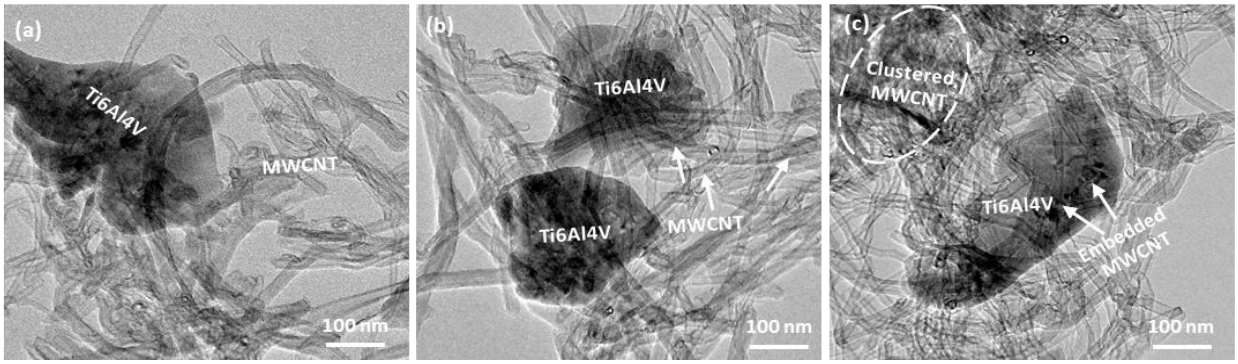

Figure 5. TEM images of the admixed composite powders (MWCNT-Ti6Al4V) comprise 0.5 wt.% (a), 1.0 wt.% (b) and 1.5 wt.% (c) of MWCNT

Subsequently, the admixed powders were consolidated using the SPS technique at the sintering temperature of 900 ºC, 1000 ºC, and 1100 ºC respectively and the SEM images in Figure 6 (a-l) illustrate the morphology of the sintered Ti6Al4V and the nanocomposites. Figure 6 (a-c) shows the SEM images of the consolidated Ti6Al4V alloy sintered at 900 ºC, 1000 ºC, and 1100 ºC respectively. It was observed from Figure 6 (a) that the Ti6Al4V alloy sintered at 900 ºC depicted a network of alpha (α) lamellar structures which may have been formed as a result of the slow cooling process after sintering as the alloy was allowed to cool in the sintering chamber. Additionally, the Ti6Al4V was not heated up to the beta transus temperature (996 ºC) where the alpha phases will start transforming to beta phases (β).

Similarly, Figure 6 (b) shows the microstructural evolution of the Ti6Al4V sintered at 1000 ºC, it was observed that there was a massive transformation of the β to α lamellar phases since the alloy was heated above the β transus temperature during SPS and allowed to cool slowly in the sintering chamber. This massive transformation basically takes place at a lower temperature because of the limited diffusional growth of the alpha phase [35,36]. In addition, it was noticed that the α lamellar phases have a continuous and discontinuous layer of grain boundaries that nucleates preferentially at the preceding β grain boundaries. These microstructural features may be ascribed to the slow cooling of the alloy from above the β transus temperature, which allowed the α lamellar phases to nucleates preferentially [37]. Figure 6 (c) shows the SEM image which depicts the microstructural features of the Ti6Al4V alloy when sintered at 1100 ºC. From the SEM image, β phases (white) were observed

on the microstructure surrounding the α phases (grey). The usual α lamellar phases observed previously were not seen in this microstructure. This microstructural feature is an indication that the higher sintering temperature far above the β transus temperature favours the preferential formation of the β phases around the alpha phase.

Similarly, the SEM images in Figure 6 (d-l) show the morphology of the sintered nanocomposites comprising MWCNT. From the SEM micrographs, it was observed that MWCNT are present and dispersed within the matrix of the Ti6Al4V. Additionally, it was observed that the α phases were present in all the reinforced nanocomposites alongside the β phases. The presence of the α phases may be ascribed to the reinforcement (MWCNT) which is a carbon material and it usually stabilizes the α phase in titanium alloy. Moreover, it is obvious that the dispersion of the MWCNT tends to decrease with the increase in the MWCNT concentration in the nanocomposites. This dispersion characteristic is in conformation with the SEM and TEM results of the admixed powders discussed earlier which is a function of the stronger Van der Waals forces that exist between the nanotubes with a higher concentration of MWCNT.

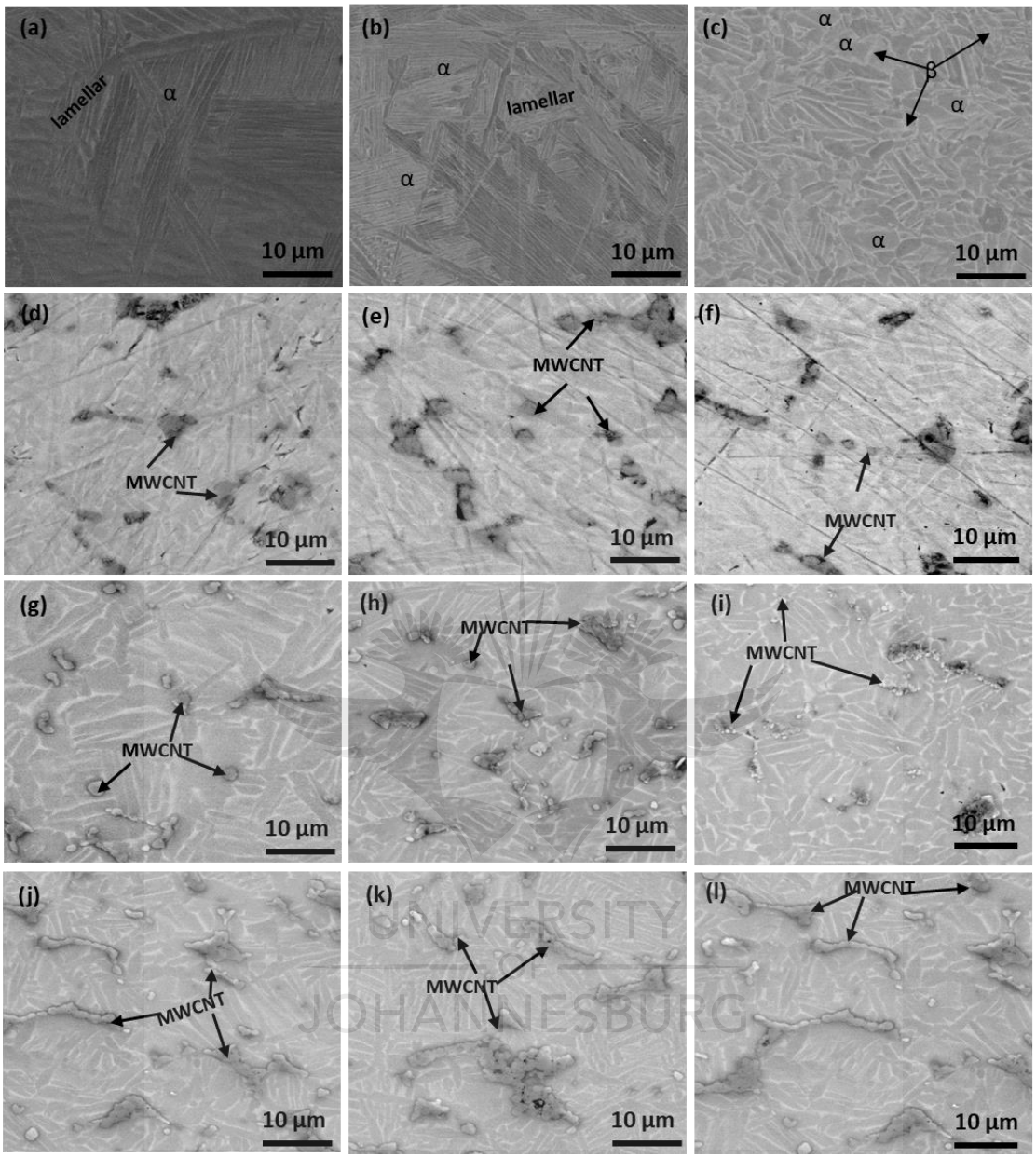

Figure 6. SEM images of the Ti6Al4V sintered at 900 oC (a), 1000 ºC (b), 1100 ºC (c), 0.5 wt.% MWCNT- Ti6Al4V sintered at 900 ºC (d), 1000 ºC (e), 1100 ºC (f), 1.0 wt.% MWCNT-Ti6Al4V sintered at 900 ºC (g) 1000 ºC (h), 1100 ºC (i) and 1.5 wt.% MWCNT- Ti6Al4V sintered at 900 ºC (g) 1000 ºC (h), 1100 ºC (i)

3.2. XRD analysis of the starting, admixed powders, sintered Ti6Al4V and MWCNT-Ti6Al4V nanocomposites

XRD technique was used to carry out the phase analysis of the starting powders, admixed nanocomposites powders, the sintered Ti6Al4V and MWCNT-Ti6Al4V nanocomposites to

understand the phase evolution that occurred during the powder processing and sintering operation. Figure 7 (a-e) shows the XRD pattern of the starting powders, admixed nanocomposites, and sintered nanocomposites.

From Figure 7 (a), which depicts the XRD pattern of the pristine MWCNT, the two graphitic peaks were fully seen at 2θ = 25.6º and 43.3 º which correspond to (002) and (100) planes respectively. Furthermore, Figure 7 (b) depicts the XRD pattern of the pristine Ti6Al4V powders, where only the following alpha titanium phases were observed at the corresponding peaks were 2θ = 35.48 º, 38.68 º, 40.52 º, 53.43 º, 63.85 º, 81.10 º, 86.92 º, 82.84 º and 88.42 º which are linked to the following; (100), (002), (101), (102), (110), (103), (112), (004) and (202) planes respectively.

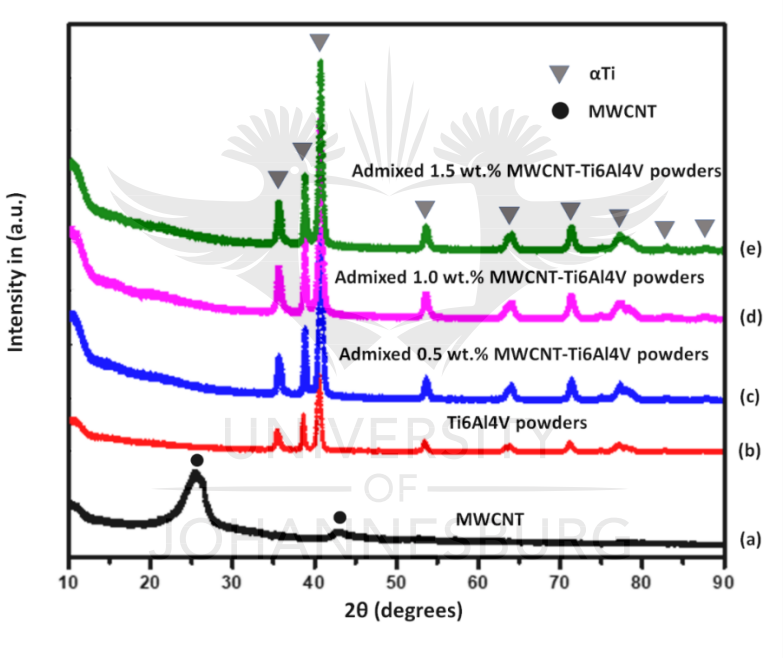

Figure 7: XRD patterns of starting and admixed MWCNT-Ti6Al4V composite powders (a) pristine MWCNT, (b) pristine Ti6Al4V, (c) 0.5 wt.% MWCNT-Ti6Al4V, (d)1.0 wt.% MWCNT-Ti6Al4V and (e) 1.5 wt.% MWCNT-Ti6Al4V nanocomposite powders

Correspondingly, it was seen from the XRD patterns in Figure 7 (c-e) of the admixed powders that there were no traces of any new phases formed after the shift speed ball milling process. Figure 7 (c) shows the XRD pattern of the admixed 0.5 wt.% MWCNT-Ti6Al4V nanocomposite powders, it was observed from the XRD pattern that the alpha titanium peaks were more pronounced after the dispersion process. This pronouncement of the peaks may be ascribed to the mechanical stresses the

powders were subjected to during the dispersion process. However, there was no trace of the MWCNT in the XRD pattern of the admixed powder.

Similarly, more pronouncement of the alpha titanium peaks were observed on the XRD pattern of 1.0 wt.% MWCNT-Ti6Al4V nanocomposite powder, shown in Figure 7 (d). A similar trend was observed from the XRD pattern of 1.5 wt.% MWCNT-Ti6Al4V nanocomposite powder, shown in Figure 7 (e). This pronouncement of the peaks with the addition of the MWCNT in the composite powders may not only be ascribed to the mechanical stresses that occurred during the dispersion process but the presence of the carbon material (MWCNT) which favours the stabilization of the alpha titanium phases. However, no other phases such as the MWCNT and carbide were observed from the XRD analysis and this may be ascribed to considerable variance in the mass absorption coefficient (for Cu Ka radiations) by the Ti and carbon (C) which are 208 and 4.6 m^2/g respectively [38]. Additionally, the dispersion process was virtually carried out at an ambient temperature which could not trigger a chemical reaction between the carbon and the titanium that will promote a phase change and the formation of carbide phases.

Meanwhile, when the admixed nanocomposite powders were sintered at 900, 1000 and 1100 ^oC, evolution in phases occurred which is observed from the XRD pattern of the sintered nanocomposites in Figure 8 (a-c). From Figure 8 (a) which depicts the XRD patterns of Ti6Al4V and the nanocomposites containing 0.5, 1.0 and 1.5 wt.% of MWCNT sintered at 900 ^oC, the MWCNT, alpha titanium, titanium, and titanium carbide phases were observed. Additionally, it was observed that these phases were more prominent as the weight fraction of the MWCNT increased from 0.5 to 1.5 wt.%. This is an indication that the sintering of the admixed powders containing MWCNT and Ti6Al4V at 900 ^oC trigger a chemical reaction between the powder particles. That resulted in a structural evolution of the nanocomposite and this reaction increased with the increasing MWCNT content in the nanocomposite, further explaining why there are more phase evolution in the nanocomposites containing 1.0 and 1.5 wt.% of MWCNT.

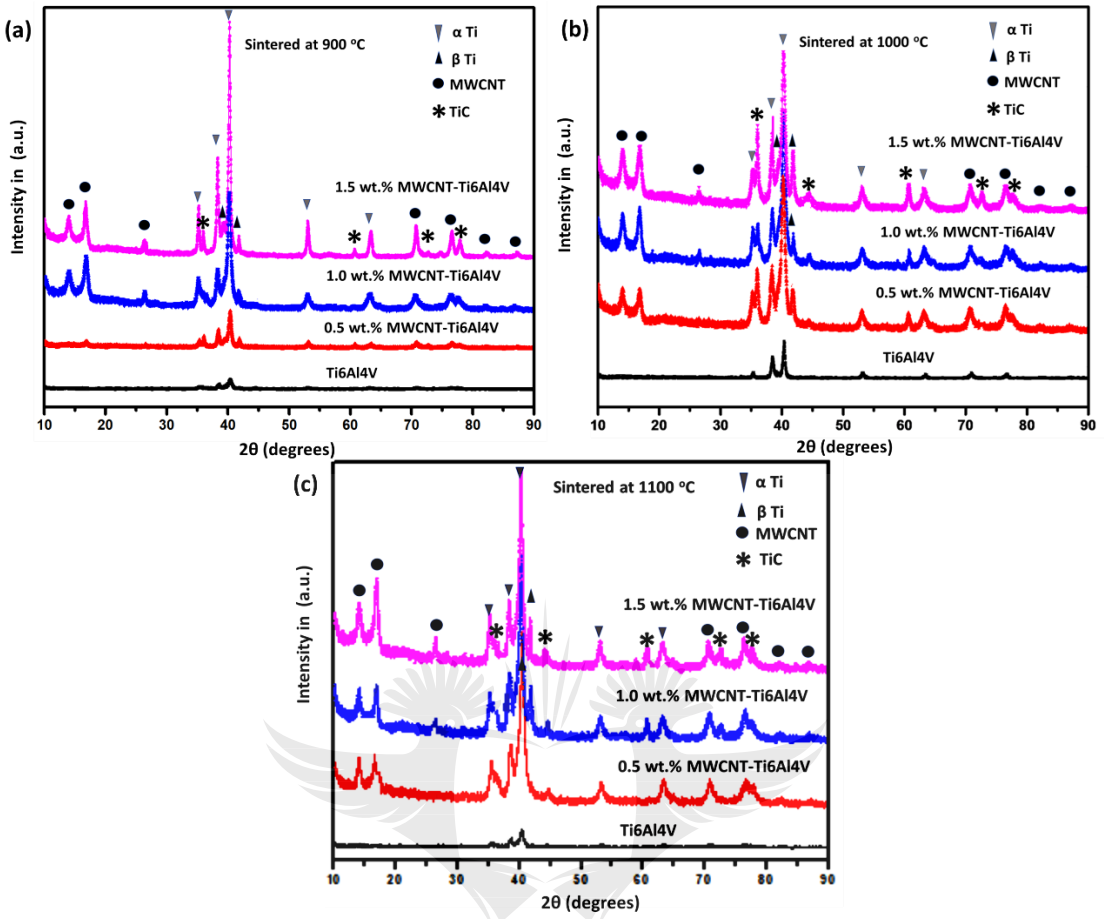

Figure 8: XRD patterns of the sintered Ti6Al4V and sintered nanocomposites MWCNT-Ti6Al4V comprising 0.5, 1.0, 1.5 wt.% of MWCNT sintered at (a) 900 °C, (b) 1000 °C and (c) 1100 °C respectively

Similarly, Figure 8 (b) depicts the XRD patterns of Ti6Al4V and the nanocomposites containing 0.5, 1.0 and 1.5 wt.% of MWCNT sintered at 1000 °C. From the XRD results, it was realized that the alpha titanium, beta titanium, and titanium carbide phases were more pronounced when the nanocomposites were fabricated at 1000 °C. Additionally, new phases were more prominent with the increase in the MWCNT content which indicates that the reaction between the titanium alloy and the MWCNT was triggered by the increase in the MWCNT, especially at elevated temperature. Likewise, the alpha titanium, beta titanium, and titanium carbide phases were observed when the nanocomposites were sintered at 1100 °C which indicates that a reaction was triggered between the composite constituent during the sintering process. The presence of the titanium carbide phase that was formed during the sintering process will help to improve the mechanical properties (tensile

strength, yield strength, elastic modulus, and hardness) and the wear resistance of the nanocomposites during service conditions.

3.3 Raman spectroscopic analysis of starting, admixed powders and sintered MWCNT-Ti6Al4V nanocomposites

The starting MWCNT, admixed MWCNT-Ti6Al4V powders, and sintered MWCNT-Ti6Al4V nanocomposites were characterized using Raman spectroscopy to ascertain the structural integrity and evolution of the nanotubes after the dispersion and sintering process. Figure 9 (a-e) shows the Raman spectra of the pristine Ti6Al4V, pristine MWCNTs and admixed powders containing the mixture of Ti6Al4V powder and varying weight fraction of MWCNT (0.5, 1.0, 1.5 wt.%).

From Figure 9 (a), which shows the Raman spectra of pristine Ti6Al4V, it was observed that the Raman result does not depict any prominent vibration peaks. Past studies have shown that this characterization technique is usually employed to ascertain the structural damages to nanotubes during their dispersion in matrix materials. This is carried out by analyzing the D band which is linked with the sp^3 defects in the carbon to carbon bond of the nanotubes and the G band which is associated with the in-plane stretching mode of the carbon to carbon bond of the nanotubes. Additionally, the G band is used to ascertain the orderliness of the carbon, degree of crystallinity, graphitization, and metallicity of the carbon to carbon bond in the nanotubes [20,39,40].

Moreover, the intensity ratio of the D and G band has been successfully used in past studies to quantify the defects on the MWCNT after dispersion and sintering. This is usually ascertained by analyzing the shift of the D band and the G band and subsequently associating the reduction and broadening of the G band to stacking disorder in the sp^2 carbon to carbon system. The changes in the G band may be as ascribed to open edges, vacancies, and damages to the walls of the nanotubes [19,41]. Figure 9 (b) shows the Raman spectrum of the pristine MWCNT where the two prominent graphitic peaks (D and G band) were observed at 1340 cm^{-1} and 1580 cm^{-1} respectively. The corresponding I_D/I_G ratio of the pristine MWCNT was calculated from the Raman spectrum in Figure 9 (b), and it has a value of 0.800. Whereas, the Raman spectrum of the admixed powder (0.5 wt.% MWCNT-Ti6Al4V) in Figure 9 (c) indicated that there was a Raman shift of the D and G band from 1340 cm^{-1} and 1580 cm^{-1} in the pristine MWCNT to 1399 cm^{-1} and 1628 cm^{-1}.

Similarly, the I_D/I_G ratio of the admixed powder containing 0.5 wt. of MWCNT increased to 0.872 which amounts to 9%. The Raman shift of the graphitic peaks and the corresponding increase in the I_D/I_G ratio indicated that the walls of the MWCNT were subjected to stresses during the dispersion process that resulted in a slight strain which reflected as changes in the D and G band of the graphitic peaks. However, there were no severe deformation or damages to the walls of the nanotubes since carbide phase was not observed on the Raman spectra. Figure 9 (d) shows the Raman spectrum of the admixed powder containing 1.0 wt.% of MWCNT, from the Raman result, it was observed that the D and G band shifted to higher wavenumbers of 1401 cm^{-1} and 1632 cm^{-1} respectively.

Likewise, there was an increase in the I_D/I_G ratio from 0.800 in the pristine MWCNT to 0.955 after dispersion in Ti6Al4V powder which amounts to 19.4%. From all indications, it was observed that there was a Raman shift to higher wavenumbers and deformation on the walls of the nanotubes. These changes may be attributed to the increase in the concentration of the MWCNT in the admixed powders which was subjected to more stresses than at lower concentration (0.5 wt.%) during the dispersion process. However, the severity of the deformation does not result in the formation of defects on the walls of the nanotubes since there were no traces of carbide phases on the Raman spectrum of the admixed powder. Subsequently, it was observed from Figure 9 (e) that the Raman spectrum of the admixed powder containing 1.5 wt.% of MWCNT depicted similar trends. The D and G band shifted to a higher wavenumber of 1412 cm^{-1} and 1640 cm^{-1} respectively.

Similarly, a higher I_D/I_G ratio of 0.985 was obtained which corresponds to 23.1% increase. This Raman feature is ascribed to the higher stresses that were subjected to the higher concentration of the MWCNT in the admixed powders that resulted in incredible changes in the graphitic peaks of the MWCNT during dispersion. Meanwhile, the SSBM conditions did not impose any damages to the walls of the nanotubes since defects such as open edges and vacancies are usually potential sites for carbide formation [20].

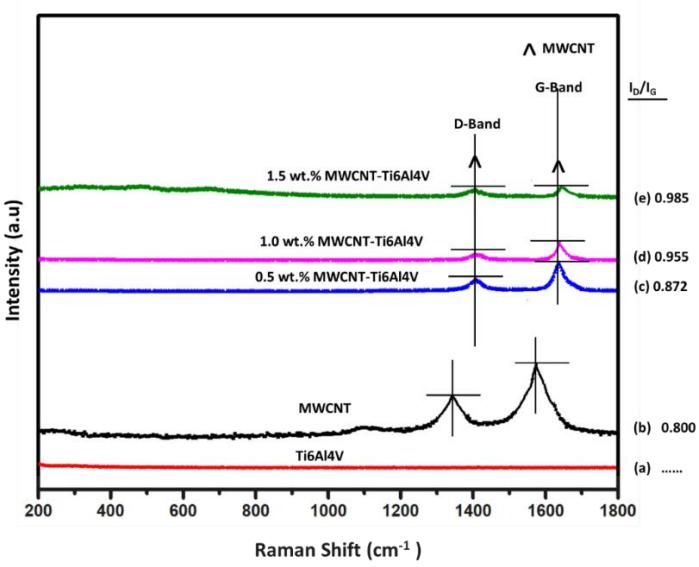

Figure 9: Raman spectra of the starting powders and admixed nanocomposite powders; (a) Pristine Ti6Al4V powders, (b) Pristine MWCNT, (c) 0.5 wt.% MWCNT-Ti6Al4V, (d) 1.0 wt.% MWCNT-Ti6Al4V and (e) 1.5 wt.% MWCNT-Ti6Al4V

Likewise, the Raman results of the sintered powders at 1000 ^{o}C are shown in Figure 10 (c-d). However, the Raman spectra in Figure 10 (a-b) are shown for comparison of the Raman shift and the change in the I_D/I_G ratio after sintering. Meanwhile, when the admixed powders were sintered, the Raman results depict new peaks which are shown in Figure 10 (c-e) which was observed at 263 cm^{-1}, 415 $cm^{-1,}$ and 602 cm^{-1} respectively. These peaks are identified as the titanium carbide (TiC) peaks formed during the sintering process, and this result is in line with the previous study where TiC phases were observed on Raman spectra of titanium reinforced with MWCNT [20,42,43].

Moreover, the TiC phases formed during sintering of the nanocomposites can assist in augmenting the mechanical and tribological properties of the sintered nanocomposites [20]. From Figure 10 (c) which shows the Raman spectrum of the sintered nanocomposite consisting of 0.5 wt.% MWCNT, broadening and reduction of the D and G band was observed when compared with the Raman results of the admixed powders and pristine MWCNT. The D and G band shifted to much higher wavenumbers of 1405 cm^{-1} and 1634 cm^{-1} respectively. Likewise, the I_D/I_G ratio of the sintered nanocomposite increased from 0.800 in the pristine MWCNT to 0.935, and this amounts to a 16.4% increase. This is an indication that the walls of the MWCNT were subjected to thermal stresses during the SPS process to form the nanocomposites. The combination of both the mechanical stresses during

SSBM and the thermal stresses during SPS resulted in the deformation of the walls of the nanotubes that created open edges and vacancies where the TiC phases were formed.

Correspondingly, Figure 10 (d) shows the Raman spectrum of the sintered nanocomposites containing 1.0 wt.% of MWCNT. From the Raman spectrum, it was observed that the D and G band shifted slightly to higher wavenumbers of 1407 cm^{-1} and 1635 cm^{-1} respectively.

Similarly, the I_D/I_G ratio increased from 0.800 in the pristine MWCNT to 0.976 which corresponds to a 22% increase. This indicates that at higher concentration of MWCNT in the nanocomposites, MWCNT has a higher susceptibility to both thermal and mechanical stresses which will produce more carbide phases in the nanocomposite. Figure 10 (e) shows the Raman spectrum of the sintered nanocomposite containing 1.5 wt.% of MWCNT. From the Raman result, a similar trend was observed when the nanocomposite contained 1.0 wt.% of MWCNT. The D and G band shifted to higher wavenumbers of 1415 cm^{-1} and 1644 cm^{-1} respectively.

Likewise, the I_D/I_G ratio increased from 0.800 of the pristine MWCNT to 0.996 after sintering the nanocomposite and this amounts to a 25% increase. From all indications, it can be deduced that the sintering of the nanocomposites containing MWCNT and Ti6Al4V triggers a reaction between the titanium and carbon to form titanium carbide.

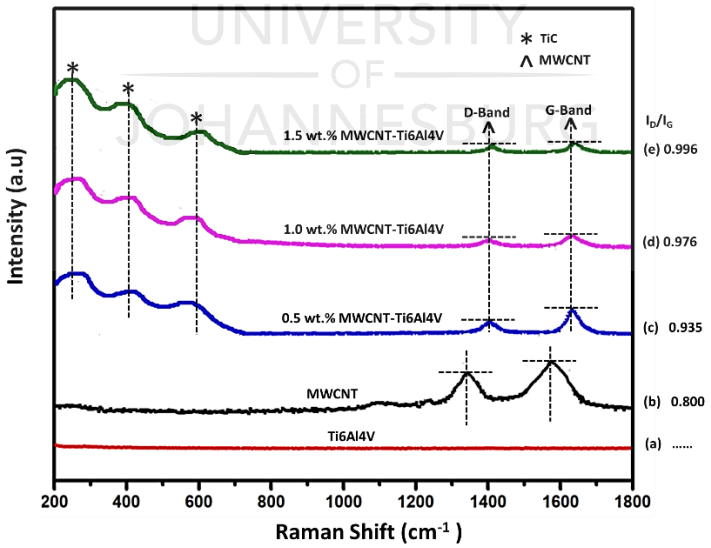

Figure 10. Raman spectra of pristine MWCNT and sintered MWCNT-Ti6Al4V nanocomposites at 1000 ^oC (a) sintered Ti6Al4V powders, (b) Pristine MWCNTs, (c) 0.5 wt.% MWCNT-Ti6Al4V, (d) 1.0 wt.% MWCNT-Ti6Al4V, and (e) 1.5 wt.% MWCNT-Ti6Al4V

3.4 Sintering behaviours of the sintered Ti6Al4V and MWCNT-Ti6Al4V nanocomposites

The sinterability of the fabricated Ti6Al4V and MWCNT-Ti6Al4V nanocomposites were evaluated from the sintering data acquired after the spark plasma sintering process. Figure 11 (a-f) shows the sintering behaviours of the fabricated titanium alloy, and the nanocomposites sintered at distinct sintering temperature (900, 1000 and 1100 ^{o}C). Displacement of the punches during the sintering process which depicts the deformation of the samples under the influence of compressive pressure at the varying sintering temperatures was also investigated.

From Figure 11 (a), which shows the sintering cycle of the Ti6Al4V and nanocomposites sintered at 900 ^{o}C which indicates the sintering behaviour of the titanium alloy and the fabricated nanocomposites, it was observed that the temperature of 250 ^{o}C was upheld for 400 s after which the temperature increased to 900 ^{o}C (sintering temperature). This was accompanied by a holding time for 600 s to achieve considerable grain growth and subsequent cooling. However, it was seen that the nanocomposite samples containing MWCNT (0.5-1.5 wt.%) underwent slow heating process as the starting temperature of 250 ^{o}C was upheld for about 412 s for the nanocomposite containing 1.5 wt.% MWCNT. This sintering behaviour may be ascribed to the presence of pores in the compacted admixed powders which was imposed by the introduction of MWCNT into the Ti6Al4V matrix [44]. Furthermore, the nanocomposites containing 1.0 and 1.5 wt.% completed the sintering cycle at a later time when compared with the sintered Ti6Al4V and the 0.5 wt.% MWCNT-Ti6Al4V. This is an indication that the presence of MWCNT in the Ti6Al4V matrix retarded the sintering process of the sintered nanocomposites.

Additionally, Figure 11 (b) shows the sintering cycle of the Ti6Al4V and nanocomposites sintered at 1000 ^{o}C. A similar trend, as depicted by Figure 11 (a), was observed where the presence of MWCNT tends to delay the start of the heating process during the sintering of the nanocomposites. Furthermore, similar trends were observed with the sintering cycles of the Ti6Al4V and nanocomposites sintered at 1100 ^{o}C. This can further be explained that the introduction of MWCNT into the Ti6Al4V matrix induced the presence of pores which reduced the thermal conductivity of the green compact and retard the sintering process.

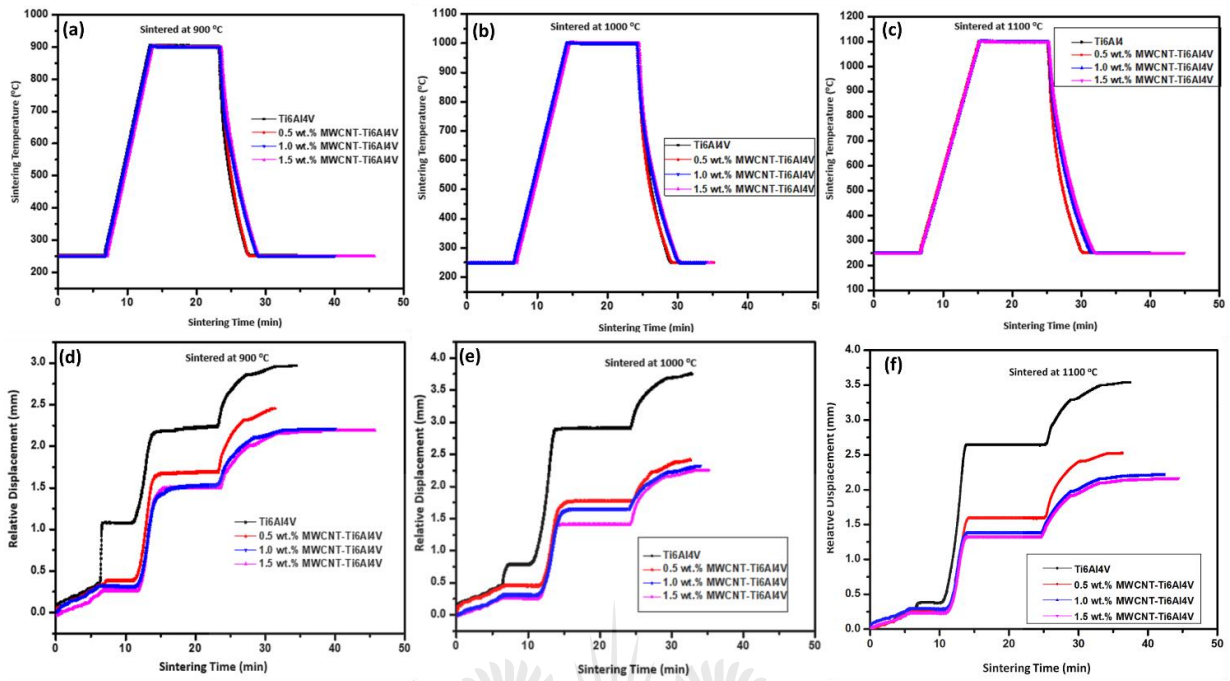

Figure 11. Sintering behaviour of the Ti6Al4V and the fabricated nanocomposites (a-c) and the displacement curves of the punches (d-f) during sintering at 900 ^{o}C, 1000 ^{o}C, and 1100 ^{o}C respectively.

Apart from the sintering cycle of the sintered titanium alloy and the nanocomposites shown in Figure 11 (a-c), the relative displacement of the punches during the sintering process was used to explain the sintering behaviours of the alloy and nanocomposites. Figure 11 (c-d) shows the relative displacement of the punches against sintering time which further explains the deformation of the samples during the sintering process.

Figure 11 (c) shows the relative displacement plots of the titanium alloy and the nanocomposites sintered at 900 ^{o}C; it was observed that the relative displacement of the Ti6Al4V increased with sintering time from 0-0.37 mm after sintering for 390 s. This sintering behaviour may be ascribed to the influence of compressive pressure applied on the green compact during the early stage of sintering although the sintering temperature at this stage is too low to influence the displacement of the punches. Immediately after this stage, the increase in temperature resulted in the rapid displacement of the punches (0.37-1.07 mm) which was influenced by the increase in temperature that softens the green compact and resulted in the rearrangement of particles of the Ti6Al4V sample. Subsequently, this was accompanied by the escape of trapped gases from the green compact after

which the displacement was constant and stable with an increase in sintering time. This sintering behaviour is in line with the result reported by Falodun et al. [45] when titanium-based nanocomposites were fabricated using spark plasma sintering.

Subsequently, the sintering process was accompanied by the necking and neck growth of the particles, resulting from evaporation and condensation as the sintering temperature increases [46]. During the sintering process, a snap displacement of the punch from 1.07-2.16 mm within a slight increase in sintering time was recorded when the temperature rises to 900 ^{o}C. This led to the change in the physical structure of the compact which is ascribed to the thermal softening of the sample that resulted in smoothening and grain reshaping [45]. The displacement further increased from 2.16 to 2.24 during the holding period (600 s) where the material almost attained its maximum density. This was accompanied by a sharp increase in displacement due to the shrinkage of the sample during the cooling process. From all indication, the sintering process depicts an increase in densification with the sintering temperature after attaining a maximum temperature of 900 ^{o}C.

Similarly, the fabricated nanocomposites containing MWCNT (0.5-1.5 wt.%) undergo the same displacement trend. However, immediately after the increase in displacement resulting from the applied compressive pressure on the green compact, a stable and constant displacement at lower sintering temperature was observed. This constant displacement at lower sintering temperature may be ascribed to the presence of the MWCNT in the Ti6Al4V matrix which created pores and retarded the sintering process. Meanwhile, with the increase in temperature, a sharp displacement was observed which may be ascribed to the thermal softening and grain reshaping that fill up the pores and promotes the densification process.

Figure 11 (e-f), which shows the displacement plot against sintering time of Ti6Al4V and the nanocomposites sintered at 1000 ^{o}C and 1100 ^{o}C respectively, depicted similar displacement trend. However, the rapid displacement observed during the sintering temperature of Ti6Al4V at 900 ^{o}C that resulted in the rearrangement of particle tends to decrease with the increase in sintering temperature (900-1100 ^{o}C). The decrease in displacement at this stage, especially at the higher sintering temperature, may be ascribed to the lower thermal transfer. Although, during the sintering of the nanocomposites with lower content of MWCNT (0.5 wt.%), a higher displacement of the punches was observed when compared with the sintering of nanocomposites containing 1.0 & 1.5

wt.% of MWCNT. This sintering behaviour may also be attributed to the presence of much pores in the nanocomposites with higher concentration of MWCNT which eventually reduced the conductivity of the green compacts and retards the sintering process.

3.5 Densification behaviour of the sintered Ti6Al4V and MWCNT-Ti6Al4V nanocomposites

In a bid to understand the densification behaviour of the Ti6Al4V and the nanocomposites sintered at 900, 1000 and 1100 ^{o}C using the SPS technique, the shrinkage rate data were acquired and plotted against the sintering time. This data assists in explaining the shrinking of the samples during the sintering process. Figure 12 (a-c) shows the shrinkage rate in relation with sintering time of the titanium-based alloy and the nanocomposites sintered at 900-1100 ^{o}C.

From Figure 12 (a), which shows the shrinkage rate of the Ti6Al4V powder when sintered at 900 ^{o}C, it was observed that the shrinkage rate of the Ti6Al4V depicts three different stages of shrinkages. The initial shrinkage stage was experienced within the first 10 min of sintering which explained the initial rearrangement of the alloy particles, the elimination of trapped gases from the powder and the production of sparks between the powder particles [47]. This was accompanied by the second shrinkage stage which occurred between 10-20 min of sintering, and this shrinkage stage is as a result of Joule heating effect that leads to the localized plastic deformation of the powder particles. This shrinkage stage is also associated with the formation of necking and neck growth, production of atomic diffusion within the particles that result in the plastic flow [48].

Moreover, the surface of the Ti6Al4V becomes activated due to the high pulse discharge plasma produced at the powder contacts. As the sintering process prolongs with time, the Joule heating effect results in the increase in temperature that promotes the softening and the necking of the powders particles. This further leads to the melting and evaporation process in the neck region. This shrinkage stage aids the densification of the sample resulting from the plastic flow by the Joule heating effect and the applied compressive pressure. It was seen that the final stage commenced after 20 min of the sintering process where a lower shrinkage rate was observed. The densification at this stage may be attributed to mass transportation and the reduction in the shrinkage rate may be ascribed to the decrease in temperature during the cooling process of the chamber to ambient temperature [49,50].

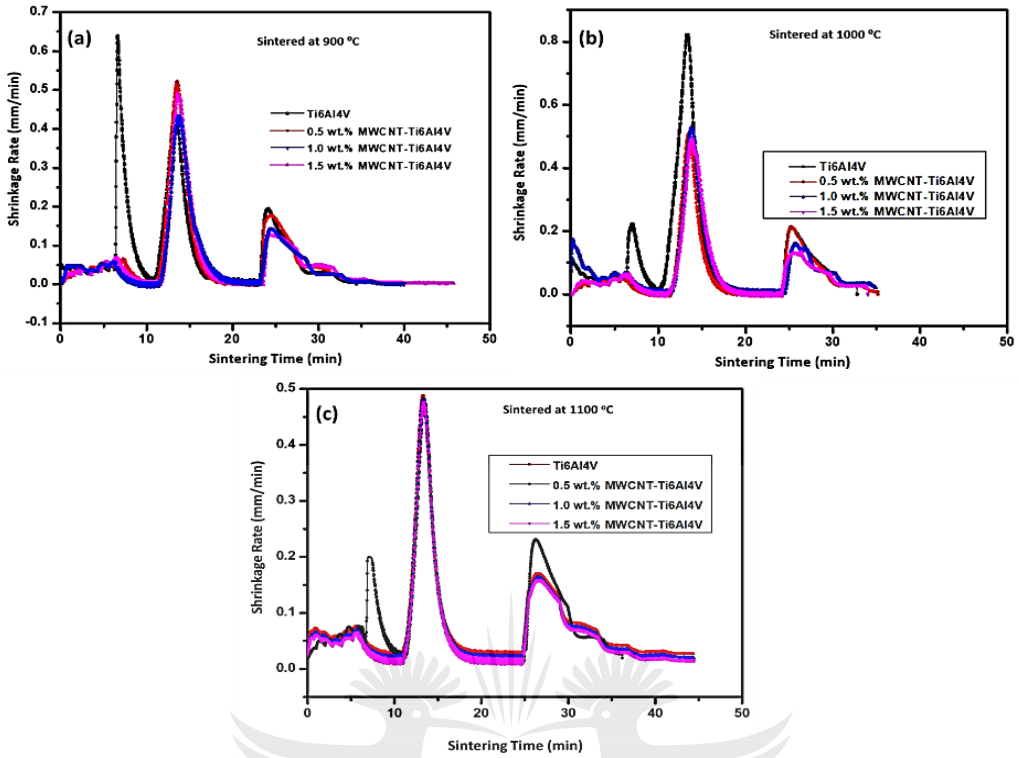

Figure 12. Shrinkage rate against sintering time of the Ti6Al4V and the fabricated nanocomposites (a-c) during sintering at 900 °C, 1000 °C and 1100 °C respectively

Furthermore, the shrinkage rate depicted similar trends during the sintering of Ti6Al4V powders at 1000 and 1100 °C. However, during the sintering of the nanocomposites at 900-1100 °C, it was observed that the shrinkage rate of the nanocomposites only depicted two distinctive shrinkage stages which are similar to the shrinkage stages reported by Vasanthakumar et al. [51] when titanium reinforced with carbon was sintered using similar sintering technique. The first shrinkage stage observed during the sintering of the pristine Ti6Al4V may be attributed to the homogeneity of the structure and the lower melting point when compared with the nanocomposites. The initial shrinkage stage during the sintering of the nanocomposites is majorly dominated by the diffusion process where about 70-90% of the densification takes place and this is supported by previous studies on the densification of TiN [52] and other ceramics [53].

Conversely, the second shrinkage stage is majorly dominated by plastic flow of the nanocomposite particles which occurred when the threshold temperature and pressure had already been attained. Also, it was observed that the sintering time increased with the addition of MWCNT to the Ti6Al4V matrix which indicates that the presence of MWCNT tends to impose some difficulty in

the sintering process. This difficulty may be ascribed to the difference between the thermal conductivity of the Ti6Al4V and MWCNT. Therefore, a higher amount of energy is needed to increase the temperature of the nanocomposite powders to the threshold temperature during sintering when compared with the pristine Ti6Al4V powders [54].

3.6 Relative density of the sintered Ti6Al4V and MWCNT-Ti6Al4V nanocomposites

The relative density of the sintered Ti6Al4V and the nanocomposites are shown in Figure 13 to further explain the densification behaviour of the fabricated materials. From Figure 13, it was observed that the relative density of the sintered Ti6Al4V ranges from 99.32-100% with an increase in sintering temperature from 900 to 1100 ^{o}C. This improvement in densification at higher sintering temperature is attributed to the induced plasma that resulted in easy diffusion of atoms which eventually led to the closure of micropores between the compacted powders [55].

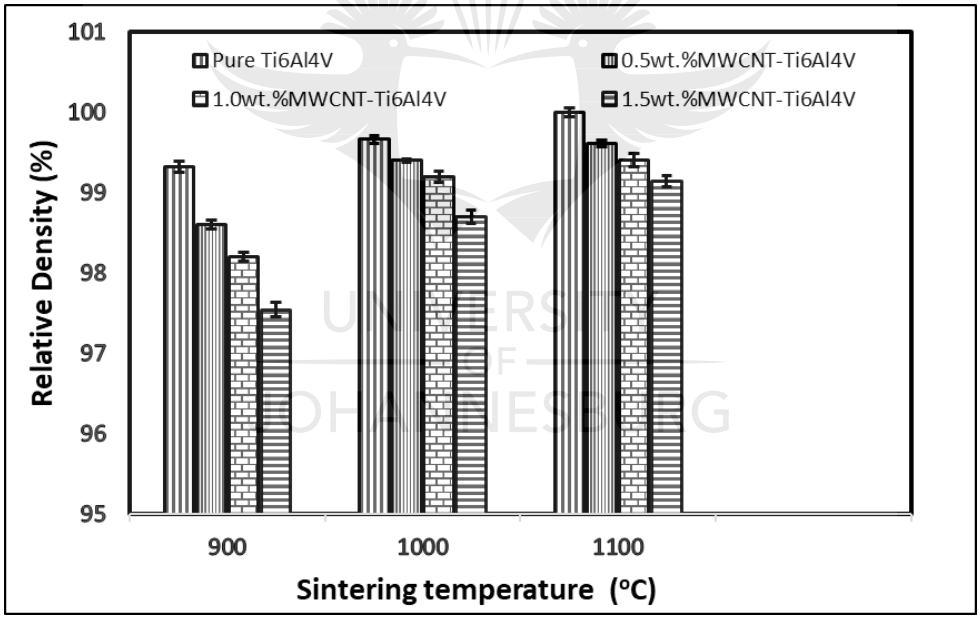

Figure 13. The relative density of the fabricated Ti6Al4V and nanocomposites sintered at 900 ^{o}C, 1000 ^{o}C and 1100 ^{o}C respectively.

Conversely, the relative density of the Ti6Al4V and the nanocomposites sintered at 900 ^{o}C decreased from 99.32-97.54% with the increase in weight fraction of the MWCNT from 0.5-1.5 wt.%. This decline in density is in accordance with the fact discussed earlier, that the presence of the MWCNT in the Ti6Al4V matrices impose some micropores into the nanocomposites. However, the employed

threshold sintering temperature was unable to fully induce bonding to form a pore-free microstructure. The presence of the MWCNT at the grain boundaries tend to hinder the full densification of the nanocomposite by inhibiting the sintering process.

Nevertheless, when the nanocomposites were sintered at higher sintering temperatures, a great improvement in the densification was recorded which indicates that higher sintering temperatures promote the full densification of the nanocomposites. This is in line with previous studies reported by Adegbenjo et al. [44] where carbon nanotubes were used to reinforce titanium alloy.

Additionally, Saheb et al. [56] reiterated that the presence of MWCNT in aluminium alloy resulted in the reduction in the densification of the metal matrix composites. From all indications, it can be deduced that the increase in weight fraction of MWCNT during the production of metal matrix composites results in the decrease in the densification of the composites. While higher sintering temperature promotes the full densification of the composites resulting from improved diffusion of atoms, good bonding and the filling of micropores.

3.7 Microhardness of the sintered Ti6Al4V and MWCNT-Ti6Al4V nanocomposites

The variation of the microhardness value of the sintered alloy and nanocomposites at different sintering temperature is shown in Figure 14. It was observed that the microhardness increased with the presence of MWCNT in the Ti6Al4V matrix.

Similarly, the microhardness of both the sintered Ti6Al4V and nanocomposites depicts tremendous improvement with an increase in sintering temperature. A thorough examination of Figure 14 revealed that the microhardness value of the sintered Ti6Al4V increased from 369-401 HV with an increase in sintering temperature from 900-1100 ^{o}C. This improvement in hardness amounts to 8% increase which is ascribed to the microstructural evolution that occurred during the sintering at a higher temperature and the employed sintering parameters that favoured the formation of both the alpha and beta phases in the alloy.

Correspondingly, it was revealed from Figure 14 that the microhardness of the sintered nanocomposites comprising 0.5 wt.% MWCNT improved significantly (458.5-502.5 HV) which amounts to about 25% increase when compared with the unreinforced alloy. This outstanding increase in hardness is ascribed to the influence of the reinforcement phase (MWCNT) owing to the

dispersion strengthening mechanism and the pinning effect that inhibits dislocation motion during the indentation [57].

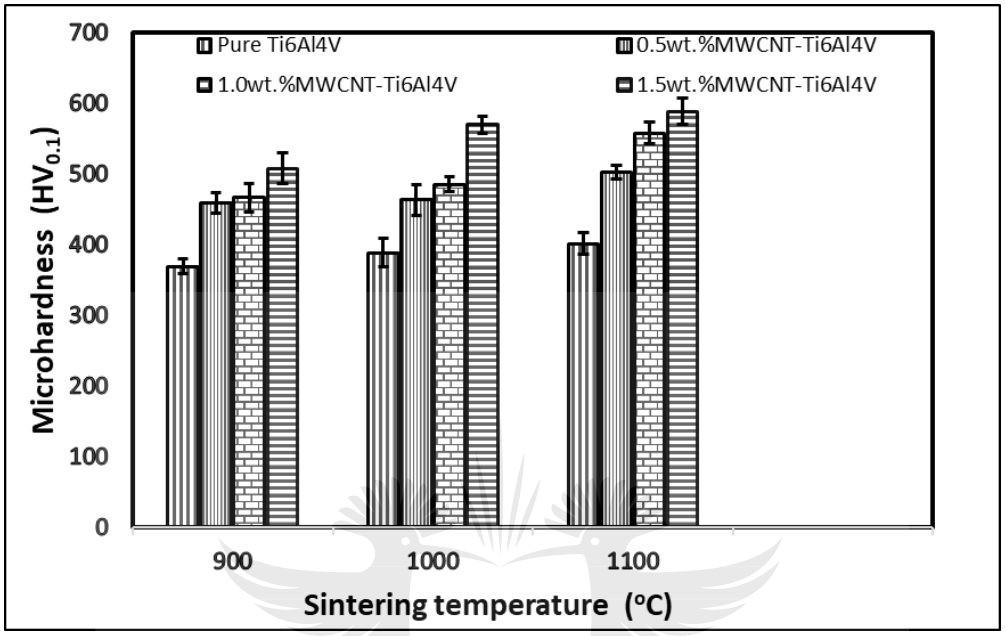

Figure 14. Microhardness of the fabricated Ti6Al4V and nanocomposites sintered at 900 °C, 1000 °C, and 1100 °C respectively

Meanwhile, during the sintering process, the reaction between the MWCNT and the titanium alloy resulted in the formation of harder phases (TiC) which assisted in improving the hardness of the nanocomposite. Similarly, the sintered nanocomposites containing 1.0 wt.% MWCNT and 1.5 wt.% MWCNT showed improvement in microhardness 466.52-557.82 HV and 507.6-588.5 HV respectively). These improvements in hardness amount to about 39.10% and 46.8% respectively when compared with the unreinforced titanium alloy sintered in the same condition.

Although, the increase in hardness by the fabricated nanocomposites despite the reduction in densification may be ascribed to the presence of the retained MWCNT and the TiC in the nanocomposites [58]. This result is in accordance with previous studies on the reinforcement of metal matrices using MWCNT [59-61]. From all indications, it can be deduced that the microhardness value of titanium alloy improves with the addition of MWCNT into its matrix and the microhardness of sintered titanium alloys and its nanocomposites increased with sintering

temperature. The employed sintering parameters for the fabrication of Ti6Al4V alloy and the nanocomposites in this study are summarized in Table 1 below.

Table 1: Shows the sintering parameters, density and the microhardness values of the Ti6Al4V and nanocomposites

Samples	**Sintering Temperature (^oC)**	**Heating Rate (^oC/min)**	**Holding Time (min)**	**Compressive Pressure (MPa)**	**Effective Density (g/cm^3)**	**Relative Density (%)**	**Microhardness ($HV_{0.1}$)**
Ti6Al4V	900	100	10	50	4.400	99.32	369
0.5 MWCNT-Ti6Al4V	900	100	10	50	4.370	98.6	458.5
1.0 MWCNT-Ti6Al4V	900	100	10	50	4.353	98.2	466.5
1.5 MWCNT-Ti6Al4V	900	100	10	50	4.321	97.54	502.6
Ti6Al4V	1000	100	10	50	4.414	99.66	388
0.5 MWCNT-Ti6Al4V	1000	100	10	50	4.403	99.40	463.1
1.0 MWCNT-Ti6Al4V	1000	100	10	50	4.394	99.20	485.3
1.5 MWCNT-Ti6Al4V	1000	100	10	50	4.371	98.7	569.8
Ti6Al4V	1100	100	10	50	4.430	100	401
0.5 MWCNT-Ti6Al4V	1100	100	10	50	4.413	99.61	502.5
1.0 MWCNT-Ti6Al4V	1100	100	10	50	4.402	99.40	557.8
1.5 MWCNT-Ti6Al4V	1100	100	10	50	4.392	99.14	588.5

4. Conclusion

In this study, Ti6Al4V and its nanocomposites comprising varying weight fractions of MWCNT were fabricated using the spark plasma sintering technique by employing different sintering temperatures and other fixed sintering parameters. The nanocomposites powders were initially

processed using the shift speed ball milling technique, and the admixed powders were further fabricated using the SPS technique. Subsequently, the sintering data were acquired and analyzed to understand the sinterability and the densification behaviour of the titanium alloy and the nanocomposites. Additionally, density measurements and microhardness tests were conducted on the sintered samples, and the following conclusions were drawn from the investigations:

1. The utilization of shift speed ball milling is a viable technique for effective dispersion of MWCNT in metal matrices.
2. Sintering temperature has tremendous impacts on the densification behaviour, sinterability, microhardness and microstructural evolution of titanium alloy and its nanocomposites fabricated by SPS.
3. The addition of MWCNT into the Ti6Al4V matrix led to the increase in sintering time of the nanocomposites during SPS.
4. The incorporation of MWCNT into Ti6Al4V matrix resulted in the increase of microhardness and the reduction of the density of the nanocomposites.

Acknowledgement

The authors would like to appreciate the National Research Foundation of South Africa in association with the World Academy of Science (NRF-TWAS) and the Global Excellence and Stature of the University of Johannesburg, South Africa for funding this research.

Reference

[1] M. Tokita, Development of large-size ceramic/metal bulk FGM fabricated by spark plasma sintering, in: Mater. Sci. Forum, Trans Tech Publ, 1999: pp. 83-88.

[2] Z.A. Munir, U. Anselmi-Tamburini, M. Ohyanagi, The effect of electric field and pressure on the synthesis and consolidation of materials: A review of the spark plasma sintering method, J. Mater. Sci. 41 (2006) 763-777.

[3] A.M. Okoro, S.S. Lephuthing, S.R. Oke, O.E. Falodun, M.A. Awotunde, P.A. Olubambi, A Review of Spark Plasma Sintering of Carbon Nanotubes Reinforced Titanium-Based Nanocomposites: Fabrication, Densification, and Mechanical Properties, JOM. (2018) 567-584.

[4] C.O. Ujah, O.M. Popoola, V.S. Aigbodion, Optimisation of spark plasma sintering parameters of Al-CNTs-Nb nano-composite using Taguchi Design of Experiment, Int. J. Adv. Manuf. Technol. 100 (2019) 1563-1573.

[5] O.E. Falodun, B.A. Obadele, S.R. Oke, O.O. Ige, P.A. Olubambi, Effect of TiN and TiCN additions on spark plasma sintered Ti6Al4V, Part. Sci. Technol. (2018) 1-10.

[6] O.E. Falodun, B.A. Obadele, S.R. Oke, A.M. Okoro, P.A. Olubambi, Titanium-based matrix composites reinforced with particulate, microstructure, and mechanical properties using spark plasma sintering technique: a review, Int. J. Adv. Manuf. Technol. (2019) 1-13.

[7] K. Yamazaki, S.H. Risbud, H. Aoyama, K. Shoda, PAS (plasma activated sintering): transient sintering process control for rapid consolidation of powders, J. Mater. Process. Technol. 56 (1996) 955-965.

[8] E. Ghasali, A. Fazili, M. Alizadeh, K. Shirvanimoghaddam, T. Ebadzadeh, Evaluation of microstructure and mechanical properties of Al-TiC metal matrix composite prepared by conventional, microwave and spark plasma sintering methods, Materials (Basel). 10 (2017) 1255.

[9] E. Ghasali, A. Pakseresht, A. Rahbari, H. Eslami-Shahed, M. Alizadeh, T. Ebadzadeh, Mechanical properties and microstructure characterization of spark plasma and conventional

sintering of Al-SiC-TiC composites, J. Alloys Compd. 666 (2016) 366-371.

[10] Y. Liu, J. Wang, Q. Fang, B. Liu, Y. Wu, S. Chen, Preparation of superfine-grained high entropy alloy by spark plasma sintering gas atomized powder, Intermetallics. 68 (2016) 16-22.

[11] H.Z. Niu, Y.F. Chen, D.L. Zhang, Y.S. Zhang, J.W. Lu, W. Zhang, P.X. Zhang, Fabrication of a powder metallurgy Ti2AlNb-based alloy by spark plasma sintering and associated microstructure optimization, Mater. Des. 89 (2016) 823-829.

[12] Z.-H. Ge, Y. Chang, F. Li, J. Luo, P. Fan, Improved thermoelectric properties of PEDOT: PSS polymer bulk prepared using spark plasma sintering, Chem. Commun. 54 (2018) 2429-2431.

[13] K. Wei, G.S. Nolas, Enhanced thermoelectric properties of polymer/inorganic bulk composites through EG treatment and spark plasma sintering processing, Scr. Mater. 150 (2018) 70-73.

[14] Ö. Balci, U. Burkhardt, M. Schmidt, J. Hennicke, M.B. Yaugci, M. Somer, Densification, microstructure and properties of TiB2 ceramics fabricated by spark plasma sintering, Mater. Charact. 145 (2018) 435-443.

[15] S. Grasso, T. Saunders, H. Porwal, B. Milsom, A. Tudball, M. Reece, Flash spark plasma sintering (FSPS) of α and β SiC, J. Am. Ceram. Soc. 99 (2016) 1534-1543.

[16] C. Leyens, M. Peters, Titanium and titanium alloys: fundamentals and applications, John Wiley & Sons, 2003.

[17] A.M. Okoro, M. Awotunde, O.A. Ajiteru, S.S. Lephuthing, P.A. Olubambi, R. Machaka, Effects of carbon nanotubes on the mechanical properties of spark plasma sintered titanium matrix composites - A review, in: 2018 IEEE 9th Int. Conf. Mech. Intell. Manuf. Technol. ICMIMT 2018, 2018 54-59.

[18] V.A.R. Henriques, P.P. de Campos, C.A.A. Cairo, J.C. Bressiani, Production of titanium alloys for advanced aerospace systems by powder metallurgy, Mater. Res. 8 (2005) 443-446.

[19] A.M. Okoro, R. Machaka, S.S. Lephuthing, M. Awotunde, P.A. Olubambi, Structural

integrity and dispersion characteristics of carbon nanotubes in titanium-based alloy, in: IOP Conf. Ser. Mater. Sci. Eng., 2018.

[20] A.M. Okoro, R. Machaka, S.S. Lephuthing, M.A. Awotunde, S.R. Oke, O.E. Falodun, P.A. Olubambi, Dispersion characteristics, interfacial bonding and nanostructural evolution of MWCNT in Ti6Al4V powders prepared by shift speed ball milling technique, J. Alloys Compd. (2019) 356-366..

[21] K. Kondoh, T. Threrujirapapong, H. Imai, J. Umeda, B. Fugetsu, Characteristics of powder metallurgy pure titanium matrix composite reinforced with multi-wall carbon nanotubes, Compos. Sci. Technol. 69 (2009) 1077-1081.

[22] B.G. Demczyk, Y.M. Wang, J. Cumings, M. Hetman, W. Han, A. Zettl, R.O. Ritchie, Direct mechanical measurement of the tensile strength and elastic modulus of multiwalled carbon nanotubes, Mater. Sci. Eng. A. 334 (2002) 173-178.

[23] R.S. Ruoff, D. Qian, W.K. Liu, Mechanical properties of carbon nanotubes: theoretical predictions and experimental measurements, Comptes Rendus Phys. 4 (2003) 993-1008.

[24] K.S. Munir, Y. Li, D. Liang, M. Qian, W. Xu, C. Wen, Effect of dispersion method on the deterioration, interfacial interactions and re-agglomeration of carbon nanotubes in titanium metal matrix composites, Mater. Des. 88 (2015) 138-148.

[25] K. Vasanthakumar, S.R. Bakshi, Effect of C/Ti ratio on densification, microstructure and mechanical properties of TiCxprepared by reactive spark plasma sintering, Ceram. Int. 44 (2018) 484-494.

[26] K.S. Munir, M. Qian, Y. Li, D.T. Oldfield, P. Kingshott, D.M. Zhu, C. Wen, Quantitative Analyses of MWCNT-Ti Powder Mixtures using Raman Spectroscopy: The Influence of Milling Parameters on Nanostructural Evolution, Adv. Eng. Mater. 17 (2015) 1660-1669.

[27] B. Debalina, N. Vaishakh, M. Jagannatham, K. Vasanthakumar, N.S. Karthiselva, R. Vinu, P. Haridoss, S.R. Bakshi, Effect of different nano-carbon reinforcements on microstructure and properties of TiO2composites prepared by spark plasma sintering, Ceram. Int. 42 (2016) 14266-14277.

[28] K.S. Munir, Y. Zheng, D. Zhang, J. Lin, Y. Li, C. Wen, Improving the strengthening efficiency of carbon nanotubes in titanium metal matrix composites, Mater. Sci. Eng. A. 696 (2017) 10-25.

[29] R. Spectrometers, Standard Guide for Raman Shift Standards for Spectrometer Calibration 1, 96 (2014) 1-11.

[30] E.W. Wong, P.E. Sheehan, C.M. Lieber, Nanobeam mechanics: elasticity, strength, and toughness of nanorods and nanotubes, Science (80). 277 (1997) 1971-1975.

[31] C.A. Handwerker, J.E. Blendell, R.L. Coble, Sintering of ceramics, in: Sci. Sinter., Springer, (1989) 3-37.

[32] J.H. Lehman, M. Terrones, E. Mansfield, K.E. Hurst, V. Meunier, Evaluating the characteristics of multiwall carbon nanotubes, Carbon N. Y. 49 (2011) 2581-2602.

[33] K.S. Munir, Y. Zheng, D. Zhang, J. Lin, Y. Li, C. Wen, Microstructure and mechanical properties of carbon nanotubes reinforced titanium matrix composites fabricated via spark plasma sintering, Mater. Sci. Eng. A. 688 (2017) 505-523.

[34] K.S. Munir, Y. Li, M. Qian, C. Wen, Identifying and understanding the effect of milling energy on the synthesis of carbon nanotubes reinforced titanium metal matrix composites, Carbon N. Y. 99 (2016) 384-397.

[35] M.R. Plichta, J.C. Williams, H.I. Aaronson, On the existence of the β→αm transformation in the alloy systems Ti-Ag, Ti-Au, and Ti-Si, Metall. Trans. A. 8 (1977) 1885-1892.

[36] M.R. Plichta, H.I. Aaronson, J.H. Perepezko, The thermodynamics and kinetics of the β → α.m transformation in three Ti-X system, Acta Metall. 26 (1978) 1293-1305.

[37] A.A. Antonysamy, Microstructure, texture and mechanical property evolution during additive manufacturing of Ti6Al4V alloy for aerospace applications, The University of Manchester (United Kingdom), 2012.

[38] L.L. Ye, M.X. Quan, Synthesis of nanocrystalline TiC powders by mechanical alloying, Nanostructured Mater. 5 (1995) 25-31.

[39] A.C. Ferrari, Raman spectroscopy of graphene and graphite: disorder, electron--phonon coupling, doping and nonadiabatic effects, Solid State Commun. 143 (2007) 47-57.

[40] K.S. Munir, D.T. Oldfield, C. Wen, Role of Process Control Agent in the Synthesis of Multi-Walled Carbon Nanotubes Reinforced Titanium Metal Matrix Powder Mixtures, Adv. Eng. Mater. 18 (2016) 294-303.

[41] P. Delhaes, M. Couzi, M. Trinquecoste, J. Dentzer, H. Hamidou, C. Vix-Guterl, A comparison between Raman spectroscopy and surface characterizations of multiwall carbon nanotubes, Carbon N. Y. 44 (2006) 3005-3013.

[42] B.H. Lohse, A. Calka, D. Wexler, Raman spectroscopy sheds new light on TiC formation during the controlled milling of titanium and carbon, J. Alloys Compd. 434 (2007) 405-409.

[43] M. V Klein, J.A. Holy, W.S. Williams, Raman scattering induced by carbon vacancies in Ti C x, Phys. Rev. B. 17 (1978) 1546.

[44] A.O. Adegbenjo, P.A. Olubambi, J.H. Potgieter, M.B. Shongwe, M. Ramakokovhu, Spark plasma sintering of graphitized multi-walled carbon nanotube reinforced Ti6Al4V, Mater. Des. 128 (2017) 119-129.

[45] O.E. Falodun, B.A. Obadele, S.R. Oke, M.E. Maja, P.A. Olubambi, Effect of sintering parameters on densification and microstructural evolution of nano-sized titanium nitride reinforced titanium alloys, J. Alloys Compd. 736 (2018) 202-210.

[46] Z.H. Zhang, X.B. Shen, F.C. Wang, S.K. Lee, L. Wang, Densification behavior and mechanical properties of the spark plasma sintered monolithic TiB2 ceramics, Mater. Sci. Eng. A. 527 (2010) 5947-5951.

[47] S.R. Oke, O.O. Ige, O.E. Falodun, B.A. Obadele, M.B. Shongwe, P.A. Olubambi, Optimization of process parameters for spark plasma sintering of nano structured SAF 2205 composite, J. Mater. Res. Technol. 7 (2018) 126-134.

[48] C.S. Bonifacio, J.F. Rufner, T.B. Holland, K. van Benthem, In situ transmission electron microscopy study of dielectric breakdown of surface oxides during electric field-assisted sintering of nickel nanoparticles, Appl. Phys. Lett. 101 (2012) 93107.

[49] E. Ghasali, K. Shirvanimoghaddam, A.H. Pakseresht, M. Alizadeh, T. Ebadzadeh, Evaluation of microstructure and mechanical properties of Al-TaC composites prepared by spark plasma sintering process, J. Alloys Compd. 705 (2017) 283-289.

[50] S.R. Oke, O.O. Ige, O.E. Falodun, A.M. Okoro, M.R. Mphahlele, P.A. Olubambi, Powder metallurgy of stainless steels and composites: a review of mechanical alloying and spark plasma sintering, Int. J. Adv. Manuf. Technol. (2019) 1-20.

[51] K. Vasanthakumar, S.R. Bakshi, Effect of C/Ti ratio on densification, microstructure and mechanical properties of TiCx prepared by reactive spark plasma sintering, Ceram. Int. 44 (2018) 484-494.

[52] S. Xu, M. Wang, L. Qiao, J. Bing, Q. Zou, Y. Zhao, Enhancing the sintering ability of TiNx by introduction of nitrogen vacancy defects, Ceram. Int. 41 (2015) 9514-9520.

[53] M. Gendre, A. Maitre, G. Trolliard, Synthesis of zirconium oxycarbide (ZrCxOy) powders: Influence of stoichiometry on densification kinetics during spark plasma sintering and on mechanical properties, J. Eur. Ceram. Soc. 31 (2011) 2377-2385.

[54] Y. Cheng, Z. Cui, L. Cheng, D. Gong, W. Wang, Effect of particle size on densification of pure magnesium during spark plasma sintering, Adv. Powder Technol. 28 (2017) 1129-1135.

[55] Y. Song, Y. Li, Z. Zhou, Y. Lai, Y. Ye, A multi-field coupled FEM model for one-step-forming process of spark plasma sintering considering local densification of powder material, J. Mater. Sci. 46 (2011) 5645-5656.

[56] N. Saheb, Sintering behavior of CNT reinforced Al6061 and Al2124 Nanocomposites, Adv. Mater. Sci. Eng. 2014 (2014).

[57] D. Lin, M. Saei, S. Suslov, S. Jin, G.J. Cheng, Super-strengthening and stabilizing with carbon nanotube harnessed high density nanotwins in metals by shock loading, Sci. Rep. 5 (2015) 15405.

[58] A.O. Adegbenjo, P.A. Olubambi, J.H. Potgieter, M.B. Shongwe, M. Ramakokovhu, Spark plasma sintering of graphitized multi-walled carbon nanotube reinforced Ti6Al4V, Mater.

Des. 128 (2017) 119-129.

[59] S. Li, B. Sun, H. Imai, T. Mimoto, K. Kondoh, Powder metallurgy titanium metal matrix composites reinforced with carbon nanotubes and graphite, Compos. Part A Appl. Sci. Manuf. 48 (2013) 57-66.

[60] A.M.K. Esawi, K. Morsi, A. Sayed, M. Taher, S. Lanka, Effect of carbon nanotube (CNT) content on the mechanical properties of CNT-reinforced aluminium composites, Compos. Sci. Technol. 70 (2010) 2237-2241.

[61] K.S. Munir, Y. Li, J. Lin, C. Wen, Interdependencies between graphitization of carbon nanotubes and strengthening mechanisms in titanium matrix composites, Materialia. (2018) 122-138.

Paper 4: Effect of multiwall carbon nanotubes addition on the microstructural evolution and mechanical properties of spark plasma sintered Ti6Al4V nanocomposites

Status: Submitted to Journal

Abstract

Recent development in advanced material engineering has fostered an improvement in the properties of conventional materials by the incorporation of nanomaterials with outstanding properties into their matrices. In this study, the influence of multiwall carbon nanotubes (MWCNT) additions on the microstructural evolution and mechanical properties of sintered Ti6Al4V based nanocomposites was investigated. This was carried out by dispersing different concentrations (0.5, 1.0 and 1.5 wt.%) of MWCNT into the Ti6Al4V matrix using shift speed ball milling technique. Thereafter, the Ti6Al4V and the nanocomposites were consolidated via the spark plasma sintering technique. Various characterization techniques such as scanning electron microscopy (SEM), transmission electron microscopy (TEM) and optical microscopy (OM) were employed to understand the microstructural evolution of the samples after the dispersion and sintering process. Subsequently, micromechanical and nanoindentation was conducted to reveal the hardness, nanohardness, elastic modulus and load-displacement behaviours of the fabricated alloy and nanocomposites. The morphological examination using SEM and TEM revealed the dispersibility of MWCNT dispersed within the Ti6Al4V matrix. Besides, the selected area diffraction (SAED) and the fast Fourier Transform (FFT) pattern demonstrated that the increase in concentration of the MWCNT exposed the nanotubes to adverse stresses during the dispersion process. Furthermore, the addition and increase in concentration of the MWCNT resulted in microstructural and phase evolution of the nanocomposites. Meanwhile, the nanocomposites displayed tremendous improvement in microhardness, nanohardness and elastic modulus up to 46.86%, 150.8%, and 169.5% respectively with the highest concentration of MWCNT.

Keywords: Microstructural evolution; Mechanical properties; Titanium alloy; multiwall carbon nanotubes; Spark plasma sintering

1. Introduction

Multiwall carbon nanotubes (MWCNT) are highly desirable in diverse engineering applications due to their notable thermal, mechanical and electrical properties [1]. They have tubular morphology with ultra-high aspect ratio in the range of 100-100000 and lightweight of 1.7-2.0 g/cm^3 [2]. Additionally, it has a tensile strength close to 150 GPa, a distinctly high elastic modulus of up to 1 Tera Pascal [3], thermal conductivity of up to 0.000004 W/m/K [4] and electrical conductivity of 0.000002 Ωcm [5]. These outstanding properties of MWCNT are traceable to the strong graphitic carbon to carbon network in its structures, nanoscale dimensions and tubular morphology [6–8]. MWCNT has been successfully utilized as a reinforcing material to improve the thermal, mechanical and electrical properties of various engineering materials. In recent years, properties such as toughness of ceramics has been effectively enhanced using MWCNT [9] and strength of polymeric materials has been augmented by MWCNT [10]. In addition, the lightweight, strength, toughness and tribological properties of various metal matrices has been successfully enhanced by the addition of MWCNT to form metal matrix composites [11–13].

Amongst the metal matrix composites used in numerous engineering applications, the demand for titanium-based nanocomposites have spurred unprecedented attention in various automobile, biomedical and aerospace industries [14]. Furthermore, titanium and its alloys are highly desirable in various industrial and technological applications owing to their excellent corrosion resistance, biocompatibility, weldability, specific strength and lightweight [15–17]. Titanium alloys are classified into various grades depending on their compositions, phases and properties. However, the grade 5 of the titanium alloy popularly called Ti6Al4V is the most highly employed titanium alloy for various applications owing to its higher strength and heat-treatability [18]. It has a dual phase microstructure consisting of the alpha and beta phases, which changes at various operating temperature. The alpha phases exist at lower operating temperatures below 884 ^oC and it has a hexagonal closed packed structure (HCP). Conversely, the beta phase occurs at higher operating temperatures (between 884-1668 ^oC) with body centered cubic structure (BCC) [19]. The combination of the different crystal structures resulting from allotropic transformation in the dual phase titanium alloy is responsible for its improved properties than other grades of titanium-based alloy.

Regardless of the outstanding properties and flexibility of Ti6Al4V, its elastic modulus is twice as less as the elastic modulus of iron [20]. This implies that the elastic strain energy required for the formation of a new phase in Ti6Al4V during allotropic transformation is absolutely lesser than elastic strain energy during the allotropic transformation of iron. In addition, it possessed low wear resistance and hardness that is far lesser than that of super-duplex stainless steels and nickel-based alloys, which are widely applied in the production of turbine blades [21].

In recent years, various attempts have been made to augment the mechanical properties of Ti6Al4V using numerous ceramics-based reinforcements by fabricating titanium matrix composites. Falodun et al., [22] achieved tremendous improvement in the hardness Ti6Al4V after reinforcing the alloy with TiN and TiCN. Similarly, Zhao et al., [23] reported an improvement in the tribological properties of Ti6Al4V reinforced with titanium carbide (TiC) and titanium diboride (TiB) powders. However, owing to the remarkable properties of MWCNT has shown that it's a best candidate to augment the properties of Ti6Al4V.

Past studies have shown the effectiveness of MWCNT in improving the mechanical properties of various titanium-based materials. This was reported by Kondoh et al. [24], whose work confirmed the improvement in tensile strength, yield strength, microhardness and strain of commercially pure titanium by the incorporation of MWCNT as reinforcement phase. Similarly, Sun et al., [25] recorded an improvement in ultimate tensile strength and hardness of titanium by reinforcing it with MWCNT. Additionally, Munir et al., [26] realized an improvement in the mechanical and tribological properties of titanium by the integration of MWCNT into its matrix. These improvements in properties of titanium are traceable to the uniform dispersion, load-carrying abilities and unique mechanical properties of MWCNT.

To fabricate titanium-based nanocomposites using MWCNT as reinforcing materials, it is pertinent to accomplish uniform dispersion of MWCNT in the titanium-based matrices without compromising its structural integrity. This is paramount for effective load transfer from the matrix to the reinforcement phase. However, MWCNT tend to cluster into bundles which inhibits their homogeneous dispersion in the metal matrix [8,27]. This dispersion characteristics of MWCNT is ascribed to the strong Van der Waal forces between its tubes, nanoscale dimensions and high aspect

ratio [28]. Conversely, an effective dispersion technique is required to achieve uniform dispersion of MWCNT in metal matrices without destroying the structures of the MWCNT.

The quest to reinforced titanium-based matrices using MWCNT, diverse powder metallurgy techniques have been employed in dispersing MWCNT in the metal matrix. Sonication [6], low energy ball milling [29] and high energy ball milling (HEBM) [30] have been employed to disperse MWCNT in titanium-based matrices. However, each of these dispersion techniques have their pros and cons. Meanwhile, high energy ball milling dispersion technique has the tendency of achieving homogeneous dispersion of MWCNT in the metal matrix [31]. However, it has a propensity of destroying the tubular structures of the MWCNT and creating structural defects on the nanotubes, especially at higher milling speed and prolonged time [6]. These HEBM-induced defects on the MWCNT can exists as open edges and vacancies in the form of sp3 C-C bond [32].

Additionally, the destruction of the walls of the MWCNT results in the conversion of the sp2 carbon to carbon network into sp3 (amorphous carbon), which can easily react with the titanium to form interfacial products (carbides) [33]. Meanwhile, the interfacial products can assist in load bearing capability of the composites alongside with the reinforcing ability of the MWCNT, thus resulting in a composites with improved mechanical properties [34].

Recent innovations in materials development have emphasized on the reinforcing capabilities of MWCNT in improving the mechanical properties of titanium-based matrices. This has engendered the exploitation of the vital load bearing ability of MWCNT to form composites with improved properties. Besides the utilization of MWCNT to enhance the properties of titanium-based matrices, the application of improved consolidation technique is very paramount in synthesizing nanocomposites with enhanced properties.

Over the years, spark plasma sintering (SPS) which is an improved consolidation technique has been successfully utilized to fabricate titanium-based nanocomposites of outstanding properties. This was reported by Munir et al.[1], where improvement in elastic modulus and nanohardness was achieved on commercially pure titanium using MWCNT as reinforcement and SPS as the consolidation technique. Likewise, Wang et al.[35], achieved a tremendous improvement in compressive strength of up to 61 % on pure titanium after reinforcing the metal matrix with MWCNT and sintering the compact with SPS technique. Additionally, they reported an improvement in the microhardness and

thermal diffusivity of the fabricated composites with the addition and increase in concentration of MWCNT. These improvements in mechanical and tribological properties of pure titanium by the addition of MWCNT can be ascribed to the load-bearing ability of the MWCNT and the modification of the microstructure titanium matrix. Owing to the interfacial reaction between MWCNT and the titanium matrix during milling or sintering, a hard carbide phase (TiC) is usually formed which assist in augmenting the mechanical and tribological properties of the titanium during the addition of MWCNT [36]. In addition, the strengthening of the titanium matrix may be linked to the dispersion of the MWCNT in the metal matrix, which in turn helps to pin down dislocation motion during plastic deformation of the composites [37].

To date, the influence of MWCNT addition on the microstructural evolution, mechanical properties and fracture behaviour of Ti6Al4V has not been satisfactorily studied yet. Hence, in this study, MWCNT of varying concentrations were dispersed in Ti6Al4V using shift speed ball milling. Afterwards, the admixed powders were sintered using the SPS technique. Furthermore, the microstructural changes, mechanical and fracture behaviour of the sintered nanocomposites were quantitatively investigated.

2. Materials and Method

2.1. As-received materials

The MWCNT powders used for this study comprises of 99.7 % purity and it was acquired from Nanocycl Belgium. Also, it has a diameter of 9.5 nm and a length of 1.5 mm. Meanwhile, the prealloyed Ti6Al4V powders which served as the matrix material was outsourced from TLS Technik GmbH & Co Germany. Consequently, the stearic acid used as a process control agent during the milling of the powders was purchased from Glass blown & Volumetric Glassware & Chemicals in Johannesburg, South Africa.

2.2 Dispersion of MWCNT in Ti6Al4V matrix using shift speed ball milling technique

The Ti6Al4V powders was weighed alongside with MWCNT powders of varying concentrations (0.5, 1.0 & 1.5 wt. %) and stearic acid (1.0 wt.%) and subsequently placed into a steel vial. The steel vial comprises of outer diameter of 250 mm and inner diameter of 100 mm. Steel balls of 5 mm and 10 mm were added to the measured powders as milling aid. The steel vial, which comprises the

measured powders and steel ball, was then transferred into a low-speed ball mill (Retch 100 PM) for preliminary milling operation. The milling operation was carried out with the following milling parameters; milling speed of 150 revolution per minute (rpm), time of 8 hours (h) and ball to powders ratio of 10:1 respectively. Meanwhile, a relaxation time of 10 min for every 10 minutes of milling was used to prevent the charged powders from overheating and further minimizes the tendency of interfacial reaction during the milling operation.

Afterwards, the steel vial comprising the pre-milled powders was transferred into a high-speed ball mill (Retch 400 PM). This is for additional milling of the powders to aid homogeneous dispersion of the MWCNT in the Ti6Al4V powders. The additional milling operation was carried out with a speed of 100 rpm for 1 h. The milling operation is schematically presented in Figure 1.

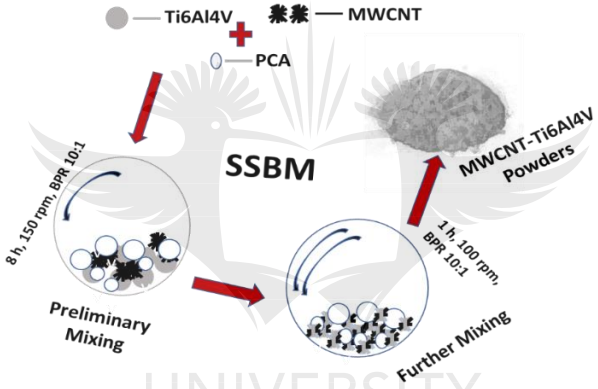

Figure 1: Schematic diagram of the processing of nanocomposite powders [8]

2.3. Sintering of the Ti6Al4V and Ti6Al4V nanocomposites using SPS technique

Prior to the sintering operation, the admixed powders were weighed and charged into a cylindrical graphite die of Ø 20 mm diameter. Subsequently, the charged powders were compacted under a force of 10 KN to promote green strength and conductivity between the die and the charged powders. Afterwards, the compacted nanocomposite powder was transferred into the SPS (model HHPD-25, FCT Germany) sintering chamber for the fabrication process. The sintering parameters used for the fabrication process include sintering temperature of 1000 ^{o}C, heating rate of 100 ^{o}C/min, compressive pressure of 50 MPa, and holding time of 10 min. After the fabrication process, the sintered samples were left to cool in the sintering chamber and subsequently sandblasted to remove graphite foils from the surface.

2.4. Characterization of starting, admixed powders and fabricated MWCNT-Ti6Al4V nanocomposites

To understand the morphology of the as-received and the mixed powders after the SSBM operations, the microstructural features of the powders were characterized using scanning electron microscope (Carl Zeiss Sigma FESEM) and JEOL-Jem 2100 transmission electron microscope (TEM). TEM was used to evaluate the walls of the MWCNT to reveal the structure of the nanotubes before and after dispersion in the Ti6Al4V matrix. Also, TEM was used to capture the fast Fourier transform (FFT) of the powders. This is to evaluate the interlayer spacing and the crystalline nature of the nanotubes before and after dispersion. The structural integrity of the MWCNT before and after dispersion in the Ti6Al4V matrix was investigated with Raman spectroscopy (WITEC 2.0). This was carried out by acquiring the Raman spectra of the powders in the range of 200 to 1800 cm^{-1} after probing ten various spots on the powder using a 514 nm laser beam at an acquisition of 50 s. Furthermore, the intensity of the acquired Raman peaks (D-band and G-band) and their corresponding positions on the Raman shift were assessed by deconvoluting the Raman spectra using the WITEC 2.10 software. Meanwhile, the Raman shifts were calibrated in accordance to ASTM E1840-96 [38]. The phase analysis of the powders and sintered nanocomposites were characterized using X-Ray diffractometer (XRD, Rigaku D/max-rB) to assess the changes in the phases of the powders during SSBM and sintering operation. The analysis was investigated by scanning the materials using Cu-Kα (λ= 0.154 nm) radiation over an angular range of 10-90^{o} at a scanning rate of 1 ^{o}/min. The various phases present in the material were assessed using ICDD card reference data.

Subsequently, the metallographic preparation (grinding) was done on the sintered samples using silicon carbide papers with various grit sizes (P320-1200). Afterwards, the samples were further grind using Aker Allegra 3 plate with 6 µm suspension to remove induced scratches from the samples. Furthermore, polishing was carried out using fused silica suspension to obtain the mirror-like feature of the samples. The polished samples were characterized using optical microscope and SEM. Also, the fractured surface of the samples was analyzed using SEM.

2.5. Densification and mechanical test of the fabricated Ti6Al4V and MWCNT-Ti6Al4V nanocomposites

The theoretical density of the fabricated Ti6Al4V and the Ti6Al4V based nanocomposites was calculated by the application of the composite rule of mixture bearing in mind that the theoretical densities of Ti6Al4V and MWCNT are 4.43 g/cm^3 and 2.11 g/cm^3 respectively. While the experimental density was ascertained from the arithmetic mean of five different density readings for each sample in accordance to ASTM B962 using the Archimedes' principle [39]. Furthermore, the densification was calculated by dividing the average density reading by the theoretical density and multiplying the result by 100%.

Subsequently, the Vickers microhardness values of the sintered alloy and the nanocomposites were investigated using INNOVA FALCON 500 series microhardness tester. This was carried out by indenting the polished surface of the sample using a diamond indenter and load of 100 gf (0.98 N) at a dwelling time of 10 s. Various phases of the sample were indented and the mean value was reported for the Vickers hardness value of the material. Furthermore, nanoindentation was carried out on the polished samples using ultra nanoindenter (UNHT) with a load of 100 mN. An average of 15 indentations were made on the polished sample to ascertain the reliability of the data generated. The major mechanical properties determined from the nanoindentation study were reduced elastic modulus and hardness, which were evaluated from the load-displacement data in accordance with Oliver and Pharr method [40]. The reduced elastic modulus (E_r) was calculated from the unloading part of the load-displacement curve. Meanwhile, the nanohardness was calculated by the application of the expression in equation (1), which indicates that nanohardness (H_N) has a relationship with the maximum load (P_{max}) and the projected contact area (A_c) at the maximum load.

$$H_N = \frac{P_{max}}{A_c} \qquad (1)$$

Besides, the reduced elastic modulus can be calculated from equation (2), where E_s and E_i are the elastic modulus of the sample and the indenter respectively [41].

$$\frac{1}{E_r} = \frac{1-v_s^2}{E_s} + \frac{1-v_i^2}{E_i} \qquad (2)$$

3. Results and discussion

3.1 Microstructural analysis of starting and mixed MWCT-Ti6Al4V powders

The microstructural analysis of the starting powders was carried out using SEM and TEM to ascertain the morphological features prior to the dispersion process. This is shown in Figure 2 (a-d). The SEM image in Figure 2 (a) represents the spherical features of the Ti6Al4V particles with average size of 25 μm while Figure 2 (b) shows the SEM image of the as-received MWCNT, which depicts the clustering of the individual multiwall nanotubes.

Moreover, the TEM image in Figure 2 (c) revealed the tubular morphology of the clustered pristine MWCNT while the inset shows the selected area diffraction pattern (SAED) of the as-received nanotubes. The SAED pattern is usually employed to confirm the amorphous and crystalline phases of the MWCNT before and after their dispersion in the matrix materials. The SAED pattern in Figure 2 (c) shows the clear rings of the graphitic planes (002) and (100) which depicts the crystalline nature of the nanotubes without any alterations of the planes [42]. Besides, a highly crystalline nanotubes is associated with similar chirality and sharp coaxial rings with fewer halo ring pattern [8]. Furthermore, the TEM image in Figure 2 (d) shows the walls of the tubular structure of the MWCNT while the inset depicts the fast Fourier transform (FFT) pattern of the pristine nanotubes. From Figure 2 (d), it was observed that there was no trace of defects in the form of deformation on the walls of the nanotubes with interlayer spacing of 0.3461 nm. This was further confirmed by the FFT pattern which shows sharp narrow peaks which indicates high crystalline nature of the pristine MWCNT [43]. Besides, the TEM image in Figure 2 (d) is in conformity with the SEM image in 2 (b) which shows the morphology of the entangled pristine MWCNT.

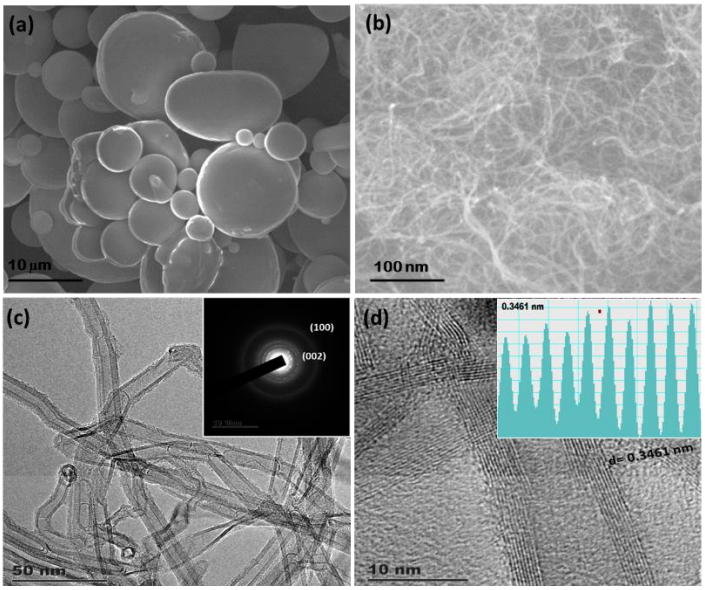

Figure 2. SEM of the starting Ti6Al4V (a), MWCNT (b), and TEM images of MWCNT (c-d) powders

3.2 Influence of SSBM on the dispersion features of MWCNT in Ti6Al4V powders

Over the years, emphasis has been made on the effective transfer of the unique properties of MWCNT into matrix materials during composite production. To realize the transfer of the nanotubes' properties into the matrix materials, the uniform dispersion and interfacial bonding of the MWCNT in the matrix must be accomplished without conceding the tubular structures of the nanotubes during dispersion [44]. Additionally, to realize homogenous dispersion and good interfacial bonding during the dispersion process requires adequate impact energy to curb the strong Van der Waals forces that occurs between the individual nanotubes [30]. The essence of the adequate impact energy during dispersion is to induce forces to de-entangle the clustered MWCNT and spread it across the matrix materials. However, the impact energy should not be too high, such that it introduces structural defects on the walls of the nanotubes.

Although, numerous techniques have been employed in recent years to achieve the uniform dispersion of MWCNT in various metal matrices [6,45,46]. However, this study employs the use of shift speed ball milling technique to uniformly disperse MWCNT into Ti6Al4V matrix. This technique involves the application of both low-speed ball mill and high-speed ball mill with regulated milling parameters to foster the homogenous dispersion of MWCNT [8,47]. The SEM images in Figure 3 (a-c) shows the dispersion features of MWCNT in Ti6Al4V powders after SSBM.

From the SEM image in Figure 3 (a), which shows the dispersion features of the mixed powder comprising of 0.5 wt.% MWCNT, it was observed that there was homogenous dispersion of the nanotubes within the Ti6Al4V matrix. Additionally, good interfacial bonding between the nanotubes and the Ti6Al4V particles was recorded. This was confirmed from the inset in Figure 3 (a), which shows the microstructural evolution and interfacial bonding at higher magnification. The microstructural evolution, interfacial bonding and dispersion characteristics of the MWCNT in the mixed powder of this nanocomposite grade is ascribed to the adequate impact energy exerted on the powders during SSBM that resulted in the deagglomeration and uniform dispersion of the nanotubes in the Ti6Al4V matrix.

The SEM image in Figure 3 (b) shows the microstructural evolution, dispersion features and interfacial bonding of the 1.0 wt.% MWCNT in Ti6Al4V powders. From the SEM image, homogenous dispersion and good interfacial bonding of the nanotubes to the Ti6Al4V particles was observed. Furthermore, the inset in the SEM image also depicts the embedment of the nanotubes in the Ti6Al4V particles which represents good bonding between the composite components. The good interfacial bonding and dispersion features of the MWCNT achieved during SSBM can be ascribed to the sufficient impact energy exerted on the powders during the dispersion process. Moreover, the SEM image in Figure 3 (c) shows the dispersion features of 1.5 wt.% MWCNT in the Ti6Al4V powders. From this SEM image, the MWCNT were agglomerated at various interstitial sites of the Ti6Al4V particles, which indicates that the nanotubes were not fully dispersed in the matrix materials. The inset in Figure 3 (c) further confirmed the agglomeration of the nanotubes on the Ti6Al4V matrix. From the dispersion features of the nanotubes, it can be deduced that there are stronger Van der Waal forces with increase in the concentration of MWCNT in this composite grade. Therefore, to achieve adequate dispersion of the 1.5 wt.% MWCNT in the Ti6Al4V powders, it is pertinent to increase the milling parameters so as produce an adequate impact energy that will eventually curb the stronger Van der Waal forces and de-entangle the nanotubes.

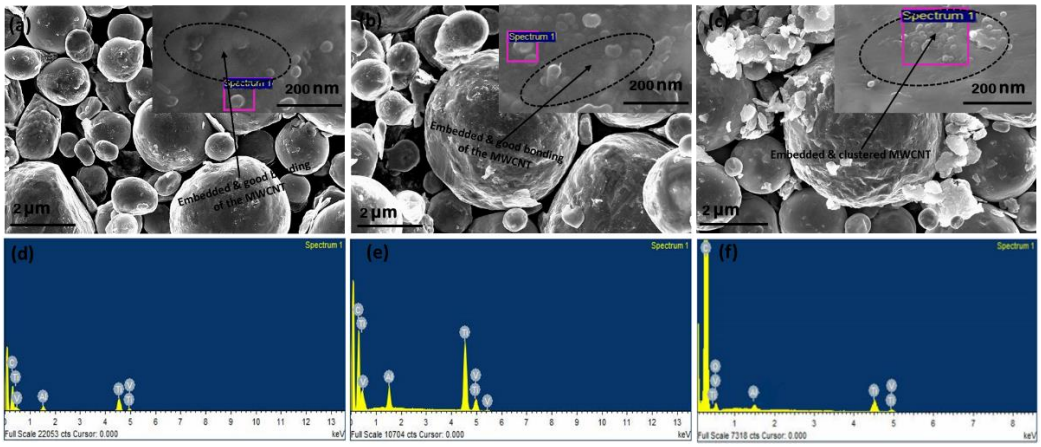

Figure 3: SEM results of the mixed composite powders (MWCNT-Ti6Al4V) comprising of 0.5 wt.% (a), 1.0 wt.% (b) and 1.5 wt.% MWCNT (c) and their conforming EDX (d-f).

To further ascertain the nano-structural evolution, dispersive features and the structural integrity of MWCNT in the mixed powders were characterized using high-resolution transmission electron microscope (HRTEM). The results of the HRTEM analysis are shown in Figure 4 (a-f). Figure 4 (a), which presents the morphology of the mixed powders comprising of 0.5 wt.% MWCNT, indicates the de-entangled, embedded and dispersed nanotubes around the Ti6Al4V powder. Meanwhile, the inset in Figure 4 (a) shows the SAED pattern of the nanotubes after dispersion in the metal matrix. From the SAED pattern, sharp rings of the graphite planes were observed, which depicts the crystalline nature of the nanotubes after the dispersion process. However, some distortion were observed in the walls of the MWCNT, which is shown in the TEM image in Figure 4 (b).. As shown in the inset in the TEM image, which represents the FFT pattern of the MWCNT after the dispersion process, a reduction in the interlayer spacing from 0.3461 nm in the pristine MWCNT to 0.3400 nm was observed. The reduction and distortion in the walls of the nanotubes may be ascribed the collapse of the walls during the dispersion process. However, the collapse of the walls of nanotubes cannot be attributed to severe defects (open edges and vacancies), which may have appeared in the form of streaks and extra spots on the SAED pattern in Figure 4 (a) [48].

The TEM image in Figure 4 (c) represents the morphology of the mixed powders comprising of 1.0 wt.% MWCNT. From the TEM image, the dispersed, deagglomerated and embedded nanotubes were observed after the SSBM process. Moreover, the inset in Figure 4 (c) shows the SAED pattern of the MWCNT after the dispersion process which depicts the fading out of the coaxial and halo ring

patterns. This feature may be attributed to the strain exerted on the MWCNT during the dispersion process. This is because an increase in the concentration of the nanotubes in the composite grade exposed more MWCNT to collision with the balls during milling. The TEM image in Figure 4 (d) shows the walls of the MWCNT while the inset indicates the FFT pattern of the nanotubes after the SSBM process. From the TEM and the FFT pattern in Figure 4 (d), distortions were observed in the walls of the nanotubes during the dispersion process. This resulted in an increase of the interlayer spacing of the walls from 0.3461 nm in the pristine MWCNT to 0.3521 nm after dispersion. The increase in the interlayer spacing and the fading out of the coaxial and halo rings of the nanotubes may be ascribed to the adequate collision of the balls on the MWCNT, which exerted some stresses on the powders during the dispersion.

Furthermore, the TEM image in Figure 4 (e) shows the dispersion features of the 1.5 wt.% MWCNT in the Ti6Al4V powders. From the TEM image, it was observed that more nanotubes were segregated out from the Ti6Al4V powders, which is an indication of stronger Van der Waals forces between the nanotubes. Besides, the SAED pattern of the nanotubes shows the presence of streaks and extra spots, which indicates some defects on the nanotube after the dispersion process [48]. Additionally, Figure 4 (f) shows the wall of the nanotubes after the dispersion process where distortions were glaringly observed. The FFT pattern of the nanotubes also indicates the increase in the interlayer spacing from 0.3461 nm of the pristine MWCNT to 0.3533 nm after the dispersion process. From all indications, it can be deduced that an increase in the concentration of MWCNT in the composite grades decreases their tendency for uniform dispersion and further expose the nanotubes to more structural strain during the dispersion process.

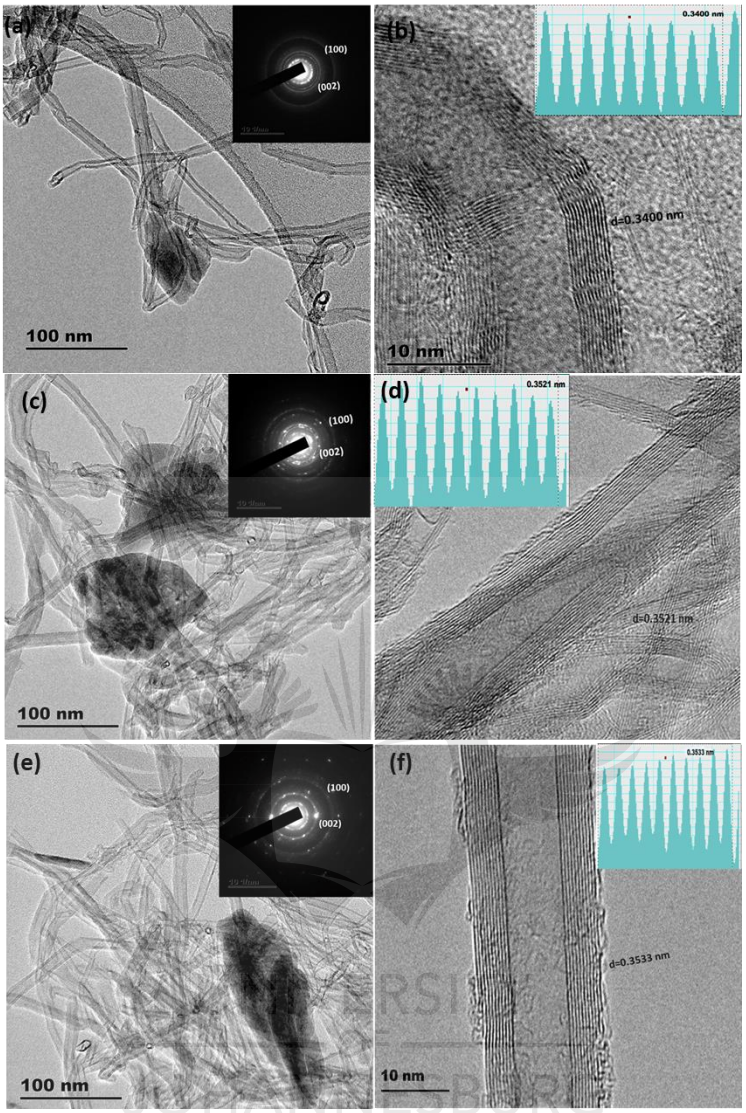

Figure 4: HRTEM images of MWCNT-Ti6Al4V comprises of 0.5 wt.% (a & b), 1.0 wt.% (c &d), and 1.5 wt.% MWCNT (e & f) after SSBM process.

3.3. Microstructural evolution of fabricated Ti6Al4V and MWCNT-Ti6Al4V nanocomposites after SPS

Immediately after the dispersion process, the starting Ti6Al4V and mixed powders were consolidated using the SPS process. Figure 5 (a-d) shows the SEM images of the fabricated Ti6Al4V and MWCNT-Ti6Al4V nanocomposites comprising of varying concentration of the nanotubes. Figure 5 (a) represents the SEM image of the fabricated Ti6Al4V alloy, which depicts a network of alpha (α) lamellar. The microstructural features observed on the SEM image of the fabricated Ti6Al4V may

be attributed to sintering above the allotropic transformation temperature of Ti6Al4V and the slow cooling process in the sintering chamber. Meanwhile, sintering of Ti6Al4V above the (α/β) transformation temperature will result in grain growth irrespective of the heating rate and cooling conditions [20].

The SEM image of the sintered MWCNT-Ti6Al4V nanocomposites comprising of 0.5 wt.% MWCNT is shown in Figure 5 (b). From the SEM micrograph, it was observed that MWCNT were dispersed across the Ti6Al4V phases. Similarly, the SEM micrograph in Figure 5 (c) shows the even dispersion of 1.0 wt.% MWCNT across the Ti6Al4V matrix. However, a more clustered MWCNT was observed in the SEM micrograph of the nanocomposite comprising of 1.5 wt.% MWCNT. These microstructural evolutions are in conformity with the SEM and TEM images of the admixed powders discussed earlier.

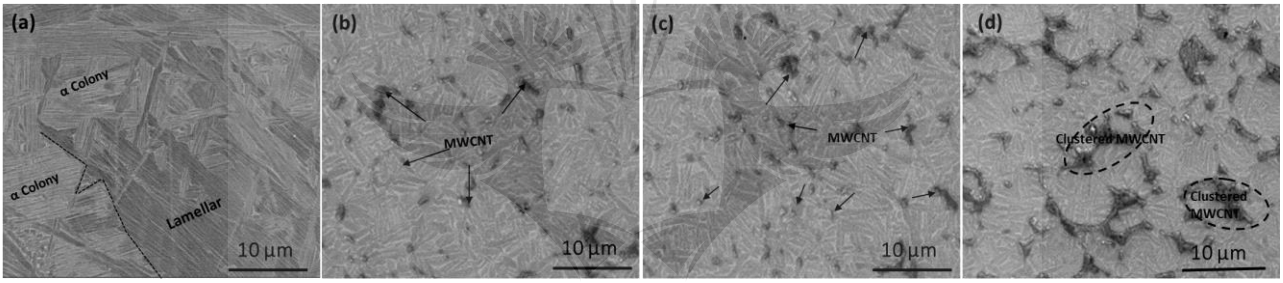

Figure 5: SEM images of the fabricated Ti6Al4V (a) and MWCN-Ti6Al4V nanocomposites comprising of 0.5 wt.% (b), 1.0 wt.% (c), and 1.5 wt.% (d) MWCNT

Subsequently, the fabricated Ti6Al4V and the corresponding nanocomposites were characterized using optical microscope and the results are shown in Figure 6. Figure 6 (a) is the optical micrograph (OM) of the fabricated Ti6Al4V alloy which depicts colonies of alpha phase lamellar. This microstructural feature, which corresponds to the SEM image discussed earlier, may be ascribed to the sintering above the (α/β) transus temperature and the slow cooling process that trapped the α lamellar phases within the alloy.

Additionally, the OM of the fabricated Ti6Al4V nanocomposites comprising of 0.5 wt.% MWCNT is shown in Figure 6 (b) where MWCNT (dark spots) were dispersed across the Ti6Al4V phases. Similarly, this microstructural feature was observed in Figure 6 (c & d) where the MWCNT were spread across the Ti6Al4V phases. However, more clustered MWCNT were seen in OM image in Figure 6 (d), which revealed the agglomeration of nanotubes at higher concentration. These results

are in conformity with the SEM micrographs discussed earlier where the dispersion features decreased with an increase in concentration of MWCNT in the nanocomposites.

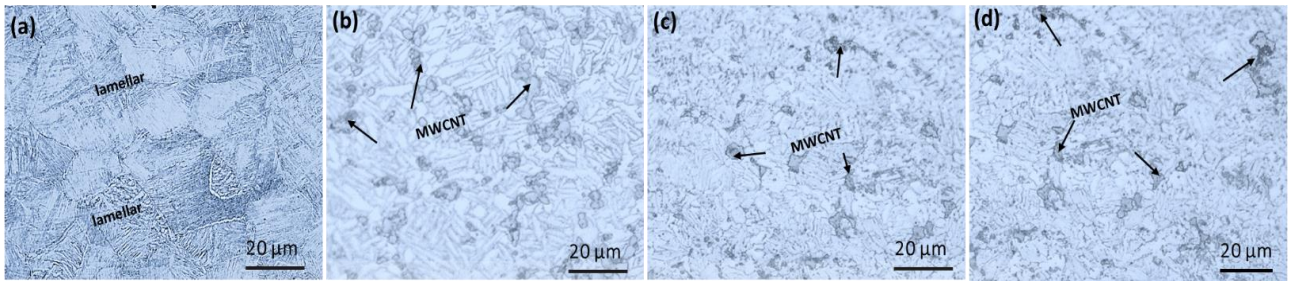

Figure 6: Optical micrographs of the fabricated Ti6Al4V (a) and MWCN-Ti6Al4V nanocomposites comprising of 0.5 wt.% (b), 1.0 wt.% (c), and 1.5 wt.% (d) MWCNT

3.4 Fracture morphology of the fabricated Ti6Al4V and MWCNT-Ti6Al4V nanocomposites

In order to further ascertain the microstructural evolution and behaviour of the fabricated Ti6Al4V and the MWCNT-Ti6Al4V nanocomposites, the fractured surface of the materials was characterized under SEM and the results are shown in Figure 7. The morphology of the fabricated alloy as shown in Figure 7 (a), which depict large dimples, revealed that the alloy undergoes ductile failure mode. Similarly, the nanocomposite grade comprising of 0.5 wt.% MWCNT shown in Figure 7 (b) depicts a dimple fracture morphology with more refined dimples and tiny voids.

Furthermore, with an increase in concentration of MWCNT to 1.0 and 1.5 wt.%, distinct fracture modes were observed. The dimple fracture morphology became more refined with a mixture of both dimple-like and cleavage-like failure. The fracture morphologies also indicated that there were reduction in the ductility of the nanocomposite with an increase in MWCNT content. However, this fracture mode suggest an improvement in the hardness and strength of the nanocomposites during loading condition. Meanwhile, the micro voids present in the fabricated nanocomposites may translate to a reduction in the density of the material. From all indications, it can be deduced that the addition and increase in MWCNT results in the microstructural changes of the fracture morphology of Ti6Al4V nanocomposites.

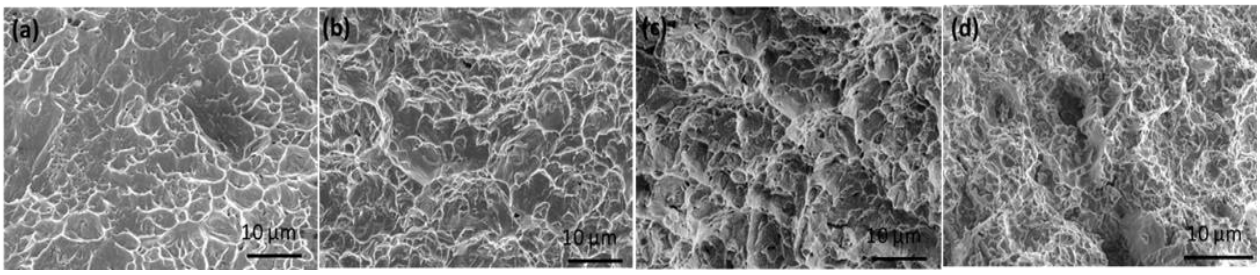

Figure 7: Fractured morphology of the fabricated Ti6Al4V (a) and MWCN-Ti6Al4V nanocomposites comprising of 0.5 wt.% (b), 1.0 wt.% (c), and 1.5 wt.% (d) MWCNT

3.5 X-Ray diffraction pattern of the starting powders, mixed powders, fabricated Ti6Al4V, and MWCN-Ti6Al4V nanocomposites

The phase evolution and analysis of the starting powders, mixed powders, fabricated Ti6Al4V and the MWCN-Ti6Al4V nanocomposites were characterized using X-Ray diffraction (XRD) techniques. The XRD pattern of the starting and mixed powders is shown in Figure 8. Figure 8 (a) shows the XRD pattern of the starting MWCNT where the two prominent graphitic peaks were glaringly observed at $2\theta = 25.6^{o}$ and 43.3^{o}, which coincides with the respective planes of (002) and (100).

Moreover, the XRD pattern of the starting Ti6Al4V powders shown in Figure 8 (b) revealed only the α phases of the titanium alloy with conforming peaks at $2\theta = 35.48^{o}$, 38.68^{o}, 40.52^{o}, 53.43^{o}, 63.85^{o}, 81.10^{o}, 86.92^{o}, 82.84^{o} and 88.42^{o}. The peaks at these diffracted angles corresponds to the respective planes of (100), (002), (101), (102), (110), (103), (112), (004) and (202). The XRD patterns of the mixed powders comprising of 0.5-1.5 wt.% MWCNT are shown in Figure 8 (c-e).

From the XRD pattern in Figure 8 (c), which shows the phase evolution of the mixed powders comprising of 0.5 wt.% MWCNT, α phases of the titanium alloy were more pronounced without any trace of the presence of MWCNT. Although, from the XRD patterns of the mixed powder comprising of 1.0 and 1.5 wt.% MWCNT, there were more increase in the peaks of the alpha titanium phases without any trace of MWCNT. The presence of the increase in the alpha titanium peaks may be ascribed to the mechanical stresses induced on the powders during the dispersion process. Besides, the absence of MWCNT in the XRD pattern of the mixed powders may be ascribed to the low concentration of the nanotubes when compared with the matrix material. Also, it can be attributed to the difference in the coefficient of mass absorption of titanium and carbon for the Cu Kα radiations

[49]. The XRD patterns of the mixed powders also revealed that no titanium carbide phases were formed despite the structural strain induced on the MWCNT during the dispersion process. Nonetheless, the structural strain only resulted in the increase in the alpha titanium peaks on the admixed powders during after milling.

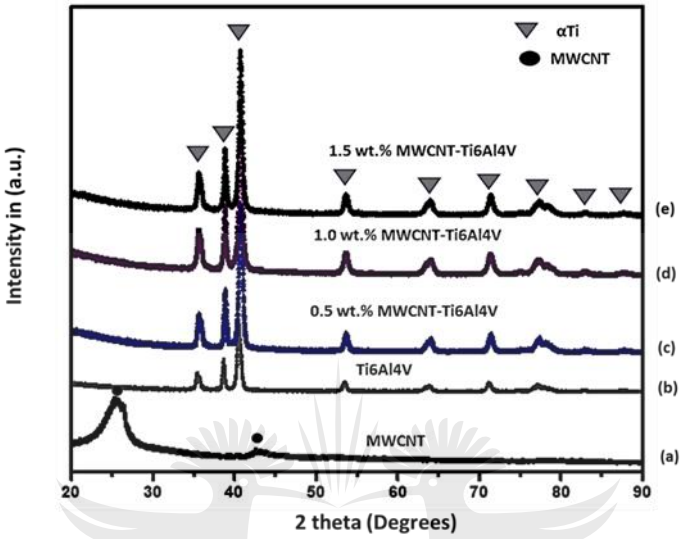

Figure 8: X-Ray diffraction patterns of starting powders (a) MWCNT, (b) starting Ti6Al4V, and mixed nanocomposite powders comprising of (c) 0.5 wt.% MWCNT (d)1.0 wt.% MWCNT, and (e) 1.5 wt.% MWCNT

Furthermore, the phase evolution of the fabricated alloy and nanocomposites after SPS is illustrated by the XRD pattern in Figure 9. Apart from the XRD pattern in Figure 9 (a), which shows the phase evolution of the fabricated Ti6Al4V where only the alpha titanium phases were observed, the XRD patterns of all the fabricated nanocomposites depict other phases. The MWCNT, α, β and TiC phases were glaringly observed on the XRD pattern of the fabricated nanocomposites. Meanwhile, more phase evolutions were observed on the XRD patterns of the fabricated nanocomposites comprising of 1.0 and 1.5 wt.% MWCNT. Nevertheless, the alpha titanium peaks was found to increase with an increase in concentration of the MWCNT. This indicates that the presence and addtion of MWCNT favours the stabilization of the alpha titanium phases owing to the fact that carbon is an alpha phase stabilizer in Ti6Al4V alloy.

The XRD pattern of the fabricated nanocomposites further revealed that sintering of the nanocomposite powders at 1000 ^{o}C accelerated a chemical reaction between the carbon and the titanium. This resulted in the formation of carbide phases, MWCNT and the beta titanium phases.

Also, this is an indication that sintering at higher temperature above the alpha-beta transus temperature promote some structural and phase evolution of the nanocomposites. Furthermore, the formation of titanium carbide (harder phase) phases after the sintering process will help to augment the strength, hardness and the anti-wear behaviour of the nanocomposites during service conditions.

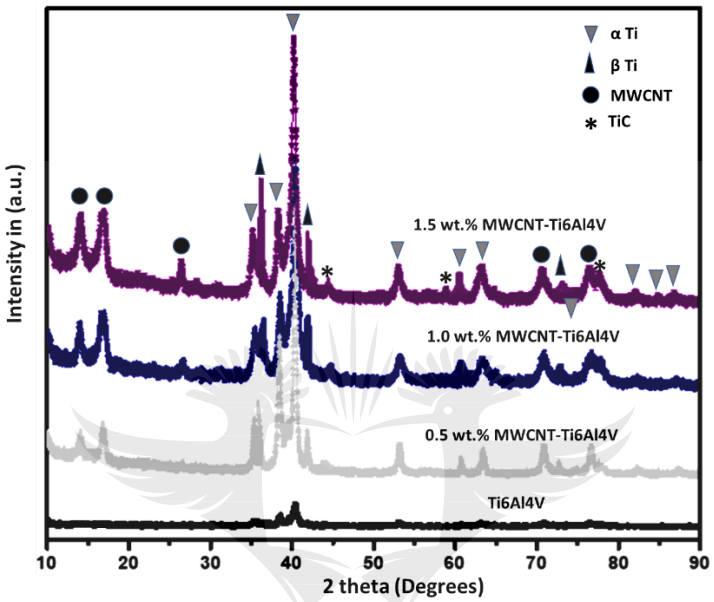

Figure 9: X-Ray diffraction patterns of the fabricated Ti6Al4V and Ti6Al4V nanocomposites comprising of MWCNT (0.5-1.5 wt.%)

3.6 Raman spectra of the starting, mixed powders, fabricated Ti6Al4V and Ti6Al4V nanocomposites

The structural evolution of the as-received MWCNT, mixed nanocomposites powders and the fabricated nanocomposites were ascertained by Raman spectroscopic technique. Figure 10 (a-e) presents the Raman result of the starting and mixed powders comprising of varying concentration of MWCNT dispersed in Ti6Al4V matrix.

The Raman spectrum in Figure 10 (a) depict the Raman result of the Ti6Al4V powder and it was observed that there were no pronounced peaks on the spectra. This is agrees with previous studies where titanium-based matrices does not display any prominent vibration peaks during Raman analysis [50–52]. Besides, Raman analysis is usually employ to confirm the structural changes in

carbon nanomaterials (graphite, graphene, graphene nanoplatelets, graphene nanoribbon, and carbon nanotubes) during their dispersion in matrix materials. Additionally, this characterization technique identifies the D and G bands, which helps to explain the structural integrity of the carbonaceous material after their processing during composite production.

Meanwhile, the D band is usually associated with the non-sp^2 defects in the C-C bond of carbon nanomaterials while the G band is linked to the stretching mode of the plane C-C network. The G band is also used to confirm the crystalline nature, degree of grphitization and orderliness of the C-C network in carbon nanomaterials [52,53].

In previous studies, the D and G band has been employed to ascertain the extent of defects on the walls of the nanotubes during the dispersion in metal matrices and consolidation process [54,55]. This is generally achieved by investigating the intensity ratio of the D and G band, the broadening, decrease and shift in the D and G band. The shift in the G band also induce structural defects, which is usually in the form of open edges and vacancies, on the nanotubes during their incorporation in matrix materials [56].

Furthermore, the Raman spectrum in Figure 10 (b) shows the Raman result of the starting MWCNT before the dispersion process. From the Raman result, it was observed that the D and G band were situated at 1340 cm^{-1} and 1580 cm^{-1} respectively. From Figure 10 (b), the intensity ratio (I_D/I_G) of the starting MWCNT was calculated to be 0.800. However, when the MWCNT was dispersed in the Ti6Al4V powder, visible changes in the Raman spectra were observed in Figure 10 (c-e). From the Raman spectrum in Figure 10 (c) which present the Raman result of the mixed powder comprising of 0.5 wt.% MWCNT, the D and G band were shifted to 1400 cm^{-1} and 1630 cm^{-1} respectively. Similarly, an incredible increase in the intensity ratio (I_D/I_G) of the D and G band from 0.800 in the starting MWCNT to 0.857 was observed. This represents a 7.13% increase in the intensity ratio (I_D/I_G) ratio of the mixed powder comprising of 0.5 wt.% MWCNT. The Raman shift and increase in the intensity ratio of the D and G band recorded maybe ascribed to the strain induced on the nanotubes during the dispersion process. However, there was no trace of carbide formed from the Raman result, which indicates severe deformation on the walls of the nanotubes during the dispersion process.

Subsequently, the Raman result of the mixed powder comprising of 1.0 wt.% MWCNT is shown in Figure 10 (d). From the Raman spectrum in Figure 10 (d), the D and G band were situated at an higher wavenumber of 1402 cm^{-1} and 1632 cm^{-1} respectively. The intensity ratio of the D and G band experienced similar increase from 0.800 in the starting MWCNT to 0.905, which represents an increase of 13.13%. Similarly, the Raman result of the mixed powder comprising of 1.5 wt.% MWCNT shown in Figure 10 (e) experienced a slight Raman shift. The D and G band were shifted to a higher wavenumbers of 1403 cm^{-1} and 1648 cm^{-1} with an increase in I_D/I_G ratio to 0.985, which amounts to 23.13% increased. A detailed analysis of the Raman shift indicates that there was a higher shift in the G band when the concentration of the MWCNT was increased to 1.5 wt.%. This implies that the MWCNT in the nanocomposite grade was exposed to considerable deformation during the dispersion process. Besides, a similar change in the SAED pattern of this nanocomposite grade was observed earlier. However, the considerable deformation on the walls of the nanotubes does not translate to the formation of carbide phases during the dispersion process.

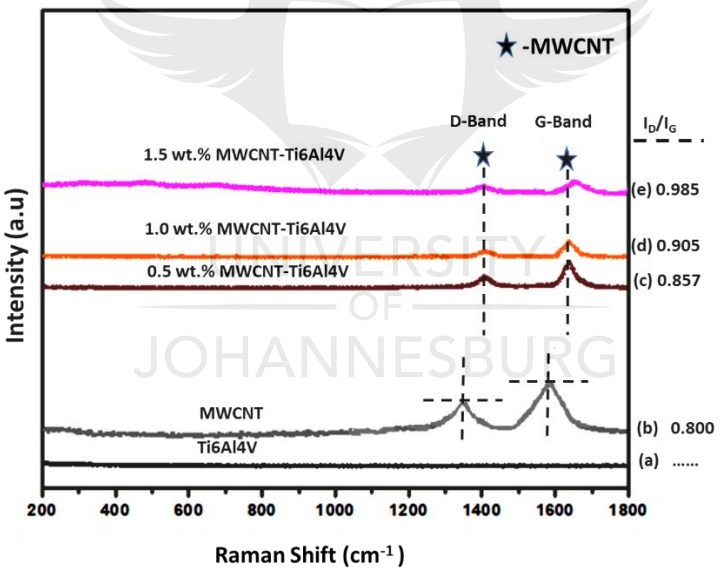

Figure 10: Raman spectra of starting powders (a) Ti6Al4V, (b) starting MWCNT, and mixed nanocomposite powders comprising of (c) 0.5 wt.% MWCNT (d)1.0 wt.% MWCNT, and (e) 1.5 wt.% MWCNT

Furthermore, the Raman results of the starting MWCNT, fabricated alloy and nanocomposites are shown in Figure 11 (a-c). A thorough examination of the Raman spectra of the fabricated nanocomposites showed the evolution of new vibration peaks at 265 cm^{-1}, 416 cm^{-1} and 602 cm^{-1}

wavenumbers. Previous studies have emphasised that these peaks are associated with the titanium carbide phases formed on the MWCNT during the consolidation process [57–59]. The Raman spectrum on Figure 11 (c) shows the Raman result of the fabricated nanocomposite comprising of 0.5 wt.% MWCNT. It was observed from the Raman result that the D and G bands were situated at higher wavenumber of 1406 cm^{-1} and 1635 cm^{-1} respectively. Correspondingly, the I_D/I_G increased from 0.800 in the starting MWCNT to 0.927, which amounts to an increase of 15.88%. Similarly, the Raman result of the fabricated nanocomposite comprising of 1.0 wt.% MWCNT is shown in Figure 11 (d). From the Raman result, it was observed that the D and G bands shifted to a higher wavenumber of 1408 cm^{-1} and 1637 cm^{-1} with an I_D/I_G ratio of 0.979, which represent an increase of 22.38%.

Moreover, a similar trend on the shift of the D and G band and an increase in I_D/I_G ratio was observed from the Raman spectrum in Figure 11 (e). The Raman spectrum in Figure 11 (e) shows the Raman result of the fabricated nanocomposites comprising of 1.5 wt.% MWCNT and it was observed that the D and G band shifted to a higher wavenumber of 1412 cm^{-1} and 1658 cm^{-1} respectively. Furthermore, the I_D/I_G ratio increased to 0.986 from 0.800 in the starting MWCNT.This amounts to an increase of 23.25%. The Raman shift of the D and G Band with the corresponding increase in the intensity ratio after the fabrication process may be ascribed to the mechanical stresses during dispersion and the thermal stresses induced on the walls of the nanotubes during consolidation. Additionally, the stresses induced on the MWCNT during consolidation resulted in the formation of carbide phases observed from the Raman spectra. Consequently, this can assist in improving the mechanical properties of the nanocomposites during service conditions.

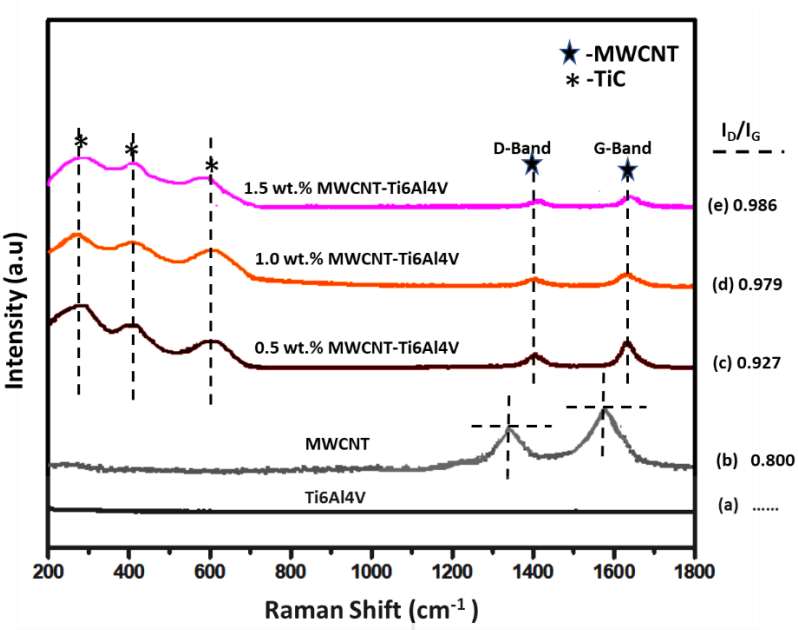

Figure 11: Raman spectra of starting MWCNT (a) fabricated Ti6Al4V (b) and consolidated nanocomposites comprising of (c) 0.5 wt.% MWCNT (d)1.0 wt.% MWCNT, and (e) 1.5 wt.% MWCNT

3.7 Densification of the fabricated Ti6Al4V and Ti6Al4V based nanocomposites

To understand the densification behaviour of the fabricated alloy and nanocomposites, the relative density of the materials were investigated and the results are shown in Figure 12. From Figure 12, it was observed that the density of the materials ranges from 98.7-99.66% and this declined with an increase in concentration of the MWCNT.

Furthermore, the fabricated alloy displayed the highest density value of 99.66%, which indicates that there were less porosity in the fabricated alloy. This was seen in the SEM morphology and fractography image presented earlier. Conversely, with the introduction and increase in the concentration of MWCNT in the Ti6Al4V matrix, the density declined intermittently. The fabricated nanocomposite with 0.5 wt.% MWCNT displayed a density value of 99.4% followed by the nanocomposite with 1.0 wt.% MWCNT, which has a relative density value of 99.2%. Meanwhile, the nanocomposite with 1.5 wt.% MWCNT displayed the least relative density value of 98.7%.

From the results of the relative density of the fabricated alloy and nanocomposites, it can be deduced that the additon of MWCNT into the Ti6Al4V matrix introduced some micropores that eventually

translate to the reduction of the density of the nanocomposites. This indicates that an increase in the concentration of MWCNT resulted in a decrease in the relative density of the fabricated nanocomposites. Also, the presence of micropores were observed in the fractography of the fabricated nanocomposites. These results are in accordance with results obtained from previous studies where MWCNT was incorporated in metal matrices to improve their properties [60,61].

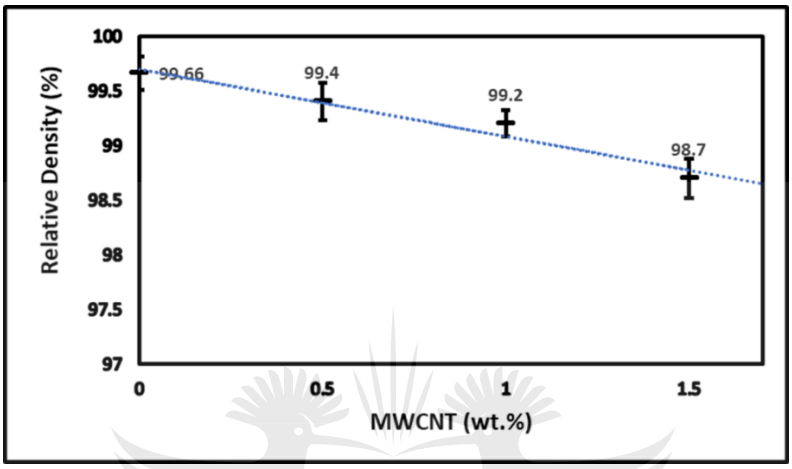

Figure 12: Densification of the consolidated Ti6Al4V and Ti6Al4V based nanocomposites

3.8 Mechanical properties of the fabricated Ti6Al4V and Ti6Al4V based nanocomposites

3.8.1 Micro and Nanohardness values of the fabricated Ti6Al4V and Ti6Al4V based nanocomposites

The mechanical properties of the fabricated alloy and nanocomposites were investigated using Vickers microhardness tester and nanoindentation technique. The results obtained from the investigations were used to derive an equation relating the microhardness and nanohardness of the fabricated materials. Furthermore, the microhardness nanohardness results and the derived relationship are presented in Figure 13.

The Vickers microhardness values of the fabricated alloy and nanocomposites are presented in Figure 13 (a). From the microhardness results, it was observed that the microhardness values increased with the addition and increase in concentration of the MWCNT in the nanocomposites. Meanwhile, the nanocomposite grade comprising of 1.5 wt.% MWCNT displayed the highest microhardness value of 569.8 HV followed by the nanocomposite grade comprising of 1.0 wt.% which has a

microhardness value of 485.3 HV. This was accompanied by the nanocomposite grade comprising of 0.5 wt.% MWCNT, which displayed a microhardness value of 463.1 HV. Conversely, the fabricated Ti6Al4V showed the least microhardness value of 388 HV. The improvement in the microhardness value can be ascribed to the addition and increase in concentration of MWCNT, which strengthened the Ti6Al4V matrix via the dispersion strengthening mechanism and the pinning effect [62]. Besides, the presence of the titanium carbide phases formed in the nanocomposites assisted in augmenting the hardness of the fabricated nanocomposites.

Similarly, the results of the nanohardness of the fabricated alloy and nanocomposites are presented in Figure 13 (b). The nanohardness results follow similar trends as the microhardness values discussed earlier. The nanohardness value improved with the addition and increase in the concentration of MWCNT. This was evident as the nanocomposite grade comprising of 0.5 wt.% MWCNT has a nanohardness of 4586.9 MPa while the 1.0 wt.% MWCNT-reinforced nanocomposite grade has a nanohardness of 6986.6 MPa. The best nanohardness of 8183.7 MPa was obtained for the nanocomposite grade reinforced with 1.5 wt% MWCNT. Nevertheless, the fabricated Ti6Al4V alloy has the least nanohardness value of 3262.6 MPa.

From all indications, the microhardness and nanohardness of the fabricated nanocomposites increased with the addition of MWCNT into the Ti6Al4V matrix. This can be ascribed to the presence of the insitu-TiC phases formed during the consolidation of the nanocomposites. Furthermore, the improvements can be attributed to the dispersion strengthening, work hardening, Orowan looping and grain boundary hardening of the MWCNT, which inhibit the dislocation motion during indentation of the nanocomposites. The work hardening effect (WHE) of the MWCNT [63] isexpressed in equation (3).

$$H_{WHE} = K_w \rho_{dis}^{1/2} = \alpha G b \rho_{dis}^{1/2} \quad (3)$$

Where K_w represent the strength index, ρ_{dis} is the dislocation density of the grain interior, α is a constant while *G* is the shear modulus of the MWCNT and *b* signifies the Burger vector. Similarly, the grain boundary hardening can be expressed as the Hall-Petch relationship [63], which is expressed in equation (4).

$$H_{GPH} = K_H d^{-1/2} \quad (4)$$

Where K_H is equivalent to 0.14 MPam$^{1/2}$ and d represents the grain size. Besides, the derived relationship between the microhardness and nanohardness is shown in equation (5).

$$H_V = 0.0316H_N + 294.72 \quad (5)$$

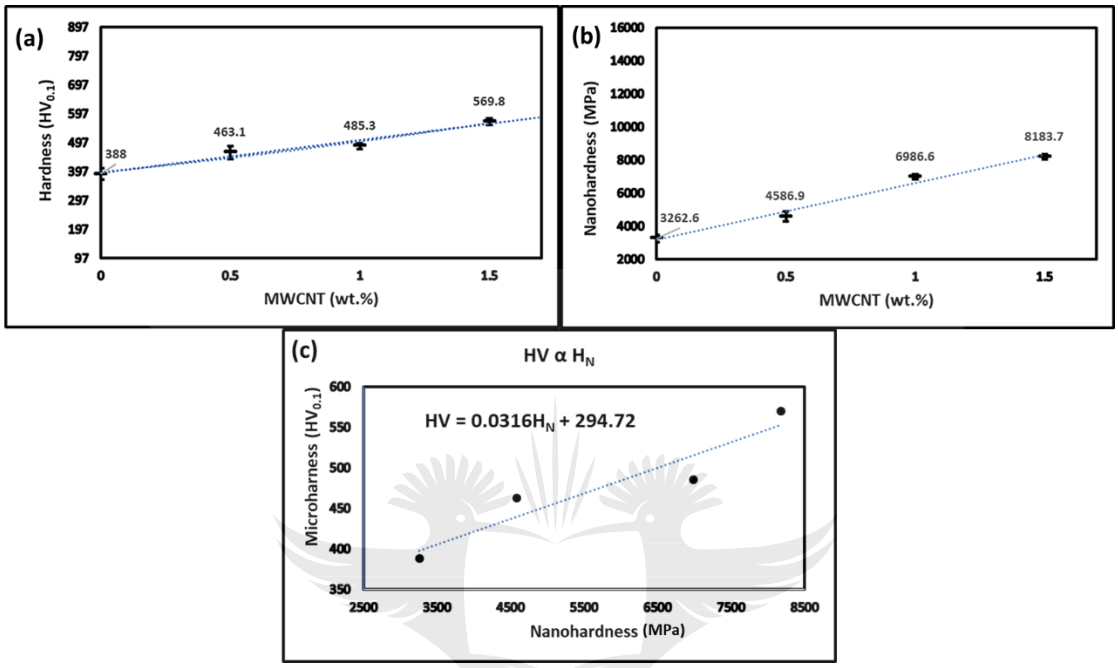

Figure 13. Micro and nanohardness of the fabricated Ti6Al4V and nanocomposites

3.8.2 Load-displacement the fabricated Ti6Al4V and Ti6Al4V nanocomposites

The mechanical behaviour of the fabricated alloy and nanocomposites was further investigated by nanoindentation technique. The load-displacement plot during nanoindentation is presented in Figure 14 (a-d). From the indentation curve in Figure 14 (a), which shows the loading and unloading curve of the fabricated alloy, it was observed that the alloy undergoes considerable plastic deformation during the indentation that was reflected in the indentation depth of 976.5 nm.

The nanocomposites grade comprising of 0.5 wt.% MWCNT displayed the least resistance to plastic deformation during the nanoindentation. This was followed by the nanocomposite grade comprising of 1.0 wt.% MWCNT with an indentation depth of 730 nm, which has a higher resistance to plastic deformation. However, the nanocomposite grade comprising of 1.5 wt.% MWCNT was found to display the highest resistance to plastic deformation among the fabricated nanocomposites with an indentation depth of 634 nm. These load-displacement results imply that the addition and increase in

the concentration of MWCNT improved its resistance to plastic deformation during nanoindentation. Therefore, the presence of MWCNT in the nanocomposite grades helps to strengthen and stiffen the Ti6Al4V matrix.

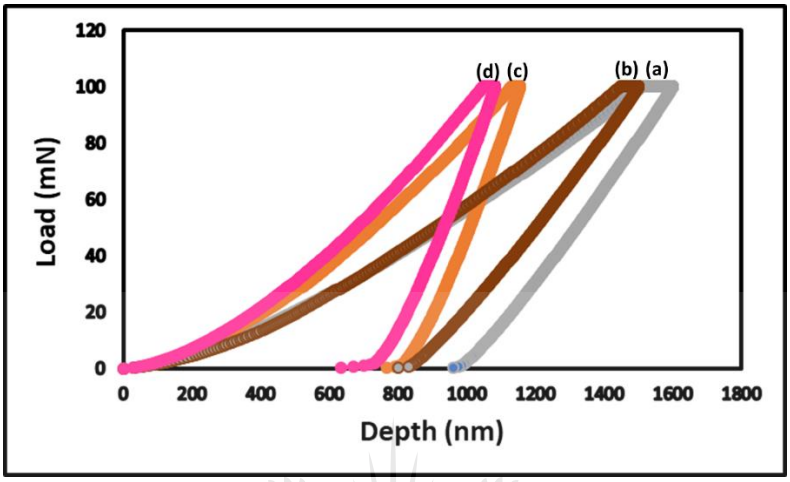

Figure 14. Load-displacement curves of the fabricated Ti6Al4V (a), and Ti6Al4V nanocomposites comprising of 0.5 wt.% MWCNT(b), 1.0 wt.% MWCNT, and 1.5 wt.% MWCNT.

3.8.3 Elastic modulus of the fabricated Ti6Al4V and Ti6Al4V nanocomposites

To further ascertain the mechanical behaviour of the fabricated alloy and nanocomposites, the elastic modulus of the materials was investigated using nanoindentation. The elastic modulus results of the fabricated materials are presented in Figure 15. From this Figure, it was observed that the elastic modulus of the materials improved with the addition and increase in the concentration of MWCNT in the nanocomposites.

Meanwhile, the fabricated Ti6Al4V displayed the least elastic modulus value of 24.51 GPa and this was followed by the nanocomposite grade comprising of 0.5 wt.% MWCNT with an elastic modulus value of 28.02 GPa. Besides, the nanocomposite grade comprising of 1.5 wt.% MWCNT exhibit the highest elastic modulus result with a value of 66.05 GPa, which further explained that this nanocomposite grade demonstrated the highest elastic resistance to linear compression from the indenter. In a nutshell, the addition of MWCNT into Ti6Al4V improved the elastic modulus of the metal matrix. This improvement can also be ascribed to the presence of the secondary carbide phases formed during the consolidation of the nanocomposites.

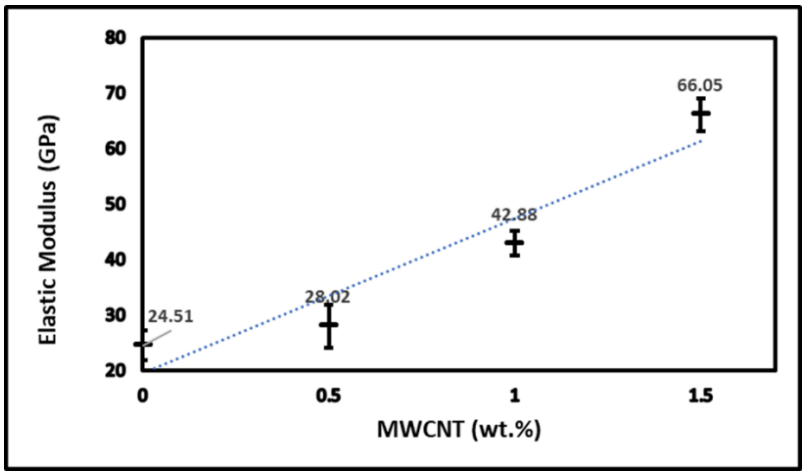

Figure 15. Elastic Modulus of the fabricated Ti6Al4V and nanocomposites

4. Conclusion

In this study, the influence of MWCNT addition on the microstructural evolution and mechanical properties of spark plasma sintered Ti6Al4V based nanocomposites was considered. Prior to the consolidation of the nanocomposites, MWCNT were dispersed in the Ti6Al4V matrix by shift speed ball milling technique and then consolidated via the spark plasma sintering technique. Various characterization techniques and mechanical tests were carried out to ascertain the influence of MWCNT addition on the microstructural evolution and properties of the nanocomposites. The following conclusions were drawn from the investigations;

1. Microstructural evolutions from the SEM, TEM and optical microscopy confirmed that the MWCNT were fully dispersed in the Ti6Al4V matrix.
2. Increase in the concentration of MWCNT adversely influence their dispersion characteristics in Ti6Al4V matrix after SSBM and SPS.
3. The addition and increase in the concentration of MWCNT in the Ti6Al4V matrix introduced some micropores in the nanocomposites, which was evident in the fractography and the relative density results.
4. Mechanical properties such as microhardness, nanohardness and elastic modulus were tremendously improved by the addition and increase in the concentration of MWCNT in the Ti6Al4V based nanocomposites.

Acknowledgement

This research was fully funded by the National Research Foundation of South Africa in association with the World Academy of Science (NRF-TWAS) and the Global Excellence and Stature (GES) of the University of Johannesburg, South Africa. Our sincere appreciation goes to the funding bodies and Adeola Borode for proofreading this manuscript.

Reference

[1] K.S. Munir, Y. Zheng, D. Zhang, J. Lin, Y. Li, C. Wen, Microstructure and mechanical properties of carbon nanotubes reinforced titanium matrix composites fabricated via spark plasma sintering, Mater. Sci. Eng. A. 688 (2017) 505–523. doi:10.1016/j.msea.2017.02.019.

[2] R.S. Ruoff, D. Qian, W.K. Liu, Mechanical properties of carbon nanotubes: theoretical predictions and experimental measurements, Comptes Rendus Phys. 4 (2003) 993–1008.

[3] E.W. Wong, P.E. Sheehan, C.M. Lieber, Nanobeam mechanics: elasticity, strength, and toughness of nanorods and nanotubes, Science (80-.). 277 (1997) 1971–1975.

[4] S. Berber, Y.-K. Kwon, D. Tománek, Unusually high thermal conductivity of carbon nanotubes, Phys. Rev. Lett. 84 (2000) 4613.

[5] T.W. Ebbesen, H.J. Lezec, H. Hiura, J.W. Bennett, H.F. Ghaemi, T. Thio, Electrical conductivity of individual carbon nanotubes, Nature. 382 (1996) 54.

[6] K.S. Munir, Y. Li, D. Liang, M. Qian, W. Xu, C. Wen, Effect of dispersion method on the deterioration, interfacial interactions and re-agglomeration of carbon nanotubes in titanium metal matrix composites, Mater. Des. 88 (2015) 138–148. doi:10.1016/j.matdes.2015.08.112.

[7] B. Chen, J. Shen, X. Ye, L. Jia, S. Li, J. Umeda, M. Takahashi, K. Kondoh, Length effect of carbon nanotubes on the strengthening mechanisms in metal matrix composites, Acta Mater. 140 (2017) 317–325. doi:10.1016/j.actamat.2017.08.048.

[8] A.M. Okoro, R. Machaka, S.S. Lephuthing, M.A. Awotunde, S.R. Oke, O.E. Falodun, P.A. Olubambi, Dispersion characteristics, interfacial bonding and nanostructural evolution of MWCNT in Ti6Al4V powders prepared by shift speed ball milling technique, J. Alloys Compd. (2019).

[9] J.-W. An, D.-H. You, D.-S. Lim, Tribological properties of hot-pressed alumina--CNT composites, Wear. 255 (2003) 677–681.

[10] P. Guo, X. Chen, X. Gao, H. Song, H. Shen, Fabrication and mechanical properties of well-dispersed multiwalled carbon nanotubes/epoxy composites, Compos. Sci. Technol. 67 (2007) 3331–3337.

[11] A.M.K. Esawi, K. Morsi, A. Sayed, M. Taher, S. Lanka, Effect of carbon nanotube (CNT) content on the mechanical properties of CNT-reinforced aluminium composites, Compos. Sci. Technol. 70 (2010) 2237–2241. doi:10.1016/j.compscitech.2010.05.004.

[12] N. Selvakumar, K. Gangatharan, Electrical resistivity, tribological behaviour of multiwalled carbon nanotubes and nanoboron carbide particles reinforced copper hybrid composites for pantograph application, Adv. Mater. Sci. Eng. 2016 (2016).

[13] K.S. Munir, Y. Zheng, D. Zhang, J. Lin, Y. Li, C. Wen, Improving the strengthening efficiency of carbon nanotubes in titanium metal matrix composites, Mater. Sci. Eng. A. 696 (2017) 10–25. doi:10.1016/j.msea.2017.04.026.

[14] A.M. Okoro, S.S. Lephuthing, S.R. Oke, O.E. Falodun, M.A. Awotunde, P.A. Olubambi, A Review of Spark Plasma Sintering of Carbon Nanotubes Reinforced Titanium-Based Nanocomposites: Fabrication, Densification, and Mechanical Properties, JOM. (2018). doi:10.1007/s11837-018-3277-2.

[15] O.E. Falodun, B.A. Obadele, S.R. Oke, A.M. Okoro, P.A. Olubambi, Titanium-based matrix composites reinforced with particulate, microstructure, and mechanical properties using spark plasma sintering technique: a review, Int. J. Adv. Manuf. Technol. (2019) 1–13.

[16] S. Li, B. Sun, H. Imai, T. Mimoto, K. Kondoh, Powder metallurgy titanium metal matrix composites reinforced with carbon nanotubes and graphite, Compos. Part A Appl. Sci. Manuf. 48 (2013) 57–66. doi:10.1016/j.compositesa.2012.12.005.

[17] A.M. Okoro, M. Awotunde, O.A. Ajiteru, S.S. Lephuthing, P.A. Olubambi, R. Machaka, Effects of carbon nanotubes on the mechanical properties of spark plasma sintered titanium matrix composites - A review, in: 2018 IEEE 9th Int. Conf. Mech. Intell. Manuf. Technol. ICMIMT 2018, 2018. doi:10.1109/ICMIMT.2018.8340420.

[18] J.D. Majumdar, I. Manna, Laser surface engineering of titanium and its alloys for improved wear, corrosion and high-temperature oxidation resistance, in: Laser Surf. Eng., Elsevier, 2015: pp. 483–521.

[19] A.K.M.N. Amin, Titanium alloys-towards achieving enhanced properties for diversified

applications, 2012.

[20] G.F. Batalha, M. Motyka, K. Kubiak, J. Sieniawski, W. Ziaja, D.J. Dos Santos, D.J. Carastan, L.B. Tavares, F. Buiochi, M.A.B. Andrade, others, Editorial Board Contributors to Volume 2 Preface xv, Compr. Mater. Process. (2014).

[21] C. Leyens, M. Peters, Titanium and titanium alloys: fundamentals and applications, John Wiley & Sons, 2003.

[22] O.E. Falodun, B.A. Obadele, S.R. Oke, O.O. Ige, P.A. Olubambi, Effect of TiN and TiCN additions on spark plasma sintered Ti--6Al--4V, Part. Sci. Technol. (2018) 1–10.

[23] B. Zhao, W.F. Ding, J.B. Dai, X.X. Xi, J.H. Xu, A comparison between conventional speed grinding and super-high speed grinding of (TiC p+ TiB w)/Ti--6Al--4V composites using vitrified CBN wheel, Int. J. Adv. Manuf. Technol. 72 (2014) 69–75.

[24] K. Kondoh, T. Threrujirapapong, H. Imai, J. Umeda, B. Fugetsu, Characteristics of powder metallurgy pure titanium matrix composite reinforced with multi-wall carbon nanotubes, Compos. Sci. Technol. 69 (2009) 1077–1081. doi:10.1016/j.compscitech.2009.01.026.

[25] X. Sun, Y. Han, S. Cao, P. Qiu, W. Lu, Rapid in-situ reaction synthesis of novel TiC and carbon nanotubes reinforced titanium matrix composites, J. Mater. Sci. Technol. 33 (2017) 1165–1171.

[26] K.S. Munir, Y. Zheng, D. Zhang, J. Lin, Y. Li, C. Wen, Improving the strengthening efficiency of carbon nanotubes in titanium metal matrix composites, Mater. Sci. Eng. A. 696 (2017) 10–25. doi:10.1016/j.msea.2017.04.026.

[27] K.S. Munir, M. Qian, Y. Li, D.T. Oldfield, P. Kingshott, D.M. Zhu, C. Wen, Quantitative Analyses of MWCNT-Ti Powder Mixtures using Raman Spectroscopy: The Influence of Milling Parameters on Nanostructural Evolution, Adv. Eng. Mater. 17 (2015) 1660–1669.

[28] E. Thostenson, Advances in the science and technology of carbon nanotubes and their composites: a review, Compos. Sci. Technol. 61 (2001) 1899–1912. doi:10.1016/S0266-3538(01)00094-X.

[29] A.M. Okoro, R. Machaka, S.S. Lephuthing, M. Awotunde, P.A. Olubambi, Structural integrity

and dispersion characteristics of carbon nanotubes in titanium-based alloy, in: IOP Conf. Ser. Mater. Sci. Eng., 2018: p. 12004.

[30] K.S. Munir, Y. Li, M. Qian, C. Wen, Identifying and understanding the effect of milling energy on the synthesis of carbon nanotubes reinforced titanium metal matrix composites, Carbon N. Y. 99 (2016) 384–397. doi:10.1016/j.carbon.2015.12.041.

[31] H. Jia, Z. Zhang, Z. Qi, G. Liu, X. Bian, Formation of nanocrystalline TiC from titanium and different carbon sources by mechanical alloying, J. Alloys Compd. 472 (2009) 97–103.

[32] P. Gill, N. Munroe, Study of carbon nanotubes in Cu-Cr metal matrix composites, J. Mater. Eng. Perform. 21 (2012) 2467–2471.

[33] L. Ci, Z. Ryu, N.Y. Jin-Phillipp, M. Rühle, Investigation of the interfacial reaction between multi-walled carbon nanotubes and aluminum, Acta Mater. 54 (2006) 5367–5375.

[34] M.R. Piggott, The interface in carbon fibre composites, Carbon N. Y. 27 (1989) 657–662.

[35] F.C. Wang, Z.H. Zhang, Y.J. Sun, Y. Liu, Z.Y. Hu, H. Wang, A. V. Korznikov, E. Korznikova, Z.F. Liu, S. Osamu, Rapid and low temperature spark plasma sintering synthesis of novel carbon nanotube reinforced titanium matrix composites, Carbon N. Y. 95 (2015) 396–407. doi:10.1016/j.carbon.2015.08.061.

[36] A.O. Adegbenjo, P.A. Olubambi, J.H. Potgieter, E. Nsiah-Baafi, M.B. Shongwe, Interfacial Reaction During High Energy Ball Milling Dispersion of Carbon Nanotubes into Ti6Al4V, J. Mater. Eng. Perform. 26 (2017) 6047–6056. doi:10.1007/s11665-017-3041-8.

[37] F. Mokdad, D.L. Chen, Z.Y. Liu, B.L. Xiao, D.R. Ni, Z.Y. Ma, Deformation and strengthening mechanisms of a carbon nanotube reinforced aluminum composite, Carbon N. Y. 104 (2016) 64–77. doi:10.1016/j.carbon.2016.03.038.

[38] R. Spectrometers, Standard Guide for Raman Shift Standards for Spectrometer Calibration 1, 96 (2014) 1–11. doi:10.1520/E1840-96R07.2.

[39] A.S. for Testing, M.C.B. on Metal Powders, M.P. Products, Standard Test Methods for Density of Compacted or Sintered Powder Metallurgy (PM) Products Using Archimedes' Principle, ASTM International, 2009.

[40] G.M. Pharr, W.C. Oliver, F.R. Brotzen, On the generality of the relationship among contact stiffness, contact area, and elastic modulus during indentation, J. Mater. Res. 7 (1992) 613–617.

[41] B.B. Medeiros, M.M. Medeiros, J. Fornell, J. Sort, M.D. Baró, A.M.J. Junior, Nanoindentation response of Cu--Ti based metallic glasses: Comparison between as-cast, relaxed and devitrified states, J. Non. Cryst. Solids. 425 (2015) 103–109.

[42] P.S.R. Sreekanth, K. Acharyya, I. Talukdar, S. Kanagaraj, Studies on structural defects on 60Co irradiated multi walled carbon nanotubes., Procedia Mater. Sci. 6 (2014) 1967–1975.

[43] J.H. Lehman, M. Terrones, E. Mansfield, K.E. Hurst, V. Meunier, Evaluating the characteristics of multiwall carbon nanotubes, Carbon N. Y. 49 (2011) 2581–2602. doi:10.1016/j.carbon.2011.03.028.

[44] K.S. Munir, Y. Zheng, D. Zhang, J. Lin, Y. Li, C. Wen, Microstructure and mechanical properties of carbon nanotubes reinforced titanium matrix composites fabricated via spark plasma sintering, Mater. Sci. Eng. A. 688 (2017) 505–523. doi:10.1016/j.msea.2017.02.019.

[45] K.S. Munir, C. Wen, Deterioration of the Strong sp2 Carbon Network in Carbon Nanotubes during the Mechanical Dispersion Processing—A Review, Crit. Rev. Solid State Mater. Sci. 41 (2016) 347–366.

[46] B. Chen, J. Shen, X. Ye, H. Imai, J. Umeda, M. Takahashi, K. Kondoh, Solid-state interfacial reaction and load transfer efficiency in carbon nanotubes (CNTs)-reinforced aluminum matrix composites, Carbon N. Y. 114 (2017) 198–208. doi:10.1016/j.carbon.2016.12.013.

[47] M. Chen, G. Fan, Z. Tan, D. Xiong, Q. Guo, Y. Su, J. Zhang, Z. Li, M. Naito, Z. Di, Design of an efficient flake powder metallurgy route to fabricate CNT/6061Al composites, Mater. Des. 142 (2018) 288–296. doi:10.1016/j.matdes.2018.01.044.

[48] M.A. Asadabad, M.J. Eskandari, Modern Electron Microscopy in Physical and Life Sciences, Mod. Electron Microsc. Phys. Life Sci. (2016) 3–26. doi:10.5772/60494.

[49] L.L. Ye, M.X. Quan, Synthesis of nanocrystalline TiC powders by mechanical alloying, Nanostructured Mater. 5 (1995) 25–31.

[50] A.O. Adegbenjo, P.A. Olubambi, J.H. Potgieter, M.B. Shongwe, M. Ramakokovhu, Spark plasma sintering of graphitized multi-walled carbon nanotube reinforced Ti6Al4V, Mater. Des. 128 (2017) 119–129. doi:10.1016/j.matdes.2017.05.003.

[51] K.S. Munir, M. Qian, Y. Li, D.T. Oldfield, P. Kingshott, D.M. Zhu, C. Wen, Quantitative Analyses of MWCNT-Ti Powder Mixtures using Raman Spectroscopy: The Influence of Milling Parameters on Nanostructural Evolution, Adv. Eng. Mater. 17 (2015) 1660–1669. doi:10.1002/adem.201500142.

[52] A.M. Okoro, R. Machaka, S.S. Lephuthing, M. Awotunde, P.A. Olubambi, Structural integrity and dispersion characteristics of carbon nanotubes in titanium-based alloy, in: IOP Conf. Ser. Mater. Sci. Eng., 2018. doi:10.1088/1757-899X/430/1/012004.

[53] A.C. Ferrari, Raman spectroscopy of graphene and graphite: disorder, electron--phonon coupling, doping and nonadiabatic effects, Solid State Commun. 143 (2007) 47–57.

[54] T. Peng, I. Chang, Mechanical alloying of multi-walled carbon nanotubes reinforced aluminum composite powder, Powder Technol. 266 (2014) 7–15. doi:10.1016/j.powtec.2014.05.068.

[55] V. Datsyuk, M. Kalyva, K. Papagelis, J. Parthenios, D. Tasis, A. Siokou, I. Kallitsis, C. Galiotis, Chemical oxidation of multiwalled carbon nanotubes, Carbon N. Y. 46 (2008) 833–840. doi:10.1016/j.carbon.2008.02.012.

[56] P. Delhaes, M. Couzi, M. Trinquecoste, J. Dentzer, H. Hamidou, C. Vix-Guterl, A comparison between Raman spectroscopy and surface characterizations of multiwall carbon nanotubes, Carbon N. Y. 44 (2006) 3005–3013.

[57] B.H. Lohse, A. Calka, D. Wexler, Raman spectroscopy sheds new light on TiC formation during the controlled milling of titanium and carbon, J. Alloys Compd. 434 (2007) 405–409.

[58] M. V Klein, J.A. Holy, W.S. Williams, Raman scattering induced by carbon vacancies in Ti C x, Phys. Rev. B. 17 (1978) 1546.

[59] K.S. Munir, Y. Li, J. Lin, C. Wen, Interdependencies between graphitization of carbon nanotubes and strengthening mechanisms in titanium matrix composites, Materialia. (2018).

[60] A. Adegbenjo, P. Olubambi, J. Potgieter, Improving the Tribological Properties of Ti6Al4V Alloy with Multi-walled Carbon Nanotube Additions, in: Int. Conf. Theor. Appl. Exp. Mech., 2018: pp. 55–61.

[61] N. Saheb, Sintering behavior of CNT reinforced Al6061 and Al2124 Nanocomposites, Adv. Mater. Sci. Eng. 2014 (2014).

[62] D. Lin, M. Saei, S. Suslov, S. Jin, G.J. Cheng, Super-strengthening and stabilizing with carbon nanotube harnessed high density nanotwins in metals by shock loading, Sci. Rep. 5 (2015) 15405.

[63] N. Hansen, Hall – Petch relation and boundary strengthening, 51 (2004) 801–806. doi:10.1016/j.scriptamat.2004.06.002.

Materials Science & Engineering A 765 (2019) 138320

Contents lists available at ScienceDirect

Materials Science & Engineering A

journal homepage: www.elsevier.com/locate/msea

Nanoindentation studies of the mechanical behaviours of spark plasma sintered multiwall carbon nanotubes reinforced Ti6Al4V nanocomposites

Avwerosuoghene Moses Okoro (M.Eng)[a,*], Ronald Machaka (PhD)[b], Senzeni Sipho Lephuthing (MTech)[a], Samuel Ranti Oke (PhD)[a], Mary Ajimegoh Awotunde (M.Eng)[a], Peter Apata Olubambi (PhD)[a]

[a] Centre for Nanoengineering and Tribocorrosion, Department of Metallurgy, School of Mining, Metallurgy and Chemical Engineering, University of Johannesburg, South Africa
[b] Council for Scientific and Industrial Research, Pretoria, South Africa

ARTICLE INFO

Keywords:
Nanoindentation studies
Multiwall carbon nanotubes
Titanium alloys
Mechanical properties
Nanocomposites

ABSTRACT

In this study, the influence of multiwall carbon nanotubes (MWCNT) additions on the mechanical properties of sintered Ti6Al4V-based nanocomposites was investigated. The nanocomposites were fabricated with varying weight fractions of MWCNT (0.5, 1.0 & 1.5 wt%) using the spark plasma sintering (SPS) technique. Investigations were carried out using nanoindentation of varying indentation loads (50 mN, 75 mN and 100 mN) to assess the nanohardness (H) and reduced elastic modulus (E_r) of the alloy and nanocomposites. Further analysis was done to evaluate the elastic recovery index $\left(\frac{w_e}{w_t}\right)$, plasticity index $\left(\frac{w_p}{w_t}\right)$, elastic strain resistance $\left(\frac{H}{E_r}\right)$ and yield pressure $\left(\frac{H^3}{E_r^2}\right)$ at the maximum load. Microstructural analysis revealed the presence of the MWCNT dispersed across the alpha and beta phases of the Ti6Al4V matrix. The nanoindentation studies showed that the nanohardness, elastic modulus, elastic recovery index, elastic strain resistance and anti-wear properties improved with the MWCNT addition and continually increased with increase in nanotubes content. Also, it was observed that the nanohardness and reduced elastic modulus of the fabricated nanocomposites are in the range of 4677–9276 MPa and 29.3–60.9 GPa respectively which declined with increase in indentation load. The sintered Ti6Al4V displayed the least resistance to plastic deformation.

Paper 5: Nanoindentation studies of the mechanical behaviours of spark plasma sintered multiwall carbon nanotubes reinforced Ti6Al4V nanocomposites

Status: Published in Journal of Materials Science and Engineering: A, p.138320

https://doi.org/10.1016/j.msea.2019.138320

Abstract

In this study, the influence of multiwall carbon nanotubes (MWCNT) additions on the mechanical properties of sintered Ti6Al4V-based nanocomposites was investigated. The nanocomposites were fabricated with varying weight fractions of MWCNT (0.5, 1.0 & 1.5 wt.%) using the spark plasma sintering (SPS) technique. Investigations were carried out using nanoindentation of varying indentation loads (50 mN, 75 mN and 100 mN) to assess the nanohardness (H) and reduced elastic modulus (E_r) of the alloy and nanocomposites. Further analysis was done to evaluate the elastic recovery index $\left({W_e}/{W_t}\right)$, plasticity index $\left({W_p}/{W_t}\right)$, elastic strain resistance $\left({H}/{E_r}\right)$ and yield pressure $\left({H^3}/{E_r^2}\right)$ at the maximum load. Microstructural analysis revealed the presence of the MWCNT dispersed across the alpha and beta phases of the Ti6Al4V matrix. The nanoindentation studies showed that the nanohardness, elastic modulus, elastic recovery index, elastic strain resistance and anti-wear properties improved with the MWCNT addition and continually increased with increase in nanotubes content. Also, it was observed that the nanohardness and reduced elastic modulus of the fabricated nanocomposites are in the range of 4677-9276 MPa and 29.3-60.9 GPa respectively which declined with increase in indentation load. The sintered Ti6Al4V displayed the least resistance to plastic deformation.

Keywords: Nanoindentation studies; Multiwall carbon nanotubes; Titanium alloys; Mechanical properties; nanocomposites

1. Introduction

The incessant needs for the replacement of conventional engineering materials with advanced materials having lightweight and improved mechanical properties have been on the rise in recent years. This has engendered the application of various advanced manufacturing technique in

fabricating materials with improved mechanical, thermal and electrical properties for aerospace, automobile and biomedical applications.

In recent times, titanium-based alloys (Ti6Al4V) have been in high demand for diverse technological applications, which span across aerospace, automobile, construction and biomedical industries. This is due to their combination of outstanding properties such as specific strength, excellent formability, weldability, high melting point, machinability, heat-treatability, lightweight, biocompatibility and good corrosion resistance [1–5]. In addition, they are cost-effective when compared to other alloys used in aerospace applications. They are widely employed for the production of biomedical implants and prostheses, gas turbine, race car gearbox, offshore drilling platforms, military airframe, aircraft jet engine, oil and gas drilling equipment, base plates, fasteners, marine engineering, power and transmission equipment, ancillary equipment, turbine compression blades and deep-sea diving device [6–9]. The widespread applications of Ti6Al4V may be linked to its dual-phase nature since it contains the alpha (α) and beta (β) phases in its microstructure, which possessed different lattice structure at both low and high temperature. The α-phase has a hexagonal closed packed lattice structure, which usually exists at a lower temperature below 883 ^{o}C, while the β-phase is associated with the body centred cubic crystal structure that is usually formed above the 883 ^{o}C. Furthermore, in the structure of Ti6Al4V, various elements favour the stability of these phases (α &β). For instance, aluminium, carbon and oxygen are good stabilizers for α-phases, while elements such as vanadium, niobium and iron favour the stability of the β-phase. Each of these phases has their specific roles in affecting the mechanical, thermal, biocompatibility of the alloy [10–12].

Despite the outstanding properties of Ti6Al4V, past studies revealed that it exhibits some limitations such as ease of oxidation, low hardness and wear resistance when compared with duplex stainless steels and super nickel alloys that are in high demand for production of turbine blades. Additionally, they possessed a high coefficient of friction, prone to ductile-brittle failure and has limited creep strength since they undergo creep above 300 ^{o}C. These inferior properties have limited their widespread use in structural applications in many industries [13–15]. Therefore, advancement in materials engineering has fostered the augmentation of the properties of Ti6Al4V by developing advanced composites materials using ceramics and other carbon-based reinforcements.

Recently, the properties of Ti6Al4V has been tremendously improved by reinforcing the alloy with ceramics and carbon-based materials. Materials such as silica, zirconia, titanium nitride, tungsten carbide, graphene and carbon nanotubes (CNT) has been adequately employed to improve the properties of Ti6Al4V for diverse engineering applications [16–21]. Among these reinforcing materials, which are used to improve the properties of Ti6Al4V, the application of CNT has spurred unprecedented interest in the materials research community in recent years owing to their lightweight, excellent mechanical, thermal and electrical properties. Carbon nanotubes usually exist as single wall, double wall and multiwall structure and recent studies have shown that the application of multiwall carbon nanotubes (MWCNT) are highly desirable for the synthesis of composite materials. The adoption of MWCNT for composite production may be ascribed to their multi-layer tubular structures, which aid the retainment of its unique properties after undergoing telescopic effect during the synthesis of composite materials [22,23].

Furthermore, MWCNT possessed excellent strength in the range of 140-150 gigapascal, young modulus up to 1 TPa, lightweight between 1.7 to 2.1 kg/m^3 and extremely high aspect ratio in the range of 100 to 100000 [24,25]. These outstanding properties are attributed to the graphitic structure of the carbon to carbon network in their outer layers, strong carbon-carbon bonds in their shells and the tubular structure of the MWCNT [23,26]. Nevertheless, in order to transfer the unique properties of MWCNT into Ti6Al4V, the uniform dispersion of the nanotubes within the Ti6Al4V is very paramount.

Past works on the effective dispersion of MWCNT in Ti6Al4V have emphasized that the nanotubes tend to agglomerate into bundles during the synthesis of Ti6Al4V nanocomposites and this dispersion behaviour is attributed to the strong van der Waal forces, high aspect ratio and the great surface area that exist between the individual MWCNT [20,23,27,28]. Conversely, during the uniform dispersion of MWCNT in Ti6Al4V, there are tendencies of damaging the structures of the nanotubes, thereby compromising the excellent properties of the MWCNT. Meanwhile, our past work has established that MWCNT can be effectively and efficiently dispersed by the adoption of shift speed ball milling without compromising the structural integrity of the nanotubes [23]. Apart from the adoption of an effective technique in dispersing MWCNT in Ti6Al4V matrix, the utilization of an efficient sintering technique is very vital to fabricate nanocomposites with excellent mechanical, thermal and electrical properties.

In recent years, various fabrication techniques such as hot isostatic pressing, microwave sintering, hot pressing and spark plasma sintering (SPS) have been successfully employed in producing metal matrix composites with outstanding mechanical properties. Among the aforementioned fabrication techniques, SPS has attracted enormous attention because of its unique features and the possibility of producing near net-shape materials. Additionally, it can be used to fabricate materials at lower sintering temperature and higher sintering rate up to 1000 ^{o}C in a short time with accompanying higher densification and improved mechanical properties [29,30]. This was buttressed by Munir et al.[31] whose work emphasized the advantages of SPS over other conventional sintering technique.

Over the past decades, various micro and macro mechanical testing techniques have been employed to evaluate the mechanical properties such as tensile strength, hardness, toughness, flexural properties, young modulus to mention but a few. Meanwhile, the revolution in material testing has unveiled a unique technique called nanoindentation to easily evaluate various mechanical properties of different materials. This testing technique can be used to investigate the mechanical properties of broad selections of materials such as metals, alloys, ceramics and composites materials. Also, it can be used to evaluate the mechanical properties of small-scale materials ranging from nanometer to micrometre scale length at a higher testing speed [32,33].

Recently, nanoindentation has been effectively utilized to evaluate the mechanical properties of thin films, coatings on various materials substrates and small volume samples [34]. The major pros of this testing technique over other conventional micro and macro testing technique is its features of probing small samples and carrying out an in-situ evaluation of the properties of materials without impelling the microstructural features of the materials [35]. Additionally, it is a highly sensitive measuring technique that employs precise resolutions to obtain the elastic modulus, elastic-plastic deformation of materials and the nanohardness of tested materials without machining the samples into any specific shape and size [36,37]. The application of this testing technique was confirmed by Attar et al. [35] as they evaluated the nanohardness, elastic modulus and wear behaviour of titanium and titanium-boride composites using the nanoindentation measurements. Similarly, Maja et al.[19] measured the mechanical properties of titanium alloy and titanium-reinforced titanium nitride where the elastic modulus and nanohardness were evaluated from the load-displacement curve generated during nanoindentation. In this research, the mechanical properties of titanium-based nanocomposites reinforced with MWCNT have been studied using nanoindentation testing

technique. To the best of our knowledge, the utilization of this testing method to evaluate the mechanical properties of spark plasma sintered titanium-based nanocomposites reinforced with MWCNT has not been reported in past studies.

2. Materials and Methods

The materials employed in this study are as described in this section. The starting materials are in powder forms and effective powder mixing technique was utilized to achieve homogeneity of the powders. Afterwards, powder consolidation was carried out using spark plasma sintering and the nanomechanical properties of the sintered samples were tested using nanoindentation technique.

2.1 Mixing and fabrication of Ti6Al4V and MWCNT-Ti6Al4V nanocomposites by SPS

Argon atomized prealloyed Ti6Al4V outsourced from TLS Technik GmbH & Co Germany was used as the starting matrix powder. MWCNT powders acquired from Nanocycl Belgium with ~99.7 % purity and diameter of 9.5 nm and length of 1.5 mm was utilized as the reinforcement phase. Consequently, 0.5, 1.0 and 1.5 wt.% of MWCNT was dispersed in the Ti6Al4V matrix using the shift speed ball milling technique reported in our preliminary study on the dispersion of MWCNT in Ti6Al4V matrix [23].

The Ti6Al4V powder and the admixed nanocomposite powders were transferred into a Ø 20 mm graphite die with 5 mm gauged height and cold compacted with a force of 10 KN to impact the powders with adequate green strength. In addition, the cold compaction assists in promoting the conductivity between the compact and the graphite die. Afterwards, the green compacts were transferred into the sintering chamber of the spark plasma sintering facility (model HHPD-23, FCT Germany) for the sintering process. The powders were sintered by using the following sintering parameters; heating rate of 100 ^{o}C/min, holding time of 10 min, pressure of 50 MPa and sintering temperature of 1100 ^{o}C. Subsequently, the sample was left to cool in the sintering chamber and further sandblasted to eliminate the graphite foils attached to the sample during sintering.

2.2 Microstructural evolution of sintered Ti6Al4V and MWCNT-Ti6Al4V nanocomposites

Prior to the nanoindentation studies of the sintered samples, metallography was carried out by grinding the samples using silica carbide papers ranging from P320 to 1200 grit size. Further grinding was done using Aker Allegra 3 plate with 6 µm suspension to eliminate scratches induced on the

samples during preliminary grinding. Fused silica suspension was utilized to polish the samples to obtain a mirror-like surface. The sintered alloy and nanocomposites were observed under a scanning electron microscope (Carl Zeiss Sigma FESEM) to reveal the morphology of the sintered materials.

2.3 Nanoindentation and Nanomechanics of the mechanical properties of the sintered Ti6Al4V and MWCNT-Ti6Al4V nanocomposites

The mechanical properties (elastic and plastic behaviour) of the sintered alloy and nanocomposites were investigated using an ultra nanoindenter (UNHT), Switzerland. This nanoindentation equipment uses the Berkovich diamond indenter, which is made up of a three-sided pyramid. Furthermore, the nanoindentation test was carried out under force control mode in accordance with ISO 14577 [38,39]. Prior to the nanoindentation test, the nanoindentation equipment was calibrated using a fused silica reference sample to obtain accurate results during the test. The indentations were carried out on the flat and polished surface of the samples by applying loads of 50, 75 and 100 mN with a loading rate of 10 mN/min. During the nanoindentation test, a minimum of 15 indentations was applied per load for each sample with a pause time of 1000 s to prevent viscoelastic effects and determine the time-dependent deformation properties of the sample. The principal mechanical properties determined from the nanoindentation test are reduced elastic modulus and hardness, which were evaluated from the load-displacement data in accordance with Oliver and Pharr method [40]. The reduced elastic modulus (E_r) was calculated from the unloading part of the load-displacement curve, while the hardness was calculated by the application of the expression in equation (1), which shows that hardness is the ratio of the maximum load (P_{max}) to the projected contact area (A_c) at the maximum load [40].

$$H = \frac{P_{max}}{A_c} \qquad (1)$$

The load-displacement indentation curve is made up of the loading and unloading part, where the indenter displacement and the load obey the power law [41,42], which is shown in the expressions in equation (2) and (3) :

$$P = \alpha_1 h^{m_1} \qquad (2)$$

$$P = \alpha(h - h_f)^m \qquad (3)$$

The expression in equation (1) represents the loading part of the indentation curve, while (2) signifies the unloading portion of the curve. P is the indentation load, h is the instantaneous indenter displacement, h_f is the final indentation depth of residual impression and m, α, m_1, α_1 are the empirical fitting parameters. Meanwhile, the value for the maximum depth (h_{max}) at the peak load P_{max} can be calculated by adding the contact depth (h_c) and the elastic surface displacement (h_e) [36,40] expressed in equation (4).

$$h_{max} = h_e + \mathrm{h}_c \qquad (4)$$

The indentation contact depth can also be expressed in a relationship with the maximum depth (h_{max}), ε is the geometry constant of the indenter which depends on the geometry of the indenter, the load (P) and the contact stiffness (S) and is shown in equation (5).

$$h_c = h_{max} - \varepsilon.\frac{P_{max}}{S} \qquad (5)$$

ε is usually expressed as 1.034 for a Berkovich indenter.

The contact stiffness can be calculated by differentiating the unloading curve at the maximum load

$$S = \left(\frac{dP}{dh}\right)_{\mathrm{h=hmax}} = \alpha m(h_{max} - h_f)^{m-1} \qquad (6)$$

Subsequently, the contact stiffness, the indented area (A) at maximum load, and the reduced elastic modulus (E_r) are related to this expression stated below in equation (7):

$$S = \frac{2}{\sqrt{\pi}} E_r \sqrt{A} \qquad (7)$$

Similarly, the reduced elastic modulus (E_r) can be expressed as a relationship of the Poisson's ratio of the sample (v_s) and the indenter (v_i) and the elastic modulus of the sample (E_s) and the indenter (E_i) respectively [43]. The elastic modulus and the Poisson's ratio of the Berkovich diamond indenter are usually expressed as E_i = 1141 GPa and v_i = 0.07.

$$\frac{1}{E_r} = \frac{1-v_s^2}{E_s} + \frac{1-v_i^2}{E_i} \qquad (8)$$

From equation (7), the reduced modulus can be expressed as

$$E_r = \frac{S}{2}\frac{\sqrt{\pi}}{\sqrt{24.5h_c^2}} \qquad (9)$$

where A is expressed as $24.5h_c^2$, this was calculated from the projected area of the Berkovich indenter, which is explained in Figure 1 below

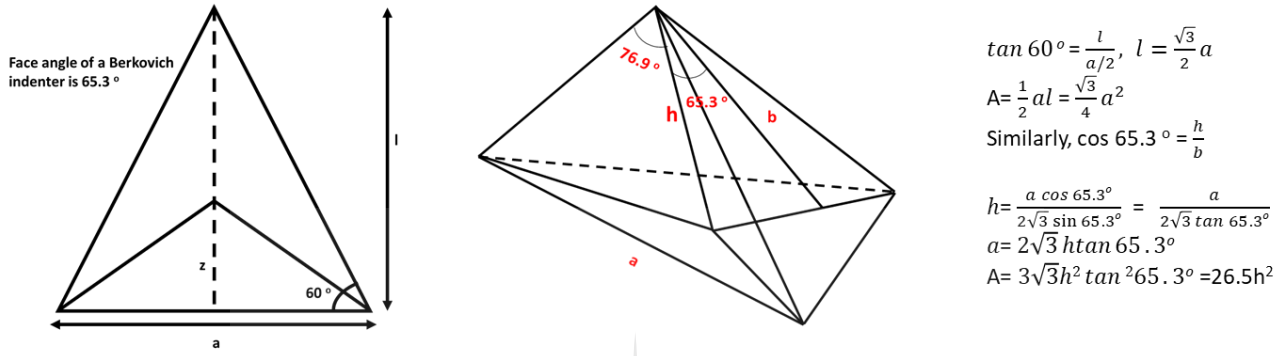

Figure 1: Mathematical derivation of the contact area of a Berkovich indenter (*A*)

By relating equation (1) and (9), a relationship between hardness, reduced elastic modulus and contact stiffness at the maximum load will be established.

$$H = \frac{4P_{max}E_r^2}{\pi S^2} \qquad (10)$$

Furthermore, Bao et al. [42], established a relationship between the elastic surface displacement h_e and the elastic recovery resistance R_e under a particular load.

$$R_e = \frac{P_{max}}{h_e^2} \qquad (11)$$

Considering the expression established by Oliver and Pharr [40] on the relationship between elastic surface displacement, maximum load and the geometry constant of the indenter (ε = 0.75 for Berkovich indenters), we can establish that

$$H = \frac{4E_r^2h_e^2}{\pi\varepsilon^2 P_{max}} \qquad (12)$$

From equation (2) and (3), the total work done by the indenter during nanoindentation can be evaluated as reported by Bao et al. [42]. The total work done by the indenter (W_t) can be used to

evaluate the elastic recovery index $\left(\frac{W_e}{W_t}\right)$ and the plasticity index $\left(\frac{W_p}{W_t}\right)$, which explains the mechanical behaviour of the sintered nanocomposites [10]. The elastic recovery index represents the amount of energy discharged from the nanocomposites after the impression of the load, which indicates the resistance of the nanocomposites to impact loading, while the plasticity index represents the inherent plasticity of the nanocomposite [44]. Meanwhile, the total energy or work done by the indenter during indentation can be expressed as

$$W_t = W_e + W_p \qquad (13)$$

Where W_e and W_p represent the elastic energy and plastic energy respectively, and these can be calculated from the area under the load-displacement nanoindentation curve as shown in Figure 2 below.

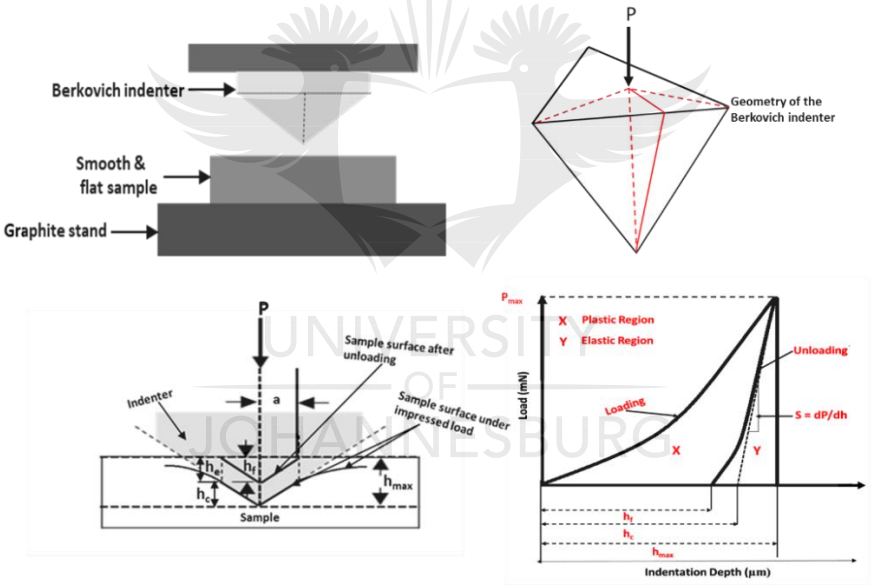

Figure 2: Nanoindentation parameters for the evaluation of mechanical properties

3. Results and Discussion

The microstructural evolution of the fabricated Ti6Al4V and titanium-based nanocomposites after spark plasma sintering are presented and discussed below. In addition, the nanoindentation technique was used to evaluate the elastic and plastic behaviour of the alloy and nanocomposites, which were comprehensively discussed in this section.

3.1 Microstructures of the sintered Ti6Al4V and Ti6Al4V nanocomposites

The microstructures of the sintered Ti6Al4V and the Ti6Al4V nanocomposites comprising 0.5, 1.0 and 1.5 wt.% of MWCNT are presented in Figure 3 below. From the SEM images in Figure 3, the morphology of the sintered Ti6Al4V and the Ti6Al4V nanocomposites were observed. The SEM image in Figure 3 (a) shows the morphology of the sintered Ti6Al4V, which depicts a combination of alpha (α) and beta (β) phases. The α phases (grey) were surrounded by the β phases (white) since the alloy was sintered at a temperature above the β transus temperature (996 ^{o}C) and was cooled slowly from above the β transus temperature, which allows the preferential nucleation of the alpha phase [45]. This microstructural feature is an indication that sintering above the β transus temperature promotes the formation of the beta phases around the alpha phases.

Conversely, the SEM images in Figure 3 (b-d) shows the morphology of the sintered Ti6Al4V nanocomposites comprising 0.5, 1.0 and 1.5 wt.% of MWCNT. From the SEM images, the presence of MWCNT was glaring and dispersed within the Ti6Al4V matrix. Furthermore, the presence of the alpha and beta phases were seen in the SEM images of the nanocomposites. The alpha phases in the SEM images of the sintered nanocomposites may be ascribed to the MWCNT that was present in the Ti6Al4V matrix, which stabilizes the alpha phases since carbon is an alpha phase stabilizer. However, it was observed that the dispersibility of MWCNT decreased with the increase in the weight fraction. This dispersion characteristic is ascribed to the stronger van der Waals forces that increased with the concentration of MWCNT in the nanocomposites. Also, the SEM image in Figure 3 (d) shows more clustering of the MWCNT in the Ti6Al4V matrix which can adversely influence the loading and unloading behaviour of the nanocomposites under nanoindentation test.

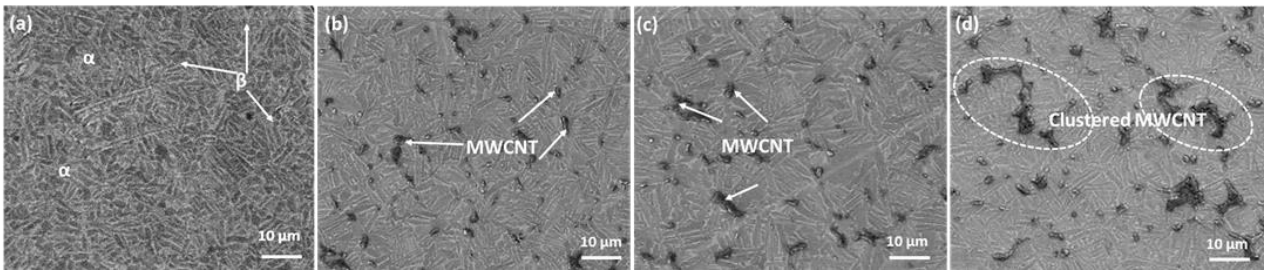

Figure 3: SEM images of the Ti6Al4V (a), 0.5 wt.% MWCNT- Ti6Al4V (b),1.0 wt.% MWCNT-Ti6Al4V (c), and 1.5 wt.% MWCNT-Ti6Al4V (d)

3.2 Nanoindentation studies of the mechanical properties of the sintered Ti6Al4V and Ti6Al4V nanocomposites

The nanoindentation testing technique was used to evaluate the nanohardness, elastic modulus, elastic recovery index, plasticity index, resistance to elastic strain to failure, and the yield pressure of the sintered Ti6Al4V and Ti6Al4V-based nanocomposites. In addition, the load-depth and displacement-time plots were used to assess the mechanical behaviour of the sintered alloy and nanocomposites in this section.

3.2.1 Load-displacement and depth-time curves of the sintered Ti6Al4V and Ti6Al4V nanocomposites

The nanoindentation load-displacement curves of the sintered Ti6Al4V and the Ti6Al4V-based nanocomposites comprising of 0.5, 1.0, & 1.5 wt.% of MWCNT when subjected to indentation loads of 50 mN, 75 mN and 100 mN respectively is as shown in Figure 4 (a-c) below. From the indentation curves, it was observed that both the sintered Ti6Al4V and the corresponding nanocomposites depict similar loading and unloading behaviours. However, the sintered alloy and nanocomposites experienced pop-in effects when subjected to the varying indentation loads. These pop-in effects may be attributed to the nucleation of dislocation and strain transfer at the vicinity of the grain boundaries of the alloy and nanocomposites, which tend to resist the dislocation motion imposed by the indentation [46,47]. Meanwhile, the pop-in effects were experienced during the loading of the samples. Additionally, the nanocomposite grade comprising of 1.5 wt.% MWCNT experienced tremendous pop-in behaviour during the indentation loading which maybe linked to the cracking and dislocation bursting of the nanocomposites resulting from the clustered MWCNT [48–50]. Furthermore, the load-displacement curves depict an elastic-plastic deformation behaviour and it was observed that the unreinforced Ti6Al4V showed the largest penetration depth at every indented load, followed by the 0.5 wt.% MWCNT-Ti6Al4V, 1.0 wt.% MWCNT-Ti6Al4V and 1.5 wt.% MWCNT-Ti6Al4V nanocomposites grades. This is an indication that the presence of MWCNT assisted in improving the resistance of the nanocomposites to plastic deformation during indentation, which further implies an improvement in hardness and stiffness resulting from load transfer from the matrix to the reinforcement.

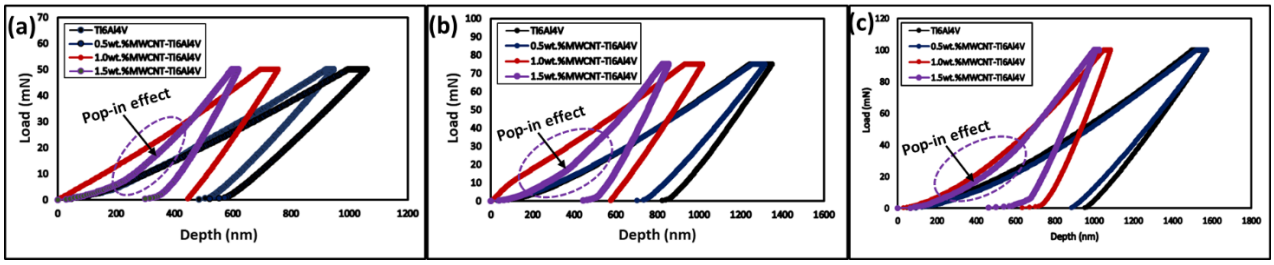

Figure 4. Load-displacement curves of the sintered Ti6Al4V and Ti6Al4V nanocomposites under indentation loads of 50 mN (a), 75 mN (b), and 100 mN (c) respectively.

Correspondingly, the penetration depth as a function of time of the sintered Ti6Al4V and Ti6Al4V-based nanocomposites comprising of 0.5, 1.0 and 1.5wt.% of MWCNT when subjected to indentation of 50 mN, 75 mN and 100 mN are shown in Figure 5 (a-c) below. It was observed that both the sintered Ti6Al4V and the Ti6Al4V-based nanocomposites experienced huge plastic deformation when subjected to a load of 100 mN. The maximum penetration depths experienced by the sintered Ti6Al4V at the varying loads are 1035 nm, 1311 nm, 1563 nm at the corresponding loads of 50 mN, 75 mN and 100 mN respectively. Meanwhile, the sintered 0.5 wt.%MWCNT-Ti6Al4V nanocomposites showed a maximum penetration depth of 924, 1307, and 1554 nm when subjected to indentation loads of 50 mN, 75 mN and 100 mN respectively. This was accompanied by the sintered 1.0 wt.%MWCNT-Ti6Al4V nanocomposite grade which shows a decline in penetration of 756, 1007 and 1083 nm when subjected to corresponding indentation loads of 50 mN, 75 mN and 100 mN respectively. However, the 1.5 wt.%MWCNT-Ti6Al4V nanocomposite grade shows the highest resistance to the indentation loads with penetration depths of 299, 444, and 462 nm under the loads 50 mN, 75 mN and 100 mN respectively. These results reflect that the hardness and stiffness of the nanocomposites were augmented by the presence of MWCNT. The improvement in mechanical properties may be attributed to the load transfer mechanism of the matrix to the reinforcement owing to the pinning effect of dislocation motion by the MWCNT in the Ti6Al4V matrix [51].

Additionally, both the sintered alloy and nanocomposites depicted similar time to complete the nanoindentation cycle. However, from Figure 5 (a-c), it was observed that the nanoindentation time increased with the indentation loads, which indicates that there was more plastic deformation of the samples when the load was increased from 50-100 mN. The plastic deformation was recorded despite

the resistance to penetration displayed by the nanocomposites grades in Figure 4 (a-c). However, there was less disparity in the elastic-plastic behaviour between the sintered titanium alloy and the nanocomposite comprising of 0.5wt.% of MWCNT especially, at 100 mN indentation load. This behaviour may be ascribed to the lower concentration of the nanotubes in the nanocomposite grade which imposed less resistance to the dislocation motion during the nanoindentation test. Meanwhile, 1.5 wt.%MWCNT-Ti6Al4V nanocomposite grade showed the highest resistance to penetration during nanoindentation under the various indentation loads and this behaviour may be ascribed to the higher concentration of the MWCNT in the Ti6Al4V matrix.

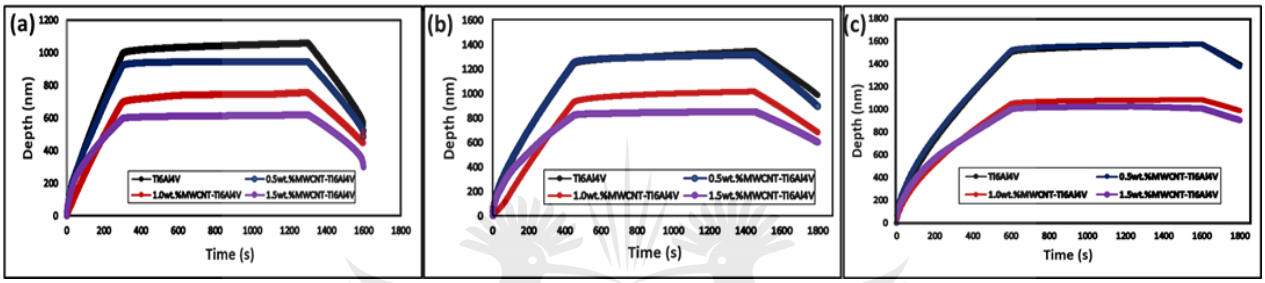

Figure 5. Displacement-time curves of the sintered Ti6Al4V and Ti6Al4V nanocomposites under indentation loads of 50 mN (a), 75 mN (b), and 100 mN (c) respectively.

3.2.2 Nanohardness and reduced elastic modulus of the sintered ti6al4v and ti6al4v nanocomposites

The nanohardness and elastic modulus of the sintered Ti6Al4V and the Ti6Al4V-based nanocomposites comprising of 0.5, 1.0 and 1.5 wt.% of MWCNT when subjected to indentation of 50 mN, 75 mN and 100 mN respectively are shown in Figure 6 (a & b). From Figure 6 (a), It was observed that the value of the nanohardness increased with the addition of MWCNT into the Ti6Al4V matrix. However, the nanohardness value decreased with the increase of the indentation load. Meanwhile, 1.5 wt.% MWCNT-Ti6Al4V nanocomposite depicted the best nanohardness values of 12823 MPa, 10975 MPa, and 10017 MPa when subjected to indentation loads of 50 mN, 75 mN and 100 mN respectively. Similarly, 1.0 wt.% MWCNT-Ti6Al4V nanocomposite displayed the nanohardness values of 9276 MPa, 8452 MPa, and 7716 MPa when subjected to indentation loads of 50 mN, 75 mN and 100 mN respectively This was accompanied by 0.5 wt.%MWCNT-Ti6Al4V nanocomposite grades, which have nanohardness values of 5864 MPa, 4964 MPa, and 4677

MPa when indented with loads of 50 mN, 75 mN and 100 mN respectively. Conversely, the sintered alloy showed lower nanohardness values of 4672 MPa, 3722 MPa, and 3393 MPa when indented with loads of 50 mN, 75 mN and 100 mN respectively. These results indicate that the nanohardness values of the sintered nanocomposites were tremendously improved by the addition of MWCNT. In addition, the hardness value increased with an increase in the concentration of the MWCNT in the Ti6Al4V matrix. The hardness values of the 1.0 wt.% MWCNT-Ti6Al4V nanocomposite grade indicate its resistance to plastic deformation, which was previously seen in the load-displacement curve in Figure 4 (a-c). In addition, there was an impediment to the dislocation motion in the nanocomposite grades owing to the presence of the MWCNT, which strengthen the Ti6Al4V matrix.

Similarly, from Figure 6 (b), remarkable improvements in reduced elastic modulus were recorded by the nanocomposite grades, which indicates that the materials elastically resist linear compression from the indenter. Furthermore, the reduced elastic modulus of the nanocomposites increased with an increase in the concentration of the MWCNT. However, the reduced elastic modulus of both the nanocomposites and alloy declined with increase in indentation loads. The best reduced elastic modulus was recorded for 1.5 wt.% MWCNT-Ti6Al4V nanocomposite grade with 88.9 GPa, 71.8 GPa, and 54.3. GPa when subjected to indentation loads of 50 mN, 75 mN and 100 mN respectively. Similarly, 1.0 wt.%MWCNT-Ti6Al4V nanocomposite grade depicts reduced elastic modulus values of 60.9 GPa, 54.8 GPa, and 43.1 GPa when subjected to indentation loads of 50 mN, 75 mN and 100 mN respectively. This was accompanied by 0.5 wt.% MWCNT-Ti6Al4V nanocomposite grade with reduced elastic modulus values of 32.0 GPa, 30.1 GPa, and 29.3 GPa under the indentation loads of 50 mN, 75 mN and 100 mN respectively. Conversely, the sintered alloy showed the least reduced elastic modulus values of 29.7 GPa, 27.6 GPa, and 25.3 GPa when indented with loads of 50 mN, 75 mN and 100 mN respectively. These results are indications that the presence of the MWCNT in the nanocomposites enhanced the stiffness effect of the fabricated materials. The improvement of both the elastic modulus and nanohardness of the reinforced nanocomposites can be ascribed to the formation of secondary carbide phases (titanium carbide) in the nanocomposites, which assist in augmenting the mechanical properties.

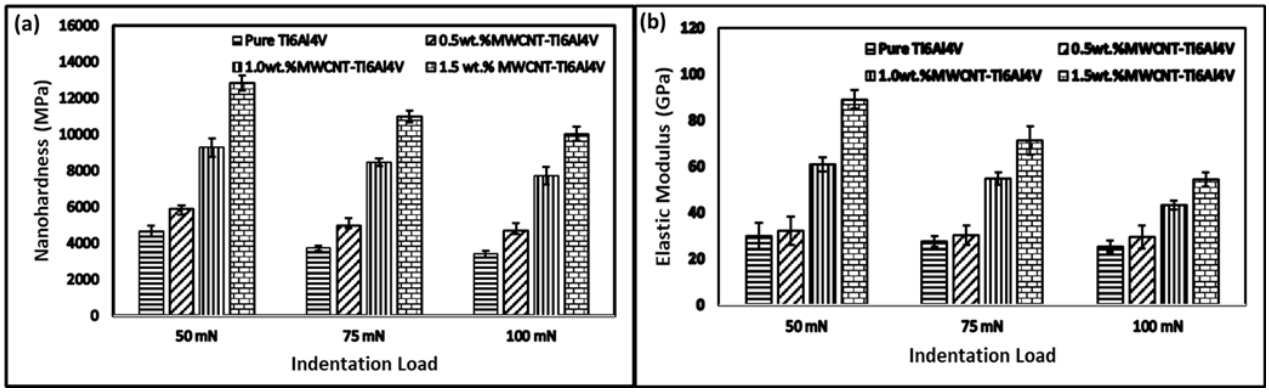

Figure 6. Nanohardness (a) and reduced elastic modulus (b) of the sintered Ti6Al4V and Ti6Al4V nanocomposites under indentation loads of 50 mN, 75 mN, and 100 mN respectively

3.2.3 Mechanical and anti-wear behaviours of the sintered Ti6Al4V and Ti6Al4V nanocomposites

The mechanical behaviours (elastic and plastic) and the anti-wear properties of the sintered Ti6Al4V and Ti6Al4V-based nanocomposites were further assessed from the nanoindentation results by evaluating the elastic recovery index $\left({}^{W_e}/_{W_t}\right)$, plasticity index $\left({}^{W_p}/_{W_t}\right)$, the ratio of the nanohardness to the reduced elastic modulus $\left({}^{H}/_{E_r}\right)$ and the yield pressure $\left({}^{H^3}/_{E_r^2}\right)$. These parameters are highly relevant in investigating the mechanical behaviours and the wear resistance of the materials during nanoindentation studies. As stated earlier, the elastic recovery index gives information about the energy released by the material under the influence of load [52], while the plasticity index is a function of the intrinsic plastic behaviour of the material. Furthermore, the ratio of the nanohardness to elastic modulus dictates the ability to materials to resist elastic strain to failure in a nanometer scale [10,53], while the yield pressure is used to assess the resistance to plastic deformation and anti-wear behaviours of materials during nanoindentation [35][54].

Figure 7 (a) shows the elastic recovery and plasticity index of the sintered Ti6Al4V and Ti6Al4V-based nanocomposites. From Figure 7 (a), it was observed that 1.5 wt.% MWCNT-Ti6Al4V nanocomposite grade depicts the highest elastic recovery index, which was accompanied by the 1.0 and 0.5 wt.% MWCNT-Ti6Al4V nanocomposite grades respectively. Meanwhile, the sintered Ti6Al4V showed the least elastic recovery index, which indicates that the presence of MWCNT in the Ti6Al4V helped to stiffen the nanocomposites and the elastic recovery index improves with increase in the concentration of the MWCNT. Conversely, the plasticity index declined with the

increase in MWCNT, which indicates that the sintered Ti6Al4V undergoes higher plastic deformation during the nanoindentation test. Also, these results buttress the fact that the presence of the MWCNT improved the resistance of the nanocomposites to plastic deformation, which has been seen in previous results of the nanohardness and elastic modulus in this study.

Subsequently, Figure 7 (b) shows the resistance to elastic strain to failure and yield pressure of the sintered Ti6Al4V and Ti6Al4V-based nanocomposites. From the results, it was observed that the resistance to elastic strain to failure improved with the presence of MWCNT. Meanwhile, 1.5 wt.%MWCNT-Ti6Al4V nanocomposite grade depicts the highest resistance to elastic strain to failure and the unreinforced Ti6Al4V showed the least resistance to elastic strain to failure. Similarly, the yield pressure of the sintered materials improved with an increase in MWCNT with 1.5 wt.%MWCNT-Ti6Al4V nanocomposite grade having the highest yield pressure. The improvement of the yield pressure and the resistance to elastic strain to failure implies good resistance to impact loading and wear of the nanocomposites [55].

From all indications in Figure 7 (a & b), the elastic recovery index, resistance to elastic strain and the yield pressure of both the sintered Ti6Al4V and the nanocomposites are directly proportional. This relationship is similar to the trend reported by Hynowska et al.[10] as they investigated the mechanical properties of titanium-based nanostructured materials using nanoindentation technique.

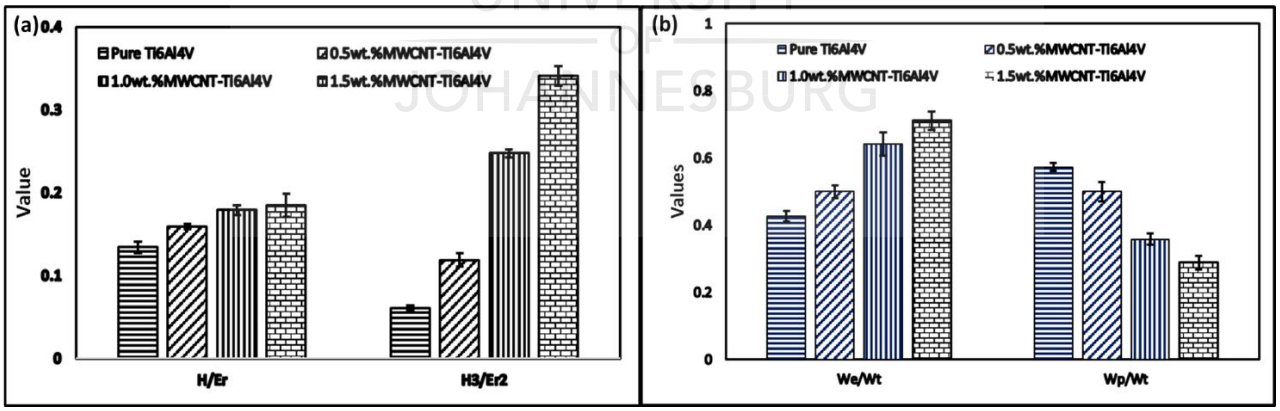

Figure 7. Elastic recovery and plasticity index (a), and elastic strain resistance to failure and yield pressure (b) of the sintered Ti6Al4V and Ti6Al4V nanocomposites under indentation load of 100 mN.

4. Conclusion

In this study, the influence of MWCNT additions on the mechanical properties of spark plasma sintered Ti6Al4V-based nanocomposites was investigated. The mechanical properties of the sintered Ti6Al4V and Ti6Al4V-based nanocomposites were evaluated using the nanoindentation technique and the following conclusions were drawn from the investigations:

1. Nanoindentation is a viable technique for evaluating the nanomechanical properties of alloys and nanocomposite materials.
2. The increase in indenter loads resulted in the reduction of the nanohardness and elastic modulus of both the sintered Ti6Al4V and Ti6Al4V-based nanocomposites.
3. The addition of MWCNT improved the nanohardness, elastic modulus, elastic recovery index, resistance to elastic strain to failure, and anti-wear behaviour of the nanocomposites.
4. The sintered Ti6Al4V displayed the least resistance to plastic deformation by depicting a huge plasticity index than the fabricated nanocomposites.

Acknowledgement

The authors would like to thank the National Research Foundation of South Africa in association with the World Academy of Science (NRF-TWAS) and the Global Excellence and Stature of the University of Johannesburg, South Africa for funding this research.

References

[1] O.E. Falodun, B.A. Obadele, S.R. Oke, A.M. Okoro, P.A. Olubambi, Titanium-based matrix composites reinforced with particulate, microstructure, and mechanical properties using spark plasma sintering technique: a review, Int. J. Adv. Manuf. Technol. (2019) 1–13.

[2] A.M. Okoro, M. Awotunde, O.A. Ajiteru, S.S. Lephuthing, P.A. Olubambi, R. Machaka, Effects of carbon nanotubes on the mechanical properties of spark plasma sintered titanium matrix composites - A review, in: 2018 IEEE 9th Int. Conf. Mech. Intell. Manuf. Technol. ICMIMT 2018, 2018.

[3] K.S. Munir, Y. Zheng, D. Zhang, J. Lin, Y. Li, C. Wen, Improving the strengthening efficiency of carbon nanotubes in titanium metal matrix composites, Mater. Sci. Eng. A. 696 (2017) 10–25.

[4] S. Li, B. Sun, H. Imai, T. Mimoto, K. Kondoh, Powder metallurgy titanium metal matrix composites reinforced with carbon nanotubes and graphite, Compos. Part A Appl. Sci. Manuf. 48 (2013) 57–66.

[5] I. Gurrappa, Characterization of titanium alloy Ti-6Al-4V for chemical, marine and industrial applications, Mater. Charact. 51 (2003) 131–139.

[6] L.E. Murr, S.A. Quinones, S.M. Gaytan, M.I. Lopez, A. Rodela, E.Y. Martinez, D.H. Hernandez, E. Martinez, F. Medina, R.B. Wicker, Microstructure and mechanical behavior of Ti--6Al--4V produced by rapid-layer manufacturing, for biomedical applications, J. Mech. Behav. Biomed. Mater. 2 (2009) 20–32.

[7] H.-C. Chen, A.J. Pinkerton, L. Li, Fibre laser welding of dissimilar alloys of Ti-6Al-4V and Inconel 718 for aerospace applications, Int. J. Adv. Manuf. Technol. 52 (2011) 977–987.

[8] C. Veiga, J.P. Davim, A.J.R. Loureiro, others, Properties and applications of titanium alloys: a brief review, Rev. Adv. Mater. Sci. 32 (2012) 133–148.

[9] A.M. Okoro, S.S. Lephuthing, S.R. Oke, O.E. Falodun, M.A. Awotunde, P.A. Olubambi, A Review of Spark Plasma Sintering of Carbon Nanotubes Reinforced Titanium-Based Nanocomposites: Fabrication, Densification, and Mechanical Properties, JOM. (n.d.) 1–18.

[10] A. Hynowska, E. Pellicer, J. Fornell, S. González, N. van Steenberge, S. Suriñach, A. Gebert, M. Calin, J. Eckert, M.D. Baró, others, Nanostructured $β$-phase Ti--31.0 Fe--9.0 Sn and sub-$μ$m structured Ti--39.3 Nb--13.3 Zr--10.7 Ta alloys for biomedical applications: Microstructure benefits on the mechanical and corrosion performances, Mater. Sci. Eng. C. 32 (2012) 2418–2425.

[11] M. Geetha, A.K. Singh, R. Asokamani, A.K. Gogia, Ti based biomaterials, the ultimate choice for orthopaedic implants--a review, Prog. Mater. Sci. 54 (2009) 397–425.

[12] M. Long, H.J. Rack, Titanium alloys in total joint replacement—a materials science perspective, Biomaterials. 19 (1998) 1621–1639.

[13] C. Leyens, M. Peters, Titanium and titanium alloys: fundamentals and applications, John Wiley & Sons, 2003.

[14] W. Pang, H.C. Man, T.M. Yue, Laser surface coating of Mo--WC metal matrix composite on Ti6Al4V alloy, Mater. Sci. Eng. A. 390 (2005) 144–153.

[15] A. Agapovichev, A. Sotov, V. Kokareva, V. Smelov, Possibilities and limitations of titanium alloy additive manufacturing, in: MATEC Web Conf., 2018: p. 1064.

[16] Y.W. Gu, K.A. Khor, D. Pan, P. Cheang, Activity of plasma sprayed yttria stabilized zirconia reinforced hydroxyapatite/Ti--6Al--4V composite coatings in simulated body fluid, Biomaterials. 25 (2004) 3177–3185.

[17] Y.-J. Kim, H. Chung, S.-J.L. Kang, Processing and mechanical properties of Ti--6Al--4V/TiC in situ composite fabricated by gas--solid reaction, Mater. Sci. Eng. A. 333 (2002) 343–350.

[18] S. Misra, M. Hussain, A. Gupta, V. Kumar, S. Kumar, A.K. Das, Fabrication and characteristic evaluation of direct metal laser sintered SiC particulate reinforced Ti6Al4V metal matrix composites, J. Laser Appl. 31 (2019) 12005.

[19] M.E. Maja, O.E. Falodun, B.A. Obadele, S.R. Oke, P.A. Olubambi, Nanoindentation studies on TiN nanoceramic reinforced Ti--6Al--4V matrix composite, Ceram. Int. 44 (2018) 4419–4425.

[20] A.O. Adegbenjo, P.A. Olubambi, J.H. Potgieter, M.B. Shongwe, M. Ramakokovhu, Spark

plasma sintering of graphitized multi-walled carbon nanotube reinforced Ti6Al4V, Mater. Des. 128 (2017) 119–129.

[21] X. Song, H. Li, X. Zeng, L. Zhang, Brazing of C/C composites to Ti6Al4V using graphene nanoplatelets reinforced TiCuZrNi brazing alloy, Mater. Lett. 183 (2016) 232–235.

[22] A. Dorri Moghadam, E. Omrani, P.L. Menezes, P.K. Rohatgi, Mechanical and tribological properties of self-lubricating metal matrix nanocomposites reinforced by carbon nanotubes (CNTs) and graphene - A review, Compos. Part B Eng. 77 (2015) 402–420.

[23] A.M. Okoro, R. Machaka, S.S. Lephuthing, M.A. Awotunde, S.R. Oke, O.E. Falodun, P.A. Olubambi, Dispersion characteristics, interfacial bonding and nanostructural evolution of MWCNT in Ti6Al4V powders prepared by shift speed ball milling technique, J. Alloys Compd. (2019).

[24] K. Morsi, A.M.K. Esawi, S. Lanka, A. Sayed, M. Taher, Spark plasma extrusion (SPE) of ball-milled aluminum and carbon nanotube reinforced aluminum composite powders, Compos. Part A Appl. Sci. Manuf. 41 (2010) 322–326.

[25] S.S. Lephuthing, A.M. Okoro, M. Lesufi, O.O. Ige, P.A. Olubambi, Effect of milling parameters on the dispersion characteristics of multi-walled carbon nanotubes in transition metal oxides, in: IOP Conf. Ser. Mater. Sci. Eng., 2018.

[26] A.M. Okoro, R. Machaka, S.S. Lephuthing, M. Awotunde, P.A. Olubambi, Structural integrity and dispersion characteristics of carbon nanotubes in titanium-based alloy, in: IOP Conf. Ser. Mater. Sci. Eng., 2018.

[27] E.W. Wong, P.E. Sheehan, C.M. Lieber, Nanobeam mechanics: elasticity, strength, and toughness of nanorods and nanotubes, Science (80-.). 277 (1997) 1971–1975.

[28] K.S. Munir, Y. Li, D. Liang, M. Qian, W. Xu, C. Wen, Effect of dispersion method on the deterioration, interfacial interactions and re-agglomeration of carbon nanotubes in titanium metal matrix composites, Mater. Des. 88 (2015) 138–148.

[29] A.M. Okoro, S.S. Lephuthing, S.R. Oke, O.E. Falodun, M.A. Awotunde, P.A. Olubambi, A Review of Spark Plasma Sintering of Carbon Nanotubes Reinforced Titanium-Based

Nanocomposites: Fabrication, Densification, and Mechanical Properties, JOM. (2018).

[30] P. Cavaliere, B. Sadeghi, A. Shabani, Spark Plasma Sintering: Process Fundamentals, in: Spark Plasma Sinter. Mater., Springer, 2019: pp. 3–20.

[31] Z.A. Munir, U. Anselmi-Tamburini, M. Ohyanagi, The effect of electric field and pressure on the synthesis and consolidation of materials: A review of the spark plasma sintering method, J. Mater. Sci. 41 (2006) 763–777.

[32] M.L. Oyen, R.F. Cook, A practical guide for analysis of nanoindentation data, J. Mech. Behav. Biomed. Mater. 2 (2009) 396–407.

[33] J.M. Wheeler, J. Michler, Invited Article: Indenter materials for high temperature nanoindentation, Rev. Sci. Instrum. 84 (2013) 101301.

[34] K.D. Sattler, Handbook of nanophysics: functional nanomaterials, CRC Press, 2010.

[35] H. Attar, S. Ehtemam-Haghighi, D. Kent, I. V Okulov, H. Wendrock, M. Bönisch, A.S. Volegov, M. Calin, J. Eckert, M.S. Dargusch, Nanoindentation and wear properties of Ti and Ti-TiB composite materials produced by selective laser melting, Mater. Sci. Eng. A. 688 (2017) 20–26.

[36] A.E. Ozmetin, O. Sahin, E. Ongun, M. Kuru, Mechanical characterization of MgB2 thin films using nanoindentation technique, J. Alloys Compd. 619 (2015) 262–266.

[37] C.C. Ng, M.M. Savalani, M.L. Lau, H.C. Man, Microstructure and mechanical properties of selective laser melted magnesium, Appl. Surf. Sci. 257 (2011) 7447–7454.

[38] J. Nohava, N.X. Randall, N. Conté, Novel ultra nanoindentation method with extremely low thermal drift: Principle and experimental results, J. Mater. Res. 24 (2009) 873–882.

[39] X. Li, B. Bhushan, A review of nanoindentation continuous stiffness measurement technique and its applications, Mater. Charact. 48 (2002) 11–36.

[40] W.C. Oliver, G.M. Pharr, An improved technique for determining hardness and elastic modulus using load and displacement sensing indentation experiments, J. Mater. Res. 7 (1992) 1564–1583.

[41] V. Marx, H. Balke, A critical investigation of the unloading behavior of sharp indentation, Acta Mater. 45 (1997) 3791–3800.

[42] Y.W. Bao, W. Wang, Y.C. Zhou, Investigation of the relationship between elastic modulus and hardness based on depth-sensing indentation measurements, Acta Mater. 52 (2004) 5397–5404.

[43] B.B. Medeiros, M.M. Medeiros, J. Fornell, J. Sort, M.D. Baró, A.M.J. Junior, Nanoindentation response of Cu--Ti based metallic glasses: Comparison between as-cast, relaxed and devitrified states, J. Non. Cryst. Solids. 425 (2015) 103–109.

[44] E. Zhang, H. Chen, F. Shen, Biocorrosion properties and blood and cell compatibility of pure iron as a biodegradable biomaterial, J. Mater. Sci. Mater. Med. 21 (2010) 2151–2163.

[45] A.A. Antonysamy, Microstructure, texture and mechanical property evolution during additive manufacturing of Ti6Al4V alloy for aerospace applications, The University of Manchester (United Kingdom), 2012.

[46] C.A. Schuh, A.C. Lund, Application of nucleation theory to the rate dependence of incipient plasticity during nanoindentation, J. Mater. Res. 19 (2004) 2152–2158.

[47] Z. Wang, Influences of sample preparation on the indentation size effect and nanoindentation pop-in on nickel, (2012).

[48] M. Suárez, A. Fernández-Camacho, J.L. Menéndez, R. Torrecillas, Challenges and opportunities for spark plasma sintering: a key technology for a new generation of materials, InTech, 2013.

[49] A.A. Najimi, H.R. Shahverdi, Effect of milling methods on microstructures and mechanical properties of Al6061-CNT composite fabricated by spark plasma sintering, Mater. Sci. Eng. A. 702 (2017) 87–95.

[50] M.A. Awotunde, A.O. Adegbenjo, O.O. Ayodele, A.M. Okoro, M.B. Shongwe, P.A. Olubambi, Interdependence of carbon nanotubes agglomerations, its structural integrity and the mechanical properties of reinforced nickel aluminide composites, J. Alloys Compd. (2019).

[51] D. Lin, M. Saei, S. Suslov, S. Jin, G.J. Cheng, Super-strengthening and stabilizing with carbon nanotube harnessed high density nanotwins in metals by shock loading, Sci. Rep. 5 (2015) 15405.

[52] J. Musil, F. Kunc, H. Zeman, H. Polakova, Relationships between hardness, Young's modulus and elastic recovery in hard nanocomposite coatings, Surf. Coatings Technol. 154 (2002) 304–313.

[53] J. Xu, G. dong Wang, X. Lu, L. Liu, P. Munroe, Z.-H. Xie, Mechanical and corrosion-resistant properties of Ti--Nb--Si--N nanocomposite films prepared by a double glow discharge plasma technique, Ceram. Int. 40 (2014) 8621–8630.

[54] J. Fornell, N. Van Steenberge, A. Varea, E. Rossinyol, E. Pellicer, S. Suriñach, M.D. Baró, J. Sort, Enhanced mechanical properties and in vitro corrosion behavior of amorphous and devitrified Ti40Zr10Cu38Pd12 metallic glass, J. Mech. Behav. Biomed. Mater. 4 (2011) 1709–1717.

[55] S. Ehtemam-Haghighi, G. Cao, L.-C. Zhang, Nanoindentation study of mechanical properties of Ti based alloys with Fe and Ta additions, J. Alloys Compd. 692 (2017) 892–897.

CHAPTER FOUR

DISCUSSIONS ON SUBJECTS CONSIDERED BY THE ARTICLES

4.1 The Ideas of the Dissertation

The dissertation is targeted towards intensifying the application of powder metallurgy technique in the fabrication of Ti6Al4V alloy for widespread engineering applications through investigations and creating tangible solutions to overcome the limitations of the alloy. Furthermore, a comprehensive discussion was made addressing the dispersion of MWCNT into the Ti6Al4V matrix to enhance the properties of the alloy.

This thesis is in accordance with the framework which indicates a PhD thesis that solve research challenges through scientific results and addressing research questions. Additionally, it proffers solutions to the SPS of Ti6Al4V based nanocomposites reinforced with dispersed MWCNT and studied and added knowledge on the dispersion characteristics of MWCNT, microstructural and nanostructural evolutions of the nanotubes in Ti6Al4V matrix. Furthermore, the densification behaviour, mechanical properties of the fabricated nanocomposites, reinforcing capabilities of MWCNT and the strengthening mechanism of the nanocomposites with improved properties were covered.

In this chapter, detailed discussion of the presented articles and their interconnectivity in accordance with the specific objectives of this study are considered. The motivations of the research in each paper are reiterated and the contributions of the papers in addressing the enlisted objectives of the study is fully covered. Furthermore, it encompassed the contributions of this research to existing knowledge in spark plasma sintering of Ti6Al4V reinforced with MWCNT and the novelty of the study.

4.2 Subjects on the novelty and contributions of the study to knowledge

As stated in the chapter one of this thesis, the primary reasons for conducting this study is to effectively disperse MWCNT in the Ti6Al4V matrix and consolidate the admixed powders using SPS. Furthermore, provide information on best dispersion method and the dispersion parameters such as milling speed, milling time, BPR, relaxation time required to achieve the homogeneous

dispersion of the nanotubes without tampering with unique properties of the MWCNT after dispersion.

Additionally, the study revealed the influence of sintering temperature on the sintering behaviour, densification, evolution in the microstructure and phases and the microhardness of the fabricated alloy and nanocomposites. Besides, the effects of the MWCNT concentration on the microstructural, phase changes, fracture morphology and the nanomechanical properties of the nanocomposites were fully considered. The research findings from this study are presented in the enclosed articles of this thesis. This section presents detailed explanation on the major subjects considered in all the articles while achieving the specific objectives of this study.

4.2.1 Subjects considered from the reviewed articles on SPS of titanium-based nanocomposites

The first article in this thesis reviewed past researches carried out on the SPS of titanium-based nanocomposites reinforced with carbon nanotubes. Additionally, the effectiveness of the SPS technique in consolidation of nanostructured titanium-based nanocomposites was emphasized. It was realized that numerous researches have been conducted using SPS technique to fabricate titanium-based nanocomposites reinforced with CNT. Furthermore, the fabrication of CNT reinforced titanium-based nanocomposites has spurred great research attention in recent years owing to the demand of titanium-based composites in widespread applications such as automobile, biomedical implants, aerospace, chemical plants, petrochemical industries to mention but a few.

Also, the properties of SPSed titanium metal and its alloy can be improved on by increasing the concentration of the nanotubes in the matrix materials. Regardless of the increase in concentration of the nanotubes in the metal matrices, the utilization of appropriate sintering parameters during the consolidation process is very expedient in producing a nanocomposite with improved properties. Sintering parameters like compressive pressure, sintering temperature, holding times and heating rate have specific influence on the grain growth, evolution of phases, densification behaviours and resulting properties of the SPSed nanocomposites.

Although the SPS technique has been employed in fabricating numerous materials, the application of SPS in fabricating Ti6Al4V based nanocomposites reinforced with MWCNT are still limited.

The fabrication of titanium-based nanocomposites reinforced with CNT using the SPS technique was reviewed in this article. Owing to the fact that the SPS technique is widely employed in fabricating nanostructured materials with outstanding properties. Despite the outstanding features of this fabrication technique, optimizing the right parameters to produce materials with minimal pores, fully dense structure and improved properties is quite tasking.

However, wide range of research on the application of SPS to fabricate commercially pure titanium reinforced CNT was reported in this article, the SPS of Ti6Al4V reinforced with CNT is still scanty in literatures. Although few researches on the improvement of the properties of Ti6Al4V using nanotubes with focus on the utilization of HEBM in dispersing the reinforcements is available from past studies. These research findings do not address the issue of effective dispersion of MWCNT in Ti6Al4V matrix without tampering on the unique and promising properties of the nanotubes.

The review from this article revealed that past research has been focused on the SPS of commercially pure titanium and titanium oxide reinforced with CNT. Few articles were available on the SPS of Ti6Al4V reinforced with CNT. Hence, this motivated the application of SSBM technique to disperse MWCNT for the improvement of the properties of Ti6Al4V matrix. The need to understand the fabrication process of the composite system, the densification mechanisms, change in the phase and microstructure of the composite and how it affects the mechanical properties of the materials have engendered this study.

4.2.2 Achieving the dispersion of MWCNT in Ti6Al4V matrix

The influence of shift-speed ball milling technique in achieving homogeneous dispersion of MWCNT in the Ti6Al4V powder was reported in the **Article 2.**

Article 2 emphasized on the utilization of low-speed ball mill and high-speed ball with regulated milling speed and time to achieve effective dispersion of MWCNT in the titanium alloy without hampering the unique properties of the nanotubes. The sole aim of employing this dispersion method was to promote the effective dispersion of the nanotubes in the Ti6Al4V matrix and achieve good bonding at the composites interface without tampering with the nanostructure of the MWCNT. The **Article 2** further reported the influence of ball milling times and speed on the dispersion of the nanotubes in the titanium alloy which was confirmed from the microstructural and nanostructural

evolution of the powders. Detail TEM analysis using the selected area diffraction and the fast Fourier transform patterns was employed to reveal the nanostructural evolution of the nanotubes after the dispersion process. Further analysis using XRD and Raman spectroscopy employed to ascertain the phase and structural evolution revealed that the structural strain induced on the nanotubes during the dispersion process do not result in the loss of the excellent properties of the MWCNT. Therefore, the research reported in the **Article 2** covered the first two specific objectives of the study.

Furthermore, the **Article 2** revealed the tremendous potential of the shift-speed ball milling technique in achieving uniform dispersion of MWCNT in Ti6Al4V powders, good bonding at the composite interface without losing the structure of the nanotubes.

4.2.3 Effects of sintering temperature during spark plasma sintering

The **Article 3** presents the influence of sintering temperature on the sinterability, densification behaviour and Vickers hardness of the sintered titanium alloy and the respective nanocomposites. This article is the continuation of the dispersion of MWCNT in Ti6Al4V matrix presented in the previous article. However, various sintering temperature (900 -1100 ^{o}C) was employed to consolidate the titanium alloy and the nanocomposites comprising of MWCNT.

The focus of the article 3 was mainly to evaluate the influence of sintering temperature on the densification behaviour and microhardness of the alloy and nanocomposites fabricated by SPS. An ideal sintering temperature is highly desirable during the fabrication of alloys and nanocomposites with outstanding mechanical properties. Furthermore, the appropriate sintering temperature has the tendency of inducing the required grain growth and fusing the composites components to form materials with pores-free or minimal pores structure. Materials with micropores have the propensity of less dense structure and weak mechanical properties which eventually limit their widespread applications especially in aerospace industries. Meanwhile, the sintering temperature employed during the SPS of titanium alloy and the nanocomposites has tremendous influence on the phase and microstructural evolution of the materials. Since it is paramount to fabricate materials with uniform microstructure, high relative density, outstanding hardness, and improved chemical and thermal stability for widespread engineering applications at a lower cost.

Sintering temperature and time during spark plasma sintering usually triggers the activation and surface diffusion of powders which induce mass transfer of the powder particle and enhance the densification process. This further promote the neck formation and deformation process of the powders particles which emanate from the grain growth mechanism and eventually result in pore-free structures. Despite grain growth and densification phenomenon works simultaneously, to achieve a highly densified material, the sintering parameters must be tuned to promote more of densification and minimal grain growth. This can be further explained by minimizing the holding time during sintering of the material after attaining the threshold sintering temperature. Being cognizant that extended holding time during SPS will promote the increase in sintering time and eventually results in grain growth and larger and uneven microstructures.

Regardless of the outstanding features of the SPS technique to fabricate superior alloys and nanostructured materials with excellent properties, insufficient investigations have been conducted to understand the sintering and densification behaviour of MWCNT reinforced Ti6Al4V during the sintering process.

The consolidation of compacted powders without appropriate sintering parameters (sintering temperature, compressive pressure, holding time, and heating rate) will result in materials with micropores and defects. Meanwhile the potential of SPS of MWCNT reinforced titanium alloys with improved relative density and hardness have been reported in past studies but the understanding of the densification mechanisms and how the sintering temperature influence the movement of the punches during the sintering process has not been studied.

Considering the fact that the SPS technique employs the pulsed DC current to produce the flow of heat across the graphite die comprising the compacted sample and triggers the rise in temperature of the sample under the compress pressure. Past studies have exploited the benefit of this technique by varying the sintering parameters to achieve titanium-based nanocomposites with outstanding properties. In this article, other optimized sintering parameters (holding time, heating rate and compressive pressure) employed in previous studies was utilized alongside with varying the sintering temperature to consolidate the titanium alloy and the nanocomposites.

The research findings from the article 3 on the influence of the varying sintering temperature on the sintering and densification behaviour and how it affects the microhardness of the fabricated titanium

alloy and nanocomposites contributed to knowledge as it revealed the appropriate parameters to achieve the best densification and mechanical properties.

Furthermore, the research finding reported in this third article will assist other researchers seeking to fabricate Ti6Al4V nanocomposites reinforced with MWCNT. Additionally, the article 3 buttressed on the phase and microstructural evolutions that occurred at the utilized sintering temperatures after the consolidation process.

Hence, from the article 3, it was discovered that the following sintering parameters (sintering temperature of 1100 ^{o}C, heating rate 100 ^{o}C/min, holding time of 10 min and compressive pressure of 50 MPa) resulted in the titanium alloy and nanocomposites with the best densification and microhardness.

It is obvious from the article 3 that one of the limitations of Ti6Al4V alloy which is weak hardness was addressed since the fabricated nanocomposites showed the best microhardness values. Meanwhile, this article covered the second and third objectives of this thesis and answered the third research question of the study.

Lastly, the contributions from this article appraised the required selection and ascertain the best parameters for the consolidation of the titanium alloy and its nanocomposites using SPS. Hence, this will eradicate empirical research during the fabrication of the alloy and the nanocomposites using SPS.

4.2.4 Effect of MWCNT addition on the microstructural evolution of the nanocomposites

The effects of MWCNT addition on the microstructural evolution, fracture morphology and mechanical properties of the fabricated nanocomposites were fully covered in **Article 4.** Despite **Article 3** highlight the microstructural evolution of the fabricated alloy and nanocomposite, but it focused was on the influence of the varying sintering temperature on the microstructural and phase evolution as well as the properties of the sintered materials.

The method employed in dispersing the 1.0 wt.% of MWCNT in the titanium alloy reported in **Article 2**, was employed to disperse various concentrations of MWCNT in Ti6Al4V matrix in the **Article 4**. Furthermore, the mixed powders were characterized by employing advanced characterization using SEM, TEM (SAED, FFT), XRD, Raman to understand the dispersibility and

structural evolutions of the various concentration of the MWCNT in the Ti6Al4V matrix. The mixed powders were further consolidated at 1000 ^{o}C using the SPS technique and various characterizations were conducted using OM, SEM, XRD, Raman to reveal the dispersibility, surface and fracture morphology, phase and structural evolutions after the sintering process. The mechanical properties of the fabricated alloy and nanocomposites were also tested to understand the influence of the MWCNT addition on the property integrity of the fabricated materials.

The **Article 4** also provides basic understanding on the dispersibility of the various MWCNT content in Ti6Al4V powders and how the walls of the nanotubes were exposed to structural deformation resulting from the increase in the concentration of the MWCNT. Despite the structural deformations observed on the walls of the nanotubes after the dispersion process, detail Raman analysis and phase analysis from this study revealed that no structural defects were induced on the nanotubes during milling. Furthermore, this **article 4** also uphold the application of shift-speed ball milling for the effective dispersion of MWCNT in metal matrices.

Additionally, it was realized that steaks and blurring coaxial and halo rings were formed from the SAED pattern and the FFT pattern displayed the increase in the interlayer spacing of the nanotubes in the nanocomposite grade with the highest concentration of MWCNT.

Nevertheless, it was revealed from this **article 4** that the dispersibility of nanotubes decreased with the increase in MWCNT concentration in the nanocomposites. Meanwhile, it was recommended from the study that when the MWCNT is increased beyond 1.0 weight percent, the milling parameters should be adjusted to effect optimal dispersion of MWCNT. This will induce adequate energy on the powder mixture and result in good dispersibility of the MWCNT in the titanium alloy matrix. Since nanocomposites comprising of uniform dispersion of the secondary phases have the tendency of bearing higher load or having good load-bearing ability in service conditions.

It also emphasized on phase evolutions of the sintered nanocomposites after the sintering process where titanium carbide was formed which helps to enhance the hardness and stiffness of the nanocomposites. It was observed from the **article 4** that the addition and increase in concentration of the MWCNT in the titanium alloy favored the stabilization of alpha titanium phase owing to the fact that carbon is a good stabilizer of alpha phases in the titanium alloy.

This article also throws more light on the fracture morphology of the nanocomposites comprising of various concentration of the nanotubes. It was established from the fractography results that the addition of MWCNT into the Ti6Al4V matrix resulted in the formation of micropores in the nanocomposites which adversely affect the densification of the nanocomposites. Meanwhile, despite the reduction of the density established in this article 4, it was reported that the mechanical properties were greatly enhanced by the addition of MWCNT into the titanium alloy matrix. The microstructural and phase evolutions, and the improvement in mechanical properties reported in this article was attributed to the presence of the MWCNT in the nanocomposite system which favored the formation of both the alpha and beta phases in the nanocomposite structure. Furthermore, the notable mechanical properties of the nanotubes were fully transferred to the matrix materials that translated to the improved properties recorded.

This article added to existing knowledge on the microstructural evolution of metal matrices by the addition of MWCNT. Being cognizant that various literatures on the microstructural evolution of MWCNT reinforced metal matrices exist, there are no literature on the microstructural evolution of this composites system. Especially studies that emphasized on the microstructural evolutions during the dispersion process and after the consolidation process using the SPS technique.

From the study reported in **Article 4**, it was discovered that the fifth objective of the entire thesis was realized. Also, the fourth and fifth research questions were fully answered from this article.

4.2.5 Ascertaining the mechanical integrity of the nanocomposite system by nanoindentation

To further established the fact that MWCNT have positive influence on the mechanical properties of the fabricated nanocomposites, both the fabricated alloy and nanocomposites were subjected to nanoindentation studies. The results from the nanoindentation studies were fully reported in **Article 5** of this thesis.

Over the years, nanoindentation studies have been explicitly employed to ascertain the mechanical behaviour and anti-wear characteristics of various grade of materials ranging from composites, alloys, ceramics and polymers to mention but a few. This testing technique can be used to investigate the mechanical properties of small materials without hampering with their microstructure.

Having established the dispersion characteristic, phase and microstructural changes, sinterability and mechanical properties of the fabricated alloy and nanocomposites in previous articles, it is worthwhile to reveal the mechanical behaviour of the fabricated materials using nanoindentation studies. Since this technique will reveal the intrinsic micro and nanomechanical behaviour of the fabricated materials.

The **Article 5** revealed information on the influence of MWCNT on the nanohardness, elastic modulus, plasticity and elastic recovery index. Additionally, the resistance to strain, anti-wear properties and resistance to plastic deformation of the Ti6Al4V alloy and the nanocomposites were covered in this article.

During the nanoindentation studies reported in this article, various indentation loads were indented on the fabricated alloy and nanocomposites. It was realized that the fabricated materials responded differently to the various loads during nanoindentation. The influence of the MWCNT in the Ti6Al4V matrix came into play to resist the indentation loads in the fabricated nanocomposites. This was glaringly observed from the load-displacement curves during the nanoindentation study where the fabricated nanocomposites showed tremendous resistance to plastic deformation.

Furthermore, it was reported from the article that the fabricated titanium alloy, exhibited the lowest resistance to elastic strain to failure but showed adequate plastic deformation than the fabricated nanocomposites. It was also realized that the nanohardness, elastic modulus, anti-wear behaviour, elastic recovery to strain improved with the addition and increase in concentration of MWCNT in the nanocomposite system.

The application of nanoindentation technique has been expressly used in probing nanocomposite coatings, alloys, and various nanocomposite materials, however, this technique has not been reportedly used to probe this nanocomposite system. Therefore, this **article 5** added to the wealth of knowledge on the application of nanoindentation technique to reveal the intrinsic nanomechanical behaviour of spark plasma sintered titanium-based nanocomposites reinforced with MWCNT.

Meanwhile, the sixth objective of the research was fully covered in **article 5** and appropriate solutions were given to the last research question of this study.

4.3 Conclusions

In this study, MWCNT of varying concentrations were effectively dispersed in Ti6Al4V matrix and consolidated using the SPS technique. Appropriate milling parameters were varied during the dispersion process to achieve nanocomposites with high dispersibility of MWCNT. During the consolidation process, various sintering temperature was employed to produce materials compact of high densification standard despite the incorporation of MWCNT into the Ti6Al4V matrix. The role of MWCNT addition on the dispersion characteristic, sinterability, densification behaviour, change in microstructure, phase evolution, fracture morphology, microhardness, nanomechanical properties and anti-wear behaviour was immensely investigated. The following conclusions were established from the study:

1. The application of SSBM technique during the dispersion of MWCNT in Ti6Al4V matrix revealed that the appropriate milling parameters to achieve optimal dispersion of MWCNT with less structural strain are 8 h, 150 rpm, 10:1 of BPR and 10 min of relaxation time and 1 h, 100 rpm, 10:1 and 10 min of relaxation time during low-speed ball milling and high-speed ball milling respectively.

2. SPS of MWCNT reinforced Ti6Al4V nanocomposites at higher sintering temperature resulted in improved densification and properties with the following sintering parameters; 1100 ^{o}C of sintering temperature, holding time of 10 min, heating rate of 100 ^{o}C/min under a pressure of 50 MPa to the produced the alloy and nanocomposites of the highest density and properties.

3. The addition of MWCNT into Ti6Al4V matrix retarded the sintering process which resulted in longer sintering time during SPS. Also, it introduced the presence of micropores in the nanocomposite grades which translate to the reduction in relative density and its evidence in the fracture morphology.

4. Sintering of the nanocomposite powders comprising of MWCNT triggers a chemical reaction between the carbon and titanium that resulted in the formation of titanium carbide which in turn enhanced the mechanical properties of the nanocomposites.

5. The nanocomposite grades comprising of the highest concentration of MWCNT displayed the best microhardness and nanomechanical properties. Although, the fabricated Ti6Al4V alloy, showed the least resistance to plastic deformation during nanoindentation.

6. The nanomechanical properties of the nanocomposite grades and the fabricated alloy decreased with the increase in nanoindentation loads.

4.4 Recommendations

In this study, it was revealed that the application of SSBM technique is reliable in homogenous dispersion of MWCNT in Ti6Al4V matrix. It also established the appropriate parameters to achieve the optimal dispersion of MWCNT in the titanium alloy matrix using this dispersion technique. Furthermore, the appropriate parameters required to fabricate a fully dense Ti6Al4V alloy and its MWCNT reinforced nanocomposites with improved mechanical properties were revealed from this study. The fabricated nanocomposite comprises of high stiffness, high hardness, resistance to plastic deformation and anti-wear behaviour. These materials can be effectively employed in structural and load-bearing engineering applications that demands high mechanical properties.